



# **Nonlinear Pretensioning and Geometry Preservation of Spatial Structures**

A Dissertation

Submitted to the Council of the Erbil Technical Engineering  
College at Erbil Polytechnic University in Partial  
Fullfilment of the Requirements for the Degree of Doctor of  
Philosophy in Structural Engineering

By

**Shna Jabar Abdulkarim**  
BSc. Building Construction  
MSc. Structural Engineering

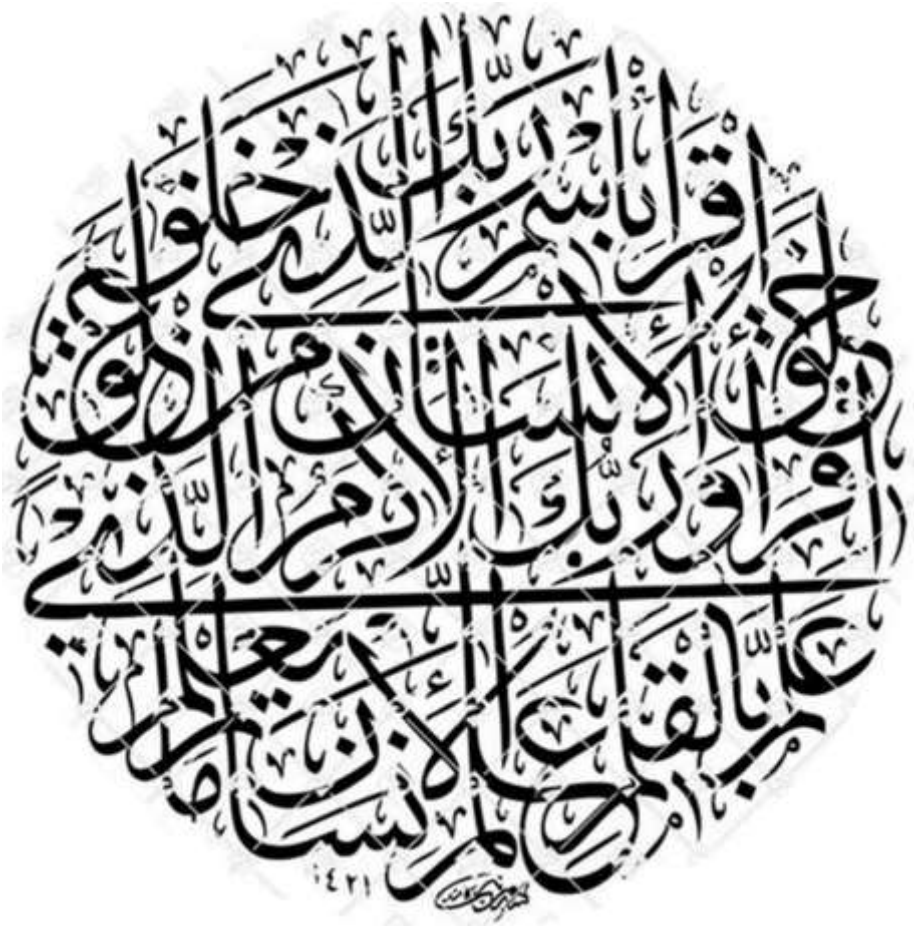
Supervised by

**Asst. Prof. Dr. Najmadeen Mohammed Saeed**

Erbil Kurdistan

October 2024

بِسْمِ اللَّهِ الرَّحْمَنِ الرَّحِيمِ



## DECLARATION

I declare that the Ph.D. Dissertation entitled: **Nonlinear Pretensioning and Geometry Preservation of Spatial Structures** is my own original work, and hereby I certify that unless stated, all work contained within this dissertation is my own independent research and has not been submitted for the award of any other degree at any institution, except where due acknowledgement is made in the text.

Signature:

Student Name: Shna Jabar Abdulkarim

Date:

## LINGUISTIC REVIEW

I confirm that I have reviewed the dissertation titled **Nonlinear Pretensioning and Geometry Preservation of Spatial Structures** from the English linguistic point of view, and I can confirm that it is free of grammatical and spelling errors.

Signature:

Name of Reviewer: Asst. Prof. Dr. Salih Ibrahim Ahmed

Date:

## SUPERVISOR CERTIFICATE

This dissertation has been written under my supervision and has been submitted for the award of the degree of Doctor of Philosophy in Structural Engineering with my approval as supervisor

Signature                      Name: Asst. Prof. Dr. Najmadeen Mohammed Saeed

Date

**I confirm that all requirements have been fulfilled.**

Signature:

Name: Asst. Prof. Dr. Bahman Omar Taha

Head of the Department of Civil Engineering Technique

Date:

**I confirm that all requirements have been fulfilled.**

Postgraduate Office

Signature:

Name: Byad Abdulqader Ahmed

Date:

## EXAMINING COMMITTEE CERTIFICATION

We certify that we have read this Dissertation: **Nonlinear Pretensioning and Geometry Preservation of Spatial Structures** and as an examining committee examined the student (Shna Jabar Abdulkarim) in its content and what is related to it. We approve that it meets the standards of a dissertation for the degree of Doctor of Philosophy in Structural Engineering.

Signature

Name: Asst. Prof. Dr. Najmadeen M. Saeed

Supervisor

Date:

Signature

Name: Asst. Prof. Dr. Wrya A. Abdullah

Member

Date:

Signature

Name: Asst. Prof. Dr. Abdulhameed A. Yaseen

Member

Date:

Signature

Name: Prof. Dr. Faris Rashied Ahmed

Member

Date:

Signature

Name: Prof. Dr. Omar Qarani Aziz

Member

Date:

Signature

Name: Prof. Dr. Mereen H. Fahmi Rasheed

Chairman

Date:

Signature

Name: Prof. Dr. Ayad Zaki Saber Agha

Dean of the Technical Engineering College

Date:

## DEDICATION

To  
My Husband  
My Mother  
My Sons

Shna Jabar Abdulkarim  
2024

## ACKNOWLEDGEMENTS

First and foremost, praise be to Allah the Almighty, the Most Kind, and the Most Merciful for His blessings granted to me during my Ph.D. study and in finalising this dissertation. May Allah's blessings be upon His final prophet Muhammad (peace be upon him), his family, and his companions.

I extend my sincere gratitude to my supervisor, Assistant Professor Dr. Najmadeen Mohammed Saeed, for his unwavering support and guidance throughout this research. I also thank my professors at Erbil Technical Engineering College, Erbil Polytechnic University, especially Assistant Professor Dr. Bahman Omar Taha and Professor Dr. Ayad Zaki Saber Agha, for their support during the preparation and evaluation courses. Profound thanks to my dissertation committee for their critical feedback, which significantly enhanced this work.

I extend my gratitude to ProLab company for providing the datalogger instrument, to Slemani Construction Laboratory for testing the cable and aluminium specimens, and to civil engineering department at the University of Raparin. I thank my brother-in-law, Mr. Omar Mahmood Ibrahim, for supplying materials from abroad. To my husband, Abubaker Mahmood Ibrahim, my sons, Awa, Aga, and Asa, and my entire family, I owe an immeasurable debt of gratitude for their unwavering love and encouragement throughout this journey. Your belief in my abilities has been the foundation of my success.

Finally, to all those who contributed to this dissertation, directly or indirectly, I offer my heartfelt thanks. Your support and contributions have made this achievement possible.



## ABSTRACT

In this dissertation, three nonlinear techniques of prestressing, analysis, and preservation were developed based on the principles of the force method to address geometric nonlinearities in pin-jointed spatial structures. These techniques provide a comprehensive framework for accurately performing prestressing, analysing, and preserving spatial assemblies, validated through rigorous numerical and experimental investigations.

The research introduces direct nonlinear approaches especially for prestressing and preservation, overcoming the limitations of iterative and linear approximation-based methods. The derived nonlinear equations, expressed as functions of joint displacements, were efficiently solved using MATLAB's *fsolve* function, demonstrating robust applicability to both simple and complex spatial systems. The proposed prestressing technique computes the desired prestress level by accurately accounting for nonlinear member alterations, preventing cable slack, and maintaining alignment with software solvers under predetermined actuation conditions.

The developed analysis method is efficient and precise, capable of calculating internal member stresses and axial forces for both rigid and flexible members while incorporating geometric nonlinearities under different loading conditions. Similarly, the preservation technique reliably restores disturbed geometries, nodal displacements, and internal forces, with targeted control of specific parameters. The effectiveness of the preservation process depends on actuator placement, bar sensitivity analysis, and the appropriate selection of actuation targets.

Validation of these techniques included numerical case studies and experimental testing on a hyperbolic paraboloid space cable net model with 64

members and 41 joints. The results demonstrated strong agreement, with maximum and minimum discrepancy ratios of 7% and 0%, respectively, between theoretical and experimental measurements. This dissertation presents a novel framework that significantly enhances the precision, efficiency, and control of structural response prediction, making substantial advancements in the field of pin-jointed spatial structures.

## TABLE OF CONTENTS

<b>DECLARATION</b> .....	<b>i</b>
<b>LINGUISTIC REVIEW</b> .....	<b>ii</b>
<b>SUPERVISOR CERTIFICATE</b> .....	<b>iii</b>
<b>EXAMINING COMMITTEE CERTIFICATION</b> .....	<b>iv</b>
<b>DEDICATION</b> .....	<b>v</b>
<b>ACKNOWLEDGEMENTS</b> .....	<b>vi</b>
<b>ABSTRACT</b> .....	<b>vii</b>
<b>TABLE OF CONTENTS</b> .....	<b>ix</b>
<b>LIST OF FIGURES</b> .....	<b>xiii</b>
<b>LIST OF TABLES</b> .....	<b>xvi</b>
<b>LIST OF NOTATIONS</b> .....	<b>xix</b>
<b>CHAPTER ONE</b> .....	<b>1</b>
<b>1 INTRODUCTION</b> .....	<b>1</b>
1.1 INTRODUCTION AND OVERVIEW .....	1
1.2 PROBLEM STATEMENT .....	5
1.3 AIMS AND OBJECTIVES .....	6
1.4 THE OUTLINE OF THE DISSERTATION.....	7
<b>CHAPTER TWO</b> .....	<b>10</b>
<b>2 LITERATURE REVIEW</b> .....	<b>10</b>
2.1 INTRODUCTION .....	10
2.2 PRESTRESSING TENSILE STRUCTURES .....	11
2.3 ANALYSIS TECHNIQUES OF SPATIAL STRUCTURES .....	13

2.4	PRESERVATION TECHNIQUES OF SPATIAL STRUCTURES ..	15
2.4.1	Geometrical Preservation .....	17
2.4.2	Member Force Preservation .....	19
2.4.3	Simultaneous Geometrical and Member Force Preservation .....	20
2.4.4	Actuators .....	22
2.5	SUMMARY .....	28
<b>CHAPTER THREE .....</b>		<b>30</b>
<b>3</b>	<b>THEORETICAL FORMULATION .....</b>	<b>30</b>
3.1	INTRODUCTION .....	30
3.2	FORMULATION OF THE PRESTRESSING TECHNIQUE.....	30
3.2.1	Deriving Nonlinear Member Alteration.....	32
3.2.2	Mathematical Expanding of Prestressed Member Alteration .....	33
3.2.3	Equilibrium Matrix at Deformed Configuration.....	35
3.2.4	Steps for Solving Nonlinear Prestressing Method .....	37
3.2.5	Illustrative Example .....	38
3.2.6	Validation of the Prestressing Technique .....	40
3.3	FORMULATION AND VALIDATION OF THE ANALYSIS TECHNIQUE .....	56
3.3.1	Two-Linked Structure .....	60
3.3.2	Flat Cable-Net Structure .....	61
3.3.3	Spatial Net Structure .....	62
3.3.4	Quarter Hyperbolic Paraboloid Net Structure.....	64
3.3.5	Saddle Net Structure .....	65
3.3.6	Cantilever Truss Structure .....	68
3.3.7	Double Layer Spherical Structure.....	70
3.4	FORMULATION OF THE PRESERVATION TECHNIQUE .....	74
3.4.1	Sensitivity Technique for the Preservation Process.....	75

3.4.2	Validation of the Preservation Technique.....	77
3.5	SUMMARY .....	84
<b>CHAPTER FOUR.....</b>		<b>86</b>
<b>4</b>	<b>DESIGN AND ASSEMBLY OF EXPERIMENTAL MODEL .....</b>	<b>86</b>
4.1	INTRODUCTION .....	86
4.2	HYPERBOLIC PARABOLOID STRUCTURE .....	86
4.2.1	Material Properties .....	89
4.2.2	Joints.....	93
4.2.3	Cable Members .....	93
4.2.4	Actuators .....	95
4.2.5	Support System .....	98
4.2.6	Experimental Measurement .....	98
4.2.7	Parameters of the Study .....	103
4.3	EXPERIMENTAL PROCEDURE .....	103
4.4	SUMMARY .....	105
<b>CHAPTER FIVE.....</b>		<b>107</b>
<b>5</b>	<b>EXPERIMENTAL FINDINGS AND DISCUSSIONS.....</b>	<b>107</b>
5.1	INTRODUCTION .....	107
5.2	PRESTRESSING PHASE RESULTS .....	107
5.2.1	Symmetric Prestressing Case 1 (PC1) .....	108
5.2.2	Symmetric Prestressing Case 2 (PC2) .....	116
5.2.3	Asymmetric Prestressing Case 3 (PC3) .....	121
5.3	ANALYSIS PHASE RESULTS.....	125
5.3.1	Vertical Nodal Loading Case (LC1) .....	125
5.3.2	Horizontal Nodal Loading Case (LC2).....	131
5.3.3	Vertical and Horizontal Nodal Loading Case (LC3) .....	136

5.4	PRESERVING PHASE RESULTS .....	140
5.4.1	Nodal Displacement Preservation Case (DPC1).....	140
5.4.2	Member Force Preservation Case (FPC2) .....	144
5.4.3	Simultaneous Preservation Case (SPC3) .....	147
5.5	SUMMARY .....	154
<b>CHAPTER SIX.....</b>		<b>156</b>
<b>6</b>	<b>CONCLUSIONS AND RECOMMENDATIONS.....</b>	<b>156</b>
6.1	CONCLUSIONS.....	156
6.2	RECOMMENDATIONS FOR FUTURE WORK .....	158
<b>REFERENCES .....</b>		<b>R1</b>
<b>LIST OF PUBLICATIONS.....</b>		<b>P1</b>
<b>APPENDIX .....</b>		<b>A1</b>
A:	MATLAB Code for Numerical Prestressing of Illustrative Example in 3.2.5 by fsolve .....	A1
B:	MATLAB Code for Numerical Analysis by fsolve .....	A4
C:	MATLAB Code for Numerical Displacement preservation by fsolve .....	A9
D:	MATLAB Code for Numerical Force preservation by fsolve .....	A13
<b>یوخته.....</b>		<b>II</b>

## LIST OF FIGURES

Fig. 1-1 The grid roof of the National Maritime Museum in the Netherlands (Pascal, 2021). .....	1
Fig. 1-2 Al-Minaa Olympic stadium in Basra, Iraq (Kaliciak, 2022).....	3
Fig. 1-3 Arrangement of dissertation .....	9
Fig. 2-1 Structural control and controlling subdomains (Korkmaz, 2011). 16	
Fig. 2-2 Geometrical preservation of double layer dome Abdulkarim et al. (2020) .....	17
Fig. 2-3 A two-dimensional cable net structure (You, 1997). .....	21
Fig. 2-4 A representative example of a turnbuckle.....	25
Fig. 2-5 Role of piezoelectric ceramic in generating electrical and mechanical effect (Yoichi, 2006).....	25
Fig. 2-6 Classification of different electromechanical actuators (Qiao <i>et al.</i> , 2018).....	26
Fig. 2-7 Deployable structure opened by shape memory alloy .....	27
Fig. 2-8 Normalized actuator attributes: power-to-weight ratio versus efficiency (Zupan <i>et al.</i> , 2002).....	28
Fig. 3-1 Two-dimensional element before and after prestressing process .	32
Fig. 3-2 Triple-link cable structure .....	39
Fig. 3-3 Cable net model designed by You (1997).....	42
Fig. 3-4 Deployable structure (Kwan and Pellegrino, 1993).....	45
Fig. 3-5 Plan view of the general state of self-stress of a unit (Kwan and Pellegrino, 1993) .....	46
Fig. 3-6 Space truss geometry by Levy et al. (1994).....	48
Fig. 3-7 Space truss grid lack of fit.....	49
Fig. 3-8 3D cable-net model with labeled nodes and members.....	51
Fig. 3-9 Conical cable-net model with labeled nodes.....	54
Fig. 3-10 Top view of the conical cable-net model with labeled cables ....	54
Fig. 3-11 Spatial bar coordinates at original and deformed configuration .	57

Fig. 3-12 Spatial equilibrium state at original and deformed configuration	57
Fig. 3-13 Two-linked structure .....	60
Fig. 3-14 Flat cable-net structure .....	61
Fig. 3-15 Spatial net structure .....	63
Fig. 3-16 Hyperbolic paraboloid net structure .....	64
Fig. 3-17 Saddle net structure .....	66
Fig. 3-18 Cantilever truss structure with nodal labels, panels spacing, and nodal loads.....	69
Fig. 3-19 Double-layer spherical model.....	70
Fig. 3-20 Supports and laterally load in (N) of double-layer spherical model .....	71
Fig. 4-1 Labelling of members and joints in the 3D experimental model with hyperbolic paraboloid geometry.....	87
Fig. 4-2 Hyperbolic paraboloid experimental model.....	88
Fig. 4-3 Members detail of experimental model.....	88
Fig. 4-4 Stress-strain diagram of (19 wire-strand) cable in tension.....	90
Fig. 4-5 Stress-strain diagram of aluminium in tension.....	91
Fig. 4-6 Top view detail of experimental member segments.....	92
Fig. 4-7 Joint detail of the experimental setup.....	93
Fig. 4-8 Tensile testing machine and cable test specimen .....	94
Fig. 4-9 Jack screw detail in the actuator.....	96
Fig. 4-10 Cutting phase of aluminium segments .....	96
Fig. 4-11 Center marking and drilling phase of aluminium segments.....	97
Fig. 4-12 Photo illustrating internal left and right threading and assembly of end joints .....	97
Fig. 4-13 Layout of supports in the experimental model.....	98
Fig. 4-14 Arrangement of lighting sources and digital camera for displacement recording.....	99



Fig. 4-15 Placement of scaled ruler and joint movement monitoring for joints .....	100
Fig. 4-16 64-channel data logger for strain measurement .....	101
Fig. 4-17 Photo illustrating steps for strain gauge sensor placement .....	101
Fig. 4-18 Connection accessories for data logger device .....	102
Fig. 4-19 Flowchart illustrating the experimental process.....	106
Fig. 5-1 Selected 24 members for prestress application in PC1 .....	108
Fig. 5-2 Displacement measurement in (mm) of joint 39 in y-z and x-z views for the experimental model .....	114
Fig. 5-3 Selected 16 members for prestress application in PC2 .....	116
Fig. 5-4 Selected 24 members for prestress application in PC3 .....	121
Fig. 5-5 Experimental model under vertical joint loads .....	126
Fig. 5-6 Joint measurements in (mm) for experimental displacement computing for LC1 .....	129
Fig. 5-7 Experimental model under horizontal joint loads .....	131
Fig. 5-8 Detailed experimental setup for horizontal load distribution.....	132
Fig. 5-9 Experimental model under vertical and horizontal joint loads ...	137
Fig. 5-10 Nodal movement for the targeted displacements in DPC1 .....	142
Fig. 5-11 Nodal movement for the targeted displacements in SPC3.....	148
Fig. 5-12 Coordinate position of nodes 7 and 35 before and after vertical displacement preservation .....	149

## LIST OF TABLES

Table 3-1 Comparison of nonlinear member alteration with You (1997) ..	42
Table 3-2 Comparison of nonlinear member alteration with the particular choice of Kwan and Pellegrino (1993).....	46
Table 3-3 Comparison of nonlinear member alteration with the optimal set of Kwan and Pellegrino (1993) .....	47
Table 3-4 Comparison of nonlinear member alteration with Hanaor and Levy (1985) .....	49
Table 3-5 Nodal coordinates for the 3D cable net model .....	52
Table 3-6 Cable prestress and $l_2$ – norm for the 3D cable net model .....	52
Table 3-7 Nodal displacement and cable actuation for the 3D cable net model .....	52
Table 3-8 Conical cable-net nodal coordinates, and displacements .....	55
Table 3-9 Conical cable-net member prestress and member actuation .....	55
Table 3-10 Nodal displacement (mm) for internal joints of the flat cable-net .....	62
Table 3-11 Cable tensile forces (N) of the flat cable-net.....	62
Table 3-12 Nodal displacements comparison (mm) of the spatial net .....	63
Table 3-13 Nodal displacements comparison (mm) in the z-direction of hyperbolic paraboloid net.....	65
Table 3-14 Nodal displacements comparison (mm) of saddle net.....	67
Table 3-15 Nodal displacements and internal bar forces of the cantilever truss by SAP2000, linear and nonlinear force methods .....	69
Table 3-16 Nodal displacement of double-layer spherical model .....	73
Table 3-17 Computed nodal displacements based on the bar sensitivity technique.....	76
Table 3-18 Computed member forces based on the bar sensitivity technique .....	77

Table 3-19 Displacement of the cantilever truss after preservation process using present technique in comparison to the linear technique by Saeed and Kwan (2016c).....	78
Table 3-20 Internal force of the cantilever truss after preservation process in comparison to the linear technique by Saeed and Kwan (2016c)	80
Table 3-21 Displacement of the cable net structure after preservation process in comparison to the linear technique by You (1997).....	82
Table 3-22 Internal force of the cable net structure after preservation process technique in comparison to the linear technique by You (1997)	82
Table 3-23 Simultaneous preservation of displacement and internal force in comparison with the studies by Xu and Luo (2009) and Saeed (2022) .....	84
Table 4-1 Nodal coordinates and member lengths of the hyperbolic paraboloid 3D model.....	89
Table 4-2 Effective combined axial stiffness of experimental members....	92
Table 5-1 Theoretical and experimental member actuation and prestressing degree in PC1 .....	110
Table 5-2 Strain data of the aluminium segments for the experimental PC1	111
Table 5-3 Theoretical and experimental displacements in PC1.....	115
Table 5-4 Theoretical and experimental member actuation and prestressing degree in PC2 .....	117
Table 5-5 Theoretical and experimental displacements in PC2.....	120
Table 5-6 Theoretical and experimental member actuation and prestressing degree in PC3 .....	123
Table 5-7 Theoretical and experimental displacements in PC3.....	124
Table 5-8 Nodal loads, theoretical and experimental member forces for LC1 .....	127
Table 5-9 Theoretical and experimental displacement under LC1 .....	130

Table 5-10 Nodal loads, theoretical and experimental member forces for LC2.....	133
Table 5-11 Theoretical and experimental displacement under LC2.....	134
Table 5-12 Nodal loads, theoretical and experimental member forces for LC3.....	138
Table 5-13 Theoretical and experimental displacement under LC3.....	139
Table 5-14 Theoretical and experimental preserved and combined displacements for DPC1.....	143
Table 5-15 Theoretical and experimental internal force for FPC2.....	146
Table 5-16 Theoretical and experimental vertical displacements before and after preservation process in SPC3.....	150
Table 5-17 Theoretical and experimental internal force before and after preservation process in SPC3.....	152
Table 5-18 Theoretical and experimental combined internal force before and after preservation process in SPC3.....	153

## LIST OF NOTATIONS

$a$	Set of coefficients for the vectors of $S$
$A(d)$	Nonlinear self-equilibrium matrix
$A_o$	Element cross-sectional area
$B(d)$	Nonlinear compatibility matrix
$c$	Number of constraints
$d$	Vectors of nodal displacement
$E$	Modulus of elasticity
$e$	Member length alteration due to $P$
$e_c(d)$	Nonlinear member actuation required for preservation after prestressing
$e_e(d)$	Nonlinear member actuation required for preservation after analysis
$e_o$	Vector of member actuation (elongation/shortening)
$e_o(d)$	Vector of nonlinear member actuation required for prestressing
$F$	Flexibility matrix
$L$	Member length before applying $P$
$L'$	Member length after prestressing member
$L_c$	Member length after deformation due to $P$
$L_o$	Initial member length
$nB$	Number of bar (element)s
$nJ$	Number of joint (node)s
$P$	External nodal load
$P_i$	external nodal load at node $i$
$P_{xi}$	$x$ component of $P_i$ at node $i$
$P_{yi}$	$y$ component of $P_i$ at node $i$
$P_{zi}$	$z$ component of $P_i$ at node $i$
$R_{eo}$	Euclidean norm ratio for member actuation
$R_t$	Euclidean norm ratio for internal force
$S$	State of self-stress matrix
$t$	Vector of prestressing force due to $e_o(d)$
$T$	Internal member force due to $P$
$t_c$	Internal member force after preservation without $P$
$T_e$	Internal member force after preservation with $P$
$tx_{i,j}$	$x$ component of vector $t$
$ty_{i,j}$	$y$ component of vector $t$

**CHAPTER ONE****INTRODUCTION****1.1 INTRODUCTION AND OVERVIEW**

A spatial structure is a three-dimensional structural system with a non-planar configuration, applied loads, internal response, and nodal transitions. The concept of spatial structures has been highlighted through numerous architecturally striking constructions in recent years. These assemblies are prominently featured in sports facilities, stadiums, bridges, malls, and museums, such as the National Maritime Museum in Amsterdam, Netherlands, as shown in Fig. 1-1.



Fig. 1-1 The grid roof of the National Maritime Museum in the Netherlands (Pascal, 2021).

Due to their distinctive geometric shape and material properties, these structures have the ability to support a broad variety of loads and withstand large spans. Spatial structures are characterised by their superior stability and strength compared to two-dimensional structures. They are specifically built to efficiently bear loads in several directions. Their exceptional capacity to endure wide areas without requiring internal supports makes them ideal for such purposes. Space structures often exhibit superior material efficiency and cost-effectiveness compared to traditional structural systems due to their inventive geometric configurations. The overall mass and material expenses decrease while maintaining the structure's reliability due to this enhanced efficiency. Space structures have versatility in design, thus they could be designed using many forms, including domes, trusses, and space frames (Schodek and Bechthold, 2014).

The construction industry plays a pivotal role in global initiatives aimed at mitigating environmental impacts (Reksowardojo and Senatore, 2023). Additionally, the lightweight properties of spatial structures have great potential to reduce material consumption and costs compared to conventional structures. Moreover, the reusability of stocked spatial structures' components makes them more sustainable and significantly supports the environmental impact of structural built-up (Brütting *et al.*, 2019). Spatial structures have been used in Kurdistan and Iraq for only a few decades. Initially, they were limited to truss roofs and small canopies, but their application has expanded to include terminals, wide-span roofs of exhibition galleries, and sports arenas such as Al-Minaa Stadium in Basra, see Fig. 1-2 (Kaliciak, 2022). For these reasons, there

is a need to attract the interest of Kurdish researchers to become familiar with spatial structures and understand the basics of this field.



Fig. 1-2 Al-Minaa Olympic stadium in Basra, Iraq (Kaliciak, 2022)

Currently, enormous space structures with cable members as the primary element of assembly are in high demand. Cables offer unique perspectives for forming enticing spatial grid structures that are highly flexible. Notably, cable nets exhibit high structural flexibility and a nonlinear response to loading. However, the absence of flexural rigidity, resulting in large displacements, presents the most challenging aspect of cable structure analysis (Kwan, 1998).

Sources of nonlinearity in structures can be classified into three categories: material nonlinearity, boundary nonlinearity, and geometric nonlinearity. Consequently, geometric nonlinearity must be considered in the analysis of cable structures due to their highly flexibility and nonlinear response for loading. Geometric nonlinearities arise when structural deformation results in



noticeable nodal displacements, making the cable's stress sufficient to produce a state of equilibrium in deformed states (Levy and Spillers, 2003).

The efficiency of cable structures depends on prestressing to attain a desirable appearance and function with the required stability. The inserted prestressing effort enhances structural rigidity, reduces structural distortion, and redistributes internal stress, resulting in a more cost-effective structure (Cinquini and Contro, 1985; Dong and Yuan, 2007; Abdulkarim and Saeed, 2023). As Kwan (1998) states, the behaviour (initial stiffness) of cable nets depends more on prestressing than on their axial stiffness. In tensile structures, the main load-bearing components do not bend or compress but instead transmit loads through direct tensile stress, making it one of the most unique and challenging problems in structural engineering.

In multiple domains of structural construction, the tolerable levels of certain structural forms and internal stresses are not only pertinent but also affect the service life of the structure (Saeed, 2014). Occasionally, deformability in spatial structures causes overstress in some cable members in tension or struts in compression. In such situations, it is necessary to adjust the stress in these cables by redistributing the internal forces among the required members through the adjustment of the length of some active members via a set of actuators. However, form alteration in these structures is unavoidable due to various reasons, such as fatigue, manufacturing imperfections, temperature changes, unpredicted loading, and looseness in joints. When shape distortion becomes intolerable, the nodal positions must be restored to their original

configuration (Saeed, 2014; Saeed and Kwan, 2016b; Manguri *et al.*, 2017; Saeed *et al.*, 2019; Abdulkarim *et al.*, 2020).

Varieties of structural types require accuracy in their geometry, and effective control of the shape, particularly in large flexible structures, is currently a significant issue of interest (Kawaguchi *et al.*, 1996; You, 1997; Xu and Luo, 2009; Yuan and Dong, 2002; Wang *et al.*, 2013; Saeed and Kwan, 2016b; Saeed and Kwan, 2016a; Saeed and Kwan, 2018; Saeed, 2019; Saeed *et al.*, 2019; Abdulkarim *et al.*, 2020). For example, bridges frequently fail due to large displacements, which is unacceptable. Therefore, there are two options: either use member length actuation to adjust the deformation to a prescribed profile, which develops stress in these members to restore the shape to a given profile, or leave it to suffer a significant displacement that ultimately leads to failure and collapse.

## **1.2 PROBLEM STATEMENT**

Recent advancements in spatial structures have led to innovative, visually iconic landmarks. However, achieving effective prestressing while preserving unaltered configurations is challenging and requires detailed structural engineering. These lightweight, long-span structures, with significant architectural value, must maintain geometric integrity within elastic limits yet exhibit marked geometric nonlinearity under loading.

Previous research efforts have introduced various techniques for computing prestress and loading effect on geometrical configuration, preserving nodal displacement, internal stress, and combined displacement-internal force control (You, 1997; Yuan and Dong, 2002; Xu and Luo, 2009; Wang *et al.*, 2013;

Saeed and Kwan, 2016a; Saeed and Kwan, 2016b; Yuan *et al.*, 2016; Li *et al.*, 2017; Manguri *et al.*, 2017; Saeed and Kwan, 2018; Saeed, 2019; Saeed *et al.*, 2019; Abdulkarim *et al.*, 2020; Saeed *et al.*, 2021; Saeed *et al.*, 2022; Saeed, 2022). These approaches, however, have primarily relied on linear control techniques applicable under limited loading conditions or iterative procedures to meet nonlinear preservation goals. Consequently, these methods have been unable to address preservation requirements effectively when large deformations necessitate direct nonlinear geometric solutions.

This dissertation aims to address a critical gap by developing a robust numerical method for prestressing, analysing, and preserving spatial structures, integrating geometric nonlinearity directly into a system of nonlinear algebraic equations. It advances analytical methods and prestressing strategies that retain geometric integrity under substantial deformation. Furthermore, this study seeks to experimentally integrate and validate all phases of nonlinear prestressing, analysis, and preservation by testing them comprehensively on a complex physical model; this level of combined analysis has not been fully achieved in previous studies.

### **1.3 AIMS AND OBJECTIVES**

The current dissertation has four main aims with the following objectives:

1. To develop a method for prestressing spatial structures that accounts for the nonlinear geometric response in both flexible and rigid pin-jointed assemblies.
  - 1.1. To derive a new prestressing technique for nonlinear geometric pin-jointed spatial systems.
  - 1.2. To compute the internal member forces resulting from members' lack of fit.

2. To formulate a nonlinear geometric analysis approach as a function of nodal displacement via deriving a comparable analysis technique for nonlinear geometric pin-jointed spatial systems.
3. To provide a direct nonlinear preservation technique for controlling nodal deformations, internal forces, and simultaneous displacement and stress.
  - 3.1. To derive a technique for positioning nodal displacements, maintaining analytical axial force below the maximum limit, and preventing slack.
  - 3.2. To identify the active members (locations of actuators) for performing prestress and shape control.
  - 3.3. To identify optimal locations for turnbuckles and determine how to achieve the target with minimal actuation.
  - 3.4. To establish an efficient number of actuators with minimal adjustment effort.
4. To apply the proposed techniques experimentally to a complex physical model for validation purposes.

#### **1.4 THE OUTLINE OF THE DISSERTATION**

The outline of this dissertation (see Fig. 1-3) is divided into six chapters as follows:

**Chapter One:** starts with an introduction and overview of the concept of spatial structure, its application, and its behaviour. The aims and objectives follow the problem statement.

**Chapter Two:** provides a detailed review of the existing prestressing, analysis, and preservation techniques for spatial structures in general and cable net structures in particular. The most crucial findings regarding the number of actuators, their locations, and types are also stated in this chapter.

**Chapter Three:** discusses the theoretical derivation and formulation of the prestressing, analysis, and preservation techniques, as well as their validation through numerical examples. The basics of the force method are utilised for the fundamental formulations, and geometric nonlinearity is introduced through member alteration using different mathematical methods for various targets.

**Chapter Four:** includes the experimental procedure for the structural model and the experimental techniques for computing nodal displacements and member forces for each of the prestressing phase, analysis phase under various loading conditions, and preserving phase of the geometry and internal stress.

**Chapter Five:** provides a presentation and discussion of both the theoretical and experimental results. This chapter also involves the comparison and validation of the techniques.

**Chapter Six:** is devoted to the conclusions of the study and the recommendations for future work.

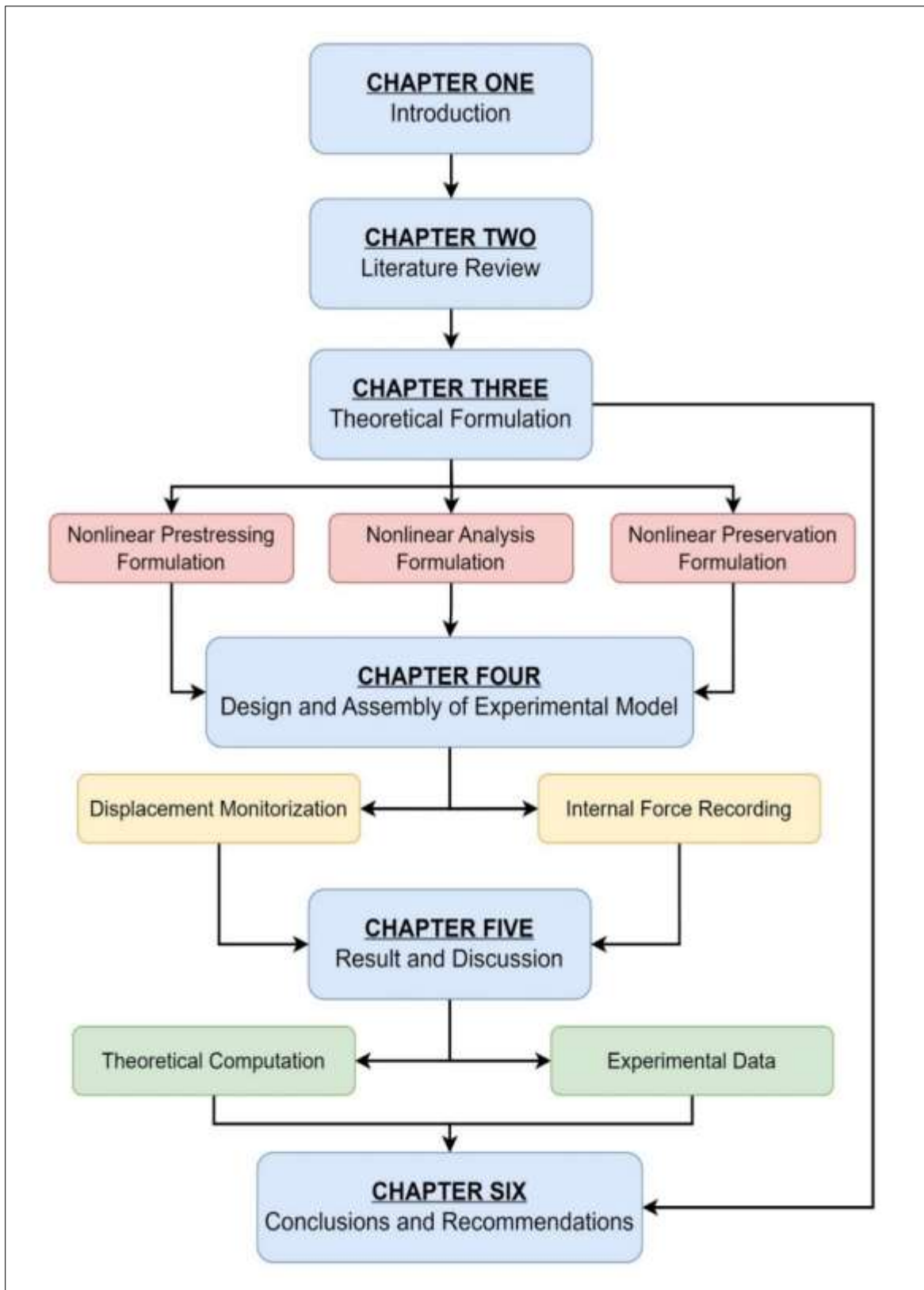


Fig. 1-3 Arrangement of dissertation

## CHAPTER TWO

### LITERATURE REVIEW

#### 2.1 INTRODUCTION

This chapter presents a literature review of prior studies pertinent to the dissertation's focus. The review begins with an examination of prestressing techniques, followed by an analysis of spatial structures, addressing both linear and geometrically nonlinear responses. Preservation techniques are then discussed, focusing on methods categorised as displacement control, member force control, or a combined approach for displacement and force control. Finally, an overview of turnbuckling members is provided.

In this dissertation, the force method is selected due to its distinct analytical advantages, which are especially suited to the specialised requirements of this study. Unlike the displacement method, where force and displacement systems are interdependent, the force method enables separate and accessible analysis of parameters influencing internal forces and external displacements, allowing for clearer management of potentially conflicting demands (Saeed, 2014). The equilibrium matrix subspaces within the force method also provide essential insights into self-stress states and structural mechanisms. The straightforward application of prestress further highlights the suitability of the force method for this research framework (Kwan, 1991; McGuire, 2000; Kassimali, 2012).

## 2.2 PRESTRESSING TENSILE STRUCTURES

Space structures are characterised by being lightweight, cost-effective, and rapid assembly. Due to their structural efficiency, spatial systems are commonly employed in applications such as wide-span roofing and deployable mesh reflectors (Kawaguchi *et al.*, 1996). Tensile members in structures have been around for decades, ranging from canopy elements in Roman times to suspension bridges for passing over rivers and deep valleys. Currently, tensile members are utilised in cable cars, cable roofs, masts, and other tall structures. They are also used in the fabrication of cable-stayed bridges, which are becoming increasingly popular due to their aesthetic appeal. Tensile assemblies are also used in temporary structures such as tents and construction equipment (Gossen, 2004; Sernizon Costa *et al.*, 2022).

The capability to allow internal stress without external loads is fundamental to most spatial structures, particularly tensile structures. Prestress is required to attain these structures' desired form, stability, and function. For structures with rigid geometry, the presence of prestress, imposed by the member's fit deficiency, can significantly enhance the design, particularly when buckling is the primary failure mode. Conversely, for flexible structures, prestress is essential to achieve the required geometrical configuration (Hanaor, 1988). Cinquini and Contro (1985) stated that the most significant feature in designing a cable-net system is the level of pretension due to its direct influence on load-carrying capacity, cost, and geometrical configuration. Also, the nonlinearity becomes more noticeable with declining pretension (Yuan and Dong, 2002). Hence, the indication of the preliminary prestress has an essential effect on the design steps.

Numerous studies have been conducted to establish the optimal prestressing levels for pin-jointed spatial structures. Additionally, various form-finding



techniques have been proposed to address aesthetic, industrial, and mechanical requirements, including iterative methods, dynamic relaxation, and force density approaches. However, these methods set limits on member stresses and nodal displacements but typically do not ensure the prestressing degree (Cinquini and Contro, 1985; Zhou *et al.*, 2017; Chen *et al.*, 2020).

Pellegrino and Calladine (1986) proposed an algorithm to provide complete details about the modes of inextensional deformation and all the states of initial stress. Pellegrino (1990) made another matrix algorithm that deals with both extensional and inextensional modes separately. The author also grouped structural assemblies into separate states of self-stress and mechanism modes. In a study by Kwan and Pellegrino (1993), an algorithm based on the linear force method was proposed to achieve a uniform degree of prestress. Choosing the correct location for prestressing actuators, the required amount of extension for the actuators, and improving the incorrect prestress state by adjusting the actuators were the basics of their working process. Additionally, based on the force method, linear and partially nonlinear internal force control has been done (Saeed *et al.*, 2021; Saeed and Kwan, 2016a; Saeed, 2014), which is part of achieving the required amount of prestressing.

Nevertheless, the simulated annealing algorithm was developed by Xu and Luo (2010); counting for geometrical stability, the optimisation model was used to find the force of tensegrity structure. Later, Li *et al.* (2013) used two different form-finding techniques on a deployable mesh reflector antenna to indicate the cable prestress to satisfy the required exterior accuracy. Guo and Zhou (2016) came up with a simulation-based pretension algorithm for a negative Gaussian-curvature cable dome. However, it depends on an iterative process between the desired internal stress for the indicated tensile force step and the prestressing degree of active tensile members. In a study by Ma *et al.* (2019), an

optimisation using a Pareto solution was made to improve the coefficient vector of self-equilibrium of prestressing design for cable strut structure. Furthermore, Zhang *et al.* (2021) presented a method for measuring the initial self-stress in a cable-strut system to achieve a specified shape and topology.

The cited studies indicate that prior research relied on specifically developed algorithms, iterative methods, and linear approaches to determine the prestressing levels of statically and kinematically indeterminate space systems. Despite the imprecision of modelling and mechanical imperfection, it was revealed that the amount of member alteration produced might produce an unbalanced state of prestress (Kwan and Pellegrino, 1993; Fraddosio *et al.*, 2021). Another comparative study concerning the member alteration to the sensitivity matrix was carried out by Xue *et al.* (2021). They indicated that the primary discrepancy between the sensitivity matrices arose from differences in geometric stiffness. Accordingly, a principal objective of this dissertation is to develop a nonlinear method for directly determining the required prestressing levels or member adjustments to achieve the desired degree of prestress in both rigid and flexible pin-jointed spatial structures. Furthermore, the proposed technique is formulated by expressing nonlinear member alterations in terms of external nodal distortions, thereby reducing the tolerance for unbalanced prestress and moving it closer to a self-equilibrated state.

### **2.3 ANALYSIS TECHNIQUES OF SPATIAL STRUCTURES**

The fundamental equations in the force method are equilibrium, compatibility, and flexibility relations. Improving the linear force method has been of interest for many researchers. For instance, Calladine (1978), based on the principle of virtual work, confirmed that the transpose of the equilibrium matrix is equal to the compatibility matrix. The force method is mostly applied in analysing

prestressed spatial structures with infinitesimal mechanisms, and an experimental investigation has been completed by Pellegrino (1990) to validate this approach. Later, Pellegrino (1993) came up with the singular value decomposition (SVD) of the equilibrium matrix to show the static and kinematic nature of the structural assemblies in relation to their physical properties when coming up with the stress and displacement formulation.

This technique has been further enhanced as a non-linear analysis approach for geometrically non-linear structures. Kwan (1998) reused the main classical equations of the force method and expressed the member actuation for prestressed cable structure in terms of displacement using the Taylor series. In addition, Luo and Lu (2006) extended the linear force method to analyse non-linear geometric cable structures. They proposed an algorithm using SVD for equilibrium matrix in every step of the iteration process. Xu and Luo (2009) implemented the non-linear force method to propose an iteration procedure for restoring the displaced joints and controlling the prestressed level of cable net systems. Similarly, Yuan *et al.* (2016) contributed the non-linear force method to control stress and shape of the cable-strut structure but utilised Moore–Penrose pseudoinverse to compute minimal necessary actuation. Moreover, Manguri and Saeed (2020), and Saeed *et al.* (2022) proposed an analysis technique which is an approximate linear force method. It is based on updating joint coordinates of the structural geometry in every iteration for the discretized applied load.

Regardless of the different solving algorithms for the force method in the previous studies, some factors give inaccurate findings, such as using the constant states of the self-stress matrix or the constant equilibrium matrix in the derivation of the analysis formulation. However, in some studies, the part of geometric nonlinearity was introduced in compatibility and equilibrium

matrices in the scheme of an iteration (Deng *et al.*, 2016; Xue *et al.*, 2021). Therefore, a direct equation for representing both compatibility and equilibrium in the completely deformed configuration as a system of algebraic nonlinear equations is required and used in deriving the proposed equation.

## 2.4 PRESERVATION TECHNIQUES OF SPATIAL STRUCTURES

A simple definition of an adjustment is a procedure that is performed to fine-tune the existing performance of a system or achieve a desired result. For instance, through shape restoration, the deformation of a structure caused by external forces can be minimised or eliminated (Ziegler, 2005; Saeed, 2014). It is possible for the structure to undergo observable deformability due to a number of factors, including but not limited to connection looseness, excessive temperatures, a large span, fatigue, and other unidentified factors. Tolerances of structural geometry and internal forces, under varying operating circumstances, are not only significant but also influence the boundary status of a structure in numerous structural engineering domains (You, 1997; Yuan *et al.*, 2016; Saeed and Kwan, 2016b; Saeed *et al.*, 2019; Abdulkarim *et al.*, 2020; Saeed, 2022). The preservation techniques can be categorised into three restoration types: restoring the disturbed nodal positions, restoring the inner member forces, or simultaneously restoring nodal positions and internal forces.

More than fifty years ago, the concept of structural control was introduced to enhance the protection of structures under extreme conditions (Korkmaz, 2011). Korkmaz (2011) categorised structural control into three subdomains: active control, adaptive control, and intelligent control (see Fig. 2-1). Active structural control employs sensors and actuators to adjust deformability and internal stress, thereby modifying the structural response. In adaptive structural

control, the adjustment process enhances the structural response irrespective of the previous loading conditions. In contrast, intelligent structural control involves a process that preserves and improves structural performance by recalling behavioural changes and actions, adapting to current objectives, and using past events to enhance future responses. Since its beginning, the implementation of structural control has been used in both civil and space structures with the aim of mitigating the adverse consequences of natural catastrophes such as earthquakes and winds, as well as addressing the detrimental effects of vibrations, geometric disturbances, and excessive internal stress.

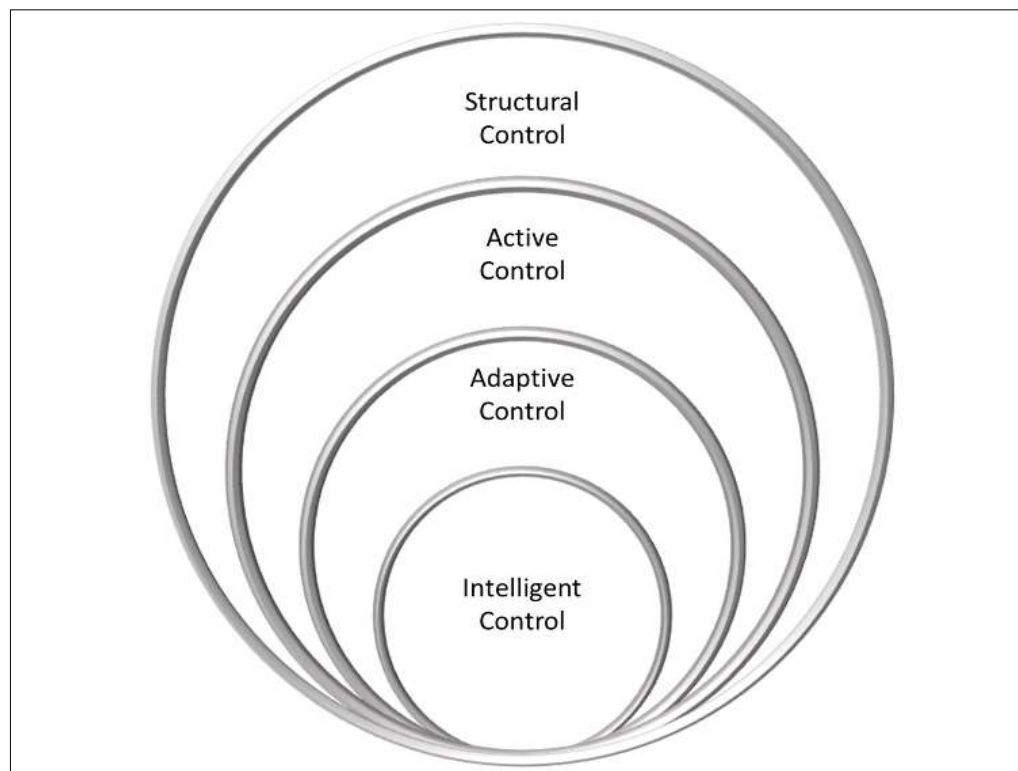


Fig. 2-1 Structural control and controlling subdomains (Korkmaz, 2011).

### 2.4.1 Geometrical Preservation

The spatial structures face geometrical deformation after being affected by external loading conditions, changes in temperature, or even imperfections in construction. To eliminate or reduce this deformation, many studies have been carried out. Because of the nonlinear geometrical property, the linear techniques can work well within a small deformation, but they become inactive or insufficient when a large disturbance is present (Xu and Luo, 2009; Yuan *et al.*, 2016; Xue *et al.*, 2021). Generally, the geometrical form of spatial structures is defined by their nodal locations. Once the components are assembled, the nodal locations must be adjusted to achieve the desired geometry. For example, the geometry of a double-layer dome was preserved, as demonstrated by Abdulkarim *et al.* (2020) in Fig. 2-2.

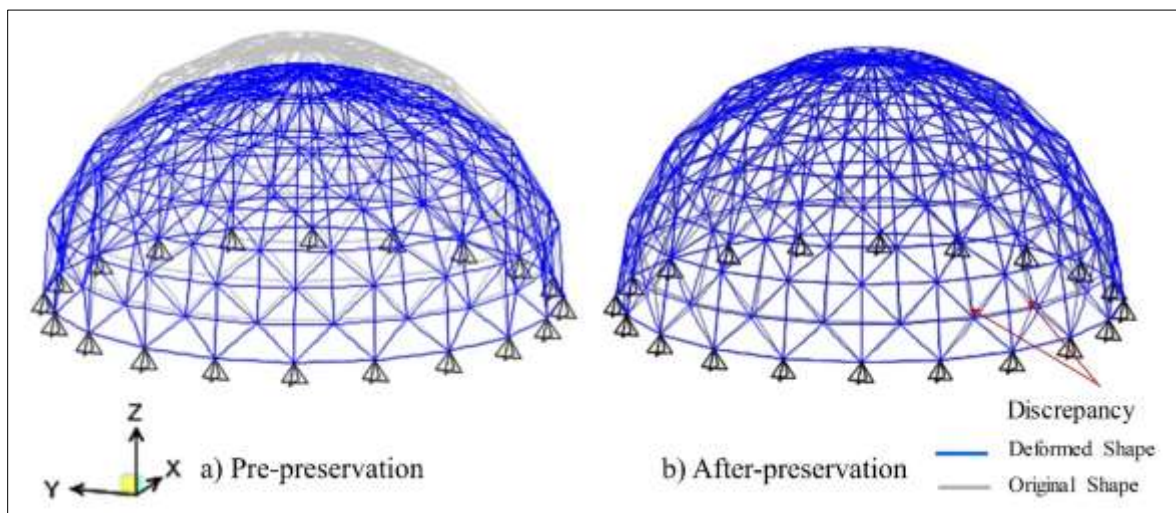


Fig. 2-2 Geometrical preservation of double layer dome Abdulkarim *et al.* (2020)

Another straightforward method involves equipping the structure with actuatable members. By adjusting the lengths of these members, the nodal

locations can be modified (You, 1997). Burdisso and Haftka (1990) were the former researchers that examined static geometrical controlling techniques, specifically with truss systems where degree of prestress is not a concern. They dealt with the manufacturing member length errors in the radiometer antenna's spatial structure. Then, through the decomposition of eigenstrain, Nyashin *et al.* (2005) improved a theorem for controlling the shape distortion. The concept claims that the load-dependent distortion pattern can be visualised by solving boundary value problems in linearized elasticity with specified nonzero displacements at the outer surface. When this type of deformation is imposed using eigenstrain, the resultant displacements are as specified, but no stress is introduced.

While various researchers have addressed geometrical restoration with regard to prestress levels, particularly for flexible spatial structures, this study focuses specifically on this issue. The first inquiry into the geometrical control of prestressed truss structures was undertaken by Kawaguchi *et al.* (1994), Pellegrino (1995), and Kawaguchi *et al.* (1996). In these studies, the proposed methods were to simultaneously control the level of prestress of selected components and the displacements of particular joints. The proposed methodology by You (1997) allows for displacement restoration of prestressed pin-jointed systems by adjusting the length of selected structural components while ensuring that the prestress value remains over a preset lower limit. Shea *et al.* (2002) conducted an investigation into the potential for adjusting the elongation of individual components in order to modify a tensegrity structure to achieve a desired configuration. This was done by combining the simulated annealing method, the dynamic relaxation technique, and the computation of nodal deflection data into a single strategy. Moreover, an optimised problem was solved by using simulated annealing with an improved technique based on

the linear-force method. It was applied to accomplish non-linear displacement restoration of prestressing cable systems (Xu and Luo, 2009).

Over the course of recent decades, several theoretical, computational, and experimental investigations have been carried out to explore the use of piezoelectricity in the monitoring and controlling of various adaptive structures. Sunar and Rao (1999) surveyed numerous studies that used piezoelectric actuators for the purpose of displacement control. Piezoelectric actuators use the reverse piezoelectric impact to transform electric signals into strain or displacement in their supporting systems.

It is important to note that the actual desired displacements are normally known after the nodal positions have been identified and compared to the actual configuration of the assembly (You, 1997; Saeed and Kwan, 2016b).

#### **2.4.2 Member Force Preservation**

The member force of some types of spatial structures may need more concern than their geometry, as in the case of preventing slack in cable nets, failing due to buckling in slender struts, or improving adaptability while facing new loading conditions during serviceability.

Kwan and Pellegrino (1993) performed prestressing with a minimum number of actuators regarding slack prevention in a deployable structure. First, the exact number of actuators was chosen to get the closest estimate of the member forces using singular value decomposition with the least squares solution technique. Later, they utilised the typical linear-programme to apply the constrained condition for optimisation purposes, so the selection of the actuators gave a more automatic procedure with an optimal solution for achieving the requested member forces. Another study was carried out for



controlling bar forces after affection by external forces by Saeed and Kwan (2016b). Even though there was an internal force due to the applied loads, the corrective amount of member actuation was calculated to give the desired vector of member forces. Moreover, a 4.9-metre Levy-shaped cable dome was used in numerical and experimental work to deal with the controlling and optimising of its member force. The central compressive members were predetermined as actuators to enhance the adaptability of the cable dome when it faces various loading conditions (Zhang *et al.*, 2023).

### **2.4.3 Simultaneous Geometrical and Member Force Preservation**

In a practical situation, it is quite probable that circumstances necessitating the regulation of geometry preservation will also impose certain demands on the internal member forces. For instance, restoring the deflected deck of the cable-stayed bridge to a horizontal level requires keeping the struts below the critical buckling force and preventing the cables from slacking.

The study of geometrical and member force control together has not been widely done. Kawaguchi *et al.* (1996) developed an analytical method for restoring deformation and internal forces in truss structures using the linear force method. Their approach involved numerical and experimental restoration of a tension-stabilised truss model by altering member lengths without applying external loads. While the study successfully adjusted the prestressing degree, it did not fully address the restoration of deformability. Similarly, You (1997) used the linear force method and proposed the control of prestressed cable nets and trusses deformation in two stages. At first, the researcher picked a group of adjustable members while keeping the prestressing degree above the initial value. Then he achieved the required amount of actuation that was determined previously. The work was applied numerically to the two-dimensional cable

net structure as shown in Fig. 2-3, but an Al-alloy truss with the same scheme as shown in Fig. 2-3 was used for the ease of experimental data collection. It should be stated that the cited technique is applicable only for small deformations and within the elastic limit. In addition, this technique would become complicated when it was applied to a more complicated system or sought for a more optimal solution.

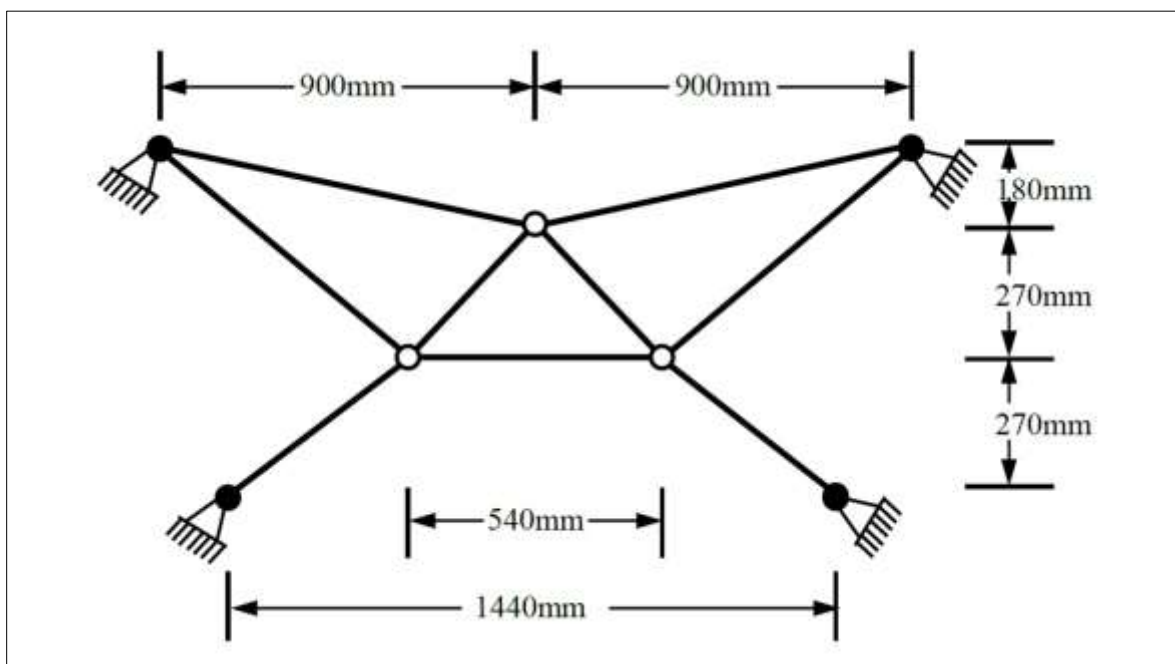


Fig. 2-3 A two-dimensional cable net structure (You, 1997).

The cable net structure in Fig. 2-3 was also examined numerically by Xu and Luo (2008) utilising multi-objective optimisation for the same target of shape restoration while keeping the same degree of prestress. However, the total computed amount of actuation was reduced by 33%, but the number of used actuators was higher. Once more, Xu and Luo (2009) used a simulated annealing algorithm in association with the developed nonlinear force method through an iteration technique for the same targets as the cited studies. The

proposed approach was tested on the cable net in Fig. 2-3, and achieved a better target when larger deformations were experienced.

Likewise, the linear force method was being solved by deploying the least squares solution (Saeed, 2014; Saeed, 2019), matrix condensation (Saeed and Kwan, 2016a), quadratic programming (Saeed, 2022) for simultaneous preservation of displacement and member force in pantographs and pin-jointed systems. Moreover, the levy cable dome has been restored numerically and experimentally by Zhang *et al.* (2023) through active control to attain the new adaptability of form and internal stress for a different loading condition. Zhang *et al.* (2023) adapted an intelligent algorithm solver for the numerical computation of the required actuation of the members. Nevertheless, the authors focused on theoretical computation and simulation modelling for control purposes. Besides, the experimental attempts were with the symmetric loading condition.

#### **2.4.4 Actuators**

Actuators are components that establish a functional link between the information-receiving component of a controller and a technical or nontechnical action (Janocha, 2004). Actuators are taking significant roles during the preservation process, either for geometrical restoration or stress control. The existence of a sufficient number of actuators, the location of actuators, and the necessary amount of actuation are key points to reaching the optimal solution for the preservation process (Kwan and Pellegrino, 1993; Saeed and Kwan, 2016b; Saeed *et al.*, 2019; Abdulkarim *et al.*, 2020).

According to a study by Haftka (1984), the optimum number and placement of actuators have been calculated, and it has been stated that the improvement of

the controlling procedure has been attained. The operations begin by establishing an initial state whereby actuators are positioned in every conceivable location. The process of identifying and eliminating the least efficient actuator is iterated until the number of actuators reaches the total number of accessible actuators. Haftka and Adelman (1985) used the integer programming technique to find the optimal actuator location among a large set of available members. Besides, the concept of the ideal actuator has been proposed to compute the required number of actuators for the preservation process (Haftka, 1991).

Many statistical techniques and various algorithms have been improved and applied for optimal actuation computation. The continuum approximation (Burdisso and Haftka, 1989) and adjoint technique and modal expansion approach (Burdisso and Haftka, 1990) were applied to optimise the actuator placement. Onoda and Hanawa (1992) were the first to introduce the simulated annealing algorithm with a genetic algorithm to search for the optimal placement of the actuators for mitigating truss distortion. Similarly, a hybrid optimisation approach was set to compute the effect of the quantity and location of actuators on the minimum weight of actively controlled assemblies (Dhingra and Lee, 1994). Kwan and Pellegrino (1993) applied a standard linear-programme to prestress a deployable structure. The number of states of self-stress was indicated as an optimal criterion for a sufficient number of actuators to perform prestress.

Saeed and Kwan (2016b) stated that the greater coefficient in the self-stress matrix shows the more active member for positioning the actuators during the preservation process. These locations for actuator placement can approach the desired target of geometry and stress control with minimal actuation. Amir Sohrabi *et al.* (2017) used electroactive actuators that have the ability to change

length and rotation employing the finite element approach for the computation of the required actuation. The authors applied the technique to the actively controlled 3D truss, which could enhance its performance and prevent disastrous system failures. Likewise, research has confirmed that the effectiveness of the preservation process is significantly influenced by the number and proximity of actuators to the controlling geometry (Saeed *et al.*, 2019; Abdulkarim *et al.*, 2020) and stress (Saeed and Kwan, 2018; Saeed, 2019; Saeed *et al.*, 2021; Mahmood *et al.*, 2022; Manguri *et al.*, 2022).

Various actuators are used in structural engineering to alter the form and stress levels of a structure. Actuators are used in a variety of applications, including adaptive assemblies, form control, stress reduction, prestressing, and the evaluation of structural health. The following sub-sections describe some types of actuators employed in geometrical and stress preservation.

#### **2.4.4.1 Turnbuckles**

The turnbuckles (see Fig. 2-4) are the main components of the actuators, and each has two threaded eye bolts or hooks that are joined by a central barrel with right-hand and left-hand threads, respectively. The tension in a cable or rod fastened to the turnbuckle's eye bolts or hooks may be increased or decreased by adjusting the turnbuckle's effective length, which is done by turning the barrel. Similarly, it can be used to preserve the geometry and internal stress of spatial structures (Saeed, 2014; Lee *et al.*, 2021).



Fig. 2-4 A representative example of a turnbuckle

#### 2.4.4.2 Piezoelectric actuators

Piezoelectric actuators are used to create modest deformations in structures, with the primary objectives being shape control, stress control, and health monitoring. The deformations exhibit rapidity, precision, and reversibility (Irschik, 2002; Janocha, 2004; Aabid *et al.*, 2021). The typical working principle of piezoelectric actuators is shown in Fig. 2-5.

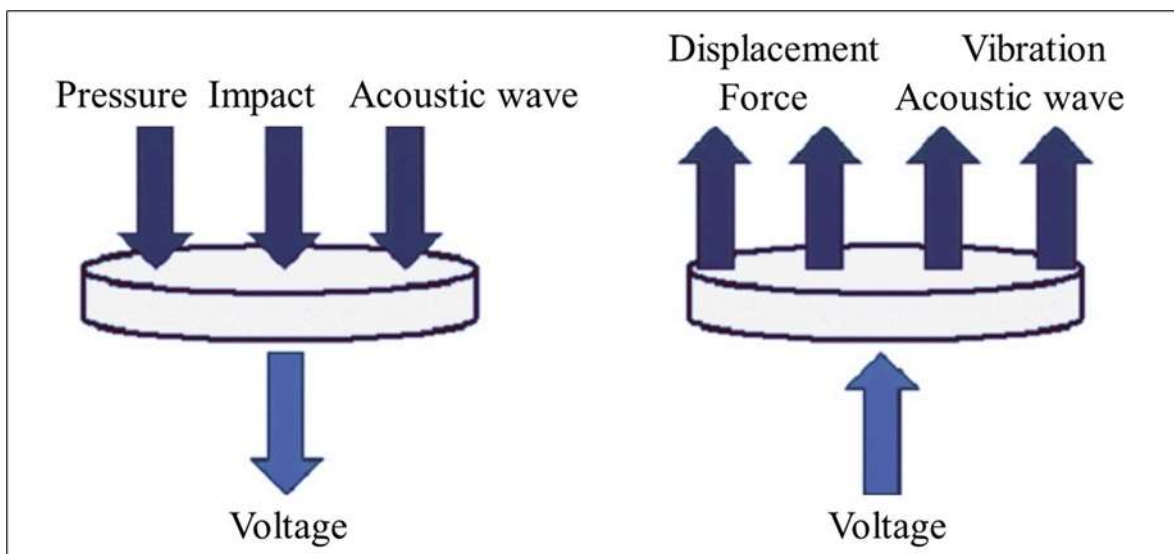


Fig. 2-5 Role of piezoelectric ceramic in generating electrical and mechanical effect (Yoichi, 2006)

### 2.4.4.3 Electromechanical actuators

A mechanical actuator that is powered electrically is called an electromechanical actuator. It is an actuator (see Fig. 2-6) that utilises both electrical and mechanical mechanisms to produce controlled motion with high precision. Where accurate linear or rotary movement is needed, electromechanical actuators are often utilised. They have a stellar reputation for dependability, accuracy, and adaptability (Janocha, 2004; Zhang *et al.*, 2023).

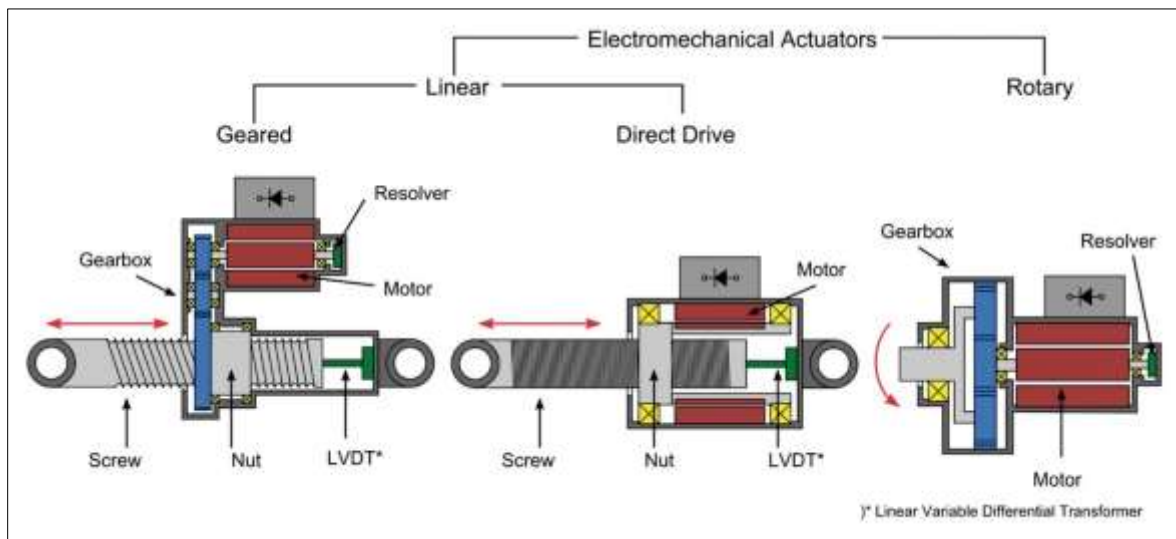


Fig. 2-6 Classification of different electromechanical actuators (Qiao *et al.*, 2018)

### 2.4.4.4 Shape memory alloy actuators

Shape-memory alloys are materials that may transform in response to variations in temperature. In the case of shape memory alloy smart materials are used to regulate and adjust the geometrical properties resulting from the semi-permanent deformation (Janocha, 2004; Bodaghi *et al.*, 2014), and noticeable

strain to produce required force. Such example is presented in Fig. 2-7 . It is used for making deployable assembly with shape stretching.

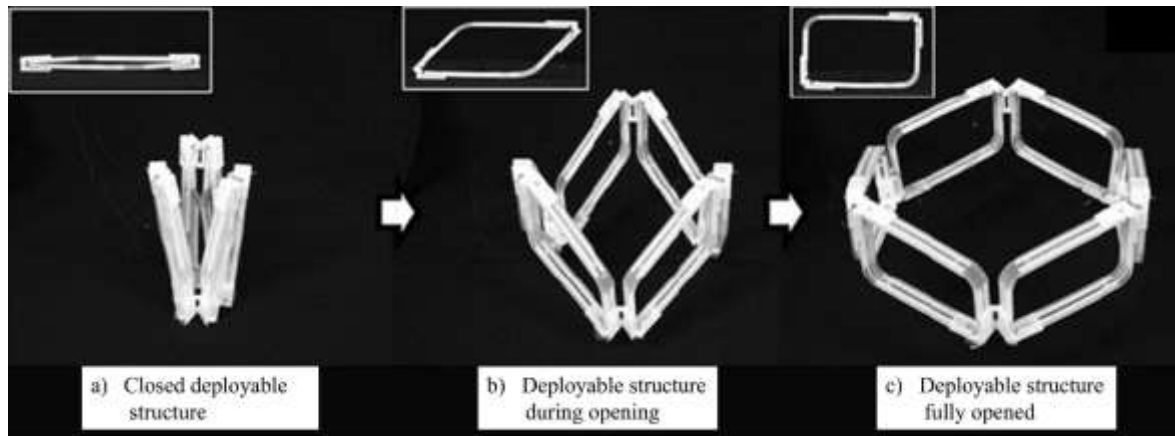


Fig. 2-7 Deployable structure opened by shape memory alloy

The process of selecting actuators in the field of structural engineering is influenced by a combination of factors, including the specific requirements of the application and the desired outcomes. Actuators may be placed to maintain the structural integrity, mitigate stress imbalances, and improve the performance and safety of a given system. Fig. 2-8 shows the normalised actuator attributes between power-to-weight ratio and their efficiency for different types of actuators made by Zupan *et al.* (2002). Fig. 2-8 was generated with data taken from Zupan's comprehensive actuator database. Certain families of actuators have similarities; however, overall, they demonstrate notable distinctions from one another. The shape-memory actuator exhibits essential inefficiency due to its dependence on heating and cooling processes. Nevertheless, the advantageous characteristic of these materials lies in their high energy density, which refers to their ability to do work per unit volume. This attribute renders them highly sought-after for use in microactuators. Piezoelectric actuators, despite their limited displacement capabilities, have the



ability to generate substantial power outputs. Due to their capacity for high-frequency cycling, they have the capability to generate significant quantities of power.

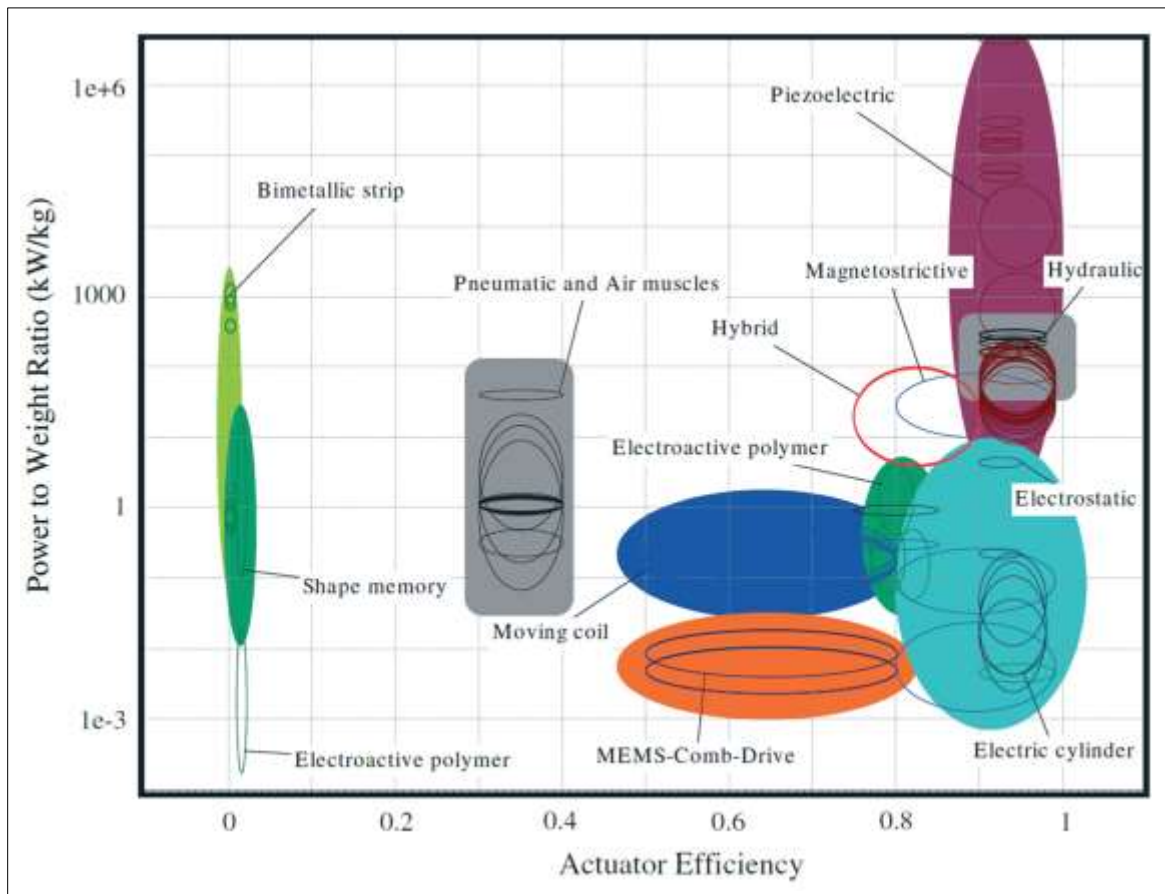


Fig. 2-8 Normalized actuator attributes: power-to-weight ratio versus efficiency (Zupan *et al.*, 2002)

## 2.5 SUMMARY

This chapter summarises the key findings of prior research relevant to the subject of this dissertation. It begins with a discussion of prestressing strategies, followed by an examination of various approaches to spatial structure analysis, including both linear and geometric nonlinear responses. Additionally, several

preservation methods are explored, including displacement control, member force control, and the combined control of displacement and force. The chapter concludes with an analysis of actuator functions, optimal actuator placement, actuator quantity and actuation methods, as well as actuator types in relation to shape and force control, with a focus on their efficiency.

The gaps in these approaches are as follows:

1. Previous methods failed to account for equilibrium in the post-deformation state, with some only ensuring compatibility in the deformed configuration.
2. Previous methods lacked the capability to directly compute nonlinear prestressing, analysis, and preservation for pin-jointed spatial structures as a system of nonlinear algebraic equations.
3. No comprehensive integration or experimental validation has been conducted for all phases of nonlinear prestressing, analysis, and preservation in a complex physical model, combining both theoretical and experimental approaches.

## **CHAPTER THREE**

### **THEORETICAL FORMULATION**

#### **3.1 INTRODUCTION**

This chapter focuses on the formulation of prestressing, statical analysis, and preservation techniques, developed based on the fundamentals of the force method. The derived equations are presented as sets of nonlinear algebraic expressions that account for the geometric nonlinearity of spatial structures, considering both elastic behaviour and small and large displacements. To further clarify the application of the prestressing technique, an illustrative numerical example is provided. The approaches are applied and validated through both simple and complex, as well as flexible and rigid, pin-jointed space structures. These techniques will be utilised in Chapter 4 for the computation of prestress levels, structural analysis, and the preservation process.

#### **3.2 FORMULATION OF THE PRESTRESSING TECHNIQUE**

One of the crucial aspects of the design of structural space systems is the degree of prestressing since it is involved in load transfer, and deformability. The prestress state can be reached via the required member alteration. This section presents a nonlinear numerical approach based on the force method for prestressing the spatial nonlinear structures to the desired level through computing nonlinear actuation as a function of external nodal displacements.

The present technique is based on the flexibility method. The three dimensional of statically indeterminate structural assemblies with  $nB$  bars,  $nJ$  joints and  $c$  support constraints are assumed to have the amount of prestress of  $t_{nB \times 1}$  without excitation by an external load  $P_{(3nJ-c) \times 1}$ . Hence, the equilibrium equation and element force of the indeterminate structure with  $s$  numbers of independent states of self-stress in its initial state (Kwan and Pellegrino, 1993; Zhou *et al.*, 2017; Fraddosio *et al.*, 2021; Saeed and Kwan, 2016b; Luo and Lu, 2006) can be expressed as:

$$A(\mathbf{d})\mathbf{t} = 0 \quad 3.1$$

$$\mathbf{t} = S\mathbf{a} \quad 3.2$$

Where  $A(\mathbf{d})_{(3nJ-c) \times nB}$  is the equilibrium matrix,  $S$  is the matrix of the independent state of self-stress, and  $\mathbf{a}$  defines the arbitrary combination coefficient vector of  $s$  independent self-stress states.

Similarly, considering geometric conditions, the relation between the strain inside a structural assembly as a vector of initial member elongations or shortenings  $e_o(\mathbf{d})$  to their nodal displacements  $\mathbf{d}$  can be written in the compatibility equation as:

$$B(\mathbf{d})\mathbf{d} = e_o(\mathbf{d}) \quad 3.3$$

$B(\mathbf{d})_{nB \times (3nJ-c)}$  is the compatibility matrix, which is proved via the principle of virtual work to be equal to  $A(\mathbf{d})^T$  (Calladine, 1978).

Taking into account the material of the structural assembly with elasticity characteristics, the constitutive equation can be set as:

$$e_o(\mathbf{d}) = F\mathbf{t} \quad 3.4$$

Where  $\mathbf{F}_{nB \times nB}$  is the flexibility matrix, which has full rank and invertible property and can be attained from the element  $L_o/EA_o$ ;  $L_o$  is the initial member length, and  $E$  and  $A_o$  are the modulus of elasticity and element cross-sectional area, respectively.

### 3.2.1 Deriving Nonlinear Member Alteration

Now the vector  $e_o$  shall be derived by taking into consideration the effect of geometric nonlinearity via experiencing the large displacement of the structural assembly of space structures. For the sake of simplicity, a two-dimensional single element of the structural assembly is considered as shown in Fig. 3-1. It has an initial length of  $L_o$ , and a new length as  $L'$  after the prestressing process. The element has initial coordinates  $(x_i, y_i)$  and  $(x_j, y_j)$  from nodes  $(i, j)$ , and is then shortened by the amount  $e_o$  reach to the new position  $(i', j')$ . The abbreviation of  $(\ )_{ji} = (\ )_j - (\ )_i$  is used in deriving the set of members alteration  $e_o$ . For the single element that is shown in Fig. 3-1.

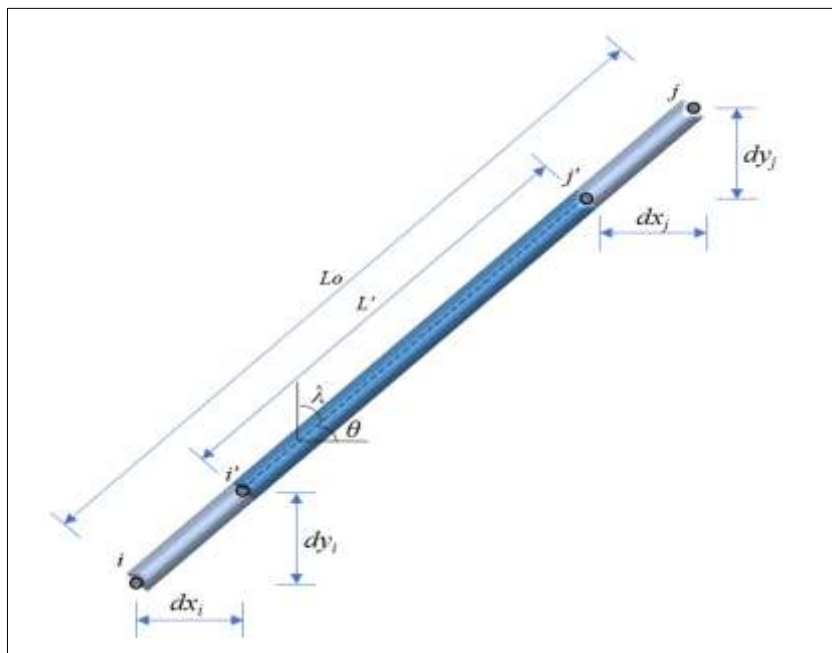


Fig. 3-1 Two-dimensional element before and after prestressing process

$$L' = L_o - e_o \quad 3.5$$

$$L' = \left\{ (x_{ji} - dx_{ji})^2 + (y_{ji} - dy_{ji})^2 \right\}^{1/2} \quad 3.6$$

Expanding Eq. 3.6 gives  $L' = \left\{ x_{ji}^2 + y_{ji}^2 - 2x_{ji}dx_{ji} + dx_{ji}^2 - 2y_{ji}dy_{ji} + dy_{ji}^2 \right\}^{1/2}$ .

Now, rearranging this expanded equation gives  $L_o^2 = x_{ji}^2 + y_{ji}^2$ , with the remaining terms, thus let the remaining terms be  $D$   $\{D = -2x_{ji}dx_{ji} + dx_{ji}^2 - 2y_{ji}dy_{ji} + dy_{ji}^2\}$ . Accordingly, the new equation will be generated as written below:

$$L' = L_o \left\{ 1 + \frac{D}{L_o^2} \right\}^{1/2} \quad 3.7$$

Now Eq. 3.7 can be expanded mathematically as a binomial function by Taylor's series (Kwan, 1998; Levy and Spillers, 2003) and as a rational function by the Pade approximation method (Baker *et al.*, 1996; Nisar *et al.*, 2021).

### 3.2.2 Mathematical Expanding of Prestressed Member Alteration

This section computes the amount of required member alteration for each element to achieve the desired degree of nonlinear prestress. Eq. 3.7 needs to be simplified in suitable mathematical ways.

### 3.2.2.1 Expansion via Taylor's series

The Eq. 3.7 can be expressed by its Taylor's series (Kwan, 1998; Levy and Spillers, 2003) as  $L' = L_o \left\{ 1 + \frac{D}{2L_o^2} - \frac{D^2}{8L_o^4} + \frac{D^3}{16L_o^6} - \dots \right\}$ , then  $L'$  can be written as:

$$L' = L_o + \frac{D}{2L_o} - \frac{D^2}{8L_o^2} \quad 3.8$$

Taking the terms only up to the second order of  $D$  is shown in Eq. 3.8, in which this accuracy is sufficient for our purpose. Now, through equalising Eq. 3.5 with Eq. 3.8,  $e_o$  can be written as:

$$e_o = -\frac{D}{2L_o} + \frac{D^2}{8L_o^2} \quad 3.9$$

By substituting the value of  $D$  expression and neglecting the small terms with higher orders, the amount of  $e_o$  can be expressed as:

$$e_o = \frac{x_{ji} dx_{ji} + y_{ji} dy_{ji}}{L_o} - \frac{dx_{ji}^2 + dy_{ji}^2}{2L_o} + \frac{x_{ji}^2 dx_{ji}^2 + y_{ji}^2 dy_{ji}^2}{2L_o^3} + \frac{x_{ji} y_{ji} dx_{ji} dy_{ji}}{L_o^3} \quad 3.10$$

Eq. 3.10 is a manifestation of the element alteration as a second-order function in terms of nodal displacements as a nonlinear compatibility condition of Eq. 3.3.

### 3.2.2.2 Expansion via Pade approximation method

Here, another mathematical method is used for arranging the relation between external nodal displacement and member alteration. In most of the instances, the Pade approximation method (Baker *et al.*, 1996; Nisar *et al.*, 2021) indicates

further improved approximant to the main function, which is Eq. 3.7 in our situation. Due to the strength of the Pade approximation, only the first order of the expanded function is considered as:

$$e_o = L_o \left\{ \frac{4 + \frac{3D}{L_o^2}}{4 + \frac{D}{L_o^2}} \right\} \quad 3.11$$

Now Eq. 3.11, which is equivalent to Eq. 3.5, then the initial member alteration can be set as:

$$e_o = -\frac{2DL_o}{4L_o^2 + D} \quad 3.12$$

Substituting  $D$  into Eq. 3.12, then it becomes:

$$e_o = \frac{2L_o (2x_{ji}dx_{ji} - dx_{ji}^2 + 2y_{ji}dy_{ji} - dy_{ji}^2)}{4L_o^2 - 2x_{ji}dx_{ji} + dx_{ji}^2 - 2y_{ji}dy_{ji} + dy_{ji}^2} \quad 3.13$$

Eq. 3.13 is the nonlinear format of Eq. 3.3, which is the representation of the amount of nonlinear member alteration with respect to external nodal displacement in the form of a rational function.

### 3.2.3 Equilibrium Matrix at Deformed Configuration

Eq. 3.1 represents the self-equilibrium state after attaining the prestressing. The equilibrium matrix and  $t$  can be set of its  $x$  and  $y$  components as  $tx_{i,j}$  and  $ty_{i,j}$  for each member as follows:

$$tx_{i,j} = t \cos \theta \quad 3.14$$

$$ty_{i,j} = t \cos \lambda \quad 3.15$$



Referring back to Fig. 3-1  $\cos\theta = x_{ji} - dx_{ji}/L'$  and  $\cos\lambda = y_{ji} - dy_{ji}/L'$ , by substituting Eq. 3.5 they become  $\cos\theta = x_{ji} - dx_{ji}/L_o - e_o$  and  $\cos\lambda = y_{ji} - dy_{ji}/L_o - e_o$ . Now substituting  $e_o$  with neglecting the second-order of displacements from Eq. 3.10  $\cos\theta$  and  $\cos\lambda$  can be expressed in the forms of Eqs. 3.16 and 3.17 based on Taylor's series expansion. Analogously, using Eq. 3.13,  $\cos\theta$  and  $\cos\lambda$  can be expressed as Eqs. 3.18 and 3.19 based on the Pade approximation method.

$$\cos\theta = \frac{x_{ji}L_o - dx_{ji}L_o}{L_o^2 - x_{ji}dx_{ji} - y_{ji}dy_{ji}} \quad 3.16$$

$$\cos\lambda = \frac{y_{ji}L_o - dy_{ji}L_o}{L_o^2 - x_{ji}dx_{ji} - y_{ji}dy_{ji}} \quad 3.17$$

$$\cos\theta = \frac{4x_{ji}L_o^2 - 2x_{ji}^2dx_{ji} - 2x_{ji}y_{ji}dy_{ji} - 4dx_{ji}L_o^2}{4L_o^3 - 6x_{ji}dx_{ji}L_o - 6y_{ji}dy_{ji}L_o} \quad 3.18$$

$$\cos\lambda = \frac{4y_{ji}L_o^2 - 2y_{ji}^2dy_{ji} - 2x_{ji}y_{ji}dy_{ji} - 4dy_{ji}L_o^2}{4L_o^3 - 6x_{ji}dx_{ji}L_o - 6y_{ji}dy_{ji}L_o} \quad 3.19$$

Hence, the internal force vector  $\mathbf{t}$  can be computed via equalising Eq. 3.4 with the Eqs. 3.10 and 3.13 as shown below:

$$\frac{x_{ji}dx_{ji} + y_{ji}dy_{ji}}{L_o} - \frac{dx_{ji}^2 + dy_{ji}^2}{2L_o} + \frac{x_{ji}^2dx_{ji}^2 + y_{ji}^2dy_{ji}^2}{2L_o^3} + \dots$$

$$\frac{x_{ji}y_{ji}dx_{ji}dy_{ji}}{L_o^3} - \mathbf{Ft} = 0 \quad 3.20$$

$$\frac{2L_o(2x_{ji}dx_{ji} - dx_{ji}^2 + 2y_{ji}dy_{ji} - dy_{ji}^2)}{4L_o^2 - 2x_{ji}dx_{ji} + dx_{ji}^2 - 2y_{ji}dy_{ji} + dy_{ji}^2} - \mathbf{Ft} = 0 \quad 3.21$$

The typified Eqs. 3.20 and 3.21, based on Taylor's series and Pade approximation method, respectively, can be solved using any technique for

solving a system of nonlinear equations. Here, `fsolve` in MATLAB (R2021a) is adopted since the form of the nonlinearity is identified and the highest order is two. `fsolve` makes an attempt to resolve an equation system by decreasing the sum of squares of the components.

In the derivation steps of the proposed technique, the matrix of  $\mathbf{S}$  in Eq. 3.2 is not used for indicating the internal force vector  $\mathbf{t}$ . In the linear force method, the self-stress state matrix is derived from the null space of equilibrium matrix ( $\mathbf{A}$ ) at the original configuration. In contrast, the proposed nonlinear approach for computing the vectors  $\mathbf{t}$  and  $\mathbf{e}_o$  relies on the  $\mathbf{A}(\mathbf{d})$  and  $\mathbf{B}(\mathbf{d})$  in Eqs. 3.1 and 3.3, which are evaluated at the fully deformed configuration.

#### 3.2.4 Steps for Solving Nonlinear Prestressing Method

Various procedures can be utilised to solve the group of nonlinear equations represented in Eqs. 3.10, 3.13, 3.20 and 3.21. In the proposed technique, `fsolve` as a built-in function in MATLAB (R2021a) has been adopted to achieve the solution of these nonlinear systems. The solving stepwise can be outlined as follows.

1. Set up the nodal coordinates of the structural geometry and boundary conditions.
2. Assign the connectivity matrix (connection between coordinates) and the desired degree of prestressing. (If finding the amount of prestressing was the goal, assign the  $\mathbf{e}_o$  instead of  $\mathbf{t}$  in step 2).
3. Assign the material properties of the elements, such as cross-sectional area and modulus of elasticity.
4. Assemble the equilibrium, compatibility, and flexibility matrices.

5. Calculate the amount of member alteration using Eqs. 3.10 or Eq. 3.13 (If finding prestress was required, use Eqs. 3.20 or 3.21 to find the value of  $t$ ).
6. Compute the rate of the Euclidean norm via Eq. 3.28 or Eq. 3.29 reliant on the target to find the cost function (see Sub Section 3.2.6 for clarification).

### 3.2.5 Illustrative Example

A simple model that consists of three-linked cables as shown in Fig. 3-2 named triple-link cable structure is selected to explain the process of applying the proposed prestressing technique. The assembly has an axial stiffness of  $10^4$  N. It is pin supported at nodes 1, 3, and 4, and has two degrees of freedom at node 2. The labelling and dimensions are presented in Fig. 3-2. The cable structure is prestressed using the derived nonlinear Eqs. 3.20 and 3.2. The process of prestressing began by shortening cable  $i$  by  $e_i$  without applying external load for simplicity. The following steps explain how to formulate the required equations for the unknowns and solve the set of algebraic nonlinear equations.

Shortening member  $i$  caused the triple-link to generate pretension in the members. Since it did not carry additional loads, the structure becomes self-equilibrated. The two equilibrium equations at joint 2 can be written as:

$$t_{ii} = t_{iii} \quad 3.22$$

$$t_i = (t_{ii} + t_{iii}) \cos \lambda \quad 3.23$$

Either Eq. 3.17 or Eq. 3.19 can be substituted into Eq. 3.23 to expand it. As both derived equations yield similar results, the equations derived via the Pade approximation method are utilised for this example. Substituting Eq. 3.19 into Eq. 3.23 can be re-written as:

$$t_i = (t_{ii} + t_{iii}) \left( \frac{30000 - 7.6dy_2 - 1.8dy_2^2}{50000 - 9dx_2 - 9dy_2} \right) \quad 3.24$$

The three compatibility equations relating the member alteration (Eq. 3.13) caused by  $e_1$  can be applied with the constitutive relationship (Eq. 3.21), resulting in the following equations:

$$\frac{10^3 (10^3 dy_2 - dx_2^2 - dy_2^2)}{10^6 - 10^3 dy_2 + dx_2^2 + dy_2^2} = t_i \frac{500}{10^4} \quad 3.25$$

$$\frac{10^3 (800dx_2 + 600dy_2 - dx_2^2 - dy_2^2)}{10^6 - 800dx_2 - 600dy_2 + dx_2^2 + dy_2^2} = t_{ii} \frac{500}{10^4} \quad 3.26$$

$$\frac{10^3 (800dx_2 + 600dy_2 - dx_2^2 - dy_2^2)}{10^6 - 800dx_2 - 600dy_2 + dx_2^2 + dy_2^2} = t_{iii} \frac{500}{10^4} \quad 3.27$$

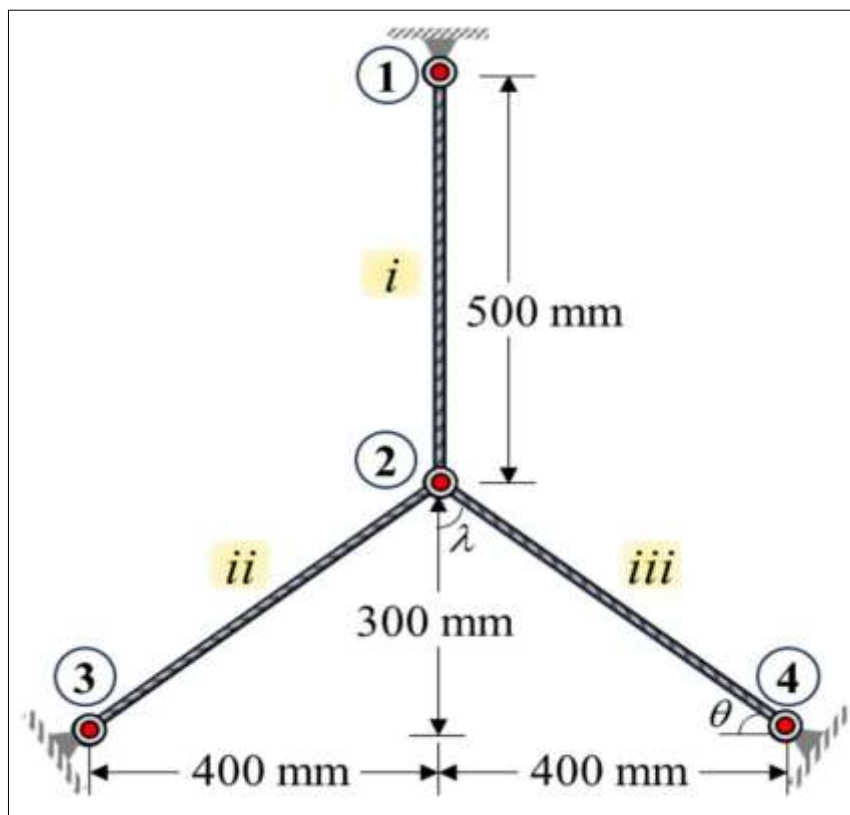


Fig. 3-2 Triple-link cable structure

Because  $t_{ii} = t_{iii}$ , the number of unknowns becomes four ( $t_i, t_{ii}$  (or  $t_{iii}$ ),  $dx_2$ , and  $dy_2$ ), with two being linear ( $t_i$ , and  $t_{ii}$ ) and the other two nonlinear ( $dx_2$ , and  $dy_2$ ). For this reason, the set of nonlinear equations needs to be solved using a nonlinear solver. Here, the `fsolve` function in MATLAB (R2021a) is used to solve the system of nonlinear equations. To utilise `fsolve` in MATLAB (R2021a), it is necessary to define the set of equations so that it can create a function that returns the equations required for solving. Then, `fsolve` must be called to provide the function and an initial guess to start solving the equations.

For this example, if the value of  $e_l$  is specified as -1 mm, the value of  $t_i, t_{ii}$ , and  $t_{iii}$  are 8.38 N, 6.97 N, and 6.97 N respectively. The displacements at node 2 ( $dx_2$ , and  $dy_2$ ) are 0, and 0.58 mm. The specific code in MATLAB using `fsolve`, written and used to achieve the reported results for the triple link structure, is as presented in Appendix -A.

### 3.2.6 Validation of the Prestressing Technique

The derived  $e_o$  in both Eqs. 3.10 and 3.13 are examined in this section via two examples, namely cable net structure and deployable structure. The prestress is also computed for the space truss grid with an imposed lack of fit. Then the results are compared with the experimental and theoretical published works.

The Euclidean norm ration (Fraddosio *et al.*, 2021; Xue *et al.*, 2021; Zhou *et al.*, 2017) between the member alterations and the internal force of the proposed technique ( $e_o$  &  $t$ ) and the previous techniques ( $e_o^*$  &  $t^*$ ) (You, 1997; Kwan and Pellegrino, 1993; Hanaor and Levy, 1985) is computed as a cost function purpose as below:

$$R_{e_o} = \frac{\|e_o - e_o^*\|_2}{\|e_o^*\|_2} \times 100 \quad 3.28$$

$$R_t = \frac{\|t - t^*\|_2}{\|t^*\|_2} \times 100 \quad 3.29$$

### 3.2.6.1 Cable net structure

A cable net structure (You, 1997) with three states of self-stress, as shown in Fig. 3-3, has seven nodes (1-7); three of them are free and the rest nodes are pinned. The structure has nine (i-ix) cables with  $EA$  equal to 431600 N. The cable network is prestressed computationally and experimentally via altering the members' length of vii, viii, and ix by the quantity of -5.02, 4.49, and -5.02 mm, respectively. The proposed technique is applied to the given structure for the same target, and the results are compared with the computational results by You (1997), as shown in Table 3-1. The results indicate a good agreement. The total amount of members varying length by the linear technique of You (1997)  $|e_o| = 14.59$  mm, while from the current nonlinear technique is only 13.51 mm, which is less than the quoted method by 7.4% via utilising both derived Eqs. 3.10 and 3.13. Besides, the rate of  $l_2$ -norm of member alteration, that is shown in Table 3-1, was 15.5% as a result of geometrical nonlinearity consideration. It can be concluded that the current method takes less effort and is consequently more economical members' length of vii, viii, and ix by the quantity of -5.02, 4.49, and -5.02 mm, respectively.

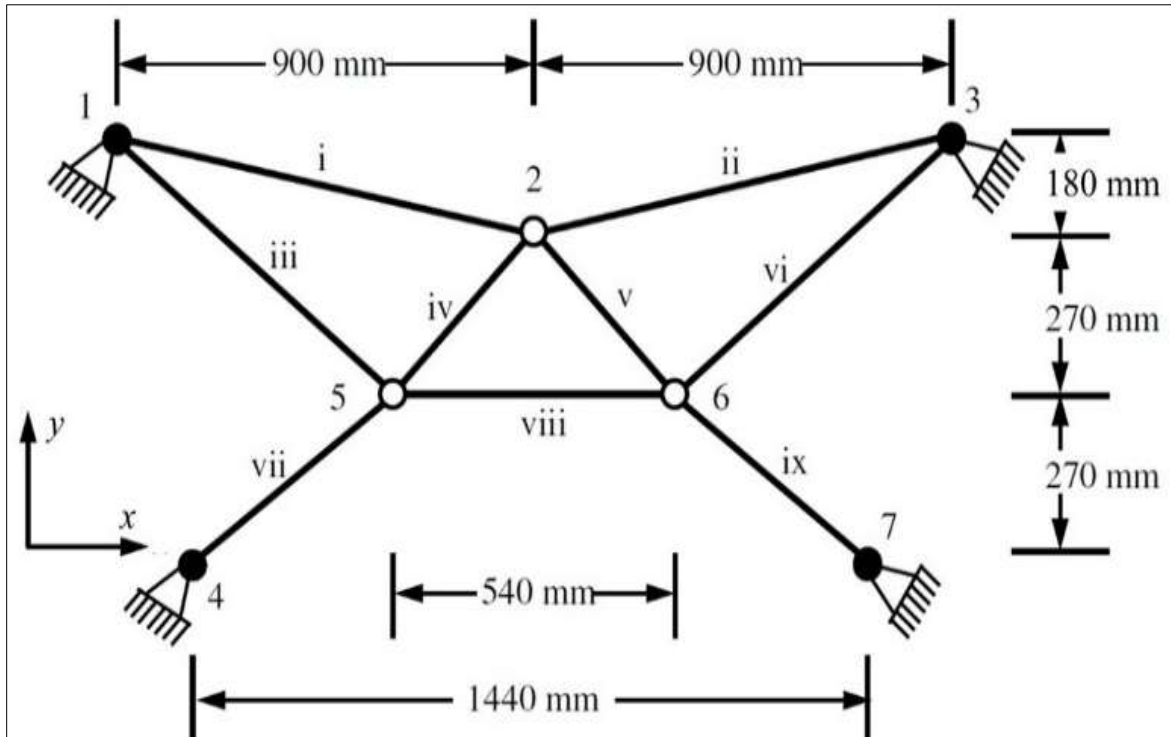


Fig. 3-3 Cable net model designed by You (1997)

Table 3-1 Comparison of nonlinear member alteration with You (1997)

Cables	$t$ (N)	$e_o$ (mm)		
		You (1997)	Eq. 3.10	Eq. 3.13
i	61.4	-	-	-
ii	61.4	-	-	-
iii	23.5	-	-	-
iv	17	-	-	-
v	17	-	-	-
vi	23.5	-	-	-
vii	50	-5.02	-4.22	-4.22
viii	50	4.49	5.07	5.07
ix	50	-5.02	-4.22	-4.22
$\sum  e_o $ (mm)		14.59	13.51	13.51
$R_{e_o}$		15.5%		

### 3.2.6.2 Deployable structure

A deployable structure that consists of six cells and sixty members is shown in Fig. 3-4 (Kwan and Pellegrino, 1993). It has twenty-four bars drawn in thick lines and thirty-six (1-12 in-plane and 13-36 out of plane) cables with six states of self-stress. Kwan and Pellegrino (1993) prestressed this structure in a fully opened configuration, which is part of the deployable mesh antenna. Fig. 3-5 shows the general state of self-stress for one unit of the structure and their in-plane connector members to the support. Each of the cables with  $EA=98$  kN and bars with  $EA=3500$  kN has a length of 500 mm. To achieve the desired prestressing level, that is 2 N for inner in-plane cables 3, 5, 7, 8, and 11, also 1 N for the remaining cables in pretension, and -1 N for all the bars.

Kwan and Pellegrino (1993) tried various ways to nominate the necessary state of prestress. In the first way of determining the total amount of member alteration, they used the Gaussian elimination method. The members with the ability to change their length were 1, 3, 4, 7, 8, and 9, which are equal to the number of states of self-stress. The total amount of actuation set-out as 0.486 mm, whereas the proposed technique determined the total actuation to be  $\sum |e_o| = 0.475$ mm. The results are tabulated in Table 3-2, and the findings by Eq. 3.10 and Eq. 3.13 of the current approach are reduced by about 2.2% and minimised the  $l_2$ -norm ratio by 6.2%.

In the second way, Kwan and Pellegrino (1993) performed a standard linear program to determine member alteration by inserting dual sets of non-negative variables to solve for an optimal total amount of actuation by a number equal to the states of self-stress. Saeed and Kwan (2016b) stated that the member with the greater arbitrary coefficients ( $\mathbf{a}$ ) of the state of self-stress can be more active during the actuation process. Therefore, using only the four members with a



coefficient  $\pm 2$ , as shown in Fig. 3-5, the structure would reach the same level of prestress instead of six elements. The participating members were 1, 3, 5, 7, 10, and 11, and the total amount of member alteration was 0.177 mm. Correspondingly, utilising the proposed technique by Eqs. 3.10 and 3.13 the  $\sum |e_o|$  was less than 50.5% and minimised the  $l_2$ -norm ratio by 72.2% as shown in Table 3-3.

The results of the nonlinear technique that tabulated in Table 3-2 and Table 3-3 show a great precision and similitude of the present findings in comparison to the highlighted linear approach. For the particular case in Table 3-2, the total actual is lesser by 2.2%, while for the optimal case, as in Table 3-3 is lesser by 50.5%, which is of a practical interest. Moreover, the nonlinear computing of member alteration produced a more compacted overall amount of member actuation and minor member alteration with fewer disturbances in geometry.

The close agreement of the findings attained by directly applying Eq. 3.10 and Eq. 3.13 shows the great potential and reduces the computational exertion producing validated results.

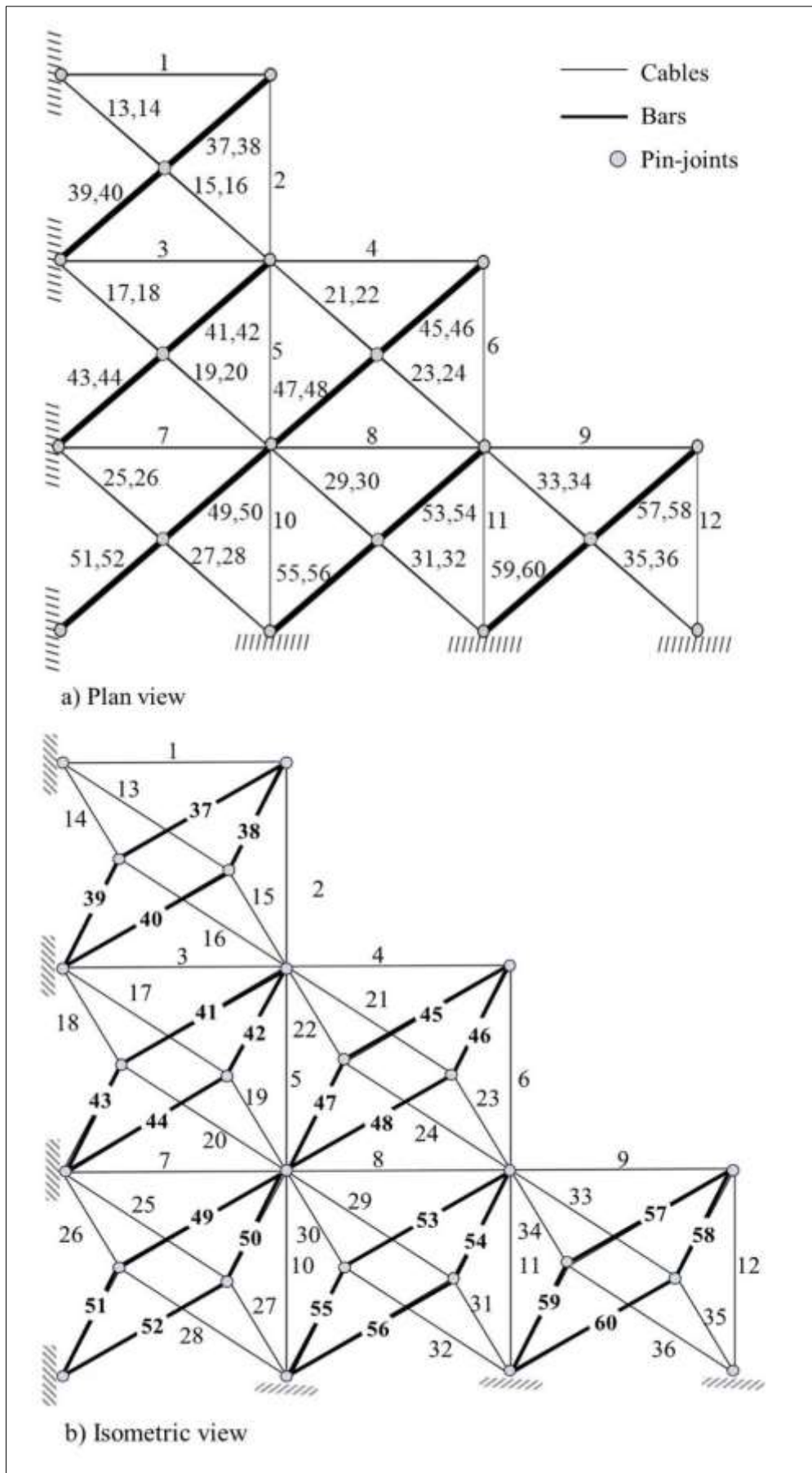


Fig. 3-4 Deployable structure (Kwan and Pellegrino, 1993)

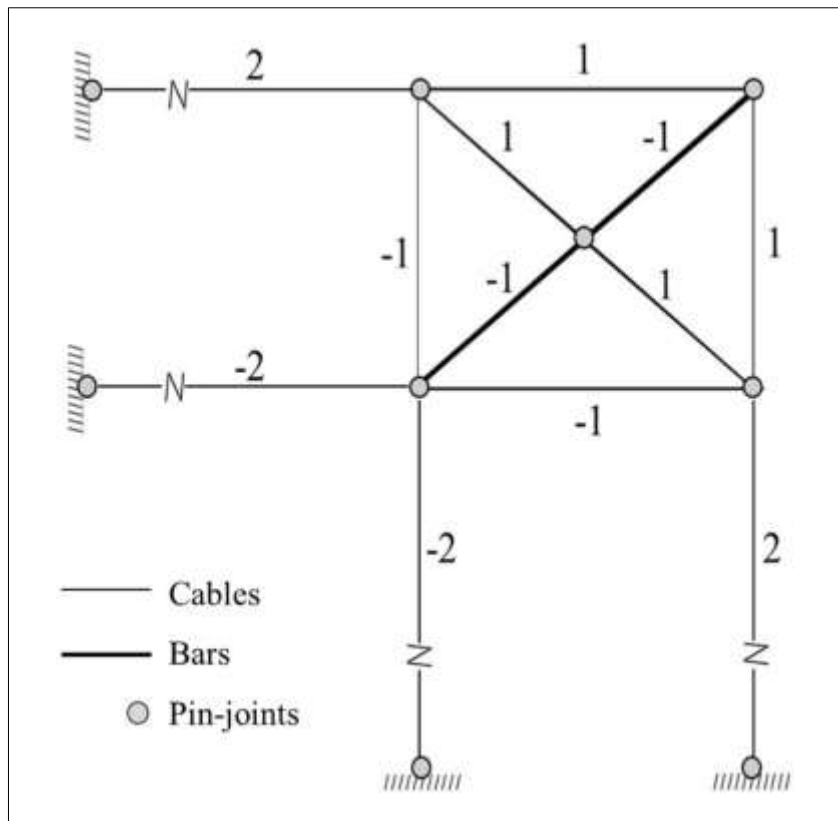


Fig. 3-5 Plan view of the general state of self-stress of a unit (Kwan and Pellegrino, 1993)

Table 3-2 Comparison of nonlinear member alteration with the particular choice of Kwan and Pellegrino (1993)

Members	$t$ (N)	$e_o$ (mm)		
		Kwan and Pellegrino (1993)	Eq. 3.10	Eq. 3.13
1	1	-0.1550	-0.15130	-0.15131
3	2	-0.0931	-0.08660	-0.08668
4	1	0.1238	0.12700	0.12701
7	2	-0.0415	-0.03360	-0.03361
8	2	0.0312	0.03908	0.03908
9	1	-0.0415	-0.03781	-0.03780
5,10,11	2	-	-	-
2,6,12-36	1	-	-	-
37-60	-1	-	-	-
$\sum  e_o $ (mm)		0.4861	0.47538	0.47549
$R_{e_o}$		6.2%		

Table 3-3 Comparison of nonlinear member alteration with the optimal set of Kwan and Pellegrino (1993)

Members	$t$ (N)	$e_o$ (mm)		
		Kwan and Pellegrino (1993)	Eq. 3.10	Eq. 3.13
1	1	-0.0104	-0.010288	-0.010288
3	2	-0.0001	0.016053	0.016053
5	2	-0.0325	0.007138	0.007141
7	2	-0.0100	0.001184	0.001185
8	2	-	-	-
10	2	-0.0727	-0.024468	-0.024471
11	2	-0.0517	-0.028590	-0.028592
2,6,9,12-36	1	-	-	-
37-60	-1	-	-	-
$\sum  e_o $ (mm)		0.1774	0.08772	0.08773
$R_{e_o}$		72.2%		

### 3.2.6.3 Space truss structure

A double-layer grid space truss system, depicted in Fig. 3-6 (a), (b), and (c), has vertical restraints applied to all perimeter joints. It comprises 25 nodes, including 16 nodes at the bottom, and 72 members (Hanaor and Levy, 1985; Levy *et al.*, 1994). The geometry shown in Fig. 3-7 forms the lack of fit amount of the truss grid assemblies. From the study by Hanaor and Levy (1985), the members' lack of fit is represented as a factor that needs to be multiplied by  $PL_o/EA_o$ , which is equal to 1 for this example. The positive and negative signs in Fig. 3-7 show the elongation and shortening of the members. The present technique is examined on this system using Eqs. and, then compared with the analytical results by Levy *et al.* (1994). The results for computing the level of prestress are presented in Table 3-4. From Fig. 3-7, the nonsymmetric distribution of the imposed lack of fit for the selected members can be seen. The reported findings by Hanaor and Levy (1985) showed symmetric prestress distribution despite the nonsymmetric distribution of members' lack of fit and this is not logical. The proposed technique results showed the effect of this

dissimilarity and minimised the  $l_2$ -norm ratio of stress vectors by 0.17% and 0.23% with respect to the outcomes of Eq. 3.20 and Eq. 3.21 respectively. It is noticeable that the outcomes of both Eqs. 3.20 and 3.21 have a good agreement with the compared one.

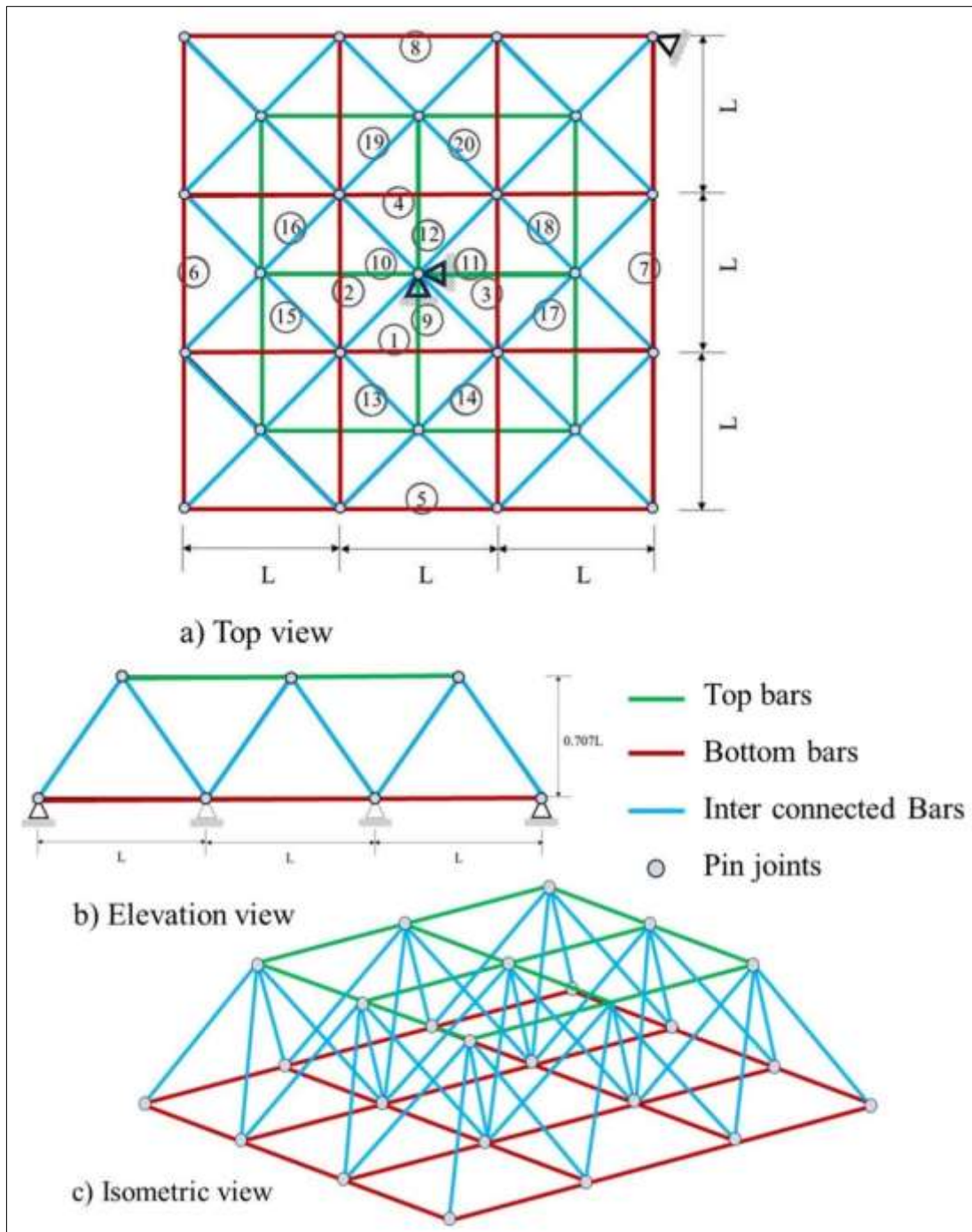


Fig. 3-6 Space truss geometry by Levy et al. (1994)

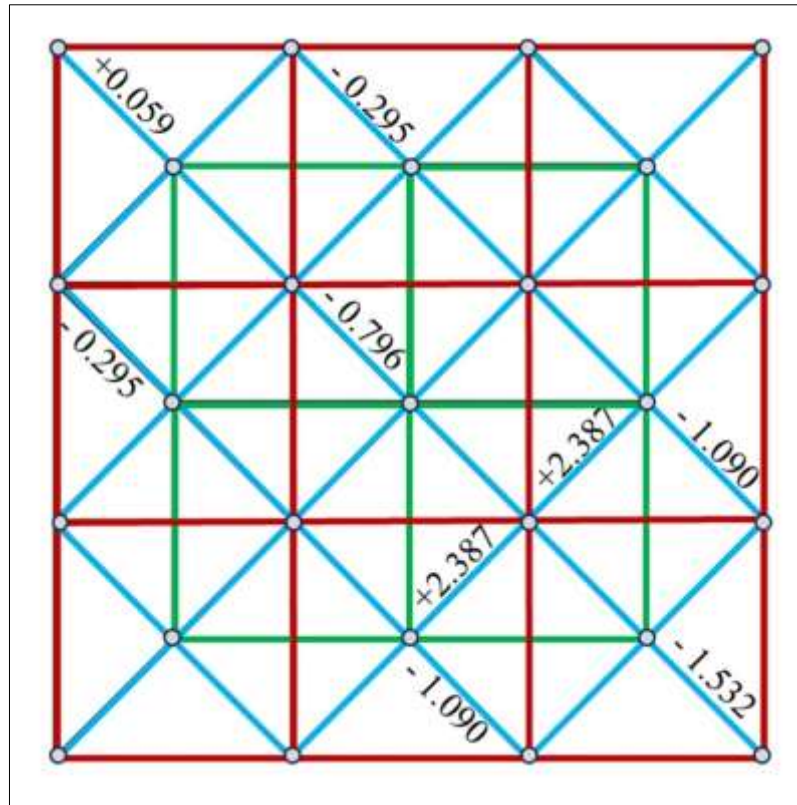


Fig. 3-7 Space truss grid lack of fit

Table 3-4 Comparison of nonlinear member alteration with Hanaor and Levy (1985)

Member No.	$t$ (N)		
	Hanaor and Levy (1985)	Present study	
		Eq. 3.20	Eq. 3.21
1,3	0.1208	0.1207	0.1206
2,4		0.1212	0.1214
5,7	-0.1620	-0.1617	-0.1616
6,8		-0.1620	-0.1622
9,11	0.2003	0.1999	0.1999
10,12		0.2004	0.2006
13,18	-0.1002	-0.1001	-0.1000
14,17		-0.0998	-0.0999
15,20		-0.1002	-0.1005
16,19		-0.1000	-0.1000
$R_t$		0.17%	0.23%

### 3.2.6.4 3D cable-net model

The 3D cable-net model shown in Fig. 3-8, has 14 nodes that the x, y, and z coordinates are shown in Table 3-5. Eight of them are pinned and shown in black solid connectors. It consists of 21 members with axial stiffness of 40,000 N. The targeted degree of prestress ( $t$ ) for all the cables is determined as shown in the 2<sup>nd</sup> column in Table 3-6. The prestressing process is performed by pre-indicating the required member pretension force for all members. The present technique has been applied to attain the targeted prestress ( $t^*$ ) using `fsolve` in MATLAB (R2021a) and the results were as shown in the 3<sup>rd</sup> column in Table 3-6. The other findings of the present technique such as 3D nodal displacements of the free nodes and the required amount of nonlinear members actuation are tabulated in Table 3-7. As a practical consideration, only members 7, 8, 9, 10, 19, 20, and 21 are selected as actuators while the remaining cables are set to have unchangeable lengths. The total amount of shortening is 13.1514 mm. Later, the results are validated using nonlinear analysis of the same model with SAP2000 finite element analysis software, version 23.2.0. When setting up the geometric nonlinearity parameters in the software, the *P-Delta plus Large Displacements* option should be used. This is because all the equilibrium equations are indicated at the deformed state of the structure, similar to the proposed technique. At this stage, the same quantity of members' shortening is assigned to the same cables. The outcomes of the computed prestress and nodal displacements are presented in the 4<sup>th</sup> column in Table 3-6 and Table 3-7.

For testing the accuracy and the closeness to the desired prestress level, the Euclidean norm ( $l_2$ -norm) (Xue et al., 2021) is used as an evaluation index as presented in Table 3-6. The  $l_2$ -norm is defined as  $\|t - t^*\|_2$  and  $\|t - t'\|_2$  to indicate the discrepancy between the vectors of targeted prestress to the calculated prestress by the present technique and SAP2000, respectively. The smaller

value of the Euclidean norm is 0.0809 with the present technique showing that it is more accurate and more approachable to the desired target in comparison to  $t'$ . Regarding the nodal displacements, the computed  $dx$ ,  $dy$ , and  $dz$  by the present technique have a very good agreement in comparison to the SAP2000 results as shown in Table 3-7. SAP2000 fails to compute the required member actuation if the targeted prestress of member forces is requested. For this reason, the output of the member actuation from the proposed technique is assigned to the cables to achieve the prestressing of the members.

For ten cables (Table 3-6) the computed prestress by SAP2000 is closer to the targeted  $t$ , while for the other 11 members, the computed one by the present technique is closer as confirmed above through the Euclidean norm index.

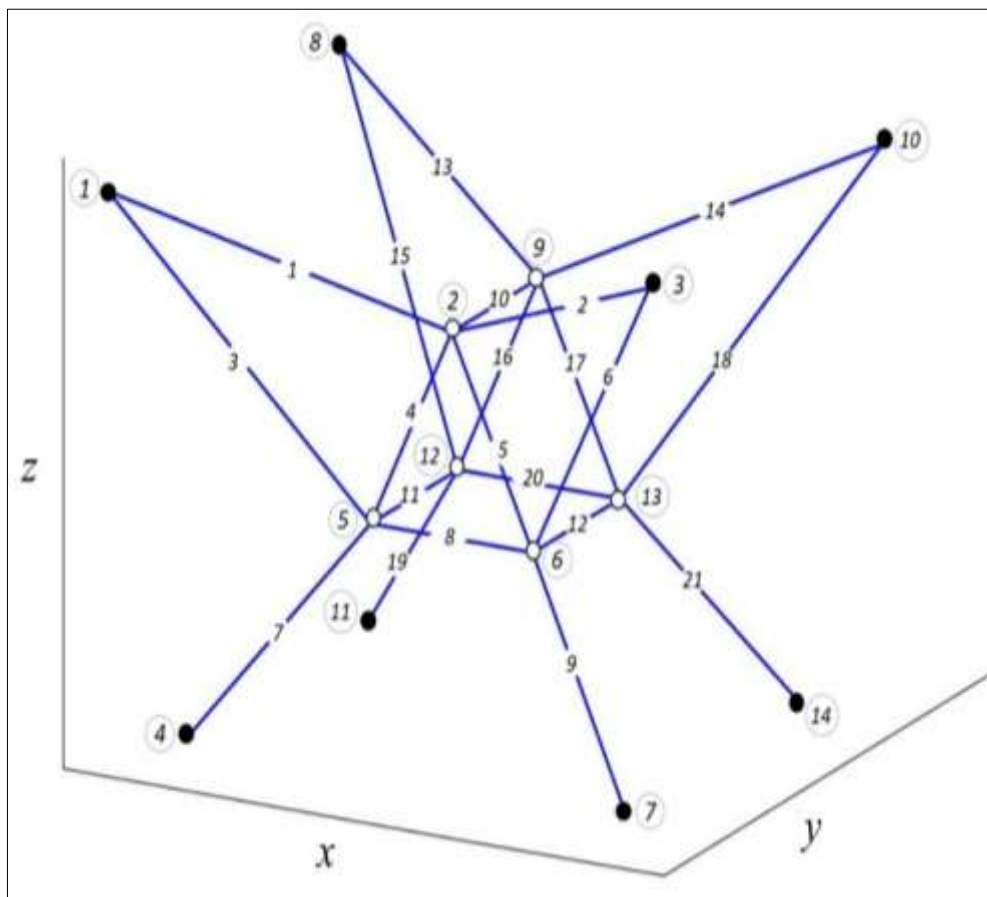


Fig. 3-8 3D cable-net model with labeled nodes and members



Table 3-5 Nodal coordinates for the 3D cable net model

Nodes	Coordinates			Nodes	Coordinates		
	x (mm)	y (mm)	z (mm)		x (mm)	y (mm)	z (mm)
1	0	720	720	8	0	-720	720
2	900	270	540	9	900	-270	540
3	1800	720	720	10	1800	-720	720
4	180	540	0	11	180	-540	0
5	630	270	270	12	630	-270	270
6	1170	270	270	13	1170	-270	270
7	1620	540	0	14	1620	-540	0

Table 3-6 Cable prestress and  $l_2$  – norm for the 3D cable net model

Cables	Prestress (N)		
	$t$	$t^*$ Present Technique	$t'$ SAP2000
1,2,13,14	51	50.8	50.92
3,6,15,18	29	29.03	28.88
4,5,16,17	12.7	12.61	12.68
7,9,19,21	51.1	51.08	51.32
8,20	50.5	50.41	50.48
10	44.5	44.35	44.83
11,12	38.1	38.07	37.99
	$\ t - t^*\ _2$	0.0809	
	$\ t - t'\ _2$	0.1909	

Table 3-7 Nodal displacement and cable actuation for the 3D cable net model

Nodes	Displacement (mm)						Actuator	$e_o$ (mm)
	Present Technique			SAP2000				
	$dx$	$dy$	$dz$	$dx$	$dy$	$dz$		
2	0	-2.5476	-1.0199	0	-2.5422	-1.022	7	-1.3796
5	0.1446	0.2569	-1.3495	0.1433	0.2559	-1.3368	8	-0.9696
6	-0.1446	0.2569	-1.3495	-0.1433	0.2559	-1.3368	9	-1.3796
9	0	2.5476	-1.0199	0	2.5422	-1.022	10	-5.6938
12	0.1446	-0.2569	-1.3495	0.1433	-0.2559	-1.3368	19	-1.3796
13	-0.1446	-0.2569	-1.3495	-0.1433	-0.2559	-1.3368	20	-0.9696
							21	-1.3796
Total Actuation (mm)								13.1514

### 3.2.6.5 Conical cable-net model

A conical cable-net structure as shown in Fig. 3-9 is prestressed by the present approach. The system consists of 24 cables labeled as shown in Fig. 3-9, and they have axial stiffness ( $EA$ ) of  $10^4$  N. The model has 18 nodes as shown in Fig. 3-10, and the coordinates are tabulated in columns 2-4 of Table 3-8. Joints 2, 4, 6, and 13-18 are restrained against x-, y-, and z- directions translation, while joints 1, 3, and 5 are restrained only in vertical (z) direction. The nodes 6-12 are free to move in all directions. The prestress of this model started by determining the members shortening of cables 19-24 by 9 mm and cables 7-12 by 5 mm as shown in column 4 of Table 3-9, which results in 66 mm of the total amount of members actuation that prevent any slack of the cables. Via using Eq. 3.20 the required pretension for all members is attained and presented in Table 3-9 (column 2). The exterior nodal displacement also came out as presented in columns 5-7 of Table 3-8.

Similarly, the conical cable-net system is modelled and prestressed in SAP2000 software with the same given properties of joints, connectivity members, and supports. The identical amount of member actuation as members deformation in the load case is assigned to the above-mentioned cables. Then it is analysed by selecting nonlinear geometrical considerations with large deformability. The joint displacements output is shown in Table 3-8 (columns 8-10), and the member pretensions output is presented in Table 3-9 (column 3). The maximum difference percent of the displacement resultant between the present technique and SAP2000 is 0.01%, while the maximum discrepancy percent for prestress level is 0.04%. These findings show great consistency and precision of the proposed approach in computing the required degree of prestress without causing slack of any member.

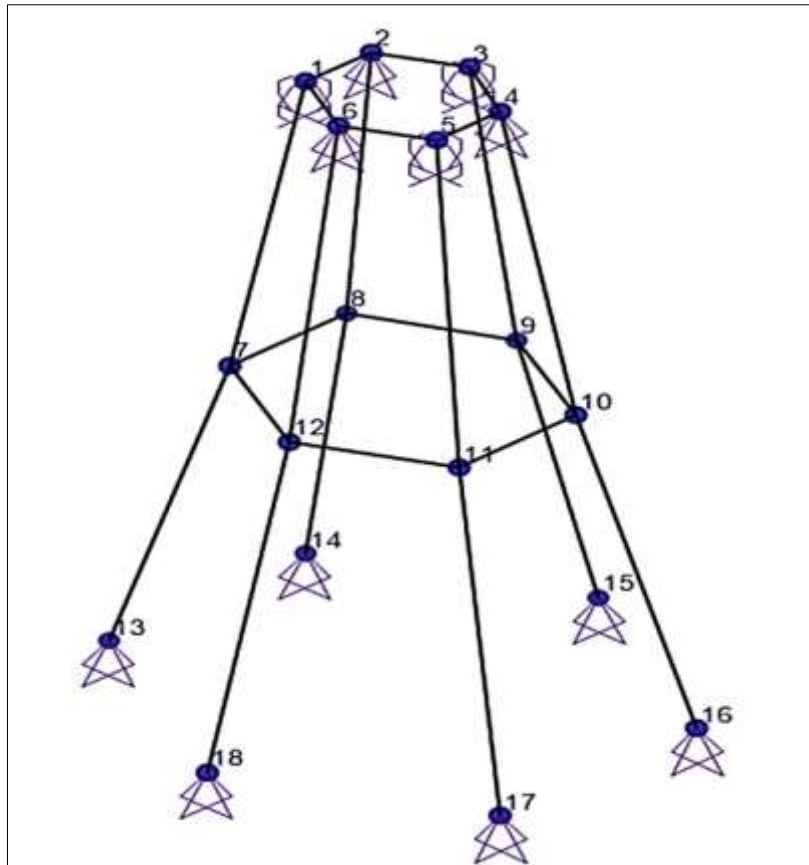


Fig. 3-9 Conical cable-net model with labeled nodes

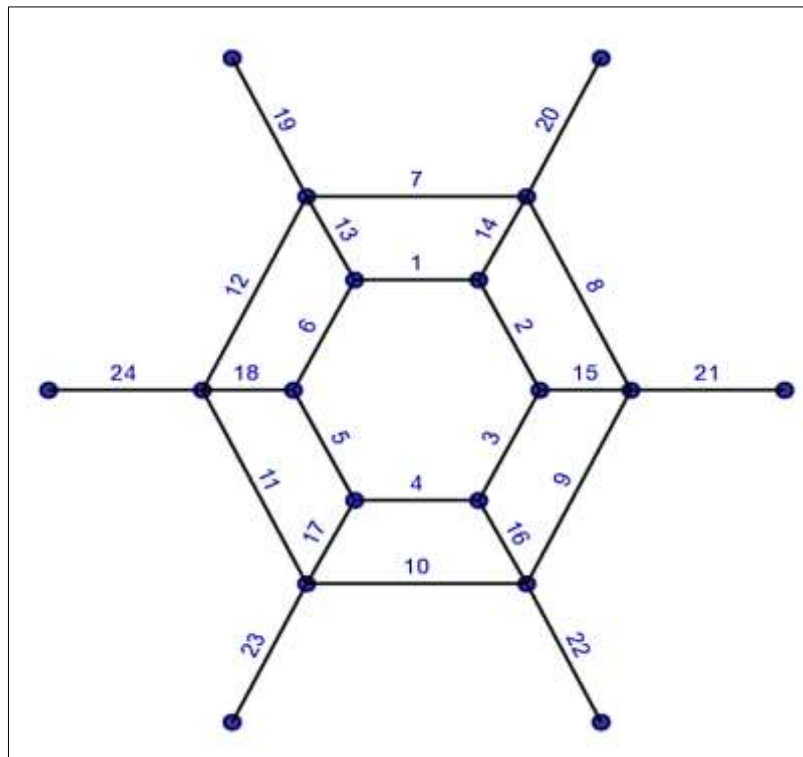


Fig. 3-10 Top view of the conical cable-net model with labeled cables

Table 3-8 Conical cable-net nodal coordinates, and displacements

Nodes	Coordinates (mm)			Displacements (mm)					
				Present technique			SAP2000		
	<i>x</i>	<i>y</i>	<i>z</i>	<i>dx</i>	<i>dy</i>	<i>dz</i>	<i>dx</i>	<i>dy</i>	<i>dz</i>
1	500	800	2000	-0.13605	0.25208	0	-0.13605	0.25207	0
2	700	800	2000	0	0	0	0	0	0
3	800	600	2000	0.36521	0	0	0.36520	0	0
4	700	400	2000	0	0	0	0	0	0
5	500	400	2000	-0.13605	-0.25208	0	-0.13605	-0.25207	0
6	400	600	2000	0	0	0	0	0	0
7	420	950	1000	2.42820	-4.61710	-5.68460	2.42818	-4.61715	-5.68466
8	780	950	1000	-2.40600	-4.57380	-5.64970	-2.40595	-4.57384	-5.64983
9	950	600	1000	-3.92790	0	-5.30870	-3.92774	0	-5.30872
10	780	250	1000	-2.40600	4.57380	-5.64970	-2.40596	4.57384	-5.64983
11	420	250	1000	2.42820	4.61710	-5.68460	2.42818	4.61714	-5.68466
12	250	600	1000	3.86180	0	-5.26860	3.86166	0	-5.26859
13	300	1200	0	0	0	0	0	0	0
14	900	1200	0	0	0	0	0	0	0
15	1200	600	0	0	0	0	0	0	0
16	900	0	0	0	0	0	0	0	0
17	300	0	0	0	0	0	0	0	0
18	0	600	0	0	0	0	0	0	0

Table 3-9 Conical cable-net member prestress and member actuation

Cable	Prestress (N)		$e_o$ (mm)
	Present technique	SAP2000	
1,4	6.8104	6.8103	0
2,3	7.3148	7.3147	
5,6	7.3676	7.3674	
7,10	4.6076	4.6075	-5
8,9	5.6949	5.6948	
11,12	5.6917	5.6917	
13,17	46.3540	46.3542	0
14,16	46.5490	46.5492	
15	45.7450	45.7446	
18	45.9650	45.9646	
19,23	47.5640	47.5639	
20,22	47.7590	47.7586	-9
21	46.7130	46.713	
24	46.9320	46.9316	
Total actuation (mm)			66

### 3.3 FORMULATION AND VALIDATION OF THE ANALYSIS TECHNIQUE

Cable-supported structures are introduced as highly flexible structures, so they distort significantly when exposed to transverse loadings. Consequently, the extra challenge is preferred in analyzing these types of non-linear geometric structures. The formulation of the present analysis approach depends on the principles of the flexibility method and the fundamentals of structural mechanics. The Pade approximation, recognised as one of the most effective approximations of a rational function of a given order, is employed to derive this non-linear equation. This approximation was initially presented and researched by Frobenius (1881) for the possibility of rational approximations of power series and then developed by Henri Eugene Pade (Nisar *et al.*, 2021). The Pade approximation is a conventional rational function whose extension is pointed to settle with the Taylor series expansion of the main function as distant as conceivable.

In most cases, the Pade approximation affords a more improved approximation for the original function and could work where the Taylor series does not converge, particularly for the functions with poles (Vazquez-Leal *et al.*, 2014). In this formulation, the cable element is considered as a general bar within the initial prestress  $t$  for preventing slack of the member, as shown in Fig. 3-11. Let the bar  $io$ - $jo$  with the original length  $L$  has the initial end coordinates at  $(x_{io}, y_{io}, z_{io})$  and  $(x_{jo}, y_{jo}, z_{jo})$ . After experiencing the deformation, its length becomes  $L_c$  in  $i_c$ - $j_c$ , and the new end coordinates are  $(x_{ci}, y_{ci}, z_{ci})$  and  $(x_{cj}, y_{cj}, z_{cj})$ , as shown in Fig. 3-11. The bar in Fig. 3-11 undergoes the deformation after being affected by external loads  $P_i$  and  $P_j$  at both ends; their horizontal and vertical components are shown in Fig. 3-12.

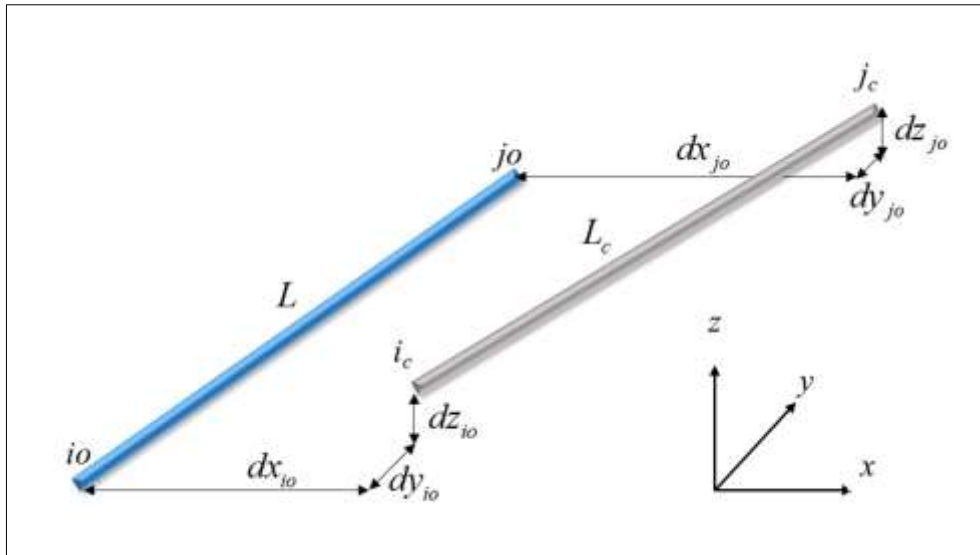


Fig. 3-11 Spatial bar coordinates at original and deformed configuration

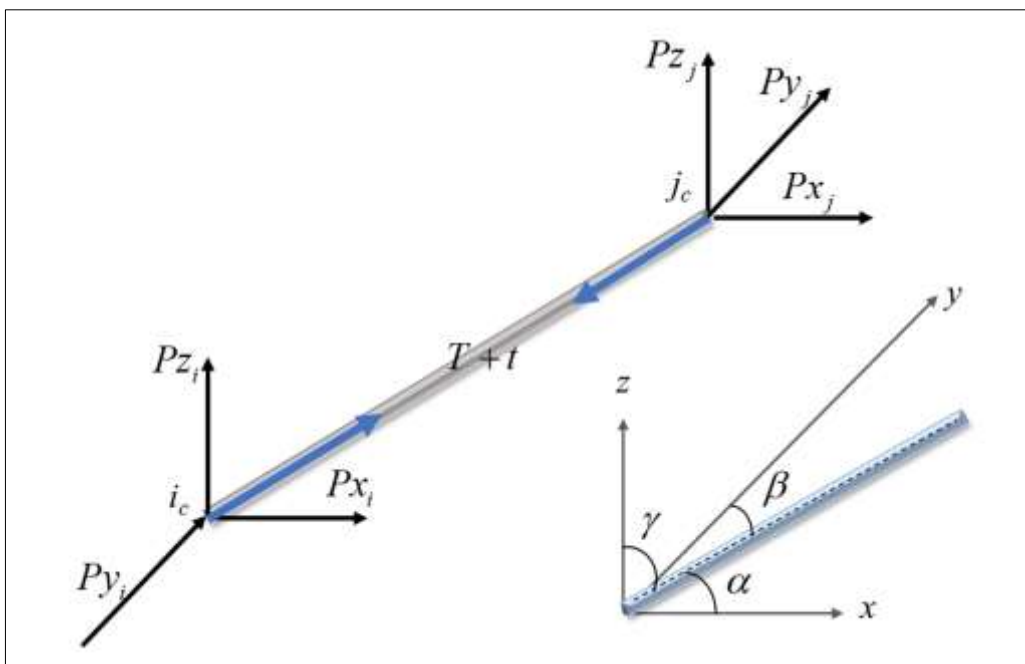


Fig. 3-12 Spatial equilibrium state at original and deformed configuration

After loading, the bar experiences bar tension  $T$  and elongation  $e$  over its original length. The abbreviation of the notation is arranged as  $( )_o = ( )_{jo} - ( )_{io}$ . Now, by reflecting the new position of the joints, the current length can be written as:

$$L_c = \left\{ (x_o + dx_o)^2 + (y_o + dy_o)^2 + (z_o + dz_o)^2 \right\}^{\frac{1}{2}} \quad 3.30$$

$$L_c = \left( L^2 + 2x_o dx_o + 2y_o dy_o + 2z_o dz_o + dx_o^2 + dy_o^2 + dz_o^2 \right)^{\frac{1}{2}} \quad 3.31$$

Let  $H = 2x_o dx_o + 2y_o dy_o + 2z_o dz_o + dx_o^2 + dy_o^2 + dz_o^2$ , thus  $L_c = \left( L^2 + H \right)^{\frac{1}{2}}$ .

Rewriting  $L_c$  gives:

$$L_c = L \left( 1 + H/L^2 \right)^{\frac{1}{2}} \quad 3.32$$

The Pade approximation is applied to extend  $\left( 1 + H/L^2 \right)^{\frac{1}{2}}$ . Due to this method's ability to accelerate or turn from the divergent to convergent function, only the first order of the asymptotic expansion is considered. Hence, the deformed bar length ( $L_c$ ) becomes:

$$L_c = L \left( \frac{4 + 3H/L^2}{4 + H/L^2} \right) \quad 3.33$$

substituting H, hence:

$$L_c = L \times \left( \frac{4 + \frac{3(2x_o dx_o + 2y_o dy_o + 2z_o dz_o + dx_o^2 + dy_o^2 + dz_o^2)}{L^2}}{4 + \frac{(2x_o dx_o + 2y_o dy_o + 2z_o dz_o + dx_o^2 + dy_o^2 + dz_o^2)}{L^2}} \right) \quad 3.34$$

The elongation of the bar can be expressed as  $e = L_c - L$ , Thus:

$$e = L \left\{ \left( \frac{4 + \frac{3(2x_o dx_o + 2y_o dy_o + 2z_o dz_o + dx_o^2 + dy_o^2 + dz_o^2)}{L^2}}{4 + \frac{(2x_o dx_o + 2y_o dy_o + 2z_o dz_o + dx_o^2 + dy_o^2 + dz_o^2)}{L^2}} \right) - 1 \right\} \quad 3.35$$

From the state of equilibrium for the deformed configuration, as shown in Fig. 3-12, the relationship between the internal and external forces with each of their components can be dedicated as shown below:

$$P_i = -(T + t) = -P_j \quad 3.36$$

Consequently, for each component in 3D becomes:

$$\begin{aligned} Px_i &= -(T + t) \cos \alpha = -Px_j \\ Py_i &= -(T + t) \cos \beta = -Py_j \\ Pz_i &= -(T + t) \cos \gamma = -Pz_j \end{aligned} \quad 3.37$$

Moreover, the terms of  $\cos \alpha$ ,  $\cos \beta$  and  $\cos \gamma$  with neglecting the high order of small displacements can be in the form:

$$\begin{aligned} \cos \alpha &= \frac{x_o + dx_o}{L_c} = \frac{4x_o L^2 + 4dx_o L^2 + 2x_o^2 dx_o + 2x_o y_o dy_o + 2x_o z_o dz_o}{4L^3 + 6L(x_o dx_o + y_o dy_o + z_o dz_o)} \\ \cos \beta &= \frac{y_o + dy_o}{L_c} = \frac{4y_o L^2 + 4dy_o L^2 + 2y_o x_o dx_o + 2y_o^2 dy_o + 2y_o z_o dz_o}{4L^3 + 6L(x_o dx_o + y_o dy_o + z_o dz_o)} \\ \cos \gamma &= \frac{z_o + dz_o}{L_c} = \frac{4z_o L^2 + 4dz_o L^2 + 2z_o x_o dx_o + 2z_o y_o dy_o + 2z_o^2 dz_o}{4L^3 + 6L(x_o dx_o + y_o dy_o + z_o dz_o)} \end{aligned} \quad 3.38$$

Employing the constitutive relationship between the tensile force of the bar and its elongation can be set up in the form:

$$e = \frac{TL}{EA_o} \quad 3.39$$

where  $E$  is the modulus of elasticity and  $A_o$  is the cross-sectional area of the cable. Via equalizing both Eqs. 3.35 and 3.39, the general analytical equation for geometrically non-linear cable and pin-jointed structures are formulated as below:

$$\left\{ \left( \frac{4L^2 + 3(2x_o dx_o + 2y_o dy_o + 2z_o dz_o + dx_o^2 + dy_o^2 + dz_o^2)}{4L^2 + (2x_o dx_o + 2y_o dy_o + 2z_o dz_o + dx_o^2 + dy_o^2 + dz_o^2)} \right) - 1 \right\} - \frac{T}{EA_o} = 0 \quad 3.40$$



For justification and presentation of the precision of the proposed non-linear approach, seven numerical examples from the quoted literature have been examined. Then the results were compared with the findings of the previous analysis techniques.

### 3.3.1 Two-Linked Structure

The two linked structure is pre-tensioned by 4448.2 N, as shown in Fig. 3-13. Each link has  $EA_o = 546920$  N, which is examined via the present technique. The middle joint vertical displacement and each internal bar force showed -166.457 mm and 303.193 N, respectively. Accordingly, the analysis of the same structure was presented by Kwan (1998) as -166.449 mm and 303.246 N for the same target correspondingly. Besides, Levy and Spillers (2003) reported -166.536 mm and 303.413 N, respectively. The outcomes showed that the current approach has a discrepancy of only 0.004% and 0.04% in displacement with Kwan (1998) and Levy and Spillers (2003), respectively. At the same time, the tensile force deviations were only 0.02% and 0.07%.

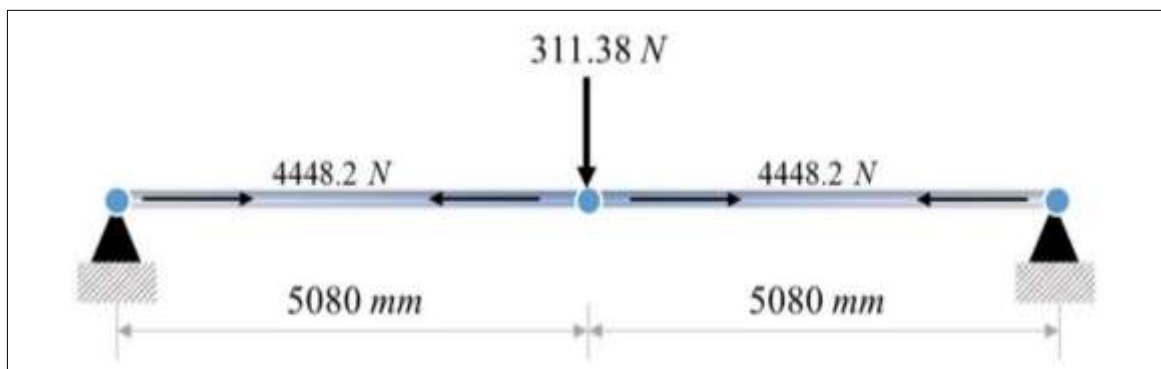


Fig. 3-13 Two-linked structure

### 3.3.2 Flat Cable-Net Structure

Figure 3-14 shows a  $3 \times 3$  square grid of flat cable-net structure, which has been numerically evaluated by numerous studies (Toklu *et al.*, 2017; Kwan, 1998; Lewis, 1987). It has a 400 mm length of cell sides, EA of 97970 N, and prestressed with 200 N. The system has 12 joints. It is supported at its perimeter from 8 joints, leaving 4 inner joints free. It was loaded by 15 N at three positions, as shown in Fig. 3-14. The present formulation is applied to the flat cable-net system and then compared with the literature. The results are presented in Table 3-10 and Table 3-11 for the joint displacements and cable tensions, respectively, which are very accurate with the other techniques.

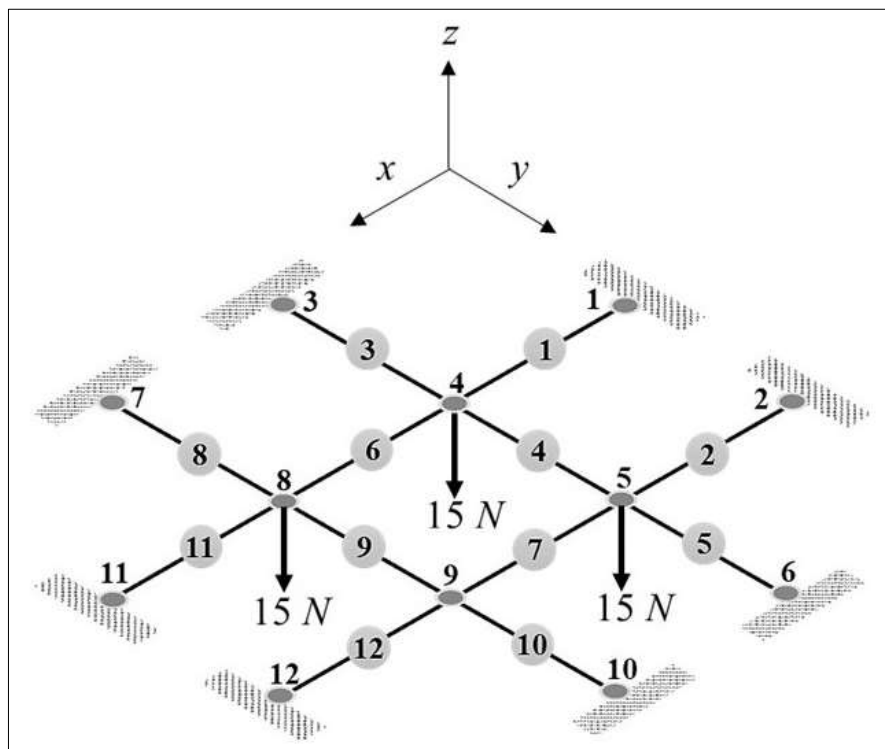


Fig. 3-14 Flat cable-net structure

Table 3-10 Nodal displacement (mm) for internal joints of the flat cable-net

Node	Present Technique			Kwan (1998)			Lewis (1987)			Toklu <i>et al.</i> (2017)		
	$dx$	$dy$	$dz$	$dx$	$dy$	$dz$	$dx$	$dy$	$dz$	$dx$	$dy$	$dz$
4	-0.07	-0.07	-12.17	-0.08	-0.08	-12.2	-0.1	-0.1	-12.2	-0.07	-0.07	-12
5	-0.08	0.04	-11.18	-0.08	0.05	-11.2	-0.1	0	-11.2	-0.08	0.04	-11
8	0.04	-0.08	-11.18	0.04	-0.08	-11.2	0	-0.1	-11.2	0.04	-0.08	-11
9	-0.04	-0.04	-5.59	-0.04	-0.04	-5.59	0	0	-5.6	-0.04	-0.04	-5.6

Table 3-11 Cable tensile forces (N) of the flat cable-net

Cable	Present technique	Kwan (1998)	Lewis (1987)
1	227.97	227.97	228.10
2	219.19	219.19	219.30
3	227.97	227.98	-
4	227.94	227.94	228.00
5	228.00	228.01	228.10
6	227.94	227.94	219.20
7	219.14	219.15	219.10
8	219.19	219.19	-
9	219.14	219.15	-
10	219.07	219.08	219.10
11	228.00	228.01	-
12	219.07	219.08	-

### 3.3.3 Spatial Net Structure

In this example, a spatial cable-net structure consists of a grid system with 24 m in the x-direction and 16 m in the y-direction, as shown in Fig. 3-15. It has 38 cables with  $EA_o$  of  $56 \times 10^6$  N and  $19.2 \times 10^6$  N in x and y-directions, respectively. Due to its central symmetry, the z-direction coordinates (z-coor.) are given for only a quarter of the structure, as presented in Table 3-12. The system is pre-tensioned by 90,000 N in the x-direction and 30,000 N in the y-direction (Toklu *et al.*, 2017; Kwan, 1998; Lewis, 1987). The present technique was applied to obtain the displacements after applying the vertical point loads

of 6800 N at all internal joints. The attained displacements were compared with the numerical findings by Lewis (1987), Abad *et al.* (2013) and Toklu *et al.* (2017), as presented in Table 3-12. These results confirmed a remarkable similarity with the established techniques.

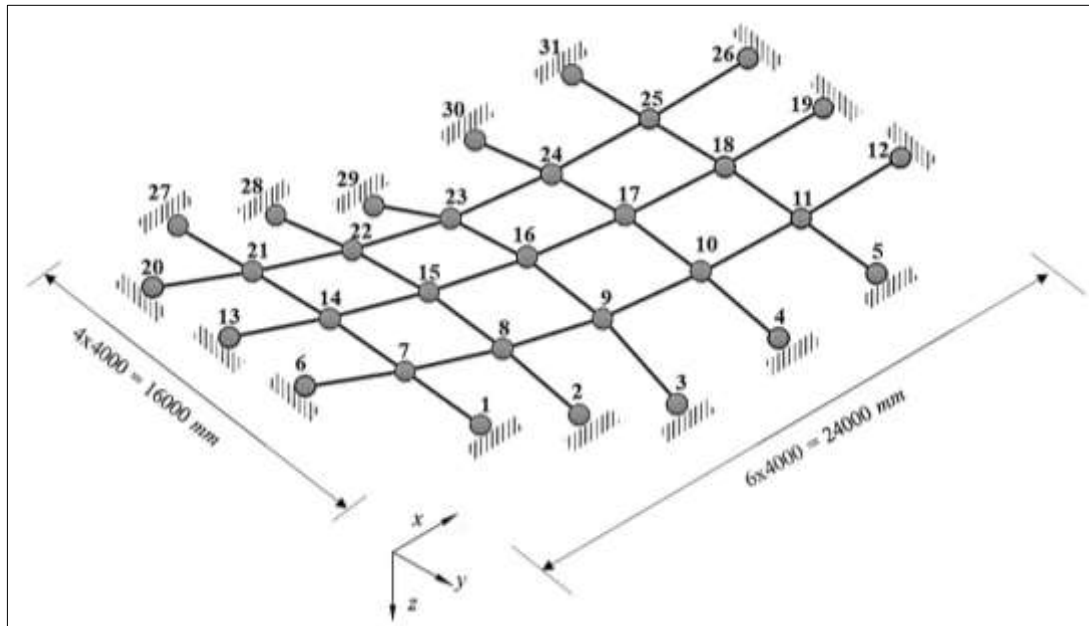


Fig. 3-15 Spatial net structure

Table 3-12 Nodal displacements comparison (mm) of the spatial net

Node	z- coord.	Present Technique			(Lewis, 1987)			Abad <i>et al.</i> (2013)			Toklu <i>et al.</i> (2017)		
		dx	dy	dz	dx	dy	dz	dx	dy	dz	dx	dy	dz
1	1000	-	-	-	-	-	-	-	-	-	-	-	-
2	2000	-	-	-	-	-	-	-	-	-	-	-	-
3	3000	-	-	-	-	-	-	-	-	-	-	-	-
6	0	-	-	-	-	-	-	-	-	-	-	-	-
7	819.5	-5.03	0.40	29.47	-5.14	0.42	30.41	-5.05	0.40	29.6	-5.03	0.40	29.46
8	1409.6	-2.23	0.40	17.12	-2.26	0.47	17.70	-2.23	0.40	17.16	-2.22	0.39	17.18
9	1676.9	0	2.39	-3.19	0	-2.27	-3.62	0	-2.36	-3.19	0	-3.12	-3.19
13	0	-	-	-	-	-	-	-	-	-	-	-	-
14	687.0	-4.93	0	42.88	-4.98	0	43.49	-4.93	0	42.94	-4.92	0	42.84
15	1147.8	-2.55	0	44.32	-2.55	0	44.47	-2.55	0	44.34	-2.55	0	44.27
16	1317.6	0	0	42.14	0	0	41.65	0	0	42.14	0	0	42.08

### 3.3.4 Quarter Hyperbolic Paraboloid Net Structure

Fig. 3-16 shows a quarter of the hyperbolic paraboloid net system consisting of 31 cables and 26 joints with 36 degrees of freedom. The axial stiffness of all members is 100200 N. The structure is concentrically loaded by 15.7 N in the z-direction at all internal nodes except 17, 21, and 22. The cable segments carry the amount of 200 N of pretension force. Several authors (Lewis *et al.*, 1984; Lewis, 1987; Kwan, 1998; Thai and Kim, 2011; Toklu *et al.*, 2017) have numerically and experimentally examined this net system via utilising different analysis techniques. For example, Dynamic relaxation (DR), which is used by Lewis (1989) and Kwan (1998), while approximation of Taylor series (ATS), elastic catenary cable element in finite element, and total potential optimisation were used by Thai and Kim (2011) and Toklu *et al.* (2017), respectively. The results for the vertical displacements of the current and previously published methods are presented in Table 3-13. It showed great accuracy and similitude of the current findings compared to the highlighted approaches.

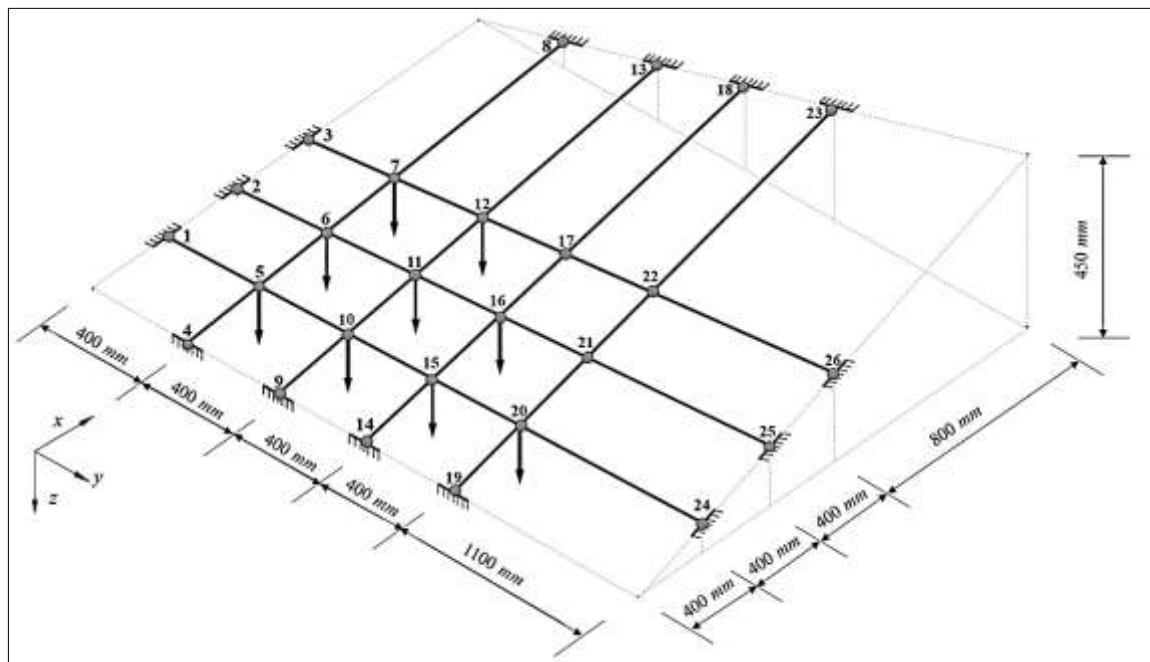


Fig. 3-16 Hyperbolic paraboloid net structure

Table 3-13 Nodal displacements comparison (mm) in the z-direction of hyperbolic paraboloid net

Node	Present technique	Lewis <i>et al.</i> (1984) Experiment	Lewis <i>et al.</i> (1984) DR	Kwan (1998) DR	Kwan (1998) ATS	Thai and Kim (2011)	Toklu <i>et al.</i> (2017)
5	19.53	19.50	19.30	19.38	19.52	19.56	19.48
6	24.66	25.30	25.30	25.62	25.35	25.70	25.59
7	23.32	22.80	23.00	22.95	23.31	23.37	23.17
10	25.88	25.40	25.90	25.57	25.86	25.91	25.75
11	34.08	33.60	33.80	33.79	34.05	34.16	33.86
12	29.52	28.80	29.40	29.32	29.49	29.60	29.27
15	25.81	25.20	26.40	25.43	25.79	25.86	25.65
16	31.33	30.60	31.70	31.11	31.31	31.43	30.96
17	21.43	21.00	21.90	21.28	21.42	21.56	21.03
20	21.49	21.00	21.90	21.16	21.48	21.57	21.33
21	20.01	19.80	20.50	19.79	20.00	20.14	19.67
22	14.41	14.20	14.80	14.29	14.4	14.55	14.04

### 3.3.5 Saddle Net Structure

The preliminary geometry of the saddle net structure, as shown in Fig. 3-17, consists of 142 cables with  $EA_o = 44.982 \times 10^6$  N and 95 joints, of which 32 of them are constrained at the perimeter. It has mirror symmetry about both centrelines, each segment has a 5000 mm distance in both x and y-directions, and the z-coordinates (z-coor.) for the one-fourth of the structure are given in Table 3-14. The saddle net structure was completed by a tensile prestressing force of 60,000 N and was affected by concentrated loads of 1000 N in x- and y-directions at the half of free nodes (11-15, ..., 66-70, and 77-81). The analysis of the proposed method is presented in Table 3-14. After comparison with the previous approaches of (Lewis, 1989; Kwan, 1998), Thai and Kim (2011), and both discrete and continuous catenary cable models by Abad *et al.*

(2013), it showed good accuracy and was verified to be comparable with the well-known methods. The maximum percentage of error for the present technique, Kwan (1998) and Thai and Kim (2011), as compared to experimental work performed by Lewis (1989), did not exceed 3.87%, while they were 5.81% and 4.91% for the discrete and continuous models of Abad *et al.* (2013), respectively, as presented in Table 3-14. In most of the studies, the saddle net is introduced as the most complex cable structure and outstanding comparable problem. It is used to confirm the effectiveness of the analysis techniques as Lewis (1987) reported that the analysis of saddle net failed in using the finite element method due to the ill-condition issue for such complicated assembly.

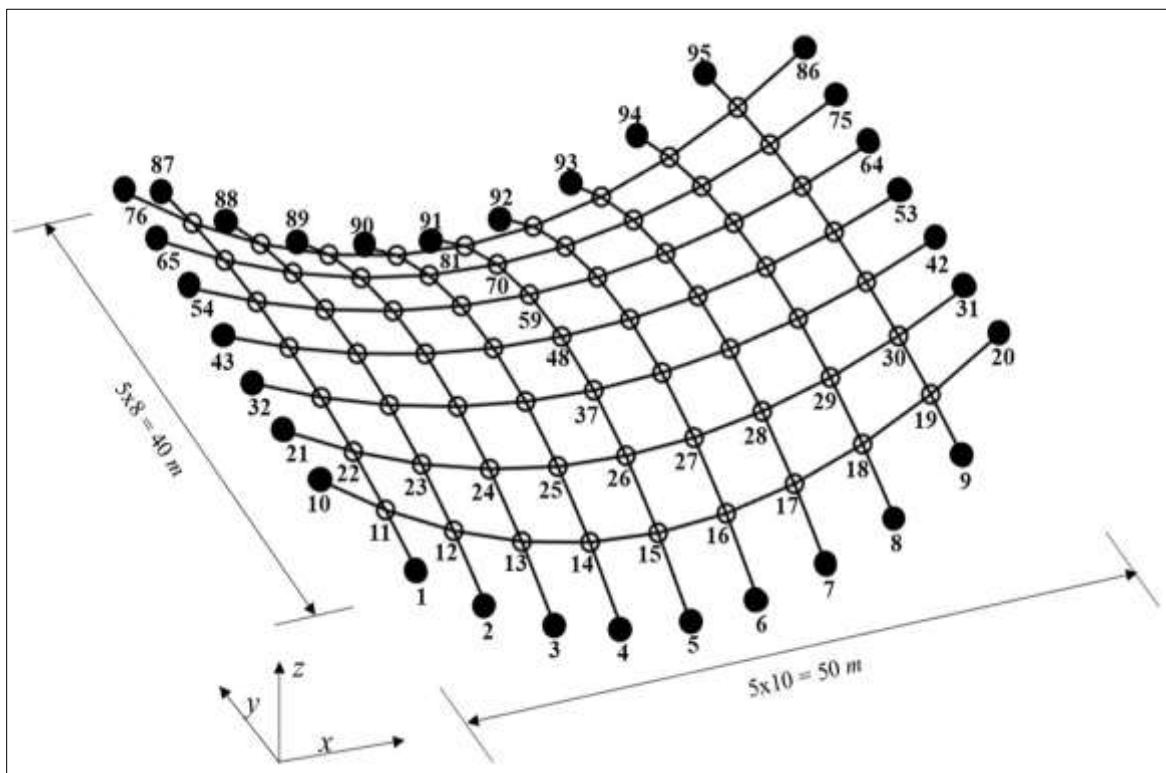


Fig. 3-17 Saddle net structure

Table 3-14 Nodal displacements comparison (mm) of saddle net

Nod	z-coor.	Lewis (1987a) experiment	Present technique	Kwan (1998b)	Thai and Kim (2011)	Abad <i>et al.</i> (2013) discrete	Abad <i>et al.</i> (2013) continuous
1	3632	0	0	0	0	0	0
2	2568	0	0	0	0	0	0
3	1808	0	0	0	0	0	0
4	1352	0	0	0	0	0	0
5	1200	0	0	0	0	0	0
10	5000	0	0	0	0	0	0
11	3968	83.53	83.28 (0.29)	83.28 (0.29)	83.24 (0.34)	83.46 (0.08)	83.38 (0.17)
12	3165	62.85	62.55 (0.48)	62.54 (0.49)	62.5 (0.56)	62.68 (0.27)	62.6 (0.4)
13	2592	34.57	34.38 (0.55)	34.38 (0.55)	34.34 (0.67)	34.47 (0.29)	34.43 (0.4)
14	2248	19	18.92 (0.42)	18.92 (0.42)	18.91 (0.47)	19.02 (-0.11)	18.96 (0.21)
15	2133	12.27	12.21 (0.49)	12.22 (0.41)	12.21 (0.49)	12.29 (-0.16)	12.26 (0.08)
21	5000	0	0	0	0	0	0
22	4208	98.4	98.27 (0.13)	98.27 (0.13)	98.23 (0.17)	98.57 (-0.17)	98.42 (-0.02)
23	3592	74.02	73.9 (0.16)	73.9 (0.16)	73.84 (0.24)	74.17 (-0.2)	74.03 (-0.01)
24	3152	32.84	32.93 (-0.27)	32.93 (-0.27)	32.89 (-0.15)	33.14 (-0.91)	33.03 (-0.58)
25	2882	11.88	12.15 (-2.27)	12.15 (-2.27)	12.14 (-2.19)	12.33 (-3.79)	12.24 (-3.03)
26	2800	12.68	12.32 (2.84)	12.32 (2.84)	12.32 (2.84)	12.12 (4.42)	12.21 (3.71)
32	5000	0	0	0	0	0	0
33	4352	93.19	93.19 (0)	93.19 (0)	93.15 (0.04)	93.56 (-0.4)	93.38 (-0.2)
34	3848	67.56	67.65 (-0.13)	67.65 (-0.13)	67.6 (-0.06)	68.02 (-0.68)	67.84 (-0.41)
35	3488	20.81	21.2 (-1.87)	21.2 (-1.87)	21.16 (-1.68)	21.51 (-3.36)	21.36 (-2.64)
36	3272	15.49	14.89 (3.87)	14.89 (3.87)	14.89 (3.87)	14.59 (5.81)	14.73 (4.91)
37	3200	36.85	36.09 (2.06)	36.09 (2.06)	36.07 (2.12)	35.77 (2.93)	35.9 (2.58)
43	5000	0	0	0	0	0	0
44	4400	-	89.36	89.36	89.31	89.75	89.56
45	3933	-	63.44	63.44	63.38	63.84	63.65
46	3600	-	15.16	15.16	15.12	15.49	15.34
47	3400	-	22.99	22.99	22.99	22.65	22.80
48	3333	-	46.11	46.12	46.09	45.74	45.89
52	4400	-	5.93	5.93	5.93	6.34	6.17
72	3152	-	30.37	30.38	30.36	30.07	30.19
81	2133	-	12.21	12.22	12.21	12.29	12.26
85	3968	-	32.67	32.67	32.65	32.89	32.79
85	3968	-	32.67	32.67	32.65	32.89	32.79

( ) shows the error percentage of the proposed technique and other quoted techniques concerning Lewis's experimental work.



### 3.3.6 Cantilever Truss Structure

A simple cantilever truss, as shown in Fig. 3-18, consists of six nodes and ten bars with an axial stiffness of 400,000 N. It is pin-supported at node number one and roller-supported at node number two. The two external point loads are applied on nodes 3 and 5 with quantities of 1000 N and 3000 N in the gravity direction, respectively. The cantilever truss has been previously used by (Saeed and Kwan, 2016b) using the linear force method. The linear analysis results were obtained using the least squares solution. The proposed nonlinear force method is applied for analyzing the same cantilever truss, and both of the findings are presented in Table 3-15. SAP2000 software is also used for the purpose of comparison, precision, and validation of the results. The output of the software analysis is basically based on finite element analysis with an improved tangent stiffness matrix, and the results for displacement and member forces are presented in columns 2-4 in Table 3-15.

To assess the proposed method's accuracy and utility, the Euclidean Norm index for internal forces (linear and nonlinear) error to internal force from SAP2000 is used. The accuracy evaluation ratio ( $RT$ ) of  $l_2$ -Norm is found using Eq. 3.29, where  $T1$  and  $T2$  are the member forces of the linear force method and SAP2000, respectively. The percent Euclidian norm ratio between linear and SAP2000 was 2.23%, while between the proposed technique and SAP2000, it was 0.05%. These ratios clearly show the precision of the present approach in considering the geometric nonlinearity during the analysis stage of spatial structures.

Further, it can be noticed that neglecting the geometric deformability in the linear force method leads to giving the internal force of bar number 7 as zero. That is due to using the equilibrium matrix in its original configuration

and the zero coefficient of the state of self-stress found in the null of the equilibrium matrix.

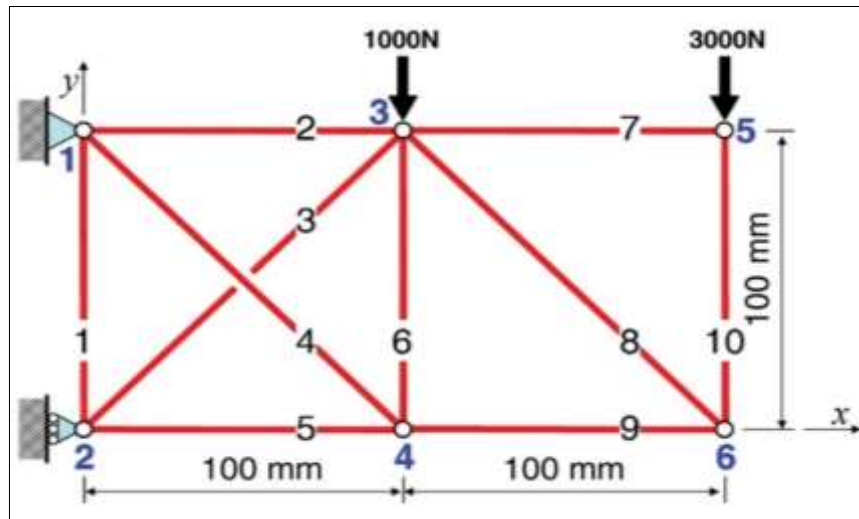


Fig. 3-18 Cantilever truss structure with nodal labels, panels spacing, and nodal loads

Table 3-15 Nodal displacements and internal bar forces of the cantilever truss by SAP2000, linear and nonlinear force methods

Nodes	Nonlinear Analysis by SAP2000			Linear Analysis by Saeed and Kwan (2016b)			Nonlinear Analysis present Study			Bars
	Nonlinear Displacement (mm)		Member Force (N)	Linear Displacement (mm)		Member Force (N)	Nonlinear Displacement (mm)		Member Force (mm)	
	$dx$	$dy$		$dx$	$dy$		$dx$	$dy$		
2	0	-0.465	1858.4	0	-0.500	2000	0	-0.465	1858.5	1
			5105.6			5000			5107.4	2
3	1.227	-3.149	-2836.8	1.250	-3.164	-2828	1.228	-3.150	-2837.8	3
			2751.8			2828			2752.4	4
4	-1.265	-2.604	-4967.4	-1.250	-2.664	-5000	-1.266	-2.605	-4970	5
			-2055.8			-2000			-2056	6
5	1.061	-9.334	98.3	1.250	-9.286	0	1.061	-9.335	98.683	7
			4304.7			4243			4303.1	8
6	-2.195	-8.532	-3012.1	-2.000	-8.536	-3000	-2.195	-8.533	-3009.4	9
			-2995.5			-3000			-2993.9	10
Euclidian Norm Ratio				<i>RTI</i>		2.23%	<i>RT</i>		0.05%	

### 3.3.7 Double Layer Spherical Structure

For apprising the validity of the proposed technique, a very complicated structure is selected. The spherical double-layer model (Mahmood *et al.*, 2022) shown in Fig. 3-19 is analysed using the technique presented in the previous section. The outer diameter of the sphere is 8000 mm and the distance between both layers is 200 mm. The model consists of 382 nodes, that 21 nodes of the outer layer from the bottom on a diameter of 1174 mm are pin supports as shown in Fig. 3-20. It has 1520 members. The axial stiffness of all the members is 15707963.3 N. The model is laterally loaded in the x-direction by 1000 N at 73 nodes on the outer surface as shown in Fig. 3-20. The lateral loads produced noticeable deformability in all of the x-, y-, and z- directions.

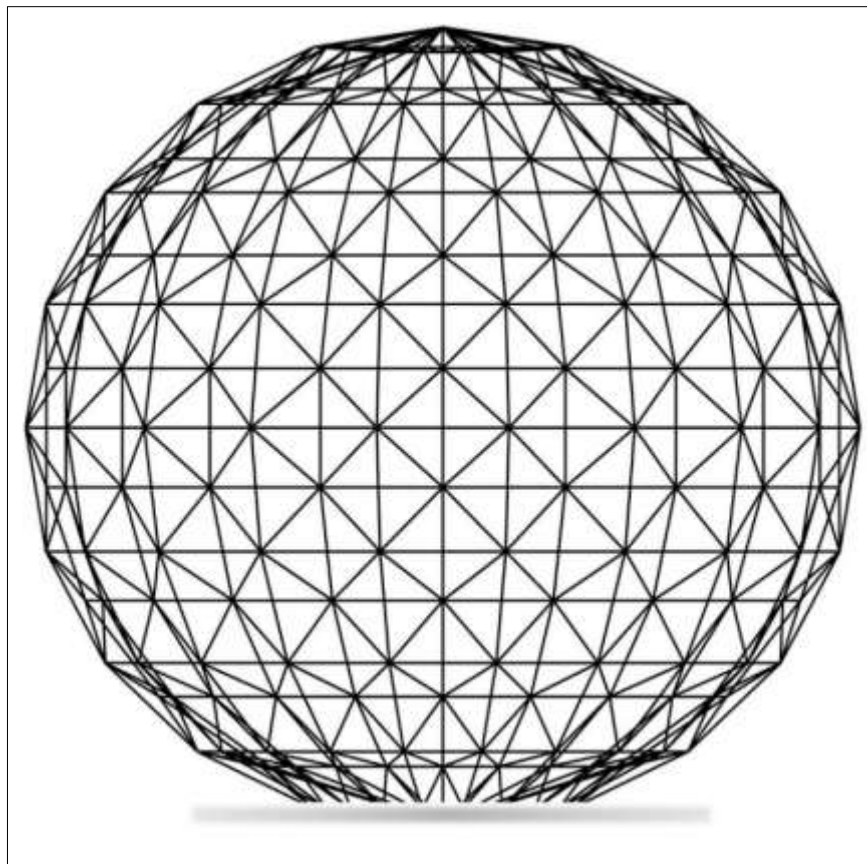


Fig. 3-19 Double-layer spherical model

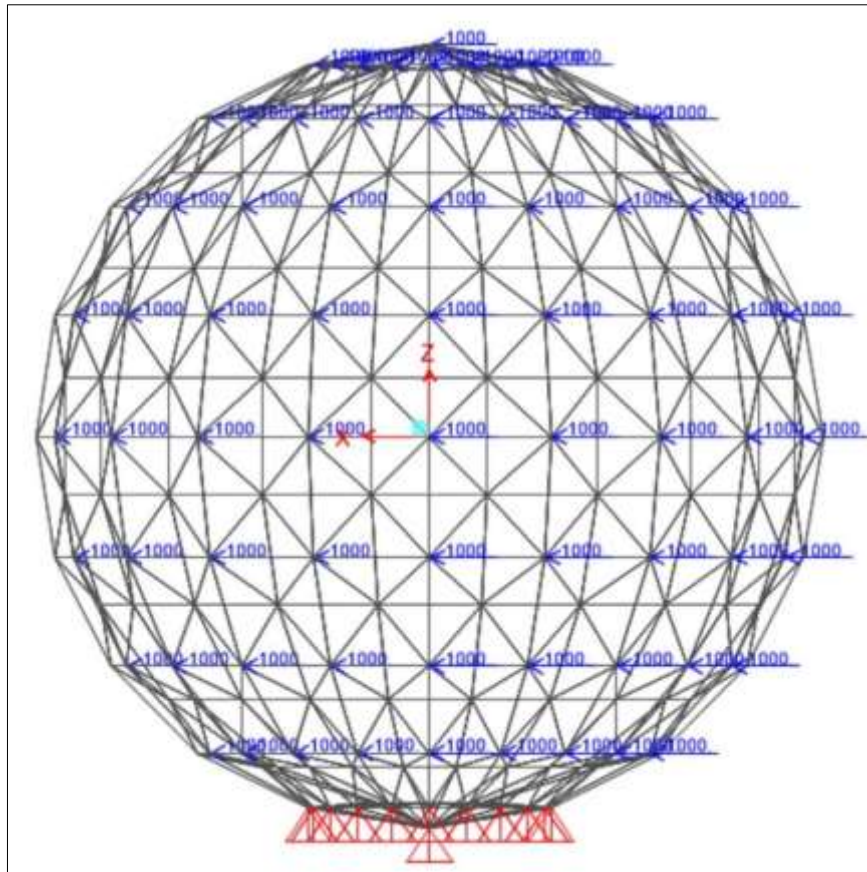


Fig. 3-20 Supports and laterally load in (N) of double-layer spherical model

The maximum axial force for this specifically applied load is located at members 862 as 45.456 kN, and 857 as -45.456 kN (Mahmood *et al.*, 2022). The present technique determined tensile 45.282 kN and compressive 45.643 kN for members 862 and 857 respectively, which are almost equal to the SAP2000 results with values 45.281 kN, -45.642 kN for the same members.

The difference of maximum member forces between the present approach and SAP2000 analysis (SNF) and also between linear technique and SAP2000 findings (SLF), were computed. The difference value between nonlinear techniques (SNF) is 0.001 N, while for SLF is 0.175 N for member 862 and 0.186 N for member 857 N. These similarities between nonlinear techniques are due to the impact of geometrical stiffness on the member force computation and vice versa.

The analysis results for the displaced selected nodes in the x-, y-, and z- directions via applying the current technique are presented in columns 2-4 of Table 3-16. Similarly, the model was analysed by nonlinear finite element analysis using SAP2000. The findings are presented in columns 5-7 of Table 3-16. Both nonlinear analysis results are in very well agreement with each other. Later, they compared with linear analysis result by Mahmood *et al.* (2022) as shown in columns 8-10 of Table 3-16.

The Euclidean norm ratio is used to find out the difference rate between the nonlinear displacement and the linear displacement. The difference rate is about 0.11%, and this rate will increase when the model faces greater loading values for the same loading condition. Moreover, the differences in resultant displacements between SAP2000 and the present non-linear technique (SND), as well as between SAP2000 and the linear technique (SLD), are evaluated. The difference between the non-linear techniques (SND) is negligible across all joints, with a maximum value of 0.002 mm. In contrast, the difference associated with the linear technique (SLD) is significant, with a maximum value of 0.146 mm, highlighting the limitations of neglecting geometric nonlinearity. Accounting for the geometric nonlinearity in systems exhibiting such behaviour yields more accurate results, particularly under conditions of large deformations.

Table 3-16 Nodal displacement of double-layer spherical model

Nodes	Present Technique (mm)			SAP2000 (mm)			Linear FM (mm)		
	$dx$	$dy$	$dz$	$dx$	$dy$	$dz$	$dx$	$dy$	$dz$
1-20	0	0	0	0	0	0	0	0	0
25	11.358	-1.018	-6.250	11.358	-1.018	-6.250	11.380	-1.050	-6.050
30	8.998	2.336	18.533	8.998	2.336	18.534	8.850	2.370	18.640
35	7.197	0.172	5.817	7.197	0.172	5.817	7.170	0.250	6.040
40	7.308	-1.587	-18.715	7.308	-1.587	-18.716	7.450	-1.570	-18.590
45	23.494	-0.691	-10.299	23.494	-0.691	-10.299	23.540	-0.680	-10.080
50	22.454	2.758	30.767	22.454	2.758	30.768	22.260	2.810	31.000
55	16.828	1.279	9.746	16.828	1.279	9.747	16.780	1.380	10.040
60	19.757	-3.576	-31.181	19.757	-3.576	-31.181	19.930	-3.520	-30.900
70	34.887	3.567	36.626	34.888	3.568	36.627	34.670	3.650	36.930
80	31.494	-4.300	-37.191	31.494	-4.300	-37.192	31.690	-4.220	-36.840
90	47.886	4.000	38.591	47.886	4.000	38.591	47.660	4.120	38.960
95	41.137	1.403	12.228	41.138	1.403	12.229	41.060	1.520	12.650
100	44.200	-4.541	-39.362	44.201	-4.541	-39.362	44.400	-4.430	-38.940
105	63.144	-1.367	-12.450	63.145	-1.367	-12.450	63.190	-1.220	-12.040
110	60.772	3.907	36.623	60.774	3.907	36.624	60.560	4.050	37.060
115	54.336	1.293	11.570	54.336	1.294	11.571	54.260	1.440	12.060
120	57.216	-4.412	-37.603	57.217	-4.412	-37.604	57.400	-4.270	-37.120
125	74.310	-1.252	-10.691	74.312	-1.252	-10.691	74.350	-1.080	-10.220
130	72.188	3.362	30.946	72.190	3.362	30.947	72.010	3.530	31.440
135	66.665	1.075	9.699	66.667	1.075	9.699	66.600	1.250	10.240
140	69.163	-3.867	-32.075	69.165	-3.867	-32.076	69.310	-3.700	-31.540
145	82.627	-1.016	-7.927	82.628	-1.016	-7.927	82.650	-0.820	-7.400
150	81.001	2.439	22.185	81.002	2.439	22.185	80.860	2.630	22.730
155	76.954	0.745	6.800	76.955	0.745	6.800	76.900	0.940	7.390
160	78.835	-2.935	-23.343	78.837	-2.935	-23.343	78.940	-2.740	-22.760
165	87.320	-0.669	-4.435	87.322	-0.669	-4.435	87.320	-0.460	-3.860
170	86.371	1.238	11.259	86.373	1.238	11.259	86.290	1.440	11.840
175	84.205	0.288	3.218	84.207	0.288	3.219	84.160	0.490	3.820
180	85.201	-1.678	-12.411	85.203	-1.678	-12.411	85.240	-1.470	-11.810
382	87.747	-0.211	-0.601	87.749	-0.211	-0.601	87.730	0	0

### 3.4 FORMULATION OF THE PRESERVATION TECHNIQUE

In situations where there is necessity to manage large displacements, particularly in the context of structural non-linearity, it becomes evident that the linear displacement and force control techniques lack precision and accuracy throughout the entirety of the process undertaken to search for a solution conducive to the effective control of large displacements (Li *et al.*, 2017). The formulation of the preservation technique starts by introducing the amount of nonlinear member alteration (shortening or elongation) as  $e_c(d)$ . Referring to elements shown in Fig. 3-1 and Fig. 3-11, the preserving quantity can be formulated with the same employed procedure of deriving Eqs. 3.10, 3.13, and 3.35, which all came from the compatibility relationship as in Eq. 3.3. Setting the element in Fig. 3-1 under preservation, the required member alteration employing Taylor's series (Eq. 3.41) and Pade approximation expansion (Eq. 3.42) can be written as the following:

$$e_c = \frac{x_{j'i'}dx_{j'i'} + y_{j'i'}dy_{j'i'}}{L} - \frac{dx_{j'i'}^2 + dy_{j'i'}^2}{2L} + \frac{x_{j'i'}^2 dx_{j'i'}^2 + y_{j'i'}^2 dy_{j'i'}^2}{2L^3} + \frac{x_{j'i'}y_{j'i'}dx_{j'i'}dy_{j'i'}}{L^3} \quad 3.41$$

$$e_c = \frac{2L(2x_{j'i'}dx_{j'i'} - dx_{j'i'}^2 + 2y_{j'i'}dy_{j'i'} - dy_{j'i'}^2)}{4L^2 - 2x_{j'i'}dx_{j'i'} + dx_{j'i'}^2 - 2y_{j'i'}dy_{j'i'} + dy_{j'i'}^2} \quad 3.42$$

To perform the preservation for displacement, internal member force, and/or displacement and internal force simultaneously, the constitutive relationship between the controlling actuation and the resulting internal force vector can be written as:

$$e_c(d) = Ft_c \quad 3.43$$

where  $t_c$  is the member force attained during the preservation process. Substituting Eqs. 3.41 and 3.42 into Eq. 3.43 yields to Taylor and Pade preservation equations respectively as shown below:

$$\frac{x_{j'i'}dx_{j'i'} + y_{j'i'}dy_{j'i'}}{L} - \frac{dx_{j'i'}^2 + dy_{j'i'}^2}{2L} + \frac{x_{j'i'}^2 dx_{j'i'}^2 + y_{j'i'}^2 dy_{j'i'}^2}{2L^3} + \frac{x_{j'i'}y_{j'i'}dx_{j'i'}dy_{j'i'}}{L^3} - Ft_c = 0 \quad 3.44$$

$$\frac{2L(2x_{j'i'}dx_{j'i'} - dx_{j'i'}^2 + 2y_{j'i'}dy_{j'i'} - dy_{j'i'}^2)}{4L^2 - 2x_{j'i'}dx_{j'i'} + dx_{j'i'}^2 - 2y_{j'i'}dy_{j'i'} + dy_{j'i'}^2} - Ft_c = 0 \quad 3.45$$

Now, the produced member force after prestressing and preservation can be computed by accumulating  $t$  and  $t_c$  as  $T_e$ , and can be expressed in terms of member length alteration as:

$$e_e(d) = FT_e \quad 3.46$$

where  $e_e(d)$  is the change in member length after both the prestressing and preserving processes.

Similarly, the derivation of the  $e_c(d)$  can be generalized to be used with rigid assemblies' preservation. When the element in Fig. 3-12 is affected by external loads ( $P$ ) at both ends, it experiences nodal deformation and member length. If the member is rigid, it does not need to be prestressed by ( $t$ ) and it will be equilibrated by just producing internal ( $T$ ). Therefore,  $T_e$  in Eq. 3.46 is the combination of  $t_c$  and  $T$ . Although  $T_e$  in Eq. 3.46 can be the combination of  $t$ ,  $t_c$ , and  $T$  if the preservation process is performed after applying an external load to the prestressed system.

### 3.4.1 Sensitivity Technique for the Preservation Process

Determining which bars to actuate is a critical point of interest during the preservation procedure. It is imperative to install actuators in structural elements where they will most effectively control future displacements and internal forces, especially when their placement is still undecided during the design phase. A specific technique involves testing the sensitivity of each



member separately by applying a unit of actuation (+1 or -1) to a single member and recording the effect on each nodal displacement and member force. This technique, referred to as bar sensitivity, was previously used by Saeed (2014) to control displacements only. However, using Eq. 3.20 or 3.21 enables observation of each member's impact as an actuator on nodal displacements and member stresses. The effect of member sensitivity can then be evaluated by observing the output to identify which member has the greatest impact on multiple joints and member forces. The sensitivity technique is applied to the cantilever truss shown in Fig. 3-18, and the computed displacements and bar forces are tabulated in Tables 3-17 and 3-18, respectively.

For example, if a 1 mm shortening is applied to the member labeled 7, it results in a displacement of -0.999 mm in the x-direction and -0.005 mm in the y-direction at node 5. It has no effect on the other joints, as shown in Table 3-17, and on the member forces, as shown in Table 3-18.

Table 3-17 Computed nodal displacements based on the bar sensitivity technique

Actuator No.	$e_c$ (mm)	Displacement (mm)								
		$dy_2$	$dx_3$	$dy_3$	$dx_4$	$dy_4$	$dx_5$	$dy_5$	$dx_6$	$dy_6$
1	-1	0.896	0.103	0.499	0.103	0.397	0.103	0.499	0.103	0.499
2	-1	-0.104	-0.897	0.494	0.102	0.396	-0.902	1.492	0.096	1.497
3	-1	0.146	-0.149	-0.709	-0.149	-0.562	-0.149	-0.709	-0.149	-0.709
4	-1	0.146	-0.149	0.709	-0.149	0.855	-0.149	0.708	-0.149	0.708
5	-1	-0.104	0.102	-0.499	-0.897	-0.598	0.097	-1.497	-0.901	-1.492
6	-1	-0.103	0.103	-0.499	0.103	0.397	0.103	-0.504	0.099	-0.504
7	-1	0	0	0	0	0	-0.999	-0.005	0	0
8	-1	0	0	0	0	0	-0.010	1.409	-0.010	1.409
9	-1	0	0	0	0	0	-0.005	-0.999	-1.004	-0.995
10	-1	0	0	0	0	0	-0.005	-0.999	0	0

Table 3-18 Computed member forces based on the bar sensitivity technique

Actuator No.	$e_c$ (mm)	Member Force (N)									
		$t_1$	$t_2$	$t_3$	$t_4$	$t_5$	$t_6$	$t_7$	$t_8$	$t_9$	$t_{10}$
1	-1	415.76	415.76	-586.51	-586.51	415.76	411.61	0	0	0	0
2	-1	415.78	415.76	-586.50	-586.51	411.61	415.75	0	0	0	0
3	-1	-584.75	-584.74	824.02	829.89	-584.74	-584.75	0	0	0	0
4	-1	-584.75	-584.74	829.89	824.02	-584.74	-584.75	0	0	0	0
5	-1	415.78	411.61	-586.51	-586.50	415.76	415.75	0	0	0	0
6	-1	411.61	415.76	-586.51	-586.51	415.76	415.76	0	0	0	0
7	-1	0	0	0	0	0	0	0	0	0	0
8	-1	0	0	0	0	0	0	0	0	0	0
9	-1	0	0	0	0	0	0	0	0	0	0
10	-1	0	0	0	0	0	0	0	0	0	0

### 3.4.2 Validation of the Preservation Technique

The precision of the proposed preservation technique is validated through numerical examples using rigid and flexible spatial structures and later through an experimental model (see Chapter 4). The preservation process has been applied, considering geometrical preservation and member force preservation separately and simultaneously.

#### 3.4.2.1 Displacement preservation without concern for member force

The displacement preservation is now being applied on the simple cantilever truss as shown in Fig. 3-18. The results of displacements during the analysis stage are presented in Table 3-15 (columns 5 and 6). The vertical displacements of unsupported joints (3 and 5) at the top of the truss are identified to be of interest. Thus, the target of preservation is defined to adjust the displacement to (-2 mm) under the applied load instead of -3.164 mm and -9.286 mm for nodes 3 and 5, respectively. The outcome of the process is tabulated in Table

3-19, then compared with the linear technique by Saeed and Kwan (2016b). The desired target of displacement was accomplished with total amount of actuation of 8.768 mm using Pade preservation equation, and 8.764 mm using Taylor preservation equation. Comparing the sum of the total actuation for attaining this prescribed vertical displacement gives a very good agreement with the linear approach. The total nonlinear actuation for the preservation process showed a discrepancy ratio of 0.44% and 0.39% when using Eqs. 3.44 and 3.45 compared to linear preservation. This discrepancy arises due to the consideration of geometric nonlinearity and equilibrium in the deformed configuration.

Members 2 and 3 are chosen as actuators because they significantly impact raising the displaced vertical joints. As shown in Table 3-17 (columns 5 and 9), shortening member 2 by 1 mm raises nodes 3 and 5 by 0.494 mm and 1.492 mm, respectively. In contrast, member 3 has the opposite effect, preventing node 3 from rising more than required.

Table 3-19 Displacement of the cantilever truss after preservation process using present technique in comparison to the linear technique by Saeed and Kwan (2016c)

Nodes	Linear preservation			Nonlinear preservation of the present study					Bars	
	Saeed and Kwan (2016b)		$e_c$ (mm)	Eq. 3.44		$e_c$ (mm)	Eq. 3.45			$e_c$ (mm)
	$dx$	$dy$		$dx$	$dy$		$dx$	$dy$		
2	0	-0.74	0	0	-0.750	0	0	-0.750	0	1
			-6.121			-6.111			-6.115	2
3	-4.630	-2	-2.682	-4.582	-2	-2.653	-4.582	-2	-2.653	3
			0			0			0	4
4	-1.009	-1741	0	-0.996	-1.717	0	-0.996	-1.717	0	5
			0			0			0	6
5	-4.630	-2	0	-4.395	-2	0	-4.394	-2	0	7
			0			0			0	8
6	-1.759	-1.250	0	-1.573	-1.263	0	-1.574	-1.263	0	9
			0			0			0	10
Total $e_c$			8.803			8.764			8.768	

### 3.4.2.2 Member force preservation without concern for joint displacement

Controlling forces in some structures is more important than minimising shape disturbances, such as preventing buckling in truss members or slack in cable systems. Similarly, the same cantilever truss in 18 is tested numerically using the present approach and compared to work by Saeed and Kwan (2016b). The analysis of member forces resulting from the applied loads is presented in Table 3-15. It was reported by Saeed and Kwan (2016b) that bars 2, 5, and 8 experienced the greatest forces, with values of 5000 N, -5000 N, and 4243 N, respectively. Thus, the target is to control these member forces.

The first aspect to consider is the computed member force for the column labeled  $t_8$  in Table 3-18, where all values are zero. This indicates that the member force  $t_8$  is independent of  $e_o$ . Similarly, bars 7, 9, and 10 on the right side of the cantilever truss are unaffected by  $e_o$  and cannot be prestressed or controlled. Therefore, they experience stress only from the applied loads.

Members 2 and 5 exhibit a similar response to member actuation, as observed in Table 3-18 when they are at their original positions. Therefore, any change in  $e_o$  results in a parallel effect on both members simultaneously, with both being reduced or increased together. The greatest effect on members 2 and 5 can be achieved by using members 3 and 4 as actuators, either separately or together, as they are associated with the maximum member force for bars 2 and 5. The findings of member forces after the preservation process for controlling member forces are presented in the Table 3.20. The target by Saeed and Kwan (2016b) was an increase of +1000 N for both members to achieve -4000 N and 6000 N for bars 2 and 5, respectively. The computed bar force was 5976 N for bar 2 and -4000 N for bar 5, with total actuation of 1.6928 mm and 1.6702 mm when bar 3 and bar 4 were used separately as actuators, respectively. However,

when both bars 3 and 4 were used together, the target was achieved with 1.6856 mm of actuation.

The computed nonlinear member force 2 using the proposed technique is less than that obtained by the linear method by Saeed and Kwan (2016b). This is attributed to the derived technique's capability to compute nonlinear member alterations after deformation has occurred and equilibrium has been achieved in the deformed configuration. Additionally, member force 2 could reach up to 6000 N, but this would cause member 5 to approach -3975 N if member 4 were selected and actuated by 1.7119 mm. This finding suggests that linear analysis underestimates internal bar forces by neglecting the stress induced by the length alterations of other bars. A similar conclusion was reported by Du Pasquier and Shea (2022) when comparing linear and nonlinear adjustments in morphing structures.

Table 3-20 Internal force of the cantilever truss after preservation process in comparison to the linear technique by Saeed and Kwan (2016c)

Bar No.	Linear preservation		Nonlinear preservation of present study					
	Saeed and Kwan (2016b)		Eq. 3.44 and Eq. 3.45					
	$t_c$ (N)	$e_c$ (mm)	$t_c$ (N)	$e_c$ (mm)	$t_c$ (N)	$e_c$ (mm)	$t_c$ (N)	$e_c$ (mm)
1	3000		2983		2984		2983	
2	6000		5975		5975		5975	
3	-4243	1.7070	-4223	1.6928	-4207		-4214	0.7880
4	1414		1430		1413	1.6702	1421	0.8976
5	-4000		-4000		-4000		-4000	
6	-1000		-1008		-1008		-1008	
7	0		0		0		0	
8	4243		4243		4243		4243	
9	-3000		-3000		-3000		-3000	
10	-3000		-3000		-3000		-3000	
Total $e_c$ (mm)		1.7070		1.6928		1.6702		1.6856

### 3.4.2.3 Simultaneous preservation of joint displacement and member force

An important feature of comprehensively controlling structural performance involves understanding the relationship between structural geometry and force distribution. In practical considerations for some structures, it is highly desirable to control both shape and internal stress simultaneously, preserving members from failure while maintaining their appearance without disturbance. The present technique is validated on the structure in Fig. 2-3, previously used by You (1997). The target is to control the displacement of joint 6 by restoring it to its original position while ensuring that the prestressing level remains unchanged. Joint 6 was successfully restored to its position in two scenarios. In Case I, small displacements for joint 6 were restored both numerically and experimentally, as reported by You (1997). In Case II, the same cable net shown in Fig. 2-3 was used, but with assumed displacements of -20 mm and 20 mm in the x- and y-directions, respectively, following the numerical studies of Xu and Luo (2009), and Saeed (2022).

#### *A. Case I: small displacement*

In the first case of simultaneous displacement and internal force preservation, small displacements were employed for validation. During the prestressing stage, as studied by You (1997), node 6 was displaced by 2.56 mm in the x-direction and -4.31 mm in the y-direction as a result of actuating cables vii, viii, and ix by -5.02, 4.49, and -5.02, respectively. Here, the cable net is indicated to have the same prestressed amount and nodal displacement as reported by You (1997), to highlight the differences during the preservation stage alone. The preservation findings for displacements and internal cable forces are presented in Table 3-21 and Table 3-22, respectively. The nonlinear technique

achieved the target with a difference rate of 1.35 % of total actuation while maintaining the prestressing level above the initial state.

Table 3-21 Displacement of the cable net structure after preservation process in comparison to the linear technique by You (1997)

Node No.	Direction	Displacement before preservation (mm)	Displacement after preservation (mm)			
			You (1997)		present study	
			$d_c$	$d_e$	$d_c$	$d_e$
2	$dx_2$	0	0.29	0.29	0.17	0.17
	$dy_2$	-6.66	-7.26	-13.92	-7.10	-13.76
5	$dx_5$	-2.56	-2.78	-5.34	-2.64	-5.20
	$dy_5$	-4.31	-4.19	-8.50	-4.18	-8.49
6	$dx_6$	2.56	-2.56	0	-2.56	0
	$dy_6$	-4.31	4.31	0	4.31	0

Table 3-22 Internal force of the cable net structure after preservation process technique in comparison to the linear technique by You (1997)

Cable No.	Cable prestress	Linear preservation by You (1997)			Nonlinear preservation of present study		
		$e_c$ (mm)	$t_c$ (N)	$T_e$ (N)	$e_c$ (mm)	$t_c$ (N)	$T_e$ (N)
1	61.4	0	80.40	141.8	0	79.7	141.1
2	61.4	0	53.60	115.0	0	53.7	115.1
3	23.5	0	9.80	33.3	0	13.3	36.8
4	17	0	0	17.0	0	0	17.0
5	17	-10.53	37.14	54.1	-10.25	36.4	53.4
6	23.5	-0.42	0	23.5	-0.82	0	23.5
7	50	-4.67	11.10	61.1	-4.59	12.8	62.8
8	50	0	17.50	67.5	0	21.8	71.8
9	50	3.79	51.10	101.1	3.49	54.8	104.8
Total $e_c$ (mm)		19.41			19.15		

### B. Case II: large displacement

In the second case, the displacement of joint 6 was set to be (-20 ,20) mm for ( $dx, dy$ ) after prestressing, maintaining the same prestress degree in the cables

as in Case I. The displacements of other free joints, such as joints 2 and 5, were not the focus of this restoration scenario. The goal was to restore joint 6 to its original position, achieving zero displacement after preservation while preventing any reduction or slackening of the member prestress.

The proposed preservation technique was applied to compute the nonlinear member alteration, using all the cables in the structure as actuators. The set of member alterations ( $e_c$ ) was calculated and presented in Table 3-23, column 11. Notably, the internal stress of the members remained unchanged during the preservation process, with total actuations amounting to 80.78 mm. This quantity is smaller, with difference ratios of 39% and 2% compared to the nonlinear studies by Xu and Luo (2009) and Saeed (2022), respectively. Another set of member alteration ( $e_c^*$ ) using the proposed approach with only four cables, resulting in total actuations of 80.551 mm, as tabulated in Table 3-23, column 12. Using only cables 5, 6, 8, and 9 as actuators restored joint 6 to its original position with less total actuation and effort, with a difference ratio of just 0.28%.

Regarding internal forces, the computed nonlinear member actuation, whether using all nine members or only four, successfully maintained the desired prestress level. In Saeed's (2022) study, the prestress level remained unchanged but required a larger total actuation with all members as actuators. Conversely, Xu and Luo (2009) restored joint 6 with 120.14 mm of total actuation, but the prestress degree was altered, though slackening was prevented. These results, obtained using the proposed technique, demonstrate the accuracy and precision of the derived preservation method.



Table 3-23 Simultaneous preservation of displacement and internal force in comparison with the studies by Xu and Luo (2009) and Saeed (2022)

Node No.	Direction	Displacement (mm)		Member No.	$t$ (N)	Xu and Luo (2009)		Saeed (2022)		Present study		
		$d$	$d_c$			$e_c$ (mm)	$T_e$ (N)	$e_c$ (mm)	$T_e$ (N)	$e_c$ (mm)	$e_c^*$ (mm)	$T_e$ (N)
6	$dx_6$	-20	0	1	61.38	-14.36	63.90	-4.38	61.38	3.90	0	61.38
				2	61.38	11.13	59.70	0.08	61.38	-1.80	0	61.38
				3	23.55	9.52	18.41	-3.07	23.55	2.98	0	23.55
				4	17.02	11.80	13.71	5.65	17.02	-0.36	0	17.02
	$dy_6$	20	0	5	17.02	-13.30	18.33	-18.62	17.02	17.50	28.284	17.02
				6	23.55	4.94	28.04	5.15	23.55	-5.20	-5.153	23.55
				7	50	-10.62	51.04	0.01	50	3.17	0	50
				8	50	-16.91	50.39	-17.99	50	15.10	19.63	50
Total $e_c$ (mm)				9	50	27.56	46.93	27.48	50	-30.77	-27.484	50
						120.14		82.43		80.78	80.551	

### 3.5 SUMMARY

This chapter presented the formulation of three nonlinear techniques: prestressing, analysis, and preservation, considering the geometric nonlinearity of spatial pin-jointed flexible and rigid structures. The proposed techniques were developed under the assumption of elastic material behaviour, accommodating both small and large displacements in pin-jointed elements. The validation of all proposed techniques was conducted through various numerical examples, and their results were compared to previously published numerical and experimental methods. Additionally, some models were validated using finite element analysis (SAP2000 – version.2023.2.0), which relies on an improved tangent stiffness matrix. The comparison of results

demonstrated exceptional agreement with cited studies, indicating that the proposed techniques, which consider both compatibility and equilibrium in the deformed configuration, produce highly accurate and dependable results. These validated methods will be crucial for computing prestress levels, conducting structural analyses, and implementing preservation processes in the subsequent chapter on the design and assembly of the experimental model.

The limitation of the derived techniques can include that the assumptions of linear elasticity, idealised pin-joints, or uniform material properties may not reflect real-world complexities. Besides, the derived equations might be sensitive to input uncertainties, leading to errors in the predictions.

## CHAPTER FOUR

### DESIGN AND ASSEMBLY OF EXPERIMENTAL MODEL

#### 4.1 INTRODUCTION

An experimental model was constructed and tested at the Structural Lab of the Civil Engineering Department at the University of Raparin to validate the theoretical concepts presented in Chapter 3. This chapter describes the model's design, its various components, the construction process, and the measuring instruments used during experimentation. The experimental system is a hyperbolic paraboloid cable net assembly, as shown in Figs. 4-1 and 4-2. Additionally, this chapter covers the testing procedure and the illustrative flowchart of the experimental findings.

#### 4.2 HYPERBOLIC PARABOLOID STRUCTURE

A three-dimensional cable net experimental model with a hyperbolic paraboloid geometry was constructed, as illustrated in Figs. 4-1 and 4-2. The labelling of the model's members and joint numbers is detailed in Fig. 4-1. The constructed structure is used for comparison purposes and to test the validity of the proposed theoretical prestress, analysis and preservation equations. The assembly consists of 64 cables and 41 joints, supported at its perimeter by 16 joints, leaving 25 inner joints free. The model's plan diagonal lengths and height are 1840 mm x 1840 mm x 800 mm, respectively. The nodal coordinates for the 3D hyperbolic paraboloid model and member lengths are presented in Table 4-1.

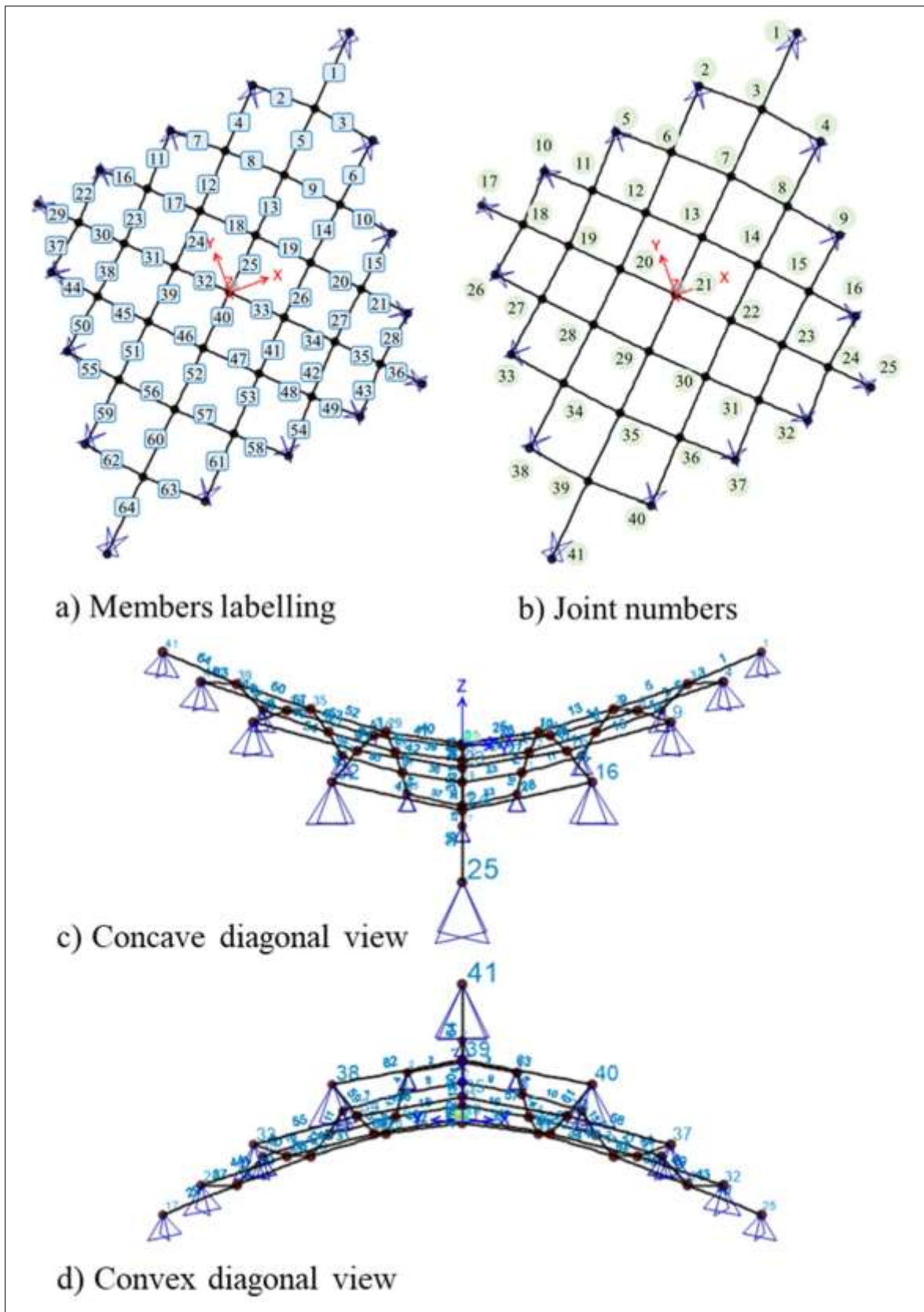


Fig. 4-1 Labelling of members and joints in the 3D experimental model with hyperbolic paraboloid geometry



Fig. 4-2 Hyperbolic paraboloid experimental model

The experimental model members are discrete elements, each consisting of four different pieces, as shown in Fig. 4-3. The joints are steel rings connected to the cables to allow free rotation, resembling pin connectors. The cable members have been cut and reconnected via actuators. The actuators comprise three segments: two aluminium female threaded turnbuckles and a single steel male threaded jack screw.

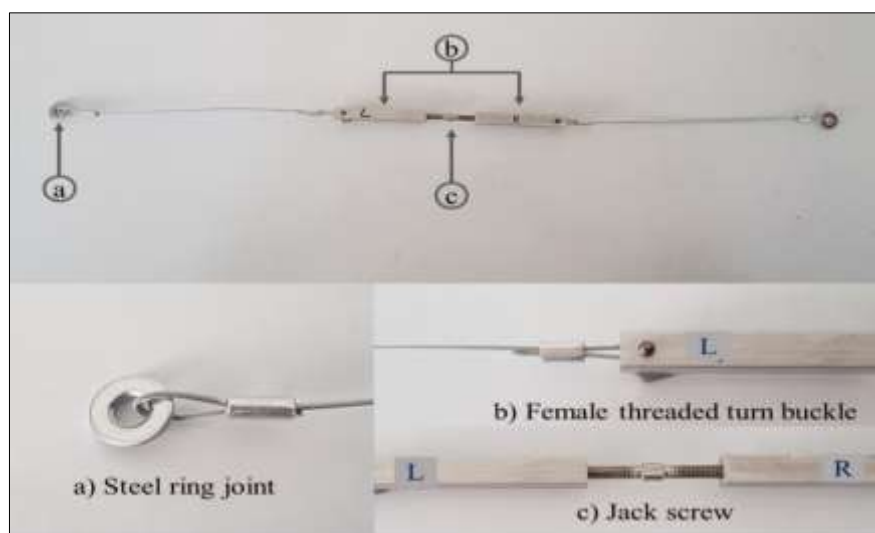


Fig. 4-3 Members detail of experimental model

Table 4-1 Nodal coordinates and member lengths of the hyperbolic paraboloid 3D model

Node No.	Coordinates (mm)			Node No.	Coordinates (mm)			Member No.	Member length (mm)
	x	y	z		x	y	z		
1	920	920	400	22	230	-230	-45		
2	460	920	200	23	460	-460	-142	1,64	354.12
3	690	690	260	24	690	-690	-270	2,3,8,9	330.76
4	920	460	200	25	920	-920	-400	62,63,56,57	
5	0	920	0	26	-920	460	-200	4,5,6	343.36
6	230	690	90	27	-690	230	-90	59,60,61	
7	460	460	150	28	-460	0	-5	7,10,11,15	337.49
8	690	230	90	29	-230	-230	50	12,14,51,53	338.86
9	920	0	0	30	0	-460	-5	50,54,55,58	
10	-460	920	-200	31	230	-690	-90	13,52	340.29
11	-230	690	-90	32	460	-920	-200	16,21,44,49	343.36
12	0	460	-5	33	-920	0	0	17,20,45,48	336.19
13	230	230	50	34	-690	-230	90	18,19,46,47	329.88
14	460	0	-5	35	-460	-460	150	22,28,37,43	332.72
15	690	-230	-90	36	-230	-690	90	23,27,38,42	329.40
16	920	-460	-200	37	0	-920	0	24,26,39,41	327.72
17	-920	920	-400	38	-920	-460	200	25,40	329.09
18	-690	690	-270	39	-690	-690	260	29,36	350.28
19	-460	460	-142	40	-460	-920	200	30,35	349.55
20	-230	230	-45	41	-920	-920	400	31,34	339.42
21	0	0	0					32,33	328.37

#### 4.2.1 Material Properties

Various materials were used in constructing the hyperbolic paraboloid cable net model. The members consist of stainless-steel cables, which incorporate aluminium female right- and left-threaded turnbuckles and steel male right- and left-threaded jack screws in the middle. The cable is a strand type consisting of

19 wires. The cable has a modulus of elasticity of 126,000 MPa (see Fig. 4-4 ) and a cross-sectional area of 1.5393 mm<sup>2</sup>, resulting in an axial stiffness (EA) of 193,951.8 N. The aluminium segments have a modulus of elasticity around 70,000 MPa, with the stress-strain diagram shown in Fig. 4-5. Both the cable and aluminium samples were tested at the Slemani Construction Laboratory. The vertical axis of both diagrams represents the tensile stress in N/mm<sup>2</sup>, and the horizontal axis which is labelled "Total Extension [%]" represents the percentage increase in length of the test specimen relative to its original length during a tensile test (strain). The third segment is a jack screw with a modulus of elasticity of 200,000 MPa and an EA of 2,389,180 N.

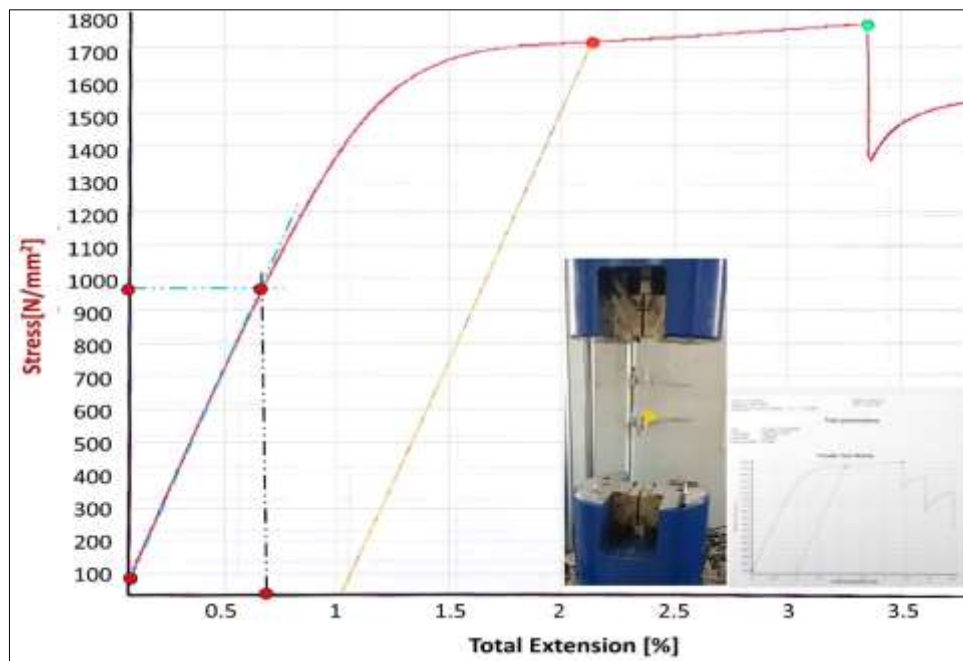


Fig. 4-4 Stress-strain diagram of (19 wire-strand) cable in tension

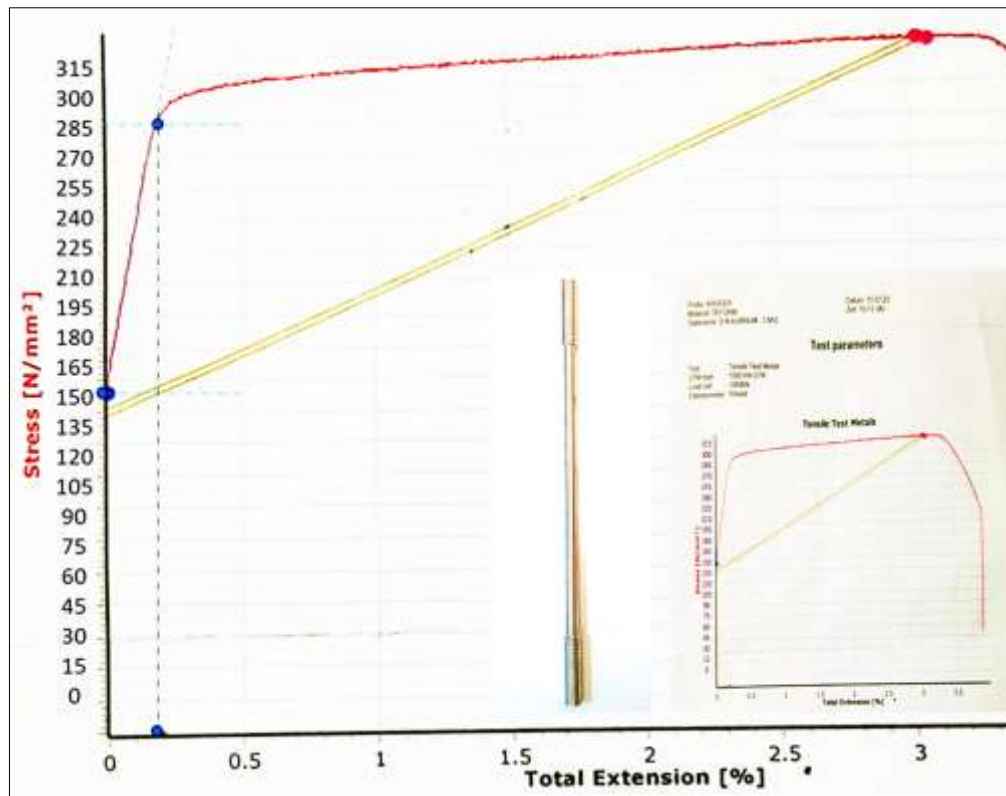


Fig. 4-5 Stress-strain diagram of aluminium in tension

Because each member of the experimental model consists of different segments, as shown in Fig. 4-6, and each segment has a different cross-section and elastic modulus, it is necessary to compute the effective axial stiffness for the combined segments using Eq. 3.47 (Saeed, 2014):

$$EA_{eff.} = \frac{L_{combined}}{\left( \frac{L_{cable}}{EA_{cable}} + \frac{L_{Al.}}{EA_{Al.}} + \frac{L_{screw}}{EA_{screw}} \right)} \quad 3.47$$

where,  $EA_{eff.}$  is the effective combined axial stiffness of the experimental members,  $L_{combined}$  is the actual length of the member that is composed of combined segments.  $L_{cable} / EA_{cable}$ ,  $L_{Al.} / EA_{Al.}$ , and  $L_{screw} / EA_{screw}$  are the ratios of length to EA for each of the cable, aluminium, and jack screw segments respectively.  $EA_{eff.}$  for all members is listed in Table 4-2.





Fig. 4-6 Top view detail of experimental member segments

Table 4-2 Effective combined axial stiffness of experimental members

Member No.	EA <sub>eff.</sub> (N)	Member No.	EA <sub>eff.</sub> (N)	Member No.	EA <sub>eff.</sub> (N)	Member No.	EA <sub>eff.</sub> (N)
1	179811.80	17	162666.37	33	165548.59	49	165034.84
2	166387.23	18	161238.01	34	164950.26	50	163100.19
3	161749.38	19	161238.01	35	165445.81	51	163434.22
4	166282.76	20	163039.52	36	172153.68	52	161987.60
5	166352.14	21	172087.92	37	162664.14	53	164188.74
6	169376.68	22	167726.70	38	160180.24	54	163100.19
7	165663.58	23	158715.67	39	160910.42	55	167620.04
8	162465.38	24	158702.74	40	160898.37	56	159484.24
9	158755.97	25	160458.22	41	158340.67	57	162086.66
10	167620.04	26	161284.35	42	161296.53	58	166440.66
11	163100.19	27	160922.71	43	164189.00	59	171369.53
12	162686.60	28	164574.69	44	166169.93	60	166352.14
13	163226.46	29	170181.03	45	163790.97	61	167045.60
14	161577.91	30	166944.71	46	159457.56	62	162125.97
15	163100.19	31	164188.74	47	159457.56	63	170043.99
16	164659.92	32	159837.54	48	160462.87	64	174389.10

### 4.2.2 Joints

Steel rings were used as pin-joint connectors to connect the members together and to the supports. Cables are connected to the rings using aluminium crimps. All internal joints connect four members (see Fig. 4-7. a) and have the ability to displace in the x-, y-, and z-directions. The parametric joints are connected to the supports via screws, as shown in Fig. 4-7. b. The load hangers pass through the hole of the ring, as shown in Fig. 4-7. c.

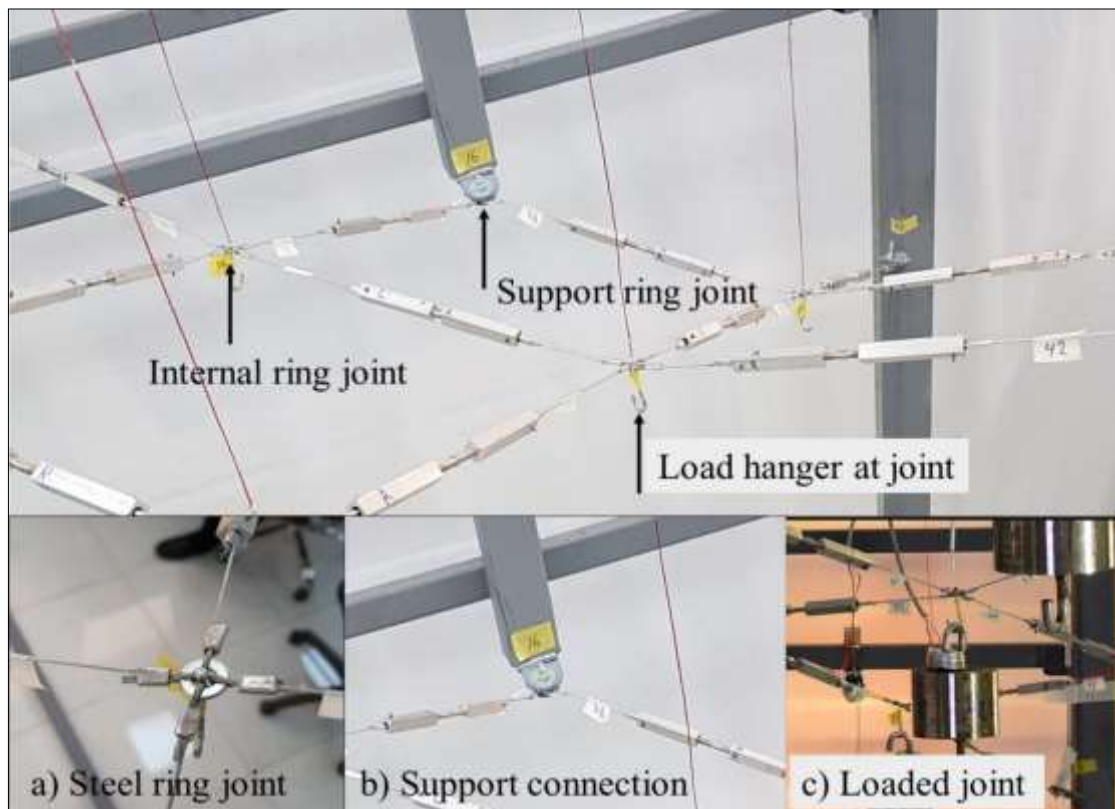


Fig. 4-7 Joint detail of the experimental setup

### 4.2.3 Cable Members

The experimental model is a space cable net structure consisting of 64 combined flexible members, as shown in Fig. 4-3. The cable members were cut

in the middle and reconnected via actuators. These cable segments are strand type, formed from 19 wires with an overall diameter of 1.4 mm. The cables are flexible members with a high ability to transform tensile force and behave elastically up to approximately 1700 N (see Fig. 4-4). The cable members need to remain taut to prevent slack and stay effective. Turnbuckles were utilised to alter the cable length during the prestressing stage and achieve the desired tautness. The strength of these cables was determined in the laboratory, and the stress-strain diagram is shown in Fig. 4-4. During testing, the ends of the cables were passed through a hole in a reinforced steel segment with 100 mm length (see Fig. 4-8.b) to fit into the tensile testing machine grips (see Fig. 4-8.a) at the Slemani Construction Laboratory.

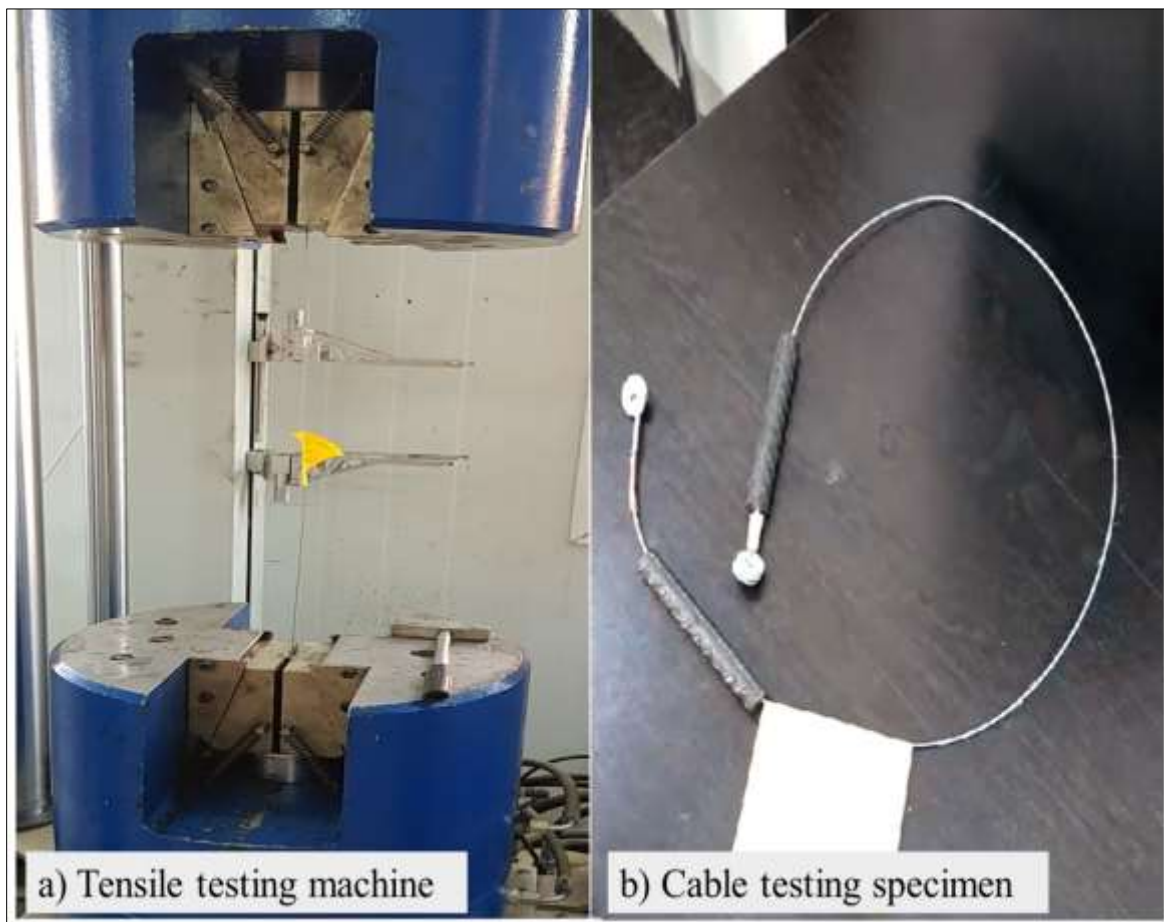


Fig. 4-8 Tensile testing machine and cable test specimen

#### 4.2.4 Actuators

To facilitate the geometrical adjustment and prestressing of the structure, it is imperative to implement some alterations to the cable length. For this reason, each cable is connected to an actuator. Each actuator is made up of two aluminium parts and one left and right-handed jack screw as shown in

Fig. 4-3. Another reason was for placing the strain gauge sensors for recording internal forces within the members.

The detail of the jack screw is shown in Fig. 4-9. It has left- and right-hand external threads with a 5 mm diameter and is connected to the aluminium segments at both ends. The turnbuckle body has a spanner width of 5 mm, allowing a wrench to twist and adjust the tensioning screw, with each wrench twist providing 1.6 mm of lengthening or shortening.

The aluminium segments were manually made in a very precise process. The aluminium bars have square cross-sections with internal circular threaded holes and a net area of 67.5698 mm<sup>2</sup>. The steps are described as follows:

- i. The aluminium bars were cut into smaller pieces, each measuring 70 mm in length, using a digital electric cutter (see Fig. 4-10).
- ii. A 4 mm diameter hole was drilled in the center of each segment parallel to its length, with the center determined using a laser indicator on the drilling machine (see Fig. 4-11).
- iii. The holes were threaded using a 5 mm internal thread tap (see Fig. 4-12), with half of the segments right-threaded and the other half left-threaded.
- iv. A 2 mm diameter hole was drilled perpendicular to the length at one end of each segment to make a connection joint to the cable segments (see



Fig. 4-12).

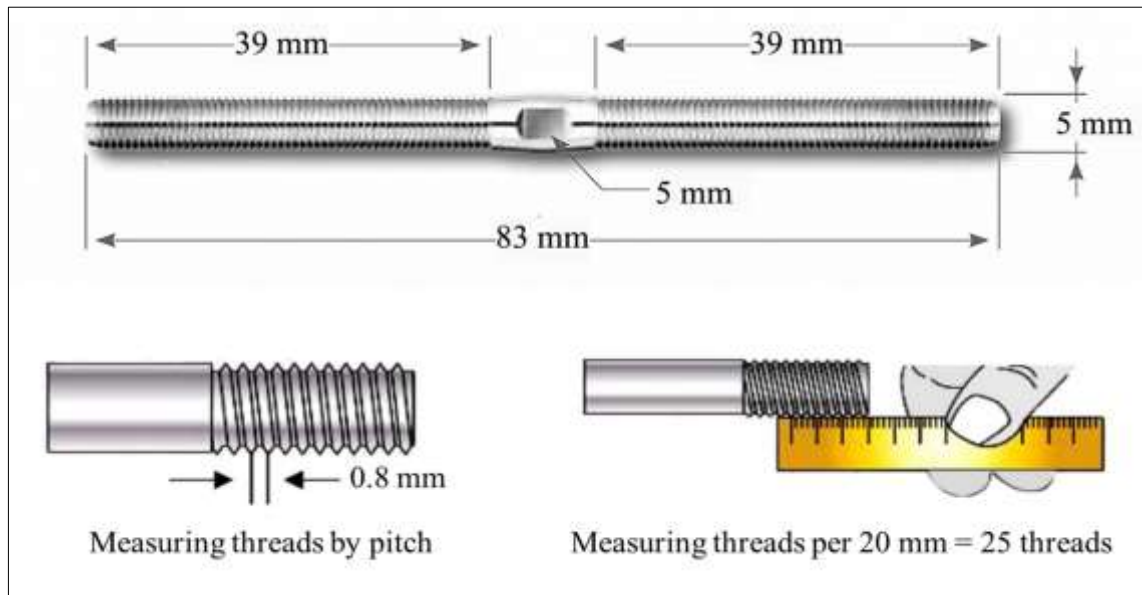


Fig. 4-9 Jack screw detail in the actuator

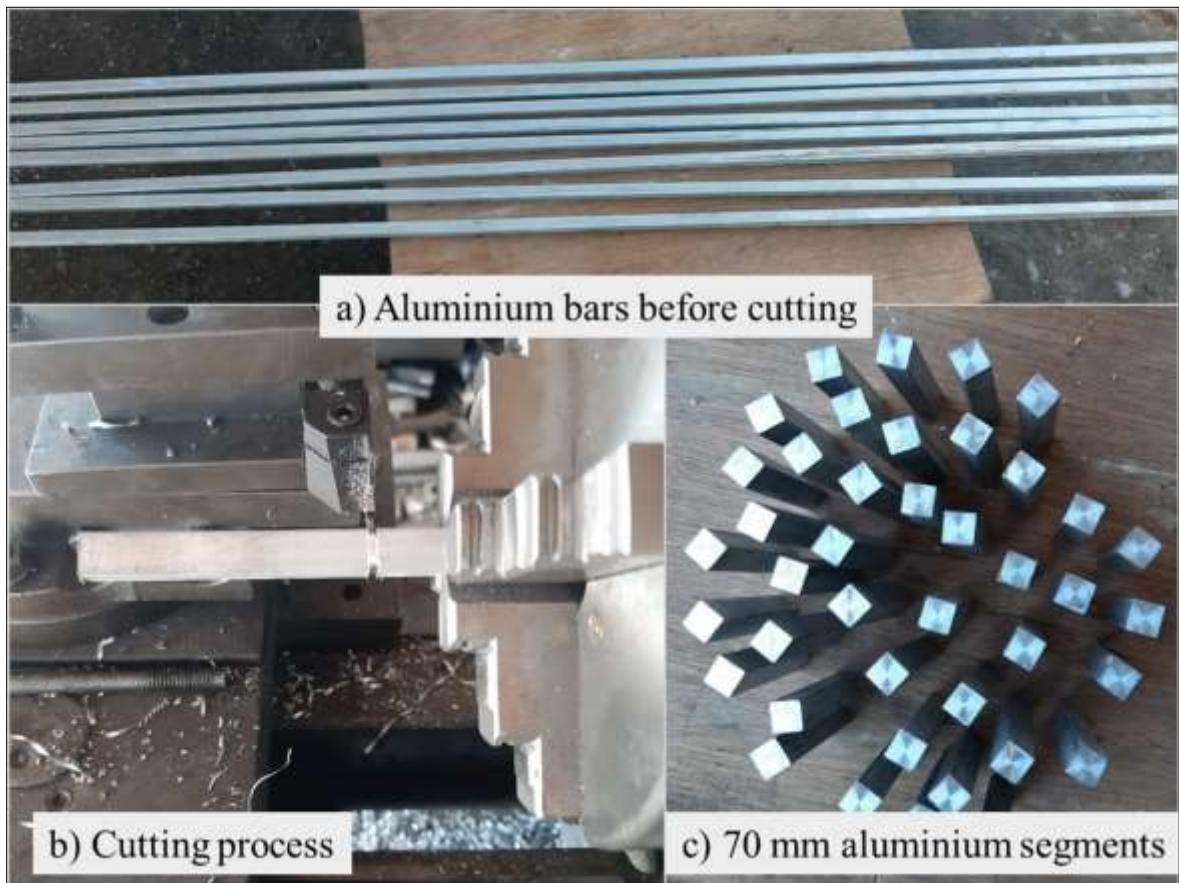


Fig. 4-10 Cutting phase of aluminium segments

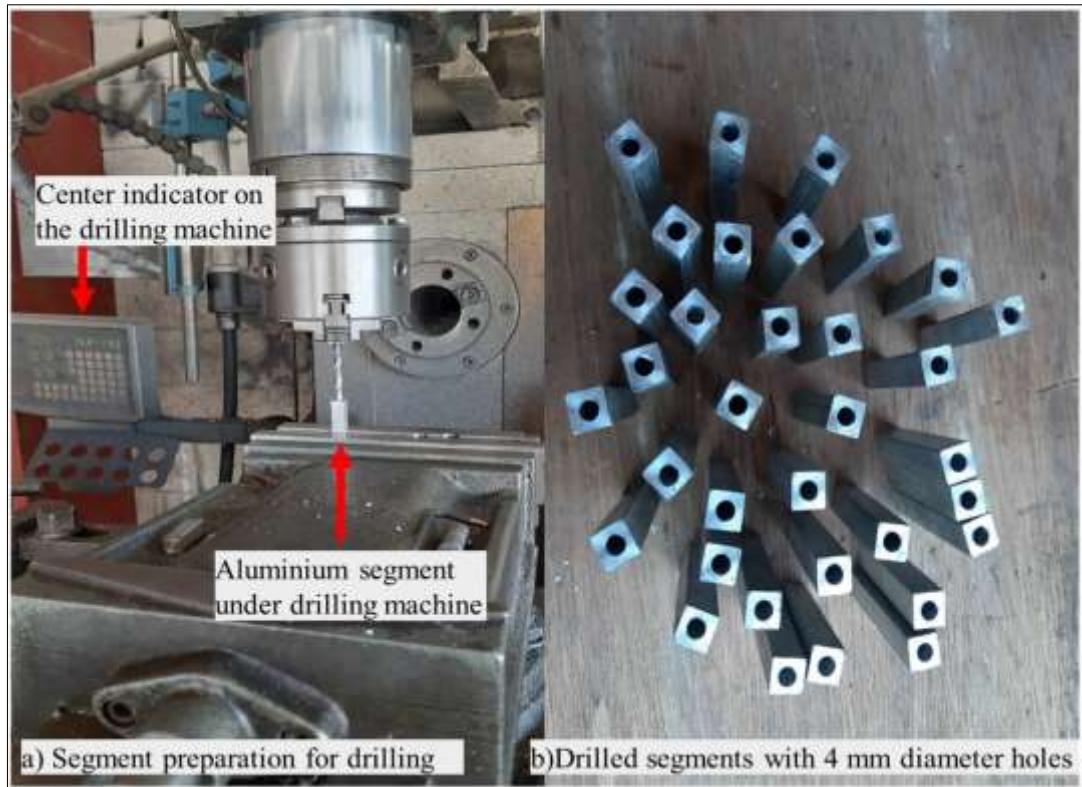


Fig. 4-11 Center marking and drilling phase of aluminium segments

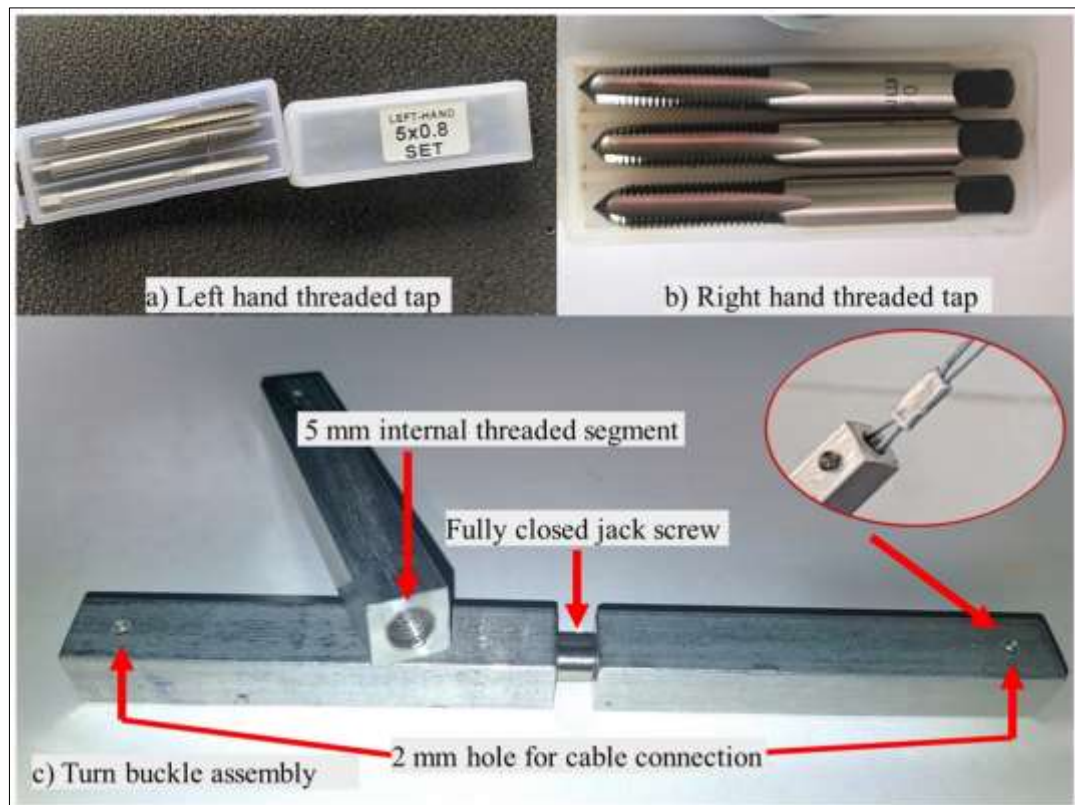


Fig. 4-12 Photo illustrating internal left and right threading and assembly of end joints

### 4.2.5 Support System

The hyperbolic paraboloid experimental model is supported by 16-pin supports positioned at its perimeter. Fig. 4-13 shows the layout of these supports, which are connected to the cables via bolts allowing free rotation. Each support's base plate, 5 mm thick, is welded to the layout frame, as depicted in Fig. 4-13.

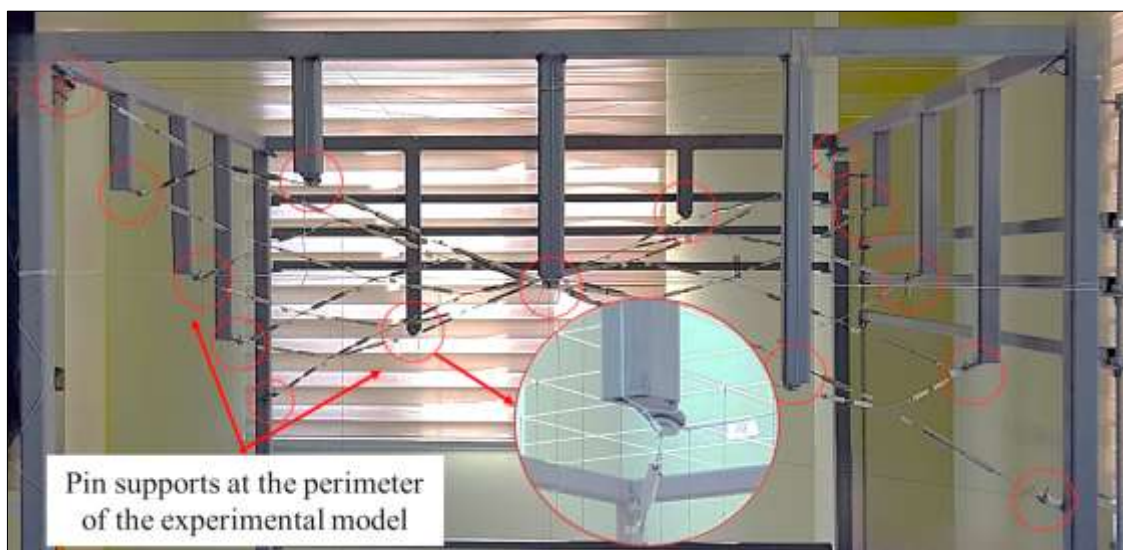


Fig. 4-13 Layout of supports in the experimental model

### 4.2.6 Experimental Measurement

It involved recording the nodal displacements of free joints and the internal forces of the combined members during the prestressing, analysis, and preservation phases. Detailed descriptions and recordings of these phases are provided in the following subsections:



#### 4.2.6.1 Nodal displacement

The model consists of 41 joints, with 25 of them free to displace in the x-, y-, and z-directions, resulting in a total of 75 degrees of freedom that need to be recorded. To achieve this, five digital cameras were utilised to capture the movement of the free nodes in the x-z and y-z planes of the 3D model (see Fig. 4-1). The used cameras were two Nikon D780 with 24.5-megapixel resolution and aspect ratio of 3:2, and three Samsung Galaxy Camera 2 with 16-megapixel and aspect ratios of 4:3, 3:2, and 16:9. Additional lighting sources were strategically positioned to ensure adequate lighting density for the cameras during data recording (see Fig. 4-14). A small red-coloured bead as in Fig. 4-15 was affixed to each free node to facilitate easy monitoring of joint movements. Above all 25 nodes, a reference scaled ruler was attached, intended to serve as a scale factor during the data collection phase. Fig. 4-14 and Fig. 4-15 provides further illustration of measuring the displacement of the experimental model.

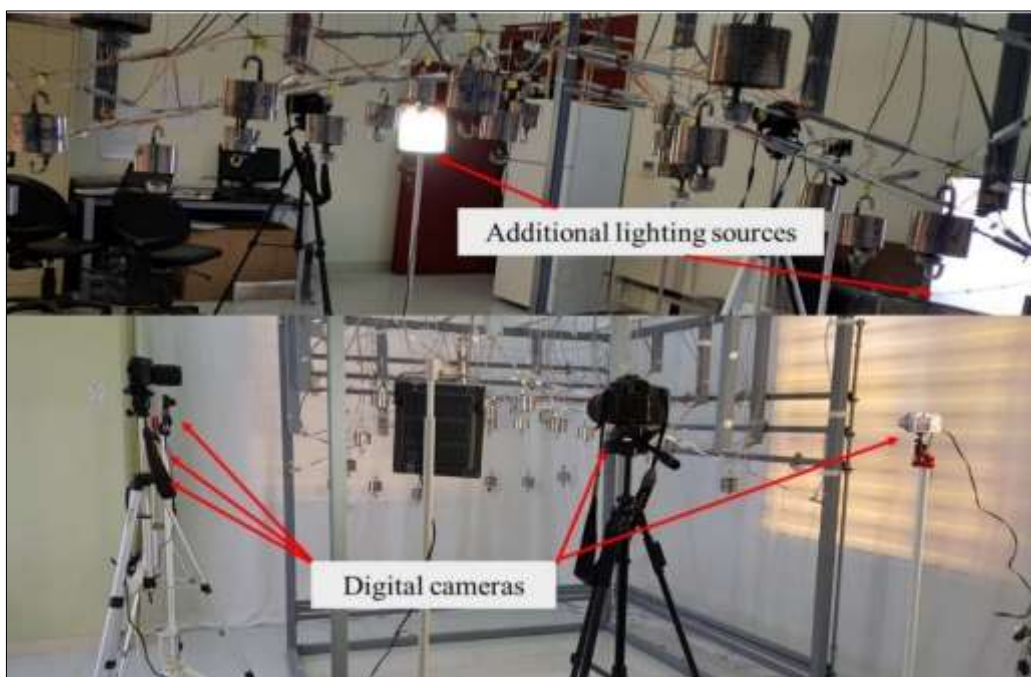


Fig. 4-14 Arrangement of lighting sources and digital camera for displacement recording



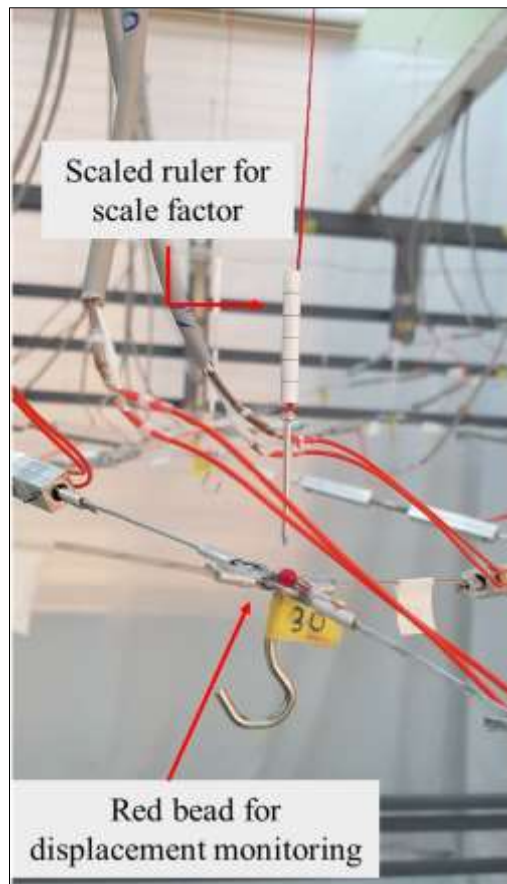


Fig. 4-15 Placement of scaled ruler and joint movement monitoring for joints

#### 4.2.6.2 Member force

Measuring the internal forces of the experimental members constitutes the second criterion in the laboratory data collection process. For this purpose, 64-channel data logger is used. The device features a touch screen LCD with a graphical resolution of 800 x 480 pixels as shown in Fig. 4-16. To measure the axial forces of the combined members in the experimental model, strain gauge sensors are provided for each member. The sensors were meticulously adhered to one side of the aluminium segments of the actuators. Specifically, the strain gauge sensor used was the BX120-3AA high-precision resistance strain gauge which has a strain gauge factor of 2.08. This strain sensor is very small, with a wire grid size of 3.0×2.3 mm, and has a nominal resistance of 120 ohms that varies with the applied force and voltage.



Fig. 4-16 64-channel data logger for strain measurement

The steps for installing the strain gauge sensors include smoothing the aluminium surface using fine grade sand paper (P320 & P400), cleaning it by toner, marking the center line for sensor placement, mounting the strain gauge on tape, applying standard type of adhesive to the sensor, and finally curing and pressing it into the surface, more illustration in Fig. 4-17.



Fig. 4-17 Photo illustrating steps for strain gauge sensor placement

Each strain gauge was welded to a lead wire measuring 150 mm, necessitating a special extension wire to connect to the data logger device. Due to the extension wires' length, ranging from 6 to 10 meters, a low-resistance cable with a double-layer shield with diameter of 0.8 mm ( $2 \times 0.5 \text{ mm}^2$ ), specifically designed for data transfer, was used for this purpose as shown in Fig. 4-18. a. The lead wires were connected to the extension wires using heat shrink wire connectors (see Fig. 4-18. b). Then, all wires were connected to the bridge strain gauge as in Fig. 4-18. c, and subsequently, the bridges were connected to the data logger channels, as depicted in Fig. 4-18. d.

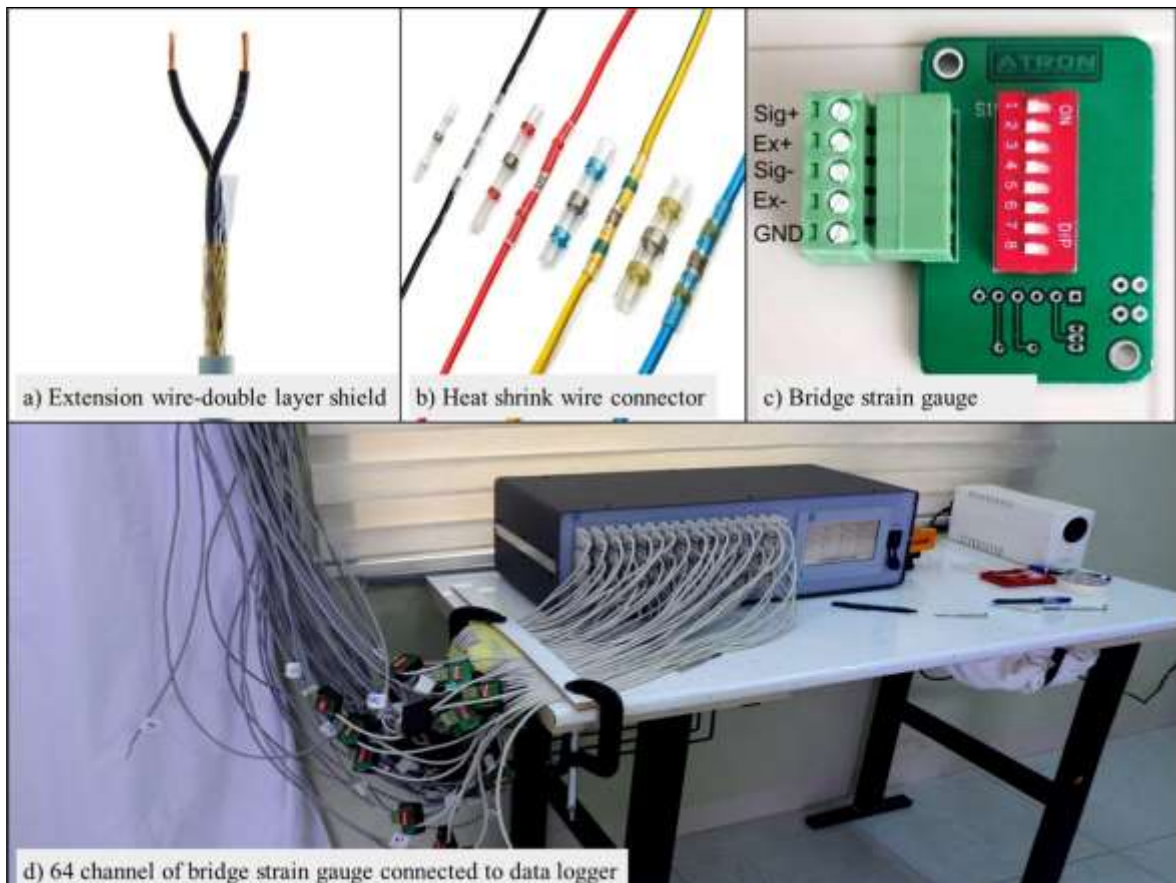


Fig. 4-18 Connection accessories for data logger device

The required calibration settings for strain readings were entered into the data logger setup. The device stores data in CSV format on an external standard USB memory in micro-strain units. During the phases of prestressing, analysis, and preservation in the experimental works, the strain readings were recorded and subsequently converted to axial forces. These measurements were then used to validate the numerical data.

#### **4.2.7 Parameters of the Study**

The parameters for this study are defined as the prestressing degree, loading cases, and preservation targets. Prestressing force serves as an independent variable, crucial to the study due to its direct influence on the displacement and internal forces within pin-jointed spatial structures. Additionally, applied nodal loads significantly affect the deformability and stress distribution within spatial assemblies. Furthermore, the restoration of geometry and/or internal forces within spatial members is essential for ensuring the longevity and optimal performance of this type of structural system.

Accordingly, the study aims to examine the impact of various prestressing degrees and loading conditions on the geometric nonlinear behaviour and overall structural performance. Similarly, it seeks to establish effective preservation techniques for structures exhibiting nonlinear responses.

### **4.3 EXPERIMENTAL PROCEDURE**

After completing all necessary settings for experimental data collection, the placement of the cameras was checked to ensure accurate capture of the targeted nodal displacements. Additionally, all channels were checked for

strain recording. It was found that 63 channels were working properly; however, channel number 22 was not functioning and was therefore removed from data recording. The hyperbolic paraboloid 3D model was then tested under various conditions, including different degrees of prestressing, different load cases, and different preservation targets.

The laboratory work began by prestressing the entire structure to the desired degree in three different scenarios: two symmetric prestressing cases using different cable members and one asymmetric case. Later, one of the prestressing cases was chosen to continue for the analysis stage. In the analysis phase, three load application cases were tested: applying nodal loads at all free joints in the gravity direction, applying loads in the horizontal direction alone, and applying loads in both the vertical and horizontal directions simultaneously.

The final phase of the experimental work included preservation in three different scenarios. The first scenario involved restoring the nodal displacement without considering the internal force, while ensuring that no slack occurred. The second scenario focused on restoring the cable force of some slackened members without considering the nodal displacement adjustment that occurred after applying one of the load cases in the analysis stage. The last scenario involved the simultaneous control of internal forces while considering the nodal displacements.

All three phases were already computed theoretically using the derived equations presented in the previous chapter. The computed theoretical member alteration ( $e_o$ ) was then carefully applied to the experimental tests by shortening or lengthening the actuators of the specific combined members, while recording the member forces and targeted nodal displacements. Finally, the experimental

data were compared to the theoretical calculations to validate the derived formulations. The results are presented in the next chapter. The layout of the experimental process is illustrated in the flowchart shown in the Fig. 4-19.

#### **4.4 SUMMARY**

This chapter discussed the design and assembly of an experimental model constructed to validate the theoretical concepts presented in Chapter 3. The model, consisting of 64 cables and 41 joints, was designed to test the proposed nonlinear equations. The chapter covered the model's components, material properties, joint and cable member details, actuator mechanisms, support system, and experimental measurement methods. The model will be tested for the three phases of prestressing, various loadings, and preservation experimentally in the next chapter, with the results and discussion presented.

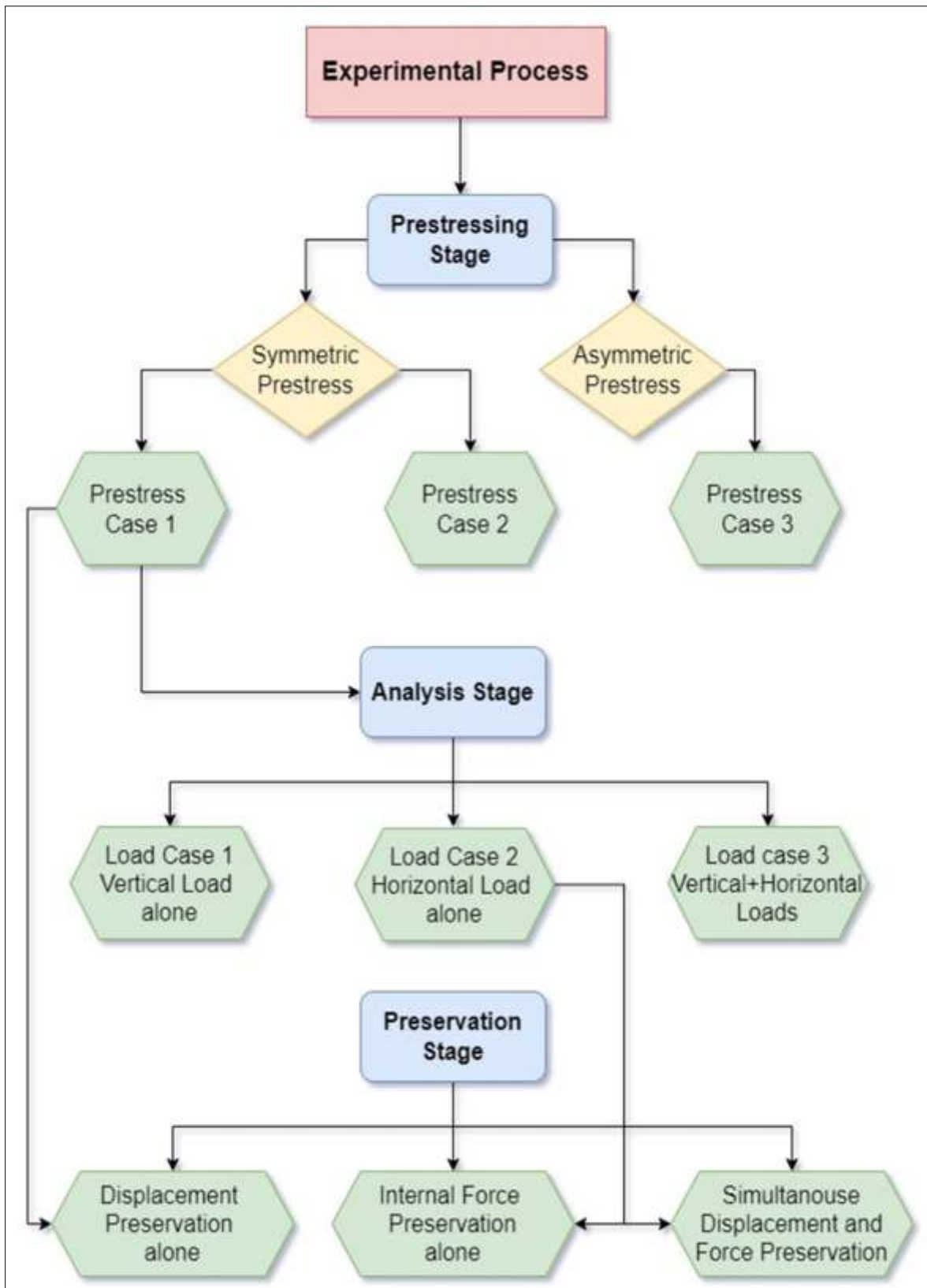


Fig. 4-19 Flowchart illustrating the experimental process



## **CHAPTER FIVE**

### **EXPERIMENTAL FINDINGS AND DISCUSSIONS**

#### **5.1 INTRODUCTION**

This chapter presents the results of the experimental phases, including the various cases of prestressing, different loading conditions, and scenarios of the preservation process. The theoretical equations derived and presented in Chapter 3 are validated through their application to the experimental model and its outcomes. A comparison between the theoretical and experimental results is also discussed.

#### **5.2 PRESTRESSING PHASE RESULTS**

The response of cable structures concerning load transfer, deformability, and forces in this type of assembly is primarily influenced by the level of prestressing. The targeted degree of prestress can always be achieved by adjusting the required member lengths. The prestressing stage was performed on the experimental model with three different degrees of prestressing. The first prestressing case (PC1) and the second prestressing case (PC2) employed an equal quantity of member actuation for equivalent members but in different amounts to achieve symmetric member actuation on the model. However, achieving the same degree of prestressing for equivalent members was not possible due to differences in the members' axial stiffness, as reported in Table 4-2. For the third prestressing case (PC3), different amounts of member



actuators were used to achieve asymmetric actuation and degrees of prestressing.

### 5.2.1 Symmetric Prestressing Case 1 (PC1)

In the first scenario of the prestressing case, 24 members, as highlighted in Fig. 5-1 were selected to achieve the required degree of prestress. The set of  $e_o$  values was determined and initially applied theoretically to the model to reach the desired level of pretension and to identify whether any cables were experiencing slack or not. The members at the perimeter of the model were then shortened by 1.6 mm each, resulting in a total actuation of 38.4 mm.

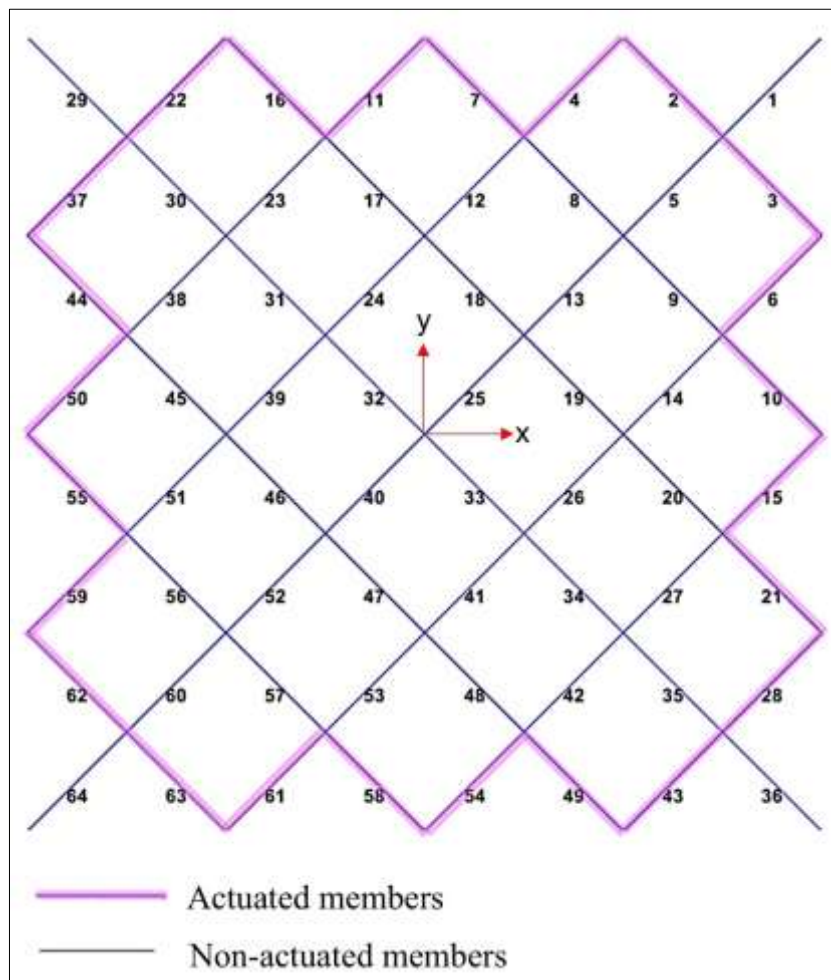


Fig. 5-1 Selected 24 members for prestress application in PC1

Both proposed Eqs. 3.20 and 3.21 used to compute the pretension of the assembly and the results are presented in columns 3,4, 8, and 9 of Table 5-1. The outcome of the calculation for the prestress level indicates a low to intermediate degree, which is very desirable for practical design (Sufian and Templeman, 1970; Sehlstrom, 2019). This helps maintain the material strength within the elastic range and prevents slack in the cables. Later, the same amount of  $e_o$  set was applied to the experimental model. The tensile strain of the members was measured via a data logger as presented in Table 5-2, and multiplied by the axial stiffness of the aluminium segments to provide the tensile force of the members. The results are presented in Table 5-1 in columns 5 and 10. The experimental results in columns 5 and 10 (Table 5-1) showed a very close, agreement between the theoretical computation and experimental measurement.

In theory, cables 1 and 64 showed maximum tensile forces of around 256 N. In the lab results, both cables recorded slightly greater prestress values, with 259.8 N and 257.5 N for cables 1 and 64, respectively. The least numerical pretension was computed in cables 22, 28, 37, and 43, with values around 19 N. Similarly, the same cables produced values close to 19 N in the lab, except for cable 22, which was not recorded due to a technical issue.

Moreover, based on the presented data in Table 5-1, the maximum discrepancy rate between the theoretical and experimental prestress values was for cable 62, with rates of 3.4% and 3.9% using the proposed Eqs. 3.20 and 3.21, respectively. Conversely, the prestress of cable 44 showed 0% and 0.1% discrepancy using the proposed Eqs. 3.20 and 3.21, respectively. The presence of a 3.9% discrepancy may be attributed to joint looseness or imperfect cycling wrench twists during the experimental procedure.

Table 5-1 Theoretical and experimental member actuation and prestressing degree in PC1

Member	Actuation (mm)	t (N)			Member	Actuation (mm)	t (N)		
		Present technique		Experiment			Present technique		Experiment
		Eq. 3.20	Eq. 3.21				Eq. 3.20	Eq. 3.21	
1		255.58	256.05	259.86	33		204.05	204.43	202.61
2	-1.6	89.07	89.57	88.48	34		208.92	209.31	210.31
3	-1.6	89.07	89.56	88.77	35		216.41	216.81	214.47
4	-1.6	122.99	123.13	122.67	36		219.35	219.78	219.53
5		243.64	244.04	243.18	37	-1.6	18.982	19.192	18.58
6	-1.6	122.96	123.10	122.81	38		82.124	82.193	82.08
7	-1.6	39.50	39.47	39.36	39		118.87	119.01	117.96
8		37.57	37.54	37.32	40		229.97	230.36	225.31
9		37.57	37.54	37.40	41		118.83	118.97	119.85
10	-1.6	39.49	39.46	39.64	42		82.18	82.249	81.02
11	-1.6	85.39	85.46	84.97	43	-1.6	18.973	19.183	18.56
12		121.58	121.72	118.23	44	-1.6	156.42	156.58	156.42
13		239.77	240.17	238.64	45		152.84	152.99	152.18
14		121.55	121.69	118.52	46		148.53	148.67	150.09
15	-1.6	85.44	85.51	83.92	47		148.51	148.66	146.61
16	-1.6	156.59	156.75	155.75	48		152.82	152.97	150.17
17		153.01	153.16	149.36	49	-1.6	156.4	156.56	156.61
18		148.71	148.86	146.15	50	-1.6	85.379	85.453	83.82
19		148.71	148.86	144.30	51		121.6	121.74	118.57
20		153.02	153.18	150.98	52		239.73	240.13	242.80
21	-1.6	156.62	156.77	156.04	53		121.56	121.7	121.25
22	-1.6	18.98	19.19	-	54	-1.6	85.436	85.51	85.05
23		82.13	82.19	80.81	55	-1.6	39.557	39.53	39.02
24		118.86	119.00	117.93	56		37.628	37.598	36.57
25		229.98	230.37	227.03	57		37.628	37.598	37.72
26		118.83	118.97	117.84	58	-1.6	39.559	39.532	39.55
27		82.18	82.25	82.44	59	-1.6	123.02	123.16	122.93
28	-1.6	18.97	19.18	19.11	60		243.6	244	242.05
29		219.33	219.77	218.99	61	-1.6	122.97	123.11	121.42
30		216.40	216.80	215.07	62	-1.6	89.106	89.599	86.05
31		208.91	209.30	207.54	63	-1.6	89.112	89.605	88.62
32		204.04	204.42	204.67	64		255.53	256	257.54
Max. discrepancy ratio				3.9%	Min. discrepancy ratio				0.1%

Although the maximum prestressed force in the experimental recording showed a difference ratio of around 2% compared to the theoretical value, most of the experimental results were smaller than the theoretical computations. This can be attributed to the extension ability and relaxation of the cable type used in the experimental model as stated by Chen *et al.* (2024) , as well as the initial geometrical state before prestressing, as confirmed by Zhang *et al.* (2023).

Table 5-2 Strain data of the aluminium segments for the experimental PC1

Member No.	Microstrain	Member No.	Microstrain	Member No.	Microstrain	Member No.	Microstrain
1	54.94	17	31.58	33	42.84	49	33.11
2	18.71	18	30.90	34	44.46	50	17.72
3	18.77	19	30.51	35	45.34	51	25.07
4	25.94	20	31.92	36	46.41	52	51.33
5	51.41	21	32.99	37	3.93	53	25.64
6	25.96	22	-	38	17.35	54	17.98
7	8.32	23	17.09	39	24.94	55	8.25
8	7.89	24	24.93	40	47.64	56	7.73
9	7.91	25	48.00	41	25.34	57	7.98
10	0.81	26	24.91	42	17.13	58	8.36
11	17.96	27	17.43	43	3.93	59	25.99
12	25.00	28	4.04	44	33.07	60	51.18
13	50.45	29	46.30	45	32.18	61	25.67
14	25.06	30	45.47	46	31.73	62	18.19
15	17.74	31	43.88	47	31.00	63	18.74
16	32.93	32	43.27	48	31.75	64	52.34

The results regarding displacement in the x, y, and z directions for theory and experiments for PC1 are presented in Table 5-3. The theoretical displacements are calculated directly using the derived Eqs. 3.20 and 3.21, and are tabulated in columns 2-7 in Table 5-3. The experimental displacements are obtained by computing the difference between the photos taken by digital cameras before

and after applying member actuations. The cameras need to be fixed in proper locations to monitor the nodal movement and should not be moved during photo capturing. In the experimental displacement recording, only specific joints are observed, particularly the nodes predicted to experience the greatest displacement during the theoretical computation.

The steps for measuring the displacement using photos are explained in detail below, utilising the dimensions depicted in Fig. 5-3 for node 39 as an illustrative example. Considering the photos a and b in Fig. 5-3 captured parallel to y-z plane:

- Reference line dimension in photo = 18 mm at both a and b in Fig. 5-3.
- Reference line dimension in reality = 25 mm

$$\therefore \text{scale factor} = \frac{25}{18} = 1.389$$

- Vertical distance ( $z_1$ ) between reference point and node 39 before prestress = -47.3 mm.
- Vertical distance ( $z_2$ ) between reference point and node 39 after prestress = -53.4 mm.

$$\therefore dz = (z_2 - z_1) \times \text{scale factor} = (-53.4 + 47.3) \times 1.389 = -8.472 \text{ mm}$$

- Horizontal distance ( $y_1$ ) between reference point and node 39 before prestress = -8.1 mm.
- Horizontal distance ( $y_2$ ) between reference point and node 39 after prestress = -9.8 mm.

$$\therefore dy = (y_2 - y_1) \times \text{scale factor} = (-9.8 + 8.1) \times 1.389 = -2.361 \text{ mm}$$

Considering the photos c and d in Fig. 5-3 captured parallel to x-z plane:

- Reference line dimension in photo = 13 mm at both a and b in Fig. 5-3.
- Reference line dimension in reality = 15 mm

$$\therefore \text{scale factor} = \frac{15}{13} = 1.154$$

- Horizontal distance ( $x_1$ ) between reference point and node 39 before prestress = -7.2 mm.
- Horizontal distance ( $x_2$ ) between reference point and node 39 after prestress = -9.2 mm.

$$\therefore dx = (x_2 - x_1) \times \text{scale factor} = (-9.2 + 7.2) \times 1.154 = -2.308 \text{ mm}$$

$$\therefore \text{Displacement of joint 39 } (dx, dy, dz) = (-2.308, -2.361, -8.472)$$

All other displacements of the selected nodes (3, 7, 13, 18, 19, 23, 24, 29, and 35) were calculated in the same way and are presented in Table 5-3. The smallest and greatest resultant displacement discrepancies between experimental and theoretical results in Table 5-3 were for joints 39 and 24, with discrepancies of 0.6% and 7%, respectively. There is a strong compatibility between the theoretical and experimental results. Additionally, all the experimental results showed slightly smaller values, which can be attributed to similar reasons observed in previous pretension lab results, such as cable extension and relaxation. Other contributing factors may include the joint connections between the cables, which may not behave as ideal hinges, as reported by Zhang *et al.* (2023).

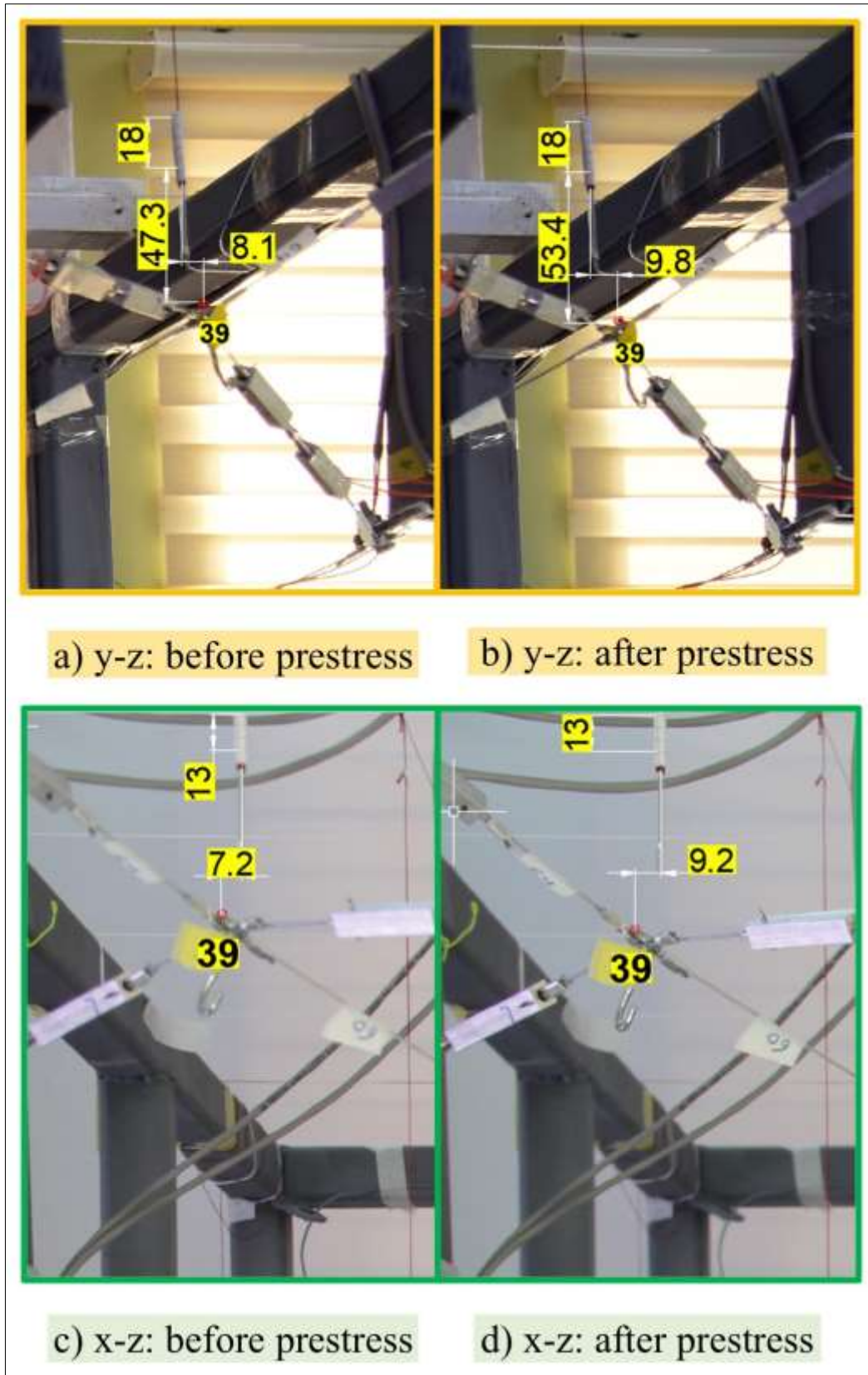


Fig. 5-2 Displacement measurement in (mm) of joint 39 in y-z and x-z views for the experimental model

Table 5-3 Theoretical and experimental displacements in PC1

Node No.	Theoretical displacement (mm)						Experimental displacement (mm)			
	Eq. 3.20			Eq. 3.21						
	$dx$	$dy$	$dz$	$dx$	$dy$	$dz$	$dx$	$dy$	$dz$	
1,2	0	0	0	0	0	0	0	0	0	
3	2.287	2.291	-8.500	2.303	2.306	-8.537	2.308	2.222	-8.889	
4,5	0	0	0	0	0	0	0	0	0	
6	-0.831	2.060	1.660	-0.833	2.059	1.671	-	-	-	
7	2.339	2.340	-10.268	2.344	2.345	-10.262	2.273	-	-10.000	
8	2.064	-0.829	1.660	2.063	-0.830	1.671	-	-	-	
9,10	0	0	0	0	0	0	0	0	0	
11	-0.354	2.047	1.028	-0.352	2.047	1.029	-	-	-	
12	-1.113	1.495	2.815	-1.115	1.494	2.823	-	-	-	
13	1.340	1.330	-7.293	1.341	1.331	-7.277	1.370	1.176	-7.059	
14	1.508	-1.120	2.811	1.508	-1.122	2.819	-	-	-	
15	2.058	-0.364	1.028	2.057	-0.363	1.029	-	-	-	
16,17	0	0	0	0	0	0	0	0	0	
18	-1.966	1.967	7.905	-1.981	1.981	7.946	-1.915	-	7.750	
19	-1.623	1.624	7.910	-1.627	1.627	7.912	-1.646	1.786	7.468	
20	-0.313	0.308	3.054	-0.312	0.307	3.048	-	-	-	
21	0.015	0.002	2.876	0.014	0.002	2.880	-	-	-	
22	0.316	-0.309	3.051	0.315	-0.309	3.045	-	-	-	
23	1.628	-1.626	7.918	1.631	-1.629	7.920	1.639	-1.875	7.500	
24	1.970	-1.970	7.904	1.985	-1.985	7.945	1.986	-1.667	7.333	
25,26	0	0	0	0	0	0	0	0	0	
27	-2.051	0.363	1.043	-2.050	0.361	1.044	-	-	-	
28	-1.506	1.124	2.845	-1.505	1.125	2.853	-	-	-	
29	-1.318	-1.312	-7.265	-1.319	-1.313	-7.249	-1.308	-1.111	-7.037	
30	1.121	-1.496	2.843	1.122	-1.496	2.851	-	-	-	
31	0.364	-2.049	1.050	0.363	-2.049	1.051	-	-	-	
32,33	0	0	0	0	0	0	0	0	0	
34	-2.066	0.829	1.667	-2.065	0.831	1.678	-	-	-	
35	-2.330	-2.330	-10.272	-2.334	-2.335	-10.266	-2.297	-2.167	-10.000	
36	0.832	-2.061	1.663	0.834	-2.060	1.674	-	-	-	
37,38	0	0	0	0	0	0	0	0	0	
39	-2.278	-2.284	-8.512	-2.294	-2.300	-8.550	-2.308	-2.361	-8.472	
40,41	0	0	0	0	0	0	0	0	0	
Max. discrepancy ratio				7%		Min. discrepancy ratio				0.6%



### 5.2.2 Symmetric Prestressing Case 2 (PC2)

The second case of symmetric prestressing was applied using 16 members, with a total actuation of 38.4 mm, as highlighted in Fig. 5-3. The eight members at the perimeter were shortened by 1.6 mm each, while the other inner members were altered by -3.2 mm. Theoretical calculations using these  $e_o$  values were performed according to derived Eqs. 3.20 and 3.21 and are presented in Table 5-4. Similar to PC1, these amounts of actuation were applied experimentally on the lab model, and the member strains were logged into the data logger. The resulting tensile forces are presented in columns 5 and 10 in Table 5-4. A good agreement can be observed between the application of the nonlinear theoretical equations and the lab results.

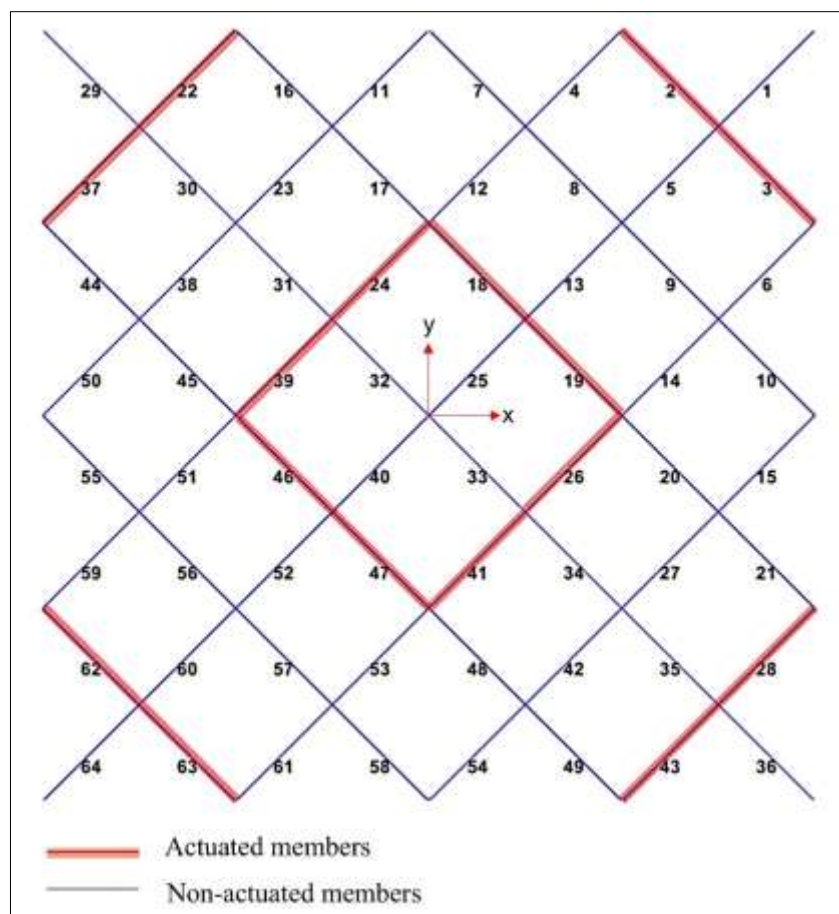


Fig. 5-3 Selected 16 members for prestress application in PC2

Table 5-4 Theoretical and experimental member actuation and prestressing degree in PC2

Member	Actuation (mm)	$t$ (N)			Member	Actuation (mm)	$t$ (N)		
		Present technique		Experiment			Present technique		Experiment
		Eq. 3.20	Eq. 3.21				Eq. 3.20	Eq. 3.21	
1		331.51	333.14	332.60	33		254.46	255.47	255.30
2	-1.6	125.53	126.42	126.10	34		267.42	268.53	267.66
3	-1.6	125.52	126.41	126.12	35		272.92	274.06	273.17
4		233.13	234.52	234.33	36		278.46	279.65	278.61
5		315.05	316.56	316.19	37	-1.6	36.146	36.462	36.25
6		233.08	234.48	232.71	38		54.355	54.613	54.12
7		7.28	7.19	7.11	39	-3.2	230.72	232.12	231.76
8		3.72	3.60	3.56	40		292.52	293.87	292.90
9		3.71	3.59	3.61	41	-3.2	230.64	232.04	231.04
10		7.25	7.16	7.20	42		54.421	54.681	53.55
11		59.92	60.22	59.87	43	-1.6	36.139	36.455	36.18
12		232.82	234.21	233.39	44		279.01	280.91	280.04
13		314.59	316.12	315.30	45		276.92	278.81	278.08
14		232.77	234.16	233.72	46	-3.2	271.04	272.92	272.44
15		59.97	60.27	59.51	47	-3.2	271.02	272.89	272.53
16		279.47	281.37	280.35	48		276.87	278.76	278.46
17		277.38	279.27	277.12	49		278.96	280.86	280.16
18	-3.2	271.53	273.41	272.95	50		59.891	60.192	59.66
19	-3.2	271.54	273.42	272.71	51		232.89	234.29	233.83
20		277.43	279.32	278.73	52		314.47	316	320.70
21		279.53	281.43	280.87	53		232.79	234.18	234.03
22	-1.6	36.15	36.46	-	54		59.963	60.265	59.51
23		54.36	54.62	54.39	55		7.426	7.335	7.23
24	-3.2	230.69	232.09	231.61	56		3.8738	3.7558	3.67
25		292.54	293.89	293.08	57		3.8751	3.7571	3.70
26	-3.2	230.63	232.03	231.54	58		7.4355	7.3445	7.20
27		54.42	54.68	54.19	59		233.21	234.6	233.64
28	-1.6	36.14	36.45	36.32	60		314.95	316.46	314.64
29		278.45	279.63	279.01	61		233.11	234.5	234.32
30		272.91	274.04	273.13	62	-1.6	125.58	126.48	126.15
31		267.41	268.52	267.69	63	-1.6	125.59	126.49	125.95
32		254.44	255.45	254.38	64		331.4	333.03	332.48
Max. discrepancy ratio				5.2%	Min discrepancy ratio				0.02%

The maximum tensile force was produced in cables 1 and 64 (see Table 5-4), with a discrepancy rate of 0.33% for Eq. 3.20 and 0.16% for Eq. 3.21. However, the minimum prestressed forces were in cables 8, 9, 56, and 57, with values around 3.7 N. The greatest discrepancy was between the experimental result and the computed result by Eq. 3.20 for cable 56, with an error ratio of 5.2%, which was the highest among all discrepancies. Similar to the previous case, the experimental data showed smaller force values due to the same reasons mentioned in PC1, which are the extension ability and relaxation of the cables. In addition, the joint connectors and actuator types also give part of error between experimental and theoretical computations (Zhang *et al.*, 2023), also not computing the axial stiffness of combined members perfectly.

The theoretical displacement findings from proposed Eqs. 3.20 and 3.21 are tabulated in columns 2-7 in Table 5-5. Both equations provide very consistent displacement values. The experimental displacements were determined using the same technique as explained in detail in the previous scenario, and the results are presented in columns 8-10 in Table 5-5. In the experimental procedure, not all 75 displacements were monitored. Only the joints that theoretically exhibited significant displacements were selected for observation. This approach allowed the cameras to zoom in on fewer points with higher resolution, thereby reducing error factors.

At nodes 13 and 29, the resultant displacement from the x, y, and z displacements in Table 5-5 was theoretically calculated around 12 mm by both proposed equations. In the lab, the resultant displacements were around the same value with an error ratio of 0.7% for node 13, and 0.8% for node 35. For all recorded lab displacements, the maximum discrepancy ratio was observed between the theoretical and experimental resultant displacement of joint 7, with

a ratio of 1.8%. The minimum discrepancy ratios were determined as 0.1% for nodes 3 and 35.

Comparing the displacement results between theory and experiment results in the second case of prestressing showed closeness and efficiency of the theoretical nonlinear computation equations (Eqs. 3.20 and 3.21) and experimental response of the 3D hyperbolic paraboloid cable net model.

The used actuation values are not optimal for prestressing using 16 members. These values were chosen to facilitate the lab work, as one full turn of the turnbuckle provides 1.6 mm of member alteration. This simplification is particularly useful when the structure needs to be returned to its original configuration for other prestressing applications. The ease of using a single cyclic wrench turn to achieve precise member alteration not only streamlines the experimental procedure but also minimises potential errors associated with more complex adjustments.

Additionally, the selected members were randomly chosen to be active in the prestressing process, ensuring a straightforward approach to the initial configuration. In the course of the experiment, some variations in member actuation were tested to explore different prestressing configurations. For instance, applying -3.2 mm (2 cycles) to the outer members and -1.6 mm to the inner members was tried. However, this actuation led to some members experiencing slack, which compromised the integrity of the prestressing process.

Table 5-5 Theoretical and experimental displacements in PC2

Node No.	Theoretical displacement (mm)						Experimental displacement (mm)		
	Eq. 3.20			Eq. 3.21					
	$dx$	$dy$	$dz$	$dx$	$dy$	$dz$	$dx$	$dy$	$dz$
1,2	0	0	0	0	0	0	0	0	0
3	2.011	2.016	-8.010	2.022	2.027	-8.037	2.018	2.010	-8.019
4,5	0	0	0	0	0	0	0	0	0
6	-3.570	-0.545	7.409	-3.574	-0.549	7.408	-3.426	-0.520	7.330
7	1.005	1.005	-5.791	1.007	1.007	-5.796	1.000	1.000	-5.688
8	-0.538	-3.564	7.410	-0.542	-3.568	7.409	-0.530	-3.432	7.324
9,10	0	0	0	0	0	0	0	0	0
11	2.284	-0.665	-4.461	2.298	-0.670	-4.483	-	-	-
12	-1.161	-1.919	3.301	-1.146	-1.930	3.268	-	-	-
13	1.832	1.814	-11.614	1.839	1.821	-11.639	1.840	1.795	-11.701
14	-1.895	-1.172	3.293	-1.906	-1.158	3.259	-	-	-
15	-0.646	2.267	-4.466	-0.652	2.281	-4.488	-	-	-
16,17	0	0	0	0	0	0	0	0	0
18	-1.814	1.815	7.712	-1.827	1.828	7.749	-1.847	-1.823	7.801
19	0.035	-0.033	2.495	0.032	-0.030	2.514	-	-	-
20	-0.817	0.808	8.269	-0.820	0.811	8.282	-0.830	0.830	8.194
21	0.020	0.004	3.426	0.020	0.004	3.432	-	-	-
22	0.821	-0.808	8.263	0.824	-0.810	8.275	0.817	-0.821	8.296
23	-0.030	0.034	2.501	-0.026	0.030	2.519			
24	1.819	-1.819	7.710	1.832	-1.832	7.748	1.811	-1.809	7.735
25,26	0	0	0	0	0	0	0	0	0
27	0.660	-2.269	-4.437	0.665	-2.283	-4.459	-	-	-
28	1.899	1.179	3.352	1.909	1.165	3.319	-	-	-
29	-1.800	-1.788	-11.564	-1.807	-1.795	-11.588	-1.798	-1.788	-11.462
30	1.173	1.917	3.349	1.159	1.928	3.315	-	-	-
31	-2.270	0.662	-4.432	-2.284	0.668	-4.454	-	-	-
32,33	0	0	0	0	0	0	0	0	0
34	0.535	3.565	7.422	0.539	3.569	7.421	0.500	3.540	7.331
35	-0.992	-0.991	-5.795	-0.994	-0.994	-5.800	-1.000	-1.040	-5.796
36	3.571	0.543	7.416	3.575	0.548	7.415	3.498	0.489	7.343
37,38	0	0	0	0	0	0	0	0	0
39	-1.999	-2.008	-8.027	-2.010	-2.019	-8.054	1.980	-2.100	-8.061
40,41	0	0	0	0	0	0	0	0	0
Max. discrepancy ratio				1.8%	Min. discrepancy ratio				0.1%

### 5.2.3 Asymmetric Prestressing Case 3 (PC3)

In the third case of applying prestress, a total of 96 mm of member shortening was achieved using 24 members to create asymmetric prestressing, referred to as PC3. The members highlighted in solid green were each altered by -4.8 mm, while the members marked with hatched blue were shortened by 3.2 mm as shown in Fig. 5-4. The  $e_o$  values (columns 2 and 7 in Table 5-6) were used in the theoretical computations, resulting in the outcomes presented in columns 3, 4, 8, and 9 in Table 5-6. Among the cables, cables 1 and 64 experienced the greatest pretension, while cables 28 and 43 exhibited the least pretension.

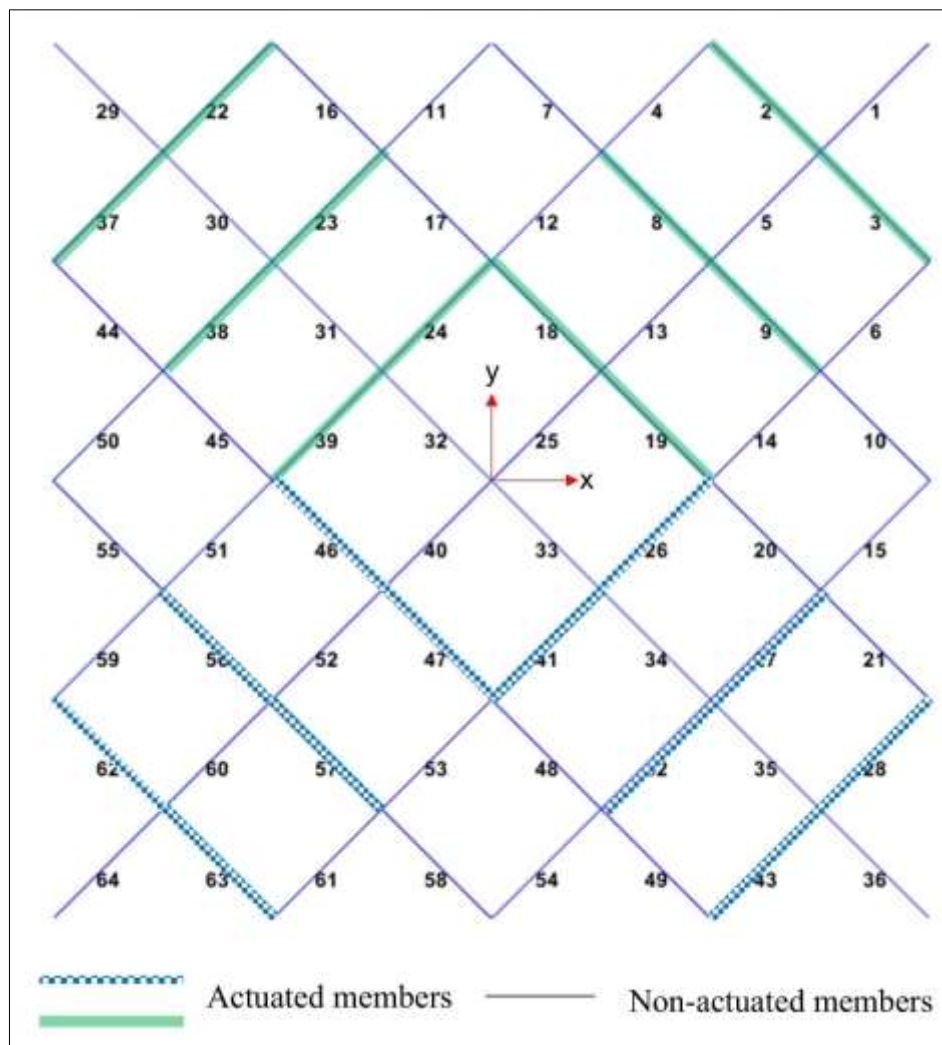


Fig. 5-4 Selected 24 members for prestress application in PC3

Similar to the previous prestress cases, the actuation amounts were applied on the marked members (see Fig. 5-4) of the lab model. The targeted asymmetric prestress achieved and recorded as a microstrain by the 64 channels data logger. These strain values transformed to the axial tensile forces and presented in columns 5 and 10 in Table 5-6. The members with the greatest and smallest prestress values were consistent with those predicted by theoretical computations. The comparison between the theoretical and experimental results showed a satisfactory agreement, demonstrating the accuracy of the derived numerical approach. The closeness between the theoretical and experimental results was tested by computing the Euclidian norm index ratio. It showed that the Euclidian distance between lab result to computed result by proposed Eq. 3.20 was 0.8 % while to proposed Eq. 3.21 was 0.36 %, thus, it can be concluded that the computed prestress by derived Eq. 3.21 gave a closer result to the experimental result.

Displacement results for both the theoretical model and the experimental model are presented in Table 5-6. The greatest resultant displacement occurred at node number 18, which measured 27.5 mm in the lab, while theoretical calculations using Eqs. 3.20 and 3.21 yielded displacements of 27.4 mm and 27.9 mm, respectively. This close agreement highlights the reliability of the theoretical models. Similar to the other two prestressing cases, nodes expected to undergo significant deformation, based on theoretical predictions, were closely monitored using digital cameras to record their displacements. This careful monitoring ensured accurate comparison data. The maximum resultant displacement from the x, y, and z displacements in Table 5-7 was observed at joints 3 and 18, as predicted by the derived Eqs. 3.20 and 3.21, with values around 27.5 mm. The experimental resultant displacements for these joints were close to this value, with a discrepancy of around 1%.

Table 5-6 Theoretical and experimental member actuation and prestressing degree in PC3

Member	Actuation (mm)	$t$ (N)			Member	Actuation (mm)	$t$ (N)		
		Present technique		Experiment			Present technique		Experiment
		Eq. 3.20	Eq. 3.21				Eq. 3.20	Eq. 3.21	
1		736.53	745.57	743.77	33		515.73	520.45	519.12
2	-4.8	647.04	665.60	663.97	34		534.72	539.64	538.13
3	-4.8	647.28	665.84	664.13	35		559.17	564.33	562.95
4		406.57	410.10	409.03	36		577.52	583.21	581.98
5		646.07	652.31	650.85	37	-4.8	254.43	267.59	267.04
6		367.95	371.32	370.35	38	-4.8	285.71	288.69	287.98
7		178.42	181.99	181.52	39	-4.8	404.6	408.21	407.12
8	-4.8	174.42	177.99	177.50	40		583.27	588.48	587.09
9	-4.8	174.88	178.46	178.17	41	-3.2	363.79	367.2	366.04
10		178.78	182.38	181.75	42	-3.2	245.91	248.26	247.63
11		291.65	294.63	293.89	43	-3.2	120.15	123.54	123.10
12		403.45	406.96	405.93	44		445.48	449.23	448.25
13		624.87	630.60	629.02	45		437.65	441.38	440.39
14		364.54	367.88	366.97	46	-3.2	428.23	431.95	430.86
15		252.35	254.72	254.03	47	-3.2	429.76	433.52	432.46
16		487.39	491.64	490.34	48		439.49	443.32	442.12
17		480.12	484.38	483.29	49		446.94	450.82	449.81
18	-4.8	472.21	476.49	475.34	50		292.02	295.03	294.29
19	-4.8	473.98	478.30	477.05	51		407.24	410.83	409.86
20		482.52	486.89	485.80	52		615.76	621.3	619.87
21		489.56	493.97	492.82	53		367.89	371.3	370.19
22	-4.8	254.21	267.36	-	54		252.68	255.08	254.47
23	-4.8	285.15	288.11	287.38	55		148.64	150.86	150.39
24	-4.8	402.99	406.59	405.59	56	-3.2	144.37	146.57	146.21
25		584.74	589.97	588.38	57	-3.2	144.81	147.02	144.97
26	-3.2	362.34	365.73	364.84	58		149	151.24	149.39
27	-3.2	245.37	247.70	247.19	59		410.44	414.06	412.15
28	-3.2	119.90	123.28	123.05	60		632.03	637.84	635.02
29		611.09	618.80	617.32	61		371.3	374.75	372.13
30		571.05	576.59	575.15	62	-3.2	352.56	358.36	355.09
31		540.95	546.08	544.77	63	-3.2	352.93	358.74	354.45
32		517.15	521.93	520.80	64		679.13	685.75	682.87
Max. discrepancy ratio				4.9%	Min discrepancy ratio				0.16%



Table 5-7 Theoretical and experimental displacements in PC3

Node No.	Theoretical displacement (mm)						Experimental displacement (mm)		
	Eq. 3.20			Eq. 3.21					
	$dx$	$dy$	$dz$	$dx$	$dy$	$dz$	$dx$	$dy$	$dz$
1,2	0	0	0	0	0	0	0	0	0
3	7.413	7.439	-25.375	7.491	7.518	-25.532	7.421	7.447	-25.200
4,5	0	0	0	0	0	0	0	0	0
6	0.636	-0.781	-2.292	0.706	-0.782	-2.450			
7	6.314	6.550	-25.380	6.379	6.619	-25.527	6.324	6.560	-25.195
8	-0.583	1.610	-4.377	-0.582	1.681	-4.531			
9,10	0	0	0	0	0	0	0	0	0
11	-1.697	-0.947	4.631	-1.719	-0.953	4.675			
12	-1.245	-2.400	3.384	-1.221	-2.411	3.328			
13	3.178	3.821	-15.785	3.198	3.853	-15.807	3.185	3.831	-15.605
14	-2.336	0.722	-0.618	-2.350	0.757	-0.679			
15	-1.080	0.045	0.695	-1.090	0.047	0.696			
16,17	0	0	0	0	0	0	0	0	0
18	-7.077	7.089	25.554	-7.227	7.239	25.937	-7.140	7.172	25.620
19	-5.022	5.236	21.716	-5.082	5.302	21.821	-5.024	5.261	21.559
20	-2.077	2.744	12.197	-2.094	2.778	12.179	-2.076	2.771	12.046
21	0.159	1.846	2.923	0.154	1.873	2.908			
22	0.615	0.097	6.937	0.615	0.113	6.919			
23	2.615	-2.394	14.043	2.632	-2.407	14.080	2.626	-2.385	13.922
24	3.949	-3.948	16.033	4.006	-4.005	16.185	3.982	-3.961	15.969
25,26	0	0	0	0	0	0	0	0	0
27	0.730	2.644	6.643	0.734	2.675	6.701	0.754	2.669	6.641
28	2.328	3.238	7.465	2.342	3.241	7.450	2.341	3.228	7.381
29	-1.447	-0.750	-10.418	-1.453	-0.746	-10.424	-1.444	-0.746	-10.295
30	1.245	2.376	3.473	1.237	2.393	3.452			
31	0.880	0.940	2.739	0.887	0.948	2.756			
32,33	0	0	0	0	0	0	0	0	0
34	0.895	1.102	1.627	0.902	1.075	1.557			
35	-3.663	-3.432	-17.592	-3.695	-3.461	-17.673	-3.655	-3.425	-17.446
36	0.148	0.770	-0.462	0.119	0.775	-0.532			
37,38	0	0	0	0	0	0	0	0	0
39	-4.166	-4.190	-16.162	-4.206	-4.230	-16.251	-4.160	-4.184	-16.044
40,41	0	0	0	0	0	0	0	0	0
Max. discrepancy ratio				1.3%	Min. discrepancy ratio				0.1%

The comparison between experimental and theoretical displacements showed a good correlation, indicating a good level of agreement between the two sets of results.

### **5.3 ANALYSIS PHASE RESULTS**

For flexible types of space structures, it is necessary to first prestress them to a sufficient level of pretensioning before subjecting them to carrying loads. From the previous section, various prestressing scenarios were applied. The analysis continues with PC1, and the loading cases are subsequently applied to the model.

The first loading case involved subjecting the model to only gravity loads at some joints. The second loading case involved applying horizontal loads alone. Finally, the last case involved applying both horizontal and vertical joint loads simultaneously.

#### **5.3.1 Vertical Nodal Loading Case (LC1)**

The first loading case involved applying a load of 20 N in the z-direction (gravity) to all joints except joints 3, 7, 35, and 39, as shown in Fig. 5-5. Theoretical calculations were performed using the derived Eq. 3.40, and the results are presented in Table 5-8. Columns 6 and 10 show the total prestress and derived force from the applied loads. These values are presented to indicate the remaining force inside the members, allowing to determine if any cable experiences slacking. The maximum remaining force was observed in cables 1 and 64, measuring 279.6 N, while the smallest force was found in cables 10, 7, 55, and 58, with 11.6 N. After the theoretical computations were completed,

the loadings were applied to the nodal experimental model. The member forces caused solely by the loadings were measured by the strain gauges and are presented in columns 8 and 12. The results for both the lab and theoretical computations showed a well-suited correlation during the analysis process under load case 1. Based on reported data in Table 5-8, the maximum and minimum error ratios between the experimental and theoretical internal forces were 7% and 0% for members 37 and 48, respectively. This 7% error ratio may be attributed to the prestressing of the cable prior to loading, as the response of the cable net system fundamentally depends on the degree of prestress rather than its axial stiffness (Kwan, 1998).

The numerical displacement of the joints after applying vertical loads was calculated using derived Eq. 3.40, and the results for the analysis stage under this specific loading condition are presented in Table 5-9. Subsequently, some specific joints that exhibited greater displacements compared to other loaded joints were selected for monitoring during the experimental displacement capturing.



Fig. 5-5 Experimental model under vertical joint loads

Table 5-8 Nodal loads, theoretical and experimental member forces for LC1

Joint No.	Nodal Load (N)			Member No.	Internal Force (N)			Member No.	Internal Force (N)			
	$P_x$	$P_y$	$P_z$		Theory		Experiment		Theory		Experiment	
					$T+t$	$T$	$T$		$T+t$	$T$	$T$	
1,2	0	0	0									
3	0	0	0	1	279.59	24.01	23.88	33	184.87	-19.17	-18.32	
4,5	0	0	0	2	107.48	18.41	17.41	34	189.86	-19.04	-18.75	
6	0	0	-20	3	107.48	18.40	18.60	35	198.32	-18.08	-18.13	
7	0	0	0	4	227.20	104.21	105.25	36	201.51	-17.83	-17.38	
8	0	0	-20	5	265.31	21.68	22.29	37	68.20	49.22	45.77	
9,10	0	0	0	6	227.16	104.21	104.73	38	163.09	80.96	79.65	
11	0	0	-20	7	11.62	-27.88	-27.45	39	215.46	96.59	94.72	
12	0	0	-20	8	12.55	-25.02	-24.61	40	253.80	23.83	23.16	
13	0	0	-20	9	12.54	-25.03	-24.81	41	215.40	96.58	95.62	
14	0	0	-20	10	11.61	-27.89	-27.23	42	163.19	81.02	79.83	
15	0	0	-20	11	169.01	83.62	82.77	43	68.17	49.19	48.46	
16,17	0	0	0	12	220.89	99.32	98.03	44	96.51	-59.91	-60.22	
18	0	0	-20	13	264.04	24.27	23.36	45	95.30	-57.54	-57.03	
19	0	0	-20	14	220.85	99.31	99.45	46	91.39	-57.14	-56.16	
20	0	0	-20	15	169.11	83.67	81.38	47	91.38	-57.13	-55.68	
21	0	0	-20	16	96.61	-59.98	-61.12	48	95.28	-57.54	-57.55	
22	0	0	-20	17	95.40	-57.61	-56.99	49	96.48	-59.92	-59.35	
23	0	0	-20	18	91.51	-57.20	-56.15	50	169.00	83.62	82.38	
24	0	0	-20	19	91.51	-57.20	-56.88	51	220.92	99.32	98.95	
25,26	0	0	0	20	95.42	-57.60	-57.92	52	264.00	24.28	24.03	
27	0	0	-20	21	96.64	-59.98	-58.59	53	220.86	99.30	100.50	
28	0	0	-20	22	68.21	49.22	0.00	54	169.11	83.68	82.32	
29	0	0	-20	23	163.08	80.96	79.54	55	11.63	-27.93	-28.01	
30	0	0	-20	24	215.45	96.59	94.96	56	12.56	-25.07	-24.43	
31	0	0	-20	25	253.80	23.83	22.81	57	12.56	-25.07	-24.72	
32,33	0	0	0	26	215.41	96.58	96.75	58	11.63	-27.93	-27.69	
34	0	0	-20	27	163.19	81.01	80.18	59	227.23	104.21	103.29	
35	0	0	0	28	68.17	49.19	49.43	60	265.28	21.69	20.57	
36	0	0	-20	29	201.49	-17.83	-18.26	61	227.16	104.20	100.12	
37,38	0	0	0	30	198.30	-18.09	-16.97	62	107.52	18.41	18.03	
39	0	0	0	31	189.86	-19.04	-17.99	63	107.52	18.41	18.52	
40,41	0	0	0	32	184.86	-19.17	-18.68	64	279.55	24.03	23.82	
Max. discrepancy ratio					7%		Min. discrepancy ratio					0.01%

Fig. 5-6 shows the lab measured values for displacement computation for the selected joints 31, 34, 35, and 36, which exhibited significant movement before and after the loading was applied. The displacements were calculated in a manner similar to that presented in detail in section 5.2.1.1.

The model showed a symmetric vertical nodal displacement for equivalent joints under the balanced applied vertical joint loads as shown in Table 5-9. The group of joints 6, 8, 34, and 36 experienced around -8 mm for both theoretical and experimental vertical movements, with a maximum discrepancy ratio of 1.2% for joint 36. For the opposite joints 7 and 35, the vertical displacements were around 4.5 mm, with a 2% error for joint 7. The other opposite joints 11, 15, 27, and 31 produced vertical displacements of around -2.85 mm in theoretical calculations, while the experimental results were slightly greater, with a maximum discrepancy rate of 2.7% at joint 31.

The maximum discrepancy ratio among the determined  $dz$  displacements was 2.8%, while the minimum discrepancy ratio was 0.2% for joints 31 and 8 respectively.

Both the theoretical results and the experimental results from the experimental model response showed good agreement with each other. This consistency is due to the predictive strength of the derived nonlinear technique in computing member forces as well as the displacements of the joints under external loads.

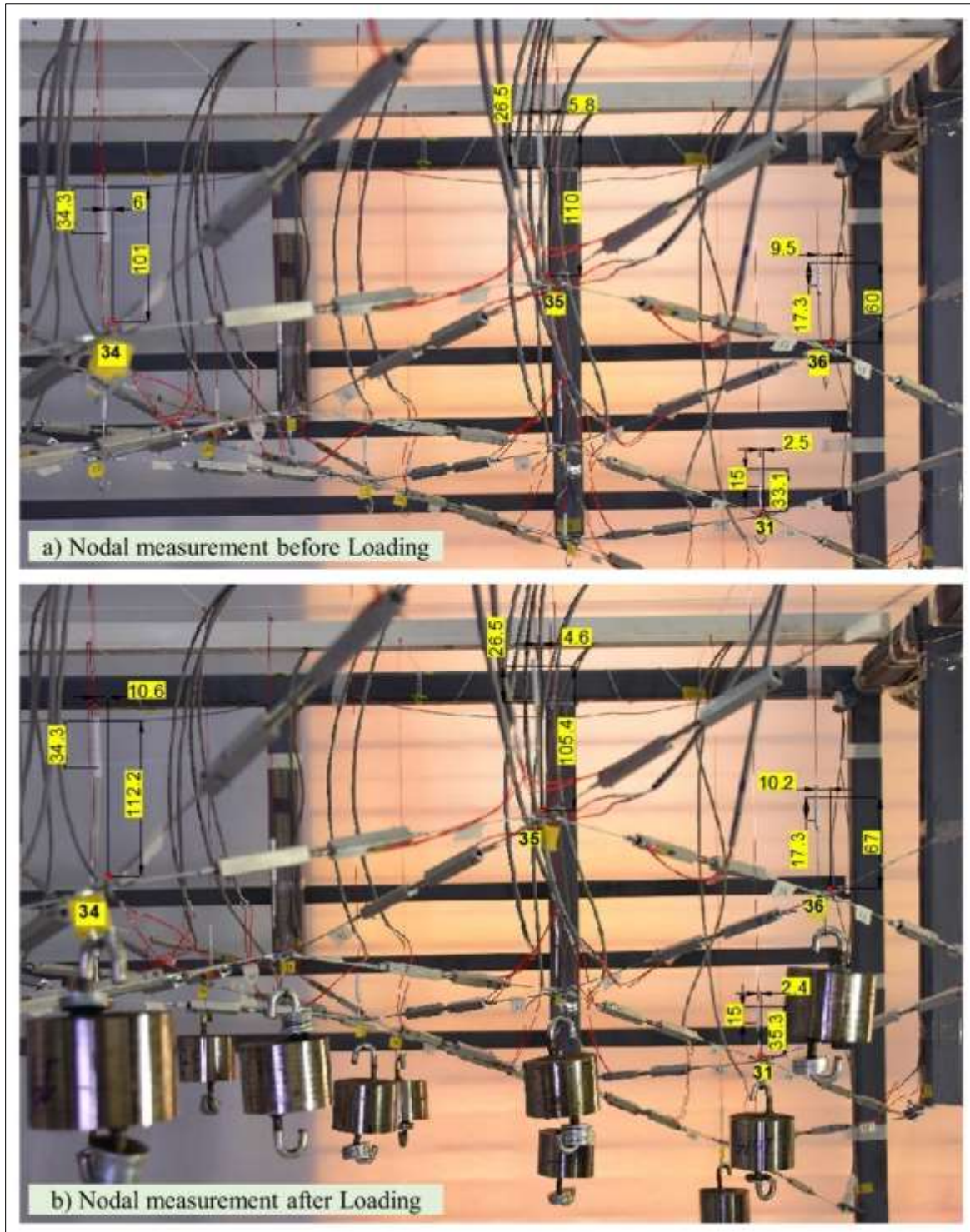


Fig. 5-6 Joint measurements in (mm) for experimental displacement computing for LC1

Table 5-9 Theoretical and experimental displacement under LC1

Node No.	Displacement (mm) due to load alone					
	Present Technique			Experiment		
	dx	dy	dz	dx	dy	dz
1,2	0	0	0	0	0	0
3	-0.117	-0.117	0.246	-	-	-
4,5	0	0	0	0	0	0
6	3.307	0.331	-8.067	-	0.316	-8.000
7	-1.116	-1.117	4.304	-1.106	-	4.204
8	0.334	3.311	-8.070	0.336	-	-8.054
9,10	0	0	0	0	0	0
11	1.022	-0.153	-2.852	1.071	-0.151	-2.870
12	0.557	0.142	-1.320	-	-	-
13	-0.226	-0.222	-0.021	-	-	-
14	0.140	0.562	-1.317	-	-	-
15	-0.157	1.021	-2.842	-0.126	-	-2.904
16,17	0	0	0	0	0	0
18	0.133	-0.131	-0.532	-	-	-
19	-0.194	0.193	0.531	-	-	-
20	-0.357	0.349	1.186	-	-	-
21	-0.001	0.000	-2.916	-	-	-
22	0.353	-0.352	1.181	-	-	-
23	0.193	-0.195	0.533	-	-	-
24	-0.133	0.133	-0.534	-	-	-
25,26	0	0	0	0	0	0
27	0.154	-1.025	-2.858	0.188	-1.012	-2.834
28	-0.145	-0.566	-1.324	-	-	-
29	0.223	0.221	-0.034	-	-	-
30	-0.563	-0.145	-1.330	-	-	-
31	-1.022	0.154	-2.853	-	0.133	-2.933
32,33	0	0	0	0	0	0
34	-0.335	-3.311	-8.066	-0.369	-3.353	-8.163
35	1.117	1.117	4.303	1.184	1.132	4.340
36	-3.307	-0.331	-8.065	-3.218	0.347	-8.092
37,38	0	0	0	0	0	0
39	0.118	0.117	0.243	-	-	-
40,41	0	0	0	0	0	0
Max. discrepancy ratio			2.8%	Min. discrepancy ratio		0.2%



### 5.3.2 Horizontal Nodal Loading Case (LC2)

Horizontal joint loads were applied to the joints located along both diagonal dimensions of the model. An 80 N load was applied to each of the 12 nodes, except for the centre joint (joint 21). Nodes 18-24 (except 21) were loaded parallel to the positive x-axis of the model, while nodes 3, 7, 13, 29, 35, and 39 were loaded parallel to the positive y-axis (see Fig. 5-7). The horizontal loads were applied using a cable that passed over a smooth pulley with a fixed flange. There are two rings at both ends of the cable: one attached to the joint rings and the other used for hanging the loads. The supports of the pulley are movable to maintain the required horizontal level with the loaded joints, as illustrated in Fig. 5-8.



Fig. 5-7 Experimental model under horizontal joint loads



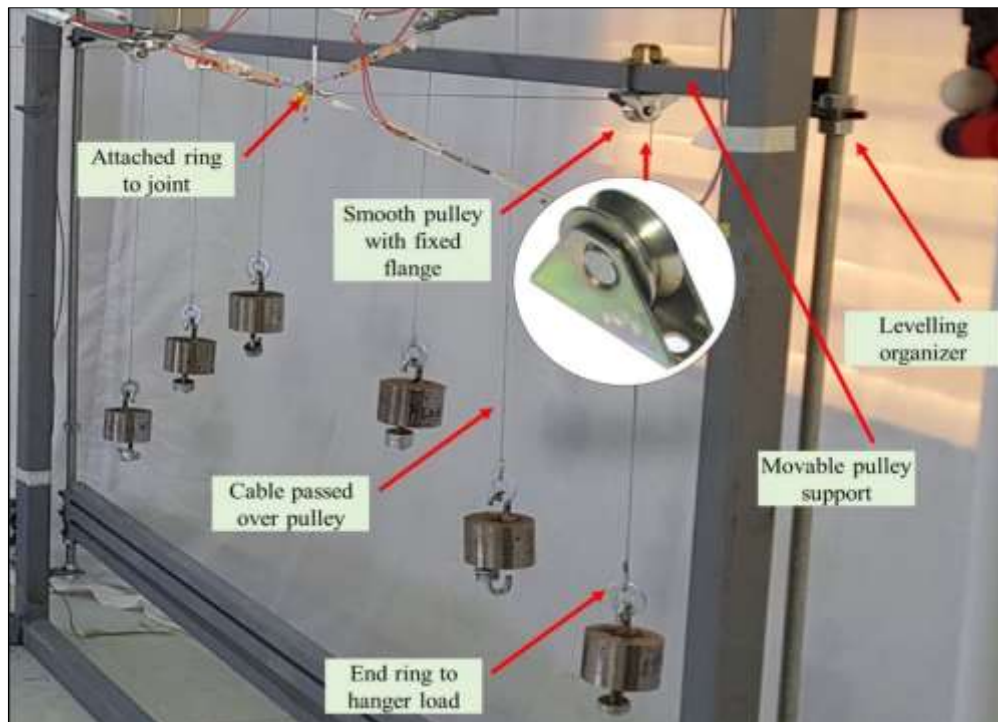


Fig. 5-8 Detailed experimental setup for horizontal load distribution

Theoretical calculations under the horizontal load condition alone in LC2 yielded the results presented in Table 5-10. It can be observed from the remaining axial force ( $T+t$ ) in columns 6 and 10 that some cables, namely members 2, 8, and 28, experienced slack due to the applied horizontal loads. This issue will be addressed in the next section (see section 5.2.3). The lowest remaining cable force, excluding the slackened ones, was in member 7 with a value of 2.43 N, while the greatest force was observed in member 64 with an amount of 558.03 N. In the lab, the same joints were loaded similarly to the theoretical model, yielding the results presented in columns 8 and 12 in Table 5-10. When the slackened cables reached zero tensile stress, they became inactive and showed zero strain readings on the data logger. This occurs because cable members cannot transfer compressive stress if they do not have a sufficient prestressing amount prior to the loading. The compressive axial force works to reduce the pretension until it reaches zero, after which the cable becomes inactive in carrying loads.

Table 5-10 Nodal loads, theoretical and experimental member forces for LC2

Joint No.	Nodal Load (N)			Member No.	Internal Force (N)			Member No.	Internal Force (N)				
					Theory		Experiment		Theory		Experiment		
	$P_x$	$P_y$	$P_z$		$T+t$	$T$	$T$		$T+t$	$T$	$T$		
1,2	0	0	0										
3	0	80	0	1	200.70	-55.35	-55.45	33	327.32	122.89	125.66		
4,5	0	0	0	2	0	0	0	34	281.09	71.78	71.00		
6	0	0	0	3	57.04	-32.52	-33.14	35	231.69	14.88	15.08		
7	0	80	0	4	142.39	19.26	20.02	36	183.52	-36.26	-36.37		
8	0	0	0	5	249.05	5.01	5.00	37	142.89	123.70	124.30		
9,10	0	0	0	6	126.73	3.63	3.53	38	200.39	118.20	120.33		
11	0	0	0	7	2.43	-37.04	-37.58	39	200.58	81.57	83.38		
12	0	0	0	8	0	0	0	40	341.66	111.30	113.09		
13	0	80	0	9	55.05	17.52	18.01	41	182.67	63.70	65.27		
14	0	0	0	10	56.99	17.53	17.92	42	74.05	-8.20	-8.68		
15	0	0	0	11	146.21	60.75	61.47	43	53.35	34.17	33.89		
16,17	0	0	0	12	142.27	20.55	25.37	44	230.18	73.60	74.08		
18	80	0	0	13	299.90	59.73	60.18	45	220.76	67.77	68.77		
19	80	0	0	14	124.96	3.27	3.34	46	211.76	63.09	63.61		
20	80	0	0	15	19.75	-65.76	-66.71	47	264.83	116.17	116.43		
21	0	0	0	16	123.34	-33.41	-34.19	48	269.23	116.26	117.93		
22	80	0	0	17	116.29	-36.87	-36.93	49	271.86	115.30	115.68		
23	80	0	0	18	109.81	-39.05	-39.28	50	205.27	119.82	121.36		
24	80	0	0	19	163.36	14.50	14.74	51	205.99	84.25	83.76		
25,26	0	0	0	20	166.18	13.00	12.94	52	410.24	170.11	172.37		
27	0	0	0	21	166.94	10.17	10.92	53	188.61	66.91	69.40		
28	0	0	0	22	85.45	66.25	-	54	79.75	-5.76	-6.07		
29	0	80	0	23	143.40	61.21	62.06	55	82.86	43.33	43.63		
30	0	0	0	24	140.73	21.73	20.82	56	79.61	42.01	42.14		
31	0	0	0	25	345.44	115.07	115.36	57	136.97	99.37	99.78		
32,33	0	0	0	26	123.37	4.40	4.41	58	140.13	100.60	100.80		
34	0	0	0	27	15.89	-66.36	-67.55	59	209.16	86.00	87.38		
35	0	80	0	28	0	0	0	60	474.35	230.35	232.49		
36	0	0	0	29	516.32	296.55	299.28	61	194.03	70.92	71.47		
37,38	0	0	0	30	446.60	229.80	228.68	62	213.05	123.45	126.51		
39	0	80	0	31	379.09	169.79	171.28	63	270.71	181.11	181.07		
40,41	0	0	0	32	319.50	115.08	117.34	64	558.03	302.03	304.25		
Max. discrepancy ratio					7%			Min. discrepancy ratio					0.02%

Table 5-11 Theoretical and experimental displacement under LC2

Node No.	Displacement (mm) due to load alone					
	Present Technique			Experiment		
	$dx$	$dy$	$dz$	$dx$	$dy$	$dz$
1,2	0	0	0	0	0	0
3	2.642	4.461	-10.179	-	4.110	-10.026
4,5	0	0	0	0	0	0
6	-4.002	-0.077	9.047	-3.996	-0.053	9.149
7	2.465	5.942	-12.849	2.501	6.163	-12.832
8	0.219	2.261	-5.175	-	2.161	-5.275
9,10	0	0	0	0	0	0
11	-2.564	0.316	5.589	-2.715	0.263	5.592
12	-3.040	0.135	6.068	-2.956	-	6.005
13	1.069	2.975	-2.288	1.134	3.055	-2.256
14	-0.120	2.083	-3.923	-	2.176	-4.028
15	-0.144	3.944	-8.843	-0.117	4.892	-8.952
16,17	0	0	0	0	0	0
18	0.831	-0.743	-1.066	-	-7.120	-1.032
19	2.312	-2.303	-5.302	2.224	-	-5.297
20	2.746	-2.991	-6.831	2.886	-3.209	-6.910
21	4.284	-0.666	-1.473	4.348	-0.705	-1.339
22	3.531	-2.816	4.337	3.615	-2.890	4.276
23	5.286	-4.190	11.976	5.349	-4.275	11.892
24	9.816	-5.192	22.339	9.730	4.998	22.011
25,26	0	0	0	0	0	0
27	0.141	1.271	2.775	-	-	-
28	0.343	0.907	1.808	-	-	-
29	1.767	2.510	3.682	1.961	2.488	3.757
30	-0.827	0.526	-0.983	-	-	-
31	-1.437	0.291	-2.885	-1.453	0.342	-2.953
32,33	0	0	0	0	0	0
34	0.196	0.100	0.082	-	-	-
35	1.583	2.081	3.483	1.523	2.153	3.499
36	-1.851	0.068	-4.179	-1.865	-	-4.315
37,38	0	0	0	0	0	0
39	1.080	1.152	1.987	-	-	-
40,41	0	0	0	0	0	0
Max. discrepancy ratio			3%	Min. discrepancy ratio		0.1%

The theoretical results for compressive forces in some members, as shown in Table 5-9, indicate that, for instance, cable number 1 has an internal compressive force of 55.35 N due to applied loads. With an initial pretension of 256.05 N, the remaining force is 200.70 N, which is sufficient to keep the cable in tension. Among all members, cable 64 experienced the maximum internal force, recorded as 302.03 N theoretically and 304.25 N experimentally, yielding an error ratio of 0.7%. Conversely, cable 14, which was less affected by the applied load, produced internal forces of 3.27 N and 3.34 N in the theoretical and experimental results, respectively. The maximum ratio of discrepancy was determined by 7% for member 21, and the zero discrepancy was for member 63.

There is satisfactory agreement between the theoretical and lab measurements regarding the results obtained during the analysis stage. Some experimental member forces were slightly smaller or greater than the numerical forces, while others were very close to each other. These discrepancies can be attributed to error sources from the previous steps prior to the analysis phase.

Similar to LC1, the theoretical and experimental displacements are presented in Table 5-11. For this loading case, among the monitored nodes, joint 24 was observed to have the maximum resultant displacement of 24.947 mm in theory and 24.579 mm in the experiment, with an error rate of 1.47%. Conversely, joint 34 experienced resultant displacements of 0.235 mm in theory, but this was not recorded experimentally and was neglected due to its small value.

Among the significant vertical displacements, the minimum and maximum discrepancy ratios were 0.1% and 3% for joints 19 and 36, respectively. The alignment of theoretical predictions with experimental observations demonstrates the reliability and accuracy of the analysis approach. Despite the

small discrepancies between the results, the proposed technique proves to be very effective for analysing such complex cable net models.

### 5.3.3 Vertical and Horizontal Nodal Loading Case (LC3)

The third loading condition applied to the model involved placing vertical and horizontal joint loads simultaneously. The free nodes, excluding joints 3, 7, 35, and 39, were loaded with -20 N, and joint 8 was loaded with -40 N to prevent the model from slacking. Only joints 3, 7, 13, 29, 35, and 39 were loaded with 20 N parallel to the positive y-axis of the model. The axial forces were computed theoretically using Eq. 3.40 and are presented in Table 5-12. The same loading was applied to the lab model, and the axial force response is also presented in Table 5-12.

The maximum compression force was observed in member 16, with a theoretical value of 73.9 N and an experimental value of 71.7 N which gives 2.9 % of discrepancy ratio. The maximum tension force was observed in member 6, with a theoretical value of 140.9 N and an experimental value of 138.6 N with 1.6 % error ratio. The maximum and minimum discrepancy ratios were computed by 7% for member 58 and 0.5% for members 7 and 11.

All the results are sufficiently close to each other, as predicted by the nonlinear calculated theory, demonstrating the accuracy and reliability of the theoretical model.

The numerical displacement of the joints, subjected to simultaneous vertical and horizontal loads as depicted in Fig. 5-9, was calculated using derived Eq. 3.40. The results from the analysis stage for this loading condition are summarized in Table 5-13. The displacements were determined similarly to the

displacements of prestress and other analysis cases. The maximum discrepancy ratio determined for node 11 with the value of 7%, while the minimum discrepancy was for joint 31 by 0.23%.

The maximum vertical displacement was computed at joint 8. The theoretical and experimental  $dz$  displacements were -17.6 mm and -17.4 mm with the discrepancy ratio of 1%, respectively.

There was good agreement between the theoretical predictions and the experimental results from the experimental model, underscoring the accuracy of the derived nonlinear technique in predicting joint displacements equivalent to member forces under combined vertical and horizontal loads.



Fig. 5-9 Experimental model under vertical and horizontal joint loads

Table 5-12 Nodal loads, theoretical and experimental member forces for LC3

Joint No.	Nodal Load (N)			Member No.	Internal Force (N)			Member No.	Internal Force (N)			
	$P_x$	$P_y$	$P_z$		Theory		Experiment		Theory		Experiment	
					$T+t$	$T$	$T$		$T+t$	$T$	$T$	
1,2	0	0	0									
3	0	20	0	1	252.20	-3.38	-3.26	33	250.09	-8.67	-8.09	
4,5	0	0	0	2	78.00	-11.09	-10.75	34	259.29	-7.05	-6.45	
6	0	0	-20	3	92.42	3.33	3.15	35	269.58	-5.94	-5.83	
7	0	20	0	4	228.36	105.36	104.69	36	276.10	-5.60	-5.08	
8	0	0	-40	5	254.03	10.39	9.48	37	92.16	50.38	48.48	
9,10	0	0	0	6	263.96	140.97	138.60	38	193.68	82.88	81.42	
11	0	0	-20	7	6.25	-33.25	-33.40	39	244.43	98.47	94.39	
12	0	0	-20	8	7.23	-30.33	-29.43	40	320.20	27.69	26.03	
13	0	20	-20	9	7.17	-30.39	-30.61	41	273.33	127.40	124.60	
14	0	0	-20	10	2.60	-36.88	-32.75	42	193.23	82.37	81.40	
15	0	0	-20	11	170.79	85.40	85.80	43	91.56	49.80	48.45	
16,17	0	0	0	12	222.25	100.67	100.09	44	132.29	-50.28	-49.23	
18	0	0	-20	13	253.30	13.52	15.01	45	129.53	-48.00	-47.26	
19	0	0	-20	14	252.17	130.59	127.80	46	126.16	-47.66	-47.33	
20	0	0	-20	15	169.64	84.20	81.93	47	140.32	-33.49	-33.10	
21	0	0	-20	16	82.71	-73.90	-71.68	48	144.64	-32.87	-31.30	
22	0	0	-20	17	81.34	-71.68	-71.39	49	147.40	-35.15	-34.30	
23	0	0	-20	18	77.14	-71.58	-69.41	50	199.84	85.72	83.56	
24	0	0	-20	19	91.12	-57.61	-58.52	51	252.05	101.52	102.32	
25,26	0	0	0	20	96.17	-56.87	-54.81	52	344.04	43.01	40.46	
27	0	0	-20	21	97.40	-59.24	-57.04	53	280.85	130.35	128.51	
28	0		-20	22	69.42	50.44	-	54	199.83	85.64	82.18	
29	0	20	-20	23	165.10	82.97	78.59	55	78.61	-20.01	-19.59	
30	0	0	-20	24	217.11	98.25	97.71	56	78.16	-17.23	-16.00	
31	0	0	-20	25	257.53	27.55	25.73	57	92.47	-2.92	-2.88	
32,33	0	0	0	26	246.89	128.03	125.17	58	93.32	-5.29	-4.91	
34	0	0	-20	27	164.01	81.84	80.36	59	261.01	106.71	101.91	
35	0	20	0	28	68.78	49.81	50.15	60	364.76	55.39	53.31	
36	0	0	-20	29	211.92	-7.41	-7.27	61	290.28	136.02	130.67	
37,38	0	0	0	30	208.55	-7.85	-8.14	62	170.22	42.26	41.45	
39	0	20	0	31	200.01	-8.90	-9.00	63	184.50	56.53	54.34	
40,41	0	0	0	32	195.17	-8.87	-8.31	64	400.52	74.89	76.15	
Max. discrepancy ratio					7%		Min. discrepancy ratio					0.5%

Table 5-13 Theoretical and experimental displacement under LC3

Node No.	Displacement (mm) due to applied load alone					
	Present Technique			Experiment		
	$dx$	$dy$	$dz$	$dx$	$dy$	$dz$
1,2	0	0	0	0	0	0
3	0.011	0.032	-0.050	-	-	-
4,5	0	0	0	0	0	0
6	2.920	0.272	-7.200	-	0.213	-7.234
7	-1.249	-1.018	4.751	-1.136	-1.111	4.667
8	1.260	7.387	-17.599	-	7.337	-17.391
9,10	0	0	0	0	0	0
11	0.683	-0.108	-2.129	0.625	-	-2.292
12	-0.026	0.161	-0.145	-	-	-
13	-0.110	0.173	-0.726	-	-	-
14	0.895	1.590	-1.993	0.862	1.500	-2.000
15	-0.162	1.061	-2.934	-0.159	1.099	-3.022
16,17	0	0	0	0	0	0
18	0.154	-0.152	-0.546	-	-	-
19	-0.141	0.021	0.249	-	-	-
20	-0.338	0.037	0.712	-	-	-
21	0.381	0.048	-3.239	0.337	-	-3.202
22	1.373	-0.125	3.368	1.364	-	3.485
23	0.184	-0.189	0.646	-	-	-
24	-0.155	0.155	-0.542	-	-	-
25,26	0	0	0	0	0	0
27	0.185	-1.194	-3.221	0.187	-1.160	-3.270
28	-0.125	-0.934	-2.100	-	-	-
29	0.590	0.390	0.273	-	-	-
30	0.280	0.121	0.561	-	-	-
31	-1.123	0.200	-3.004	-1.190	0.215	-3.011
32,33	0	0	0	0	0	0
34	-0.360	-3.544	-8.584	-0.313	-3.529	-8.627
35	1.344	1.286	4.427	1.302	1.276	4.464
36	-2.610	-0.135	-6.497	-2.651	-0.156	-6.406
37,38	0	0	0	0	0	0
39	0.321	0.338	0.648	-	-	-
40,41	0	0	0	0	0	0
Max. discrepancy ratio11			7%	Min. discrepancy ratio		0.23%



## 5.4 PRESERVING PHASE RESULTS

The derived nonlinear direct technique, using Eqs. 3.44 and 3.45, was validated through experimental control of nodal displacements alone, internal bar forces alone, and both nodal displacements and internal bar forces simultaneously on the complex structural model of a 3D hyperbolic paraboloid cable net. This phase was applied to the lab model in three different cases, each with distinct controlling targets. The detailed description of these applications is provided in the following subsections:

### 5.4.1 Nodal Displacement Preservation Case (DPC1)

The first preservation scenario (DPC1) was applied to PC1 to control the noticeable deformation that occurred during the prestressing process. The target was to reduce the nodal displacement for some nodes that exhibited the greatest vertical movement. Controlling the internal forces was not a priority, but the pretension of the members needed to be maintained without violation or slacking.

Some nodes, namely 7, 13, 19, 23, 29, and 35, showed remarkable vertical displacements during prestressing, with values of -10.27, -7.29, 7.91, 7.92, -7.26, and -10.27 mm, respectively. Thus, these nodes were selected as the targeted nodes that required restoration to reduce their displacements. Numerical calculations were performed to determine the required targeted vertical displacement for each selected node and to find the necessary  $e_0$  values for the preservation process. Ten members were allowed to be used as actuators during the preservation for displacement. These members were chosen after using a sensitivity technique to identify which members had the greatest impact

on restoring these displaced joints. Each member was examined separately; thus, these are not representing optimal actuators to provide the best preservation process.

The set of actuations was determined using the technique, and then these values were adjusted to a new set to be more practical and measurable in the lab. Therefore, actuators 5 and 60 were shortened by 1.6 mm, and the other eight actuators (8, 9, 23, 27, 38, 42, 56, 57) were lengthened by 1.6 mm. The alteration of 1.6 mm was chosen because it corresponds to one cycle of twisting the jack screw, which is easier for lab work and for returning the model to its original state after modification. The resulting numerical displacements during the preservation process are presented in Table 5-14 with the total actuation of 16 mm. These displacements were then added to the prestressed displacements to give the combined displacements after both prestressing and preservation, as shown in columns 5-7 in Table 5-14. The data presented for the theoretical preserved displacements are computed from derived Eq. 3.44. The output of proposed Eq. 3.45 is not presented because both equations yielded very similar values.

In the lab, the same amount of member actuation was applied to the specified members with the same values. The targeted joints were monitored during the experimental nodal displacement restoration, and the recorded data for displacements are presented in columns 8-10 in Table 5-14. The preserved experimental displacements, combined with the prestressed experimental displacements, are presented in columns 11-13 in Table 5-14.

Fig. 5-10 shows the illustrative profile for the nodal movement at the original configuration, prestressed configuration, and preserved configuration. It can be

clearly seen that the targeted joints have been raised to the desired position. The theoretical preserved displacements and combined displacements show an exceptional correlation with the experimental adjusted displacements, which proves the efficiency of the derived nonlinear equations. The selected set of  $e_o$  did not violate the member forces, and no slack was noticed in both the theoretical and lab models.

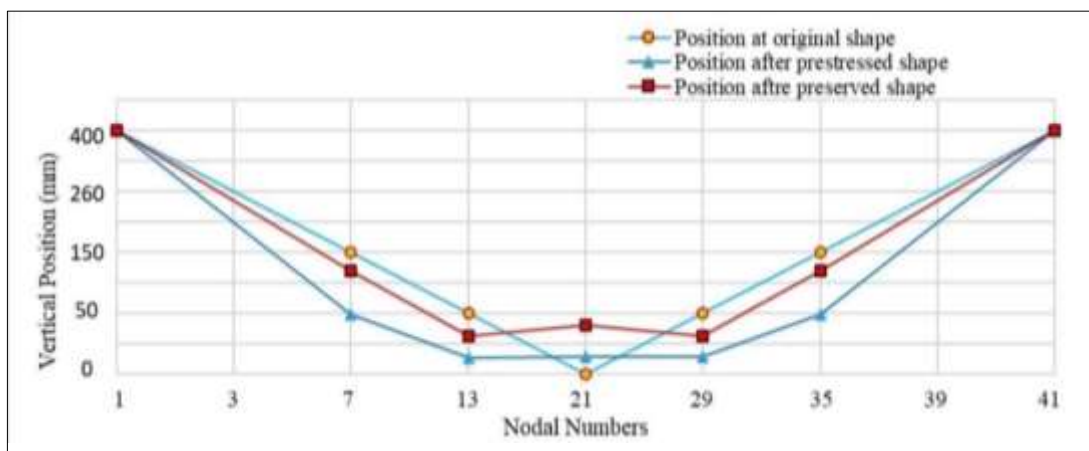


Fig. 5-10 Nodal movement for the targeted displacements in DPC1

From Fig. 5.10, node 21 deviated significantly from its original position because it was not indicated as a targeted joint to maintain its location. Additionally, the targeted joints were adjusted to be close to their original positions, but not fully restored to those positions. Achieving full restoration would have required more effort, more actuators, and a greater number of actuators. The maximum raised displacements were at joints 7 and 35, with theoretical values of 7.18 mm and experimental values of 7.04 mm with a 1.9% error ratio and 6.96 mm with a 3% error ratio, respectively. Similarly, the lowered joints 19 and 23 were indicated to reach -6.55 mm in theory. In the experiment, they approached -6.12 mm with a discrepancy rate of 6% for joint 19 and -6.2 mm with a discrepancy rate of 5% for joint 23. The maximum error ratio for the adjusted joints was recorded as 6.5% between the theoretical and

experimental preserved displacements at node 19, while the minimum error ratio was 0% at the restored nodes 13 and 29.

Table 5-14 Theoretical and experimental preserved and combined displacements for DPC1

Node	Preserved Displacement (mm)			Combined displacement of prestress and preservation			Preserved Displacement (mm)			Combined displacement of prestress and preservation			
	Present technique						Experiment						
	dx	dy	dz	dx	dy	dz	dx	dy	dz	dx	dy	dz	
3	-0.08	-0.08	0.14	2.20	2.21	-8.36	-	-	-	-	-	-	
6	-1.68	-0.11	3.84	-2.51	1.95	5.50	-	-	-	-	-	-	
7	-0.58	-0.58	7.18	1.76	1.76	-3.09	-0.51	-	7.04	1.76	-	-2.96	
8	-0.11	-1.68	3.84	1.95	-2.51	5.50	-	-	-	-	-	-	
11	2.21	-0.21	-5.05	1.86	1.84	-4.02	-	-	-	-	-	-	
12	0.52	-0.34	-0.92	-0.60	1.15	1.89	-	-	-	-	-	-	
13	0.17	0.17	3.49	1.51	1.50	-3.80	0.18	0.15	3.49	1.55	1.33	-3.57	
14	-0.34	0.51	-0.92	1.16	-0.61	1.89	-	-	-	-	-	-	
15	-0.21	2.21	-5.05	1.85	1.84	-4.02	-	-	-	-	-	-	
18	0.04	-0.04	-0.03	-1.93	1.93	7.88	-	-	-	-	-	-	
19	1.82	-1.82	-6.55	0.20	-0.20	1.36	1.87	-2.01	-6.12	0.22	-0.22	1.35	
20	0.52	-0.52	-0.10	0.20	-0.21	2.95	-	-	-	-	-	-	
21	0.00	0.00	5.15	0.02	0.00	8.03	-	-	-	-	-	-	
22	-0.52	0.52	-0.10	-0.20	0.21	2.95	-	-	-	-	-	-	
23	-1.82	1.82	-6.55	-0.20	0.20	1.37	-1.9	2.1	-6.2	-0.2	0.23	1.32	
24	-0.04	0.04	-0.03	1.93	-1.93	7.87	-	-	-	-	-	-	
27	0.21	-2.21	-5.04	-1.84	-1.85	-4.00	-	-	-	-	-	-	
28	0.34	-0.51	-0.91	-1.16	0.61	1.93	-	-	-	-	-	-	
29	-0.17	-0.17	3.49	-1.49	-1.48	-3.77	-0.18	-0.16	3.49	-1.49	-1.27	-3.54	
30	-0.51	0.35	-0.91	0.61	-1.15	1.93	-	-	-	-	-	-	
31	-2.21	0.21	-5.04	-1.85	-1.84	-3.99	-	-	-	-	-	-	
34	0.11	1.68	3.84	-1.95	2.51	5.50	-	-	-	-	-	-	
35	0.58	0.58	7.18	-1.75	-1.75	-3.10	0.55	0.52	6.96	-1.75	-1.65	-3.04	
36	1.68	0.11	3.84	2.52	-1.95	5.50	-	-	-	-	-	-	
39	0.08	0.08	0.14	-2.19	-2.20	-8.38	-	-	-	-	-	-	
Max. discrepancy ratio						6.5%	Min. discrepancy ratio						0.0%

### 5.4.2 Member Force Preservation Case (FPC2)

For the second objective of preservation, which involves controlling the member forces alone, the validation was checked using LC2 to address the slack in the members when horizontal forces were applied. In the second load case, some members, specifically cables 2, 8, and 28, became slack due to the presence of insufficient pretension when prestressed. When the horizontal nodal loads were applied, these cables experienced compressive forces greater than their pretension, rendering them inactive. For this reason, these cables need to be controlled and re-tensioned to become active again.

Theoretical calculations began by determining the desired pretension force for the slackened members and identifying the necessary member alterations to achieve this target. Referring to Table 5-10 (column 6), cables 2, 8, and 28 showed zero values. It can also be observed that the remaining pretension forces for cable 7 were 2.43 N and for cable 27 were 15.89 N. Therefore, these were also included among the targeted force preservations. Subsequently, eight members were specified to take on the role of actuators (see column 2 in Table 5-15) with a total actuation of 16 mm. The member forces during the controlling ( $t_c$ ) process were computed and are presented in columns 4 and 8 in Table 5-15. Finally, the remaining internal force ( $T+t+t_c$ ) was calculated to ensure all members were kept in tension and that slackening of different cables was prevented.

For the experimental model, the set of selected members' actuation were given to the model. The response of the cables recorded via the data logger and tabulated in columns 5 and 10 in Table 5-15. The  $t_c$  results from the experiment were very close to the numerical calculation for the preservation of internal force to overcome the slack members. In the theoretical computation, as an

example, it was requested from the proposed Eq. 3.45 to achieve a pretension of 54 N for cable 2. The computation attained 53.42 N by determining the necessary member actuation. In the laboratory, following actuation, a measurement of 54.05 N was recorded, with a discrepancy ratio of only 1.1%.

The maximum and minimum discrepancy ratios between the numerical computation and experimental forces were 2.8% and 0.02% for the members 43 and 55 respectively.

The selected members (2, 3, 7, 8, 27, 28, 36 and 43) as actuators provided satisfactory results; however, selecting different members might have yielded better results or required less efforts during the preservation process. Additionally, the member actuations were chosen to be easy for lab application. The theoretical results presented in Table 5-15 were calculated using from Eq. 3.45, which provided closer results to the lab data, with a Euclidian norm ratio of only 1.2%. In comparison, the computed forces using Eq. 3.44 in this case showed  $l_2$ -norm ratio of 9.3%. Despite these considerations, the technique remains highly effective and accurate for controlling the internal member forces in such a complicated model.

Table 5-15 Theoretical and experimental internal force for FPC2

Member No.	$e_o$ (mm)	Internal Force (N)			Member No.	$e_o$ (mm)	Internal Force (N)		
		Present technique		Experiment			Present technique		Experiment
		$T+t+t_c$	$t_c$	$t_c$			$T+t+t_c$	$t_c$	$t_c$
1		255.06	54.36	54.83	33		382.28	54.96	55.56
2	-1.6	53.42	53.42	54.05	34		337.70	56.61	57.19
3	-1.6	112.51	55.47	56.02	35		292.16	60.47	60.95
4		165.50	23.11	23.31	36	-1.6	253.94	70.42	71.37
5		295.61	46.56	46.83	37		148.98	6.09	6.27
6		139.93	13.20	13.24	38		214.97	14.58	14.67
7	-1.6	21.74	19.31	19.59	39		223.52	22.94	23.01
8	-1.6	17.65	17.65	17.74	40		384.03	42.37	42.68
9		70.64	15.59	15.76	41		196.38	13.71	13.76
10		72.64	15.65	15.76	42		104.47	30.42	30.46
11		161.01	14.80	15.03	43	-3.2	110.52	57.17	58.92
12		164.76	22.49	22.66	44		250.25	20.07	20.20
13		344.56	44.66	45.06	45		240.02	19.26	19.32
14		137.76	12.80	12.95	46		229.83	18.07	18.10
15		53.01	33.26	33.50	47		281.71	16.88	16.93
16		139.37	16.03	16.05	48		285.78	16.55	16.65
17		131.55	15.26	15.31	49		288.90	17.04	17.18
18		124.58	14.77	14.85	50		220.33	15.06	15.10
19		177.60	14.24	14.36	51		229.52	23.53	23.66
20		180.33	14.15	14.26	52		453.36	43.12	43.53
21		181.87	14.93	14.98	53		203.03	14.42	14.54
22		91.54	6.09	-	54		110.25	30.50	30.89
23		157.87	14.47	14.66	55		90.18	7.33	7.33
24		163.19	22.46	22.65	56		86.51	6.91	6.96
25		388.90	43.46	43.75	57		143.75	6.78	6.85
26		135.92	12.55	12.59	58		147.10	6.97	6.98
27	-1.6	49.32	33.44	33.85	59		232.99	23.83	24.02
28	-3.2	52.87	52.87	54.34	60		518.01	43.66	43.89
29		570.72	54.40	54.98	61		208.77	14.74	14.91
30		500.17	53.57	53.99	62		225.02	11.97	12.00
31		431.75	52.66	53.17	63		282.72	12.01	12.03
32		372.04	52.54	52.91	64		603.06	45.03	45.30
Max. discrepancy ratio				2.8%	Min. discrepancy ratio				0.02%

### 5.4.3 Simultaneous Preservation Case (SPC3)

The validation of the derived Eqs. 3.44 and 3.45 was also examined by simultaneously controlling both the internal force and nodal displacement. The same case as in FPC2 was used, but this time with an additional emphasis on displacement. In the theoretical computation, both targets for member forces and the selected nodal displacements were determined, and the necessary set of  $e_o$  values was requested to achieve these targets.

After the model was subjected to prestressing and external horizontal loads, its form was disturbed. Fig. 5-11 (a and b) shows the nodal positions of the joints on the concave and convex diagonal curves of the model. At the original position, the equivalent joints were at the same level. However, after prestressing and loading, they were no longer at the same height. Thus, the target was to restore these opposite joints to the same level. Additionally, the slackened cables required fastening and re-tensioning.

The calculation for attaining the stated targets identified the set of member actuations shown in the Table 5-15 with a total actuation of 51.7 mm. The members 2,3, 7, 8, 9, 10, 22, 24, 25, 28, 37, 38, 39, 43, 46, 47, 56, 57, 62, 63, and 64 were permitted to be used during the preservation process. The outcomes of the vertical displacements for both Eqs. 3.44 and 3.45 are presented in Table 5-16 in columns 4 and 5. Columns 2 and 3 in the Table 5-16 show the combined vertical displacement from the previous phases of prestressing and loading. The targeted joints for this preservation process are 3, 7, 13, 29, 35, and 39 on the concave diagonal curve, and joints 18-24, except central joint 21, are on the convex diagonal curve of the model, as shown in Fig. 5-11.



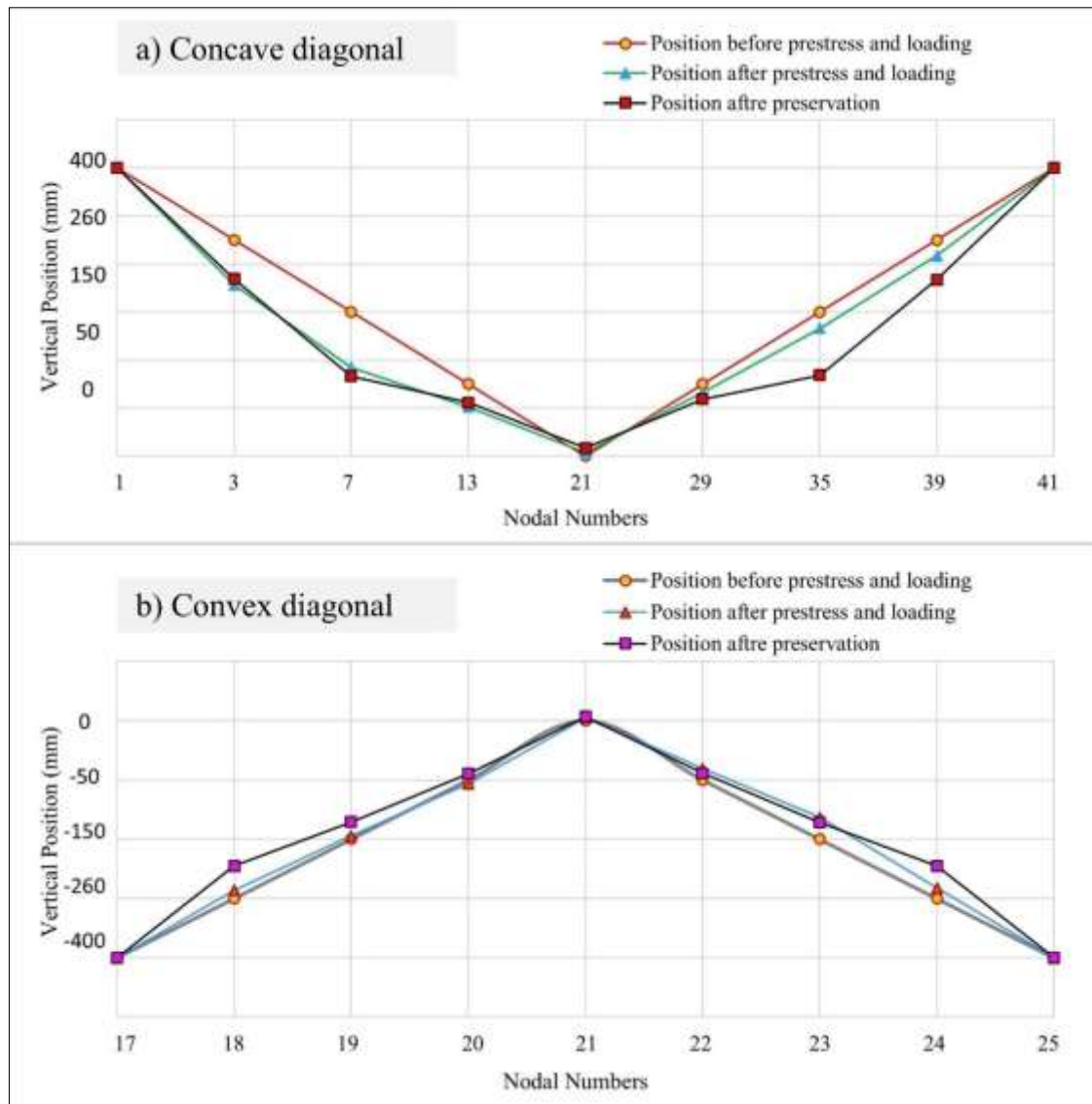


Fig. 5-11 Nodal movement for the targeted displacements in SPC3

For further clarification on the preservation of vertical displacement, the coordinates of two opposite joints, 7 and 35, are used as an example. In Fig. 5-12, the original vertical ( $z$ ) coordinates for both joints were 150 mm. After prestressing and loading, the  $z$ -coordinate of node 7 became 126.89 mm, and the  $z$ -coordinate of node 35 became 143.22 mm. The target was to bring both coordinates to the same level, and after achieving the target, they became approximately 123.5 mm theoretically. The experimental results showed that node 7 approached 123.58 mm, with a discrepancy ratio of 0.25%, and node 35 reached 124.17 mm, with a discrepancy ratio of 0.38%.

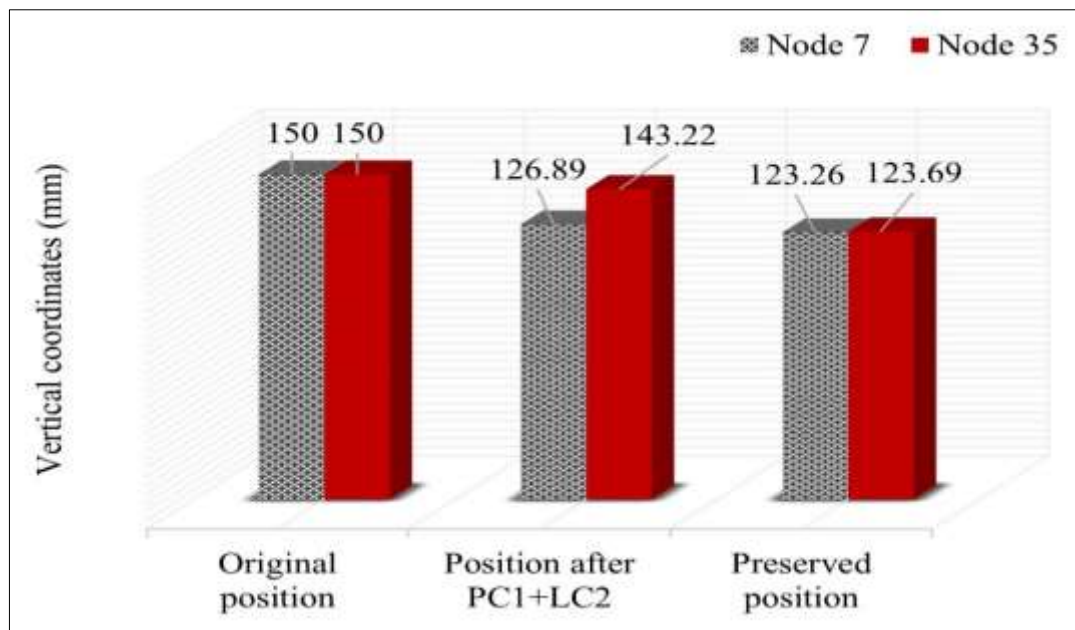


Fig. 5-12 Coordinate position of nodes 7 and 35 before and after vertical displacement preservation

The theoretical internal forces during the preservation process were also computed and are tabulated in Table 5-18. The closeness between the computed theoretical preserved forces ( $t_c$ ) using derived Eqs. 3.44 and 3.45 with the experimental  $t_c$  examined, showing that the Euclidian norm ratio between the theoretical result of Eq. 3.44 and experimental  $t_c$  was 3.2% while it was 0.49% with the theoretical result of Eq. 3.45. The combined internal forces for the model, calculated before performing the restoration stage and after the slackened cables were restored, are presented in Table 5-18. This is done to ensure that the slackened members are properly tensioned and that other members are prevented from slackening or overloading.

After the numerical calculations were set and the required member actuations identified, the lab model was examined to achieve the displacement targets. The experimental vertical displacements were recorded in the same manner as in the previous phases and are presented in columns 6 and 9 in Table 5-16. The maximum ratio of discrepancy between the theoretical and experimental

combined displacements were determined as 6% at node 29, while the minimum ratio was at node 18 by 0.4%.

Table 5-16 Theoretical and experimental vertical displacements before and after preservation process in SPC3

Node	Before preservation		After preservation					
	Combined displacement PC1+LC2 (mm)		Preserved Displacement (mm)			Combined displacement PC1+LC2+SPC3 (mm)		
	Theory	Experiment	Eq. 3.44	Eq. 3.45	Experiment	Eq. 3.44	Eq. 3.45	Experiment
	dz	dz	dz	dz	dz	dz	dz	dz
3	-18.72	-18.91	2.52	2.41	2.45	-16.20	-16.31	-16.46
6	10.72	-	-13.36	-13.51	-	-2.64	-2.79	-
7	-23.11	-22.83	-3.63	-3.68	-3.59	-26.74	-26.79	-26.42
8	-3.50	-	-5.84	-5.93	-	-9.34	-9.43	-
11	6.62	-	1.89	1.90	-	8.51	8.52	-
12	8.89	-	0.96	0.94	-	9.85	9.83	-
13	-9.56	-9.32	1.79	1.86	1.82	-7.77	-7.70	-7.50
14	-1.10	-	2.08	2.09	-	0.98	0.99	-
15	-7.81	-	3.11	3.09	-	-4.70	-4.72	-
18	6.88	6.72	20.51	20.85	21.13	27.39	27.73	27.85
19	2.61	2.17	11.97	12.02	11.94	14.58	14.63	14.11
20	-3.78	-	9.29	9.22	-	5.51	5.44	-
21	1.41	-	2.02	1.96	-	3.43	3.37	-
22	7.38	-	-1.63	-1.76	-	5.75	5.62	-
23	19.90	19.39	-5.83	-5.84	-5.67	14.07	14.06	13.72
24	30.28	29.34	-2.89	-2.42	-2.56	27.39	27.86	26.78
27	3.82	-	3.88	3.92	-	7.70	7.74	-
28	4.66	-	3.01	3.01	-	7.67	7.67	-
29	-3.57	-3.28	-2.78	-2.74	-2.69	-6.35	-6.31	-5.97
30	1.87	-	-0.34	-0.35	-	1.53	1.52	-
31	-1.83	-	0.01	-0.01	-	-1.82	-1.84	-
34	1.76	-	-9.42	-9.55	-	-7.66	-7.79	-
35	-6.78	-6.50	-19.53	-19.64	-19.33	-26.31	-26.42	-25.83
36	-2.51	-	-8.96	-9.06	-	-11.47	-11.57	-
39	-6.56	-	-9.92	-10.02	-	-16.48	-16.58	-
Max. discrepancy ratio			6%		Min. discrepancy ratio			0.4%

Initially, the slackened members recorded zero strain until they were re-tensioned, after which they recorded strain values. The member strains were transformed into axial forces and are presented in Table 5-17 (columns 4 and 8). For instance, in computing the member force of cable 2 in theoretical and recording experimental values, this cable experienced slack due to an insufficient pretension force that produced in prestressing stage (see column 6 in Table 5.11), and producing compression force from the applied loads. Therefore, it needed to overcome this compression force first and then acquire a pretension value. During the adjustment, the technique computed 78.6 N using Eq. 3.45, which became the total pretension force due to zero force at the previous stage. Similarly, during lab strain recording, it showed zero strain until it passed the compression value and then recorded a tension force of 77.43 N. Referring to Table 5-17, the maximum discrepancy between the theoretical computation by Eq. 3.45 and experimental  $t_c$  was 2.8% for cable 3, while the minimum error was for cables 13 and 41 with zero percent.

In Table 5-18, the collected experimental axial forces before and after the preservation process are shown alongside the theoretical values for comparison. The lab results regarding both the displacements and internal member forces exhibited a good correlation with the theoretical results. This level of agreement not only validates the accuracy of the theoretical models but also demonstrates the robustness of the experimental procedures. The consistent results across both theoretical and experimental data further confirm that the present approach to adjusting nodal displacement and internal stress is highly effective for complex space structures. These structures, which exhibit geometric nonlinear responses to disturbance sources, benefit greatly from this precise and reliable method of analysis and adjustment.

Table 5-17 Theoretical and experimental internal force before and after preservation process in SPC3

Member No.	Preserved internal force (N) $t_c$			Member No.	Preserved internal force (N) $t_c$		
	Eq. 3.44	Eq. 3.45	Experiment		Eq. 3.44	Eq. 3.45	Experiment
1	249.91	256.30	257.01	33	191.43	197.45	197.82
2	74.24	78.60	77.43	34	195.57	201.70	202.49
3	74.53	78.87	76.61	35	197.96	204.05	203.59
4	147.67	149.56	149.64	36	218.33	226.80	226.42
5	239.25	245.04	244.63	37	419.42	440.95	440.61
6	117.02	118.62	118.67	38	64.61	65.45	65.38
7	167.01	170.40	169.11	39	142.90	144.70	145.35
8	164.69	168.06	166.32	40	212.38	217.73	216.85
9	168.27	171.67	170.35	41	111.06	112.58	112.58
10	171.57	175.02	174.92	42	31.22	31.14	31.30
11	59.41	60.18	60.11	43	128.95	143.18	140.53
12	142.61	144.41	144.82	44	58.80	59.11	59.06
13	221.55	226.96	226.95	45	57.09	57.41	57.44
14	111.05	112.55	113.07	46	51.69	51.96	52.00
15	34.95	34.89	34.99	47	56.70	57.01	57.13
16	93.48	94.22	94.12	48	61.54	61.89	61.74
17	91.62	92.37	92.08	49	62.95	63.27	62.93
18	86.98	87.69	87.67	50	64.76	65.60	65.67
19	86.38	87.07	87.15	51	142.86	144.62	144.44
20	89.64	90.35	90.09	52	212.59	217.97	218.21
21	91.00	91.71	91.60	53	112.13	113.62	114.00
22	424.66	446.27	-	54	32.09	32.03	32.12
23	58.08	58.83	58.70	55	273.82	278.49	280.39
24	141.90	143.70	144.03	56	274.18	278.87	280.85
25	218.05	223.44	224.40	57	273.02	277.68	275.50
26	109.20	110.70	111.28	58	273.14	277.78	280.97
27	33.26	33.19	33.31	59	152.67	154.55	155.08
28	125.10	139.35	137.67	60	238.52	244.44	244.72
29	273.24	283.05	282.70	61	122.66	124.27	124.29
30	206.67	212.87	212.69	62	181.94	187.78	187.96
31	200.83	206.94	207.13	63	181.78	187.63	187.28
32	194.73	200.73	200.46	64	262.17	268.93	268.61
Max. discrepancy ratio			2.8%	Min. discrepancy ratio			0.0%

Table 5-18 Theoretical and experimental combined internal force before and after preservation process in SPC3

Member No.	$e_o$ (mm)	Combined Internal Force (N)		Member No.	$e_o$ (mm)	Combined Internal Force (N)	
		Theory	Experiment			Theory	Experiment
		T+t+t <sub>c</sub>	T+t+t <sub>c</sub>			T+t+t <sub>c</sub>	T+t+t <sub>c</sub>
1		457.00	461.42	33		524.77	526.09
2	-1.1	78.60	77.43	34		482.79	483.80
3	-1.1	135.91	132.24	35		435.74	433.14
4		291.95	292.33	36		410.32	409.58
5		494.09	492.81	37	-4	583.84	583.49
6		245.35	245.01	38	-4.8	265.84	267.79
7	-1.1	172.83	170.89	39	-2.8	345.28	346.69
8	-2.4	168.06	166.32	40		559.39	555.25
9	-2.4	226.72	225.76	41		295.25	297.70
10	-1.6	232.00	232.48	42		105.19	103.64
11		206.39	206.55	43	-3.2	196.53	192.98
12		286.68	288.42	44		289.29	289.56
13		526.86	511.17	45		278.17	278.39
14		237.51	234.93	46	0.8	263.72	265.70
15		54.64	52.20	47	-1.6	321.84	320.17
16		217.56	215.68	48		331.12	329.84
17		208.66	204.51	49		335.13	335.22
18		197.50	194.54	50		270.87	270.85
19		250.43	246.19	51		350.61	346.77
20		256.53	250.47	52		628.21	633.38
21		258.65	258.56	53		302.23	304.65
22	-4	531.71	-	54		111.77	111.10
23		202.23	201.57	55		361.35	363.04
24	-0.8	284.43	282.78	56	-5	358.47	359.56
25	-2.4	568.88	566.79	57	-5	414.65	413.00
26		234.07	233.53	58		417.91	421.32
27		49.08	48.20	59		363.71	365.39
28	-3.2	139.35	137.67	60		718.79	719.26
29		799.37	800.97	61		318.30	317.18
30		659.47	656.44	62	-1.8	400.83	400.52
31		586.03	585.95	63	-1.8	458.34	456.97
32		520.23	522.47	64	0.8	826.96	830.40
Total $e_o$ (mm)				51.7			

## 5.5 SUMMARY

This chapter presented a comprehensive validation of the theoretical models developed in Chapter 3 through a series of experimental tests on a hyperbolic paraboloid 3D cable net model. The key findings are:

- **Prestressing Phase Summary:** The experimental results for three prestressing scenarios (symmetric and asymmetric) closely aligned with theoretical predictions. Minor discrepancies arose due to factors such as cable extension and relaxation, non-ideal hinge behaviour at joints, and inaccuracies in calculating the combined axial stiffness of the members. The maximum discrepancy was observed in PC2, with a 7% error in prestressed force and a 5.2% error in resultant displacement.
- **Analysis Phase Summary:** The model was subjected to vertical, horizontal, and combined loading conditions. The experimental data showed a strong correlation with theoretical calculations, validating the accuracy of the derived equations. The discrepancies noted were primarily due to the initial prestressing conditions and the inherent characteristics of the model. The maximum error ratios were computed in LC1 among all loading cases, with 7% for internal force and 2.7% for resultant displacement.
- **Preservation Phase Summary:** The preservation techniques were tested in three scenarios: nodal displacement control, member force control, and simultaneous control of both. The experimental outcomes demonstrated that the derived nonlinear equations effectively maintained structural integrity, preventing slack and overloading in the cable members. It was confirmed in SPC3 that the derived Eq. 3.45 provided results closer to the experimental values regarding internal force, with a Euclidean norm index ratio of 0.49%, while Eq. 3.44 showed an  $l_2$ -norm distance of 3.2%.

Overall, the experimental findings confirmed the robustness and practical applicability of the theoretical models for managing the behaviour of pin-jointed spatial structures under various prestressing and loading conditions.



## CHAPTER SIX

### CONCLUSIONS AND RECOMMENDATIONS

#### 6.1 CONCLUSIONS

The conclusions of the present study can be reported as the following:

1. The derived equations express a system of algebraic nonlinear equations as a function of joint displacements.
2. The 'fsolve' function in MATLAB can be employed for solving the derived nonlinear equations.
3. The derived nonlinear prestressing methods are applicable, efficient and reliable for prestressing simple and complex space cable structures.
4. The proposed prestressing technique can numerically compute the desired degree of prestressing for spatial assemblies by accounting for the nonlinear amount of required member alteration.
5. The applied prestressing approach is accurate in computing the targeted prestress when it is predetermined to find the required member actuation.
6. The present prestressing technique is equivalent to software solvers when the amount of member actuation is pre-indicated.
7. The slack of the cables can be prevented through the required member actuation.
8. The proposed nonlinear prestressing equations, similar to those used for flexible structures, can successfully calculate the resulting axial force formed from the lack of fit of rigid members in space truss systems.
9. The proposed analysis technique is applicable for both flexible and rigid members of spatial pin-jointed systems.
10. The proposed analysis technique can accurately calculate the internal stress

of the members, considering geometric nonlinearity.

11. The proposed analysis technique is very fast and accurate for simple and complex assemblies with nonlinear geometrical response under any loading condition.
12. The proposed preservation technique effectively computes the amount of nonlinear member actuation needed for the preservation process to achieve a desired target.
13. The proposed preservation approach is applicable for preserving the nodal displacements and restoring or minimising the disturbed geometry after the prestressing procedure and/or external loads.
14. The derived preservation technique is applicable for restoring the member force of slackened members in flexible structures or reducing the tensile and compressive forces in rigid member systems.
15. The derived preservation technique can preserve the nodal position of joints and internal force simultaneously for all pin-jointed structures based on the requested target.
16. The proposed preservation technique is accurate in redistributing the internal stress of the spatial structure to prevent slacking or overloading of the members.
17. Achieving the desired target, whether it is nodal control alone, internal force control alone, or simultaneous control of displacement and force, depends on the amount of actuation and the sufficient number of actuators.
18. The location of the actuators has a direct effect on the preservation process and the required amount of total actuation for the process.
19. Bar sensitivity technique determined the effect of selective members on the nodal displacement and member forces which relies on the resulting coefficient of the bar sensitivity technique.
20. Placing the actuators within active members allows the target to be achieved easily with minimal total actuation.

21. Determining the correct target during the preservation stage can strongly affect the ease of achieving the desired adjustment with less effort.

## **6.2 RECOMMENDATIONS FOR FUTURE WORK**

1. Generalising the geometric nonlinear techniques for analysing not only pin-jointed structures but also frame systems.
2. Deriving a more advanced technique for identifying the optimal locations for actuator placement, whether for prestressing applications or adjustment processes.
3. Integrating the proposed techniques, particularly the preservation technique, into machine learning and intelligent control systems.
4. Linking the displacement monitoring using digital photos to image processing software for faster displacement computation.
5. Developing the proposed nonlinear analysis technique for dynamic analysis.
6. Testing the applicability of the proposed nonlinear analysis technique for thermal load.

### REFERENCES

- Aabid, A., Parveez, B., Raheman, M. A., Ibrahim, Y. E., Anjum, A., Hrairi, M., Parveen, N. & Mohammed Zayan, J. 2021. A review of piezoelectric material-based structural control and health monitoring techniques for engineering structures: Challenges and opportunities. *Actuators*, 10, 101.
- Abad, M. S. A., Shooshtari, A., Esmaeili, V. & Riabi, A. N. 2013. Nonlinear analysis of cable structures under general loadings. *Finite elements in analysis and design*, 73, 11-19.
- Abdulkarim, S. J. & Saeed, N. M. 2023. Nonlinear technique of prestressing spatial structures. *Mechanics Research Communications*, 127, 104040.
- Abdulkarim, S. J., Saeed, N. M. & Haji, H. A. 2020. Direct Displacement Control of Deformed Double Layer Dome. *UKH Journal of Science and Engineering*, 4, 1-14.
- Amir Sohrabi, M., Muliana, A. H. & Srinivasa, A. R. 2017. Controlling deformations of electro-active truss structures with nonlinear history-dependent response. *Finite Elements in Analysis and Design*, 129, 42-52.
- Baker, G. A., Baker Jr, G. A., Graves-Morris, P., Baker, G. & Baker, S. S. 1996. *Pade Approximants: Encyclopedia of Mathematics and It's Applications, Vol. 59 George A. Baker, Jr., Peter Graves-Morris*. Cambridge University Press.
- Bodaghi, M., Damanpack, A. R., Aghdam, M. M. & Shakeri, M. 2014. Active shape/stress control of shape memory alloy laminated beams. *Composites Part B: Engineering*, 56, 889-899.
- Brütting, J., Desruelle, J., Senatore, G. & Fivet, C. 2019. Design of Truss Structures Through Reuse. *Structures*, 18, 128-137.
- Burdisso, R. A. & Haftka, R. T. 1989. Optimal location of actuators for correcting distortions in large truss structures. *AIAA Journal*, 27, 1406-1411.
- Burdisso, R. A. & Haftka, R. T. 1990. Statistical analysis of static shape control in space structures. *AIAA Journal*, 28, 1504-1508.

## REFERENCES

---

- Calladine, C. R. 1978. Buckminster Fuller's "Tensegrity" structures and Clerk Maxwell's rules for the construction of stiff frames. *International Journal of Solids and Structures*, 14, 161-172.
- Chen, Y., Xiang, J., Xiang, J., Wang, Q. & Zhou, J. 2024. Stress relaxation behavior and its effect on the mechanical performance of a wire cable. *Mechanics of Time-Dependent Materials*, 28, 595-615.
- Chen, Y., Yan, J., Sareh, P. & Feng, J. 2020. Feasible Prestress Modes for Cable-Strut Structures with Multiple Self-Stress States Using Particle Swarm Optimization. *Journal of Computing in Civil Engineering*, 34, 04020003.
- Cinquini, C. & Contro, R. 1985. Prestressing design method for cable net structures. *Engineering Structures*, 7, 183-189.
- Deng, H., Zhang, M., Liu, H., Dong, S., Zhang, Z. & Chen, L. 2016. Numerical analysis of the pretension deviations of a novel crescent-shaped tensile canopy structural system. *Engineering Structures*, 119, 24-33.
- Dhingra, A. K. & Lee, B. 1994. Optimal placement of actuators in actively controlled structures. *Engineering Optimization*, 23, 99-118.
- Dong, S. & Yuan, X. 2007. Pretension process analysis of prestressed space grid structures. *Journal of Constructional Steel Research*, 63, 406-411.
- Du Pasquier, C. & Shea, K. 2022. Validation of a nonlinear force method for large deformations in shape-morphing structures. *Structural and Multidisciplinary Optimization*, 65, 87.
- Fraddosio, A., Pavone, G. & Piccioni, M. D. 2021. A novel method for determining the feasible integral self-stress states for tensegrity structures. *Curved and Layered Structures*, 8, 70-88.
- Frobenius, G. 1881. Ueber Eelationen zwischen den Näherungsbrüchen von Potenzreihen. *Journal fur die Reine und Angewandte Mathematik*, 1881, 1-17.
- Gossen, P. 2004. Design with Cables. *Structure*, 11, 15-16.
- Guo, J. & Zhou, D. 2016. Pretension simulation and experiment of a negative Gaussian curvature cable dome. *Engineering Structures*, 127, 737-747.

## REFERENCES

---

- Haftka, R. T. 1984. Optimum placement of controls for static deformations of space structures. *AIAA Journal*, 22, 1293-1298.
- Haftka, R. T. 1991. Limits on static shape control for space structures. *AIAA Journal*, 29, 1945-1950.
- Haftka, R. T. & Adelman, H. M. 1985. Selection of actuator locations for static shape control of large space structures by heuristic integer programming. *Computers & Structures*, 20, 575-582.
- Hanaor, A. 1988. Prestressed pin-jointed structures—flexibility analysis and prestress design. *Computers & structures*, 28, 757-769.
- Hanaor, A. & Levy, R. 1985. Imposed Lack of Fit as a Means of Enhancing Space Truss Design. *International Journal of Space Structures*, 1, 147-154.
- Irschik, H. 2002. A review on static and dynamic shape control of structures by piezoelectric actuation. *Engineering Structures*, 24, 5-11.
- Janocha, H. 2004. Introduction. In: Janocha, H. (ed.) *Actuators: Basics and Applications*. Berlin, Heidelberg: Springer Berlin Heidelberg.
- Kaliciak, G. 2022. *Al-Minaa Olympic Stadium* [Online]. Available: [http://stadiumdb.com/stadiums/irq/minaa\\_stadium](http://stadiumdb.com/stadiums/irq/minaa_stadium) [Accessed 17/07 2024].
- Kassimali, A. 2012. *Matrix Analysis of Structures*. ed. Australia.
- Kawaguchi, K.-I., Hangai, Y., Pellegrino, S. & Furuya, H. 1996. Shape and stress control analysis of prestressed truss structures. *Journal of Reinforced Plastics and Composites*, 15, 1226-1236.
- Kawaguchi, K., Furuya, H. & Pellegrino, S. 1994. *Shape and stress control of prestressed truss structures*. University of Cambridge, Department of Engineering.
- Korkmaz, S. 2011. A review of active structural control: challenges for engineering informatics. *Computers & Structures*, 89, 2113-2132.
- Kwan, A. & Pellegrino, S. 1993. Prestressing a space structure. *AIAA journal*, 31, 1961-1963.

## REFERENCES

---

- Kwan, A. S. K. 1991. *A Pantographic Deployable Mast*. University of Cambridge.
- Kwan, A. S. K. 1998. A new approach to geometric nonlinearity of cable structures. *Computers & Structures*, 67, 243-252.
- Lee, S.-H., Shin, K.-J., Shin, H.-M. & Lee, H.-D. 2021. Design Procedure and Ultimate Capacity of New Turnbuckle for Measuring Tensile Force. *International Journal of Steel Structures*, 21, 626-633.
- Levy, R., Hanaor, A. & Rizzuto, N. 1994. Experimental Investigation of Prestressing in Double-Layer Grids. *International Journal of Space Structures*, 9, 21-26.
- Levy, R. & Spillers, W. R. 2003. *Analysis of geometrically nonlinear structures*. Springer Science & Business Media.
- Lewis, J. W. 1987. A comparative study of numerical methods for the solution of pretensioned cable networks. *Proceedings of the International Conference on the Design and Construction of Non-Conventional Structures*, 27-33.
- Lewis, W. J. 1989. The efficiency of numerical methods for the analysis of prestressed nets and pin-jointed frame structures. *Computers & Structures*, 33, 791-800.
- Lewis, W. J., Jones, M. S. & Rushton, K. R. 1984. Dynamic relaxation analysis of the non-linear static response of pretensioned cable roofs. *Computers & Structures*, 18, 989-997.
- Li, A., Liang, X. & Yuan, X. 2017. Force Method for Displacement Adjustment of Prestressed Cable Structures with Dynamic Relaxation Method. *Destech Transactions on Engineering and Technology Research*.
- Li, T., Jiang, J., Deng, H., Lin, Z. & Wang, Z. 2013. Form-finding methods for deployable mesh reflector antennas. *Chinese Journal of Aeronautics*, 26, 1276-1282.
- Luo, Y. & Lu, J. 2006. Geometrically non-linear force method for assemblies with infinitesimal mechanisms. *Computers & Structures*, 84, 2194-2199.

## REFERENCES

---

- Ma, Q., Ohsaki, M., Chen, Z. & Yan, X. 2019. Multi-objective optimization for prestress design of cable-strut structures. *International Journal of Solids and Structures*, 165, 137-147.
- Mahmood, A., Katebi, J., Saeed, N. & Manguri, A. 2022. Optimized Stress and Geometry Control of Spherical structures under Lateral Loadings. *2022 8th International Engineering Conference on Sustainable Technology and Development (IEC)*, 142-148.
- Manguri, A., Kwan, A. S. K. & Saeed, N. 2017. Adjustment for shape restoration and force control of cable arch stayed bridges. *International Journal of Computational Methods and Experimental Measurements*, 5, 514-521.
- Manguri, A., Saeed, N., Mahmood, A., Katebi, J. & Jankowski, R. 2022. Optimal reshaping and stress controlling of double-layer spherical structures under vertical loadings. *Archives of Civil Engineering*, vol. 68, 591-606.
- Manguri, A. A. & Saeed, N. M. 2020. An Approximate Linear Analysis of Structures Using Incremental Loading of Force Method. *UKH Journal of Science Engineering Structures*, 4, 37-44.
- McGuire, W. 2000. *Matrix Structural Analysis*. John Wiley & Sons.
- Nisar, K. S., Ali, J., Mahmood, M. K., Ahmed, D. & Ali, S. 2021. Hybrid evolutionary padé approximation approach for numerical treatment of nonlinear partial differential equations. *Alexandria Engineering Journal*, 60, 4411-4421.
- Nyashin, Y., Lokhov, V. & Ziegler, F. 2005. Stress-free displacement control of structures. *Acta Mechanica*, 175, 45-56.
- Onoda, J. & Hanawa, Y. 1992. Optimal locations of actuators for statistical static shape control of large space structure-A comparison of approaches. *33rd Structures, Structural Dynamics and Materials Conference*, 2558.
- Pascal, T. 2021. *Spatial Structures - An Innovative Structural Solution* [Online]. Available: <https://www.structuresinsider.com/post/spatial-structures-an-innovative-structural-solution#:~:text=Spatial%20structures%20are%20formally%20defined,e xtend%20beyond%20a%20single%20plane>. [Accessed 22/03 2023].



## REFERENCES

---

- Pellegrino, S. 1990. Analysis of prestressed mechanisms. *International Journal of Solids and Structures*, 26, 1329-1350.
- Pellegrino, S. 1993. Structural computations with the singular value decomposition of the equilibrium matrix. *International Journal of Solids and Structures*, 30, 3025-3035.
- Pellegrino, S. 1995. Adaptive shape control of mesh reflectors. *Proc. ESA Workshop on Antenna Technologies*, 21-23.
- Pellegrino, S. & Calladine, C. R. 1986. Matrix analysis of statically and kinematically indeterminate frameworks. *International Journal of Solids and Structures*, 22, 409-428.
- Qiao, G., Liu, G., Shi, Z., Wang, Y., Ma, S. & Lim, T. C. 2018. A review of electromechanical actuators for More/All Electric aircraft systems. *Proceedings of the Institution of Mechanical Engineers, Part C: Journal of Mechanical Engineering Science*, 232, 4128-4151.
- Reksowardojo, A. P. & Senatore, G. 2023. Design of ultra-lightweight and energy-efficient civil structures through shape morphing. *Computers & Structures*, 289, 107149.
- Saeed, N., Manguri, A., Abdulkarim, S. & Shekha, A. 2019. Shape Restoration of Deformed Egg-Shaped Single Layer Space Frames. *2019 International Conference on Advanced Science and Engineering (ICOASE)*, 220-225.
- Saeed, N., Manguri, A., Szczepanski, M. & Jankowski, R. 2022. Non-Linear Analysis of Structures Utilizing Load-Discretization of Stiffness Matrix Method with Coordinate Update. *Applied Sciences*, 12, 2394.
- Saeed, N. M. 2014. *Prestress and deformation control in flexible structures*. PhD Dissertation, Cardiff University.
- Saeed, N. M. 2019. Simultaneous force and deformation control of cable arch stayed bridges. *Kufa Journal of Engineering*, 10, 66-75.
- Saeed, N. M. 2022. Displacement Control of Nonlinear Pin-Jointed Assemblies Based on Force Method and Optimization. *AIAA Journal*, 60, 1024-1031.

## REFERENCES

---

- Saeed, N. M. & Kwan, A. S. K. 2016a. Displacement and force control of complex element structures by matrix condensation. *Structural Engineering and Mechanics*, 59, 973-992.
- Saeed, N. M. & Kwan, A. S. K. 2016b. Simultaneous displacement and internal force prescription in shape control of pin-jointed assemblies. *AIAA journal*, 54, 2499-2506.
- Saeed, N. M. & Kwan, A. S. K. 2018. Displacement and internal force control in cable-stayed bridges. *Proceedings of the Institution of Civil Engineers - Bridge Engineering*, 171, 63-76.
- Saeed, N. M., Manguri, A. A. H. & Adabar, A. M. 2021. Shape and force control of cable structures with minimal actuators and actuation. *International Journal of Space Structures*, 36, 241-248.
- Schodek, D. L. & Bechthold, M. 2014. *Structures*, 7th ed. USA, Pearson Education.
- Sehlstrom, A. 2019. *Prestress in nature and technics*. Licentiate of Architecture, Universidade Tecnica de Lisboa (Portugal).
- Sernizon Costa, R., Cesar Campos Lavall, A., Gomes Lanna da Silva, R., Porcino dos Santos, A. & Francisco Viana, H. 2022. Cable structures: An exact geometric analysis using catenary curve and considering the material nonlinearity and temperature effect. *Engineering Structures*, 253, 113738.
- Shea, K., Fest, E. & Smith, I. F. C. 2002. Developing intelligent tensegrity structures with stochastic search. *Advanced Engineering Informatics*, 16, 21-40.
- Sufian, P. & Templeman, A. 1970. Analysis and design of cable net structures through optimization techniques. *WIT Transactions on The Built Environment*, 2.
- Sunar, M. & Rao, S. S. 1999. Recent Advances in Sensing and Control of Flexible Structures Via Piezoelectric Materials Technology. *Applied Mechanics Reviews*, 52, 1-16.
- Thai, H.-T. & Kim, S.-E. 2011. Nonlinear static and dynamic analysis of cable structures. *Finite Elements in Analysis and Design*, 47, 237-246.

## REFERENCES

---

- Toklu, Y. C., Bekdaş, G. & Temür, R. 2017. Analysis of cable structures through energy minimization. *Structural Engineering and Mechanics*, 62, 749-758.
- Vazquez-Leal, H., Benhammouda, B., Filobello-Nino, U., Sarmiento-Reyes, A., Jimenez-Fernandez, V. M., Garcia-Gervacio, J. L., Huerta-Chua, J., Morales-Mendoza, L. J. & Gonzalez-Lee, M. 2014. Direct application of Padé approximant for solving nonlinear differential equations. *SpringerPlus*, 3, 563.
- Wang, Z., Li, T. & Cao, Y. 2013. Active shape adjustment of cable net structures with PZT actuators. *Aerospace Science and Technology*, 26, 160-168.
- Xu, X. & Luo, Y.-Z. 2008. Multi-objective shape control of prestressed structures with genetic algorithms. *Proceedings of the Institution of Mechanical Engineers, Part G: Journal of Aerospace Engineering*, 222, 1139-1147.
- Xu, X. & Luo, Y. 2009. Non-linear displacement control of prestressed cable structures. *Proceedings of the Institution of Mechanical Engineers, Part G: Journal of Aerospace Engineering*, 223, 1001-1007.
- Xu, X. & Luo, Y. 2010. Force Finding of Tensegrity Systems Using Simulated Annealing Algorithm. *Journal of Structural Engineering*, 136, 1027-1031.
- Xue, Y., Wang, Y., Xu, X., Wan, H.-P., Luo, Y. & Shen, Y. 2021. Comparison of different sensitivity matrices relating element elongations to structural response of pin-jointed structures. *Mechanics Research Communications*, 118, 103789.
- Yoichi, M. 2006. Applications of piezoelectric actuator. *NEC Technical Journal*, 1, 82-86.
- You, Z. 1997. Displacement control of prestressed structures. *Computer Methods in Applied Mechanics and Engineering*, 144, 51-59.
- Yuan, X. & Dong, S. 2002. Nonlinear analysis and optimum design of cable domes. *Engineering Structures*, 24, 965-977.

## REFERENCES

---

- Yuan, X., Liang, X. & Li, A. 2016. Shape and force control of prestressed cable-strut structures based on nonlinear force method. *Advances in Structural Engineering*, 19, 1917-1926.
- Zhang, H., Lu, J., Lu, M. & Li, N. 2023. Active control experiments on a Levy cable dome. *Engineering Structures*, 278, 115450.
- Zhang, Q., Wang, X., Cai, J., Yang, R. & Feng, J. 2021. Prestress design for cable-strut structures by grouping elements. *Engineering Structures*, 244, 112010.
- Zhou, J., Chen, W., Zhao, B. & Dong, S. 2017. A feasible symmetric state of initial force design for cable-strut structures. *Archive of Applied Mechanics*, 87, 1385-1397.
- Ziegler, F. 2005. Computational aspects of structural shape control. *Computers & Structures*, 83, 1191-1204.
- Zupan, M., Ashby, M. F. & Fleck, N. A. 2002. Actuator Classification and Selection—The Development of a Database. *Advanced Engineering Materials*, 4, 933-940.

## LIST OF PUBLICATIONS

List of Published Journal Articles, DOI, and 1<sup>st</sup> Page Image

## P. 1. Nonlinear Technique of Prestressing Spatial Structures

<https://doi.org/10.1016/j.mechrescom.2022.104040>

Mechanics Research Communications 127 (2023) 104040

Contents lists available at ScienceDirect

**Mechanics Research Communications**

journal homepage: [www.elsevier.com/locate/mechrescom](http://www.elsevier.com/locate/mechrescom)






## Nonlinear technique of prestressing spatial structures

Shna Jabar Abdulkarim<sup>a,\*,b</sup>, Najmadeen Mohammed Saeed<sup>b,c</sup>

<sup>a</sup> Civil Engineering Department, Erbil Polytechnic University, Erbil, Kurdistan Region 44001, Iraq  
<sup>b</sup> Civil Engineering Department, University of Raparin, Rapara, Kurdistan Region 46012, Iraq  
<sup>c</sup> Civil Engineering Department, Tishk International University, Erbil, Kurdistan Region 44001, Iraq.

---

**ARTICLE INFO**

**Keywords:**  
 Prestress  
 Member alteration  
 Lack of fit  
 Self-equilibrate  
 Force method

**ABSTRACT**

One of the crucial aspects of the design of structural space systems is the degree of prestressing since it is involved in the load transferring, deformability and charges. The prestress state can be reached via required member alteration. This paper presents an efficient nonlinear numerical approach based on the force method for prestressing the spatial nonlinear structures to the desired level through computing nonlinear actuation as a function of external nodal displacements. Two equations are derived for indicating the required amount of member alteration  $\epsilon_0$  and prestressing level by using Taylor's series and Pade approximation methods. This technique can be applied to both rigid and flexible spatial structures. The present technique is validated based on three numerical examples, and the computational findings are in well agreement with the compared methods. The results show that the new approach requires less effort and makes greater economic sense. Moreover, the member forces with concern to nonlinear  $\epsilon_0$  of double-layer space grid structure by imposing lack of fit of some members successfully obtained.

---

### 1. Introduction

Space structures are characterized by lightweight, cost-effective, and swiftness in an erection. Due to their structural effectiveness, spatial systems are intended for claims such as structures with wide-span roofs or deployable mesh reflectors [1]. The capability to allow internal stress without having external loads is fundamental to most spatial structures. Prestress is required to attain these structures' desired form, stability, and function. For structures with rigid geometry, the existence of prestress, which is imposed via the member's fit deficiency, can noticeably improve the design, essentially when buckling is the main failure of their members. While, for the flexible type, prestress is essential to achieve the required geometrical configuration [2]. Cinquini and Contro [3] stated that the most significant feature for designing a cable-net system is the level of pretension because of the direct influence on its load-carrying capacity, expenses amount, and geometrical configuration. Also, the nonlinearity develops more noticeable with declining pretension [4]. Hence, the indication of the preliminary prestress has an essential effect in the design steps.

Numerous studies have been published to find out the optimal prestressing level of pin-jointed spatial structures. As well, many form-finding techniques have been proposed to attain desired aesthetical, industrial, and mechanical demands, such as iteration techniques, dynamic relaxation method, and force density method. However, these methods established limits on member stresses and nodal displacements but typically do not certain the prestressing degree [3].

Pellegrino and Calladine [5] proposed an algorithm to bring complete detailing about the modes for in-extensional deformation and all the states of initial stress. Another matrix algorithm was developed by Pellegrino [6], which deals with both extensional and inextensional modes distinctly; in addition, they classified the structural assemblies as an independent state of self-stress and mechanism modes. In the study by Kwan and Pellegrino [7], based on the linear force method, an algorithm was proposed which was used to gain over a uniform degree of prestress. And so on, based on the Force Method, linear and partially nonlinear internal force controlling has been done [8–10], which is a part of achieving the required amount of prestressing. Nevertheless, the simulated annealing algorithm was developed by Xu and Luo [11]; with taking care of geometrical stability, the optimization model was used for finding the force of tensegrity structure. Later, Li, Jiang [12] used two different form-finding techniques on deployable mesh reflector antenna to indicate the cable prestress to satisfy the required exterior accuracy. Even though a pretension algorithm by simulation for negative Gaussian-curvature cable dome was proposed by Guo and Zhou [13], it

---

<sup>\*</sup> Corresponding author.  
 E-mail address: [shna.jabar@uor.edu.krd](mailto:shna.jabar@uor.edu.krd) (S.J. Abdulkarim).

<https://doi.org/10.1016/j.mechrescom.2022.104040>  
 Received 30 August 2022; Received in revised form 19 December 2022; Accepted 20 December 2022  
 Available online 25 December 2022  
 0093-6413/© 2022 Elsevier Ltd. All rights reserved.



## P. 2. Nonlinear Structural Analysis Technique Based on Flexibility Method by Pade Approximants

<https://doi.org/10.24271/PSR.2024.429055.1433>




Available online at [www.garmian.edu.krd](http://www.garmian.edu.krd)

### Passer Journal

Passer 6 (Issue 1) (2024) 150-160

<http://passer.garmian.edu.krd/>



### Nonlinear structural analysis technique based on flexibility method by Pade approximants

**Shna Jabar Abdulkarim<sup>1,2</sup>, Najmadeen Mohammed Saeed<sup>2,3\*</sup>**

<sup>1</sup>Department of Civil Engineering, Technical Engineering, Erbil Polytechnic University, Erbil, Kurdistan Region, Iraq.  
<sup>2</sup>Department of Civil Engineering, University of Raparin, Rania, Kurdistan Region, Iraq.  
<sup>3</sup>Department of Civil Engineering, Faculty of Engineering, Tishk International University, Erbil, Kurdistan Region, Iraq.

Received 06 December 2023; revised 08 February 2024;  
 accepted 13 February 2024; available online 25 February 2024

DOI: 10.24271/PSR.2024.429055.1433

**ABSTRACT**

This work proposes an improved numerical methodology based on the flexibility method to study the geometric nonlinearity of space cable structures. The proposed approach makes use of the Pade approximation to enhance the performance of computation. The transformation to the Pade arrangement is particularly successful in quickly speeding up convergence and obtaining the solution when working with complex structures that demonstrate geometrically nonlinear properties. In contrast to previous approaches, the suggested method directly solves the problem by formulating an algebraic system of nonlinear equations using the Pade approximation. To arrive at an analytical solution, some of the most well-established methods that make use of iterative techniques include dynamic relaxation, finite element analysis, and minimum total potential energy. A comprehensive evaluation of the proposed technique's precision and reliability was conducted using six different numerical examples. The recommended method's accuracy, consistency, and computational efficiency are shown by carefully comparing the results with those of techniques that have been around for a long time. This work contributes to the advancement of numerical approaches for the analysis of complex structural behavior by providing a reliable and efficient alternative. Moreover, this work is beneficial for both academics and professionals working in the field.

<https://creativecommons.org/licenses/by-nc/4.0/>

**Keywords:** Cable Net Structure; Spatial Structure; Geometric Nonlinearity; Static Analysis; Force Method; Nonlinear Analysis.

**1. Introduction**

Sources of nonlinearity in structures can be classified into three categories: material nonlinearity, boundary nonlinearity, and geometric nonlinearity. Currently, large space structures are requested, mainly in which the cable member structures are the main element in assembly. Cables provide interesting perspectives to form attractive spatial grid structures with high flexibility. It is noteworthy that cable nets show great structural flexibility and nonlinear response under loading conditions. However, the most challenging aspect of cable structure analysis is the absence of flexural rigidity, which results in high displacements. Consequently, geometric nonlinearity is required to be considered in the analysis of cable structures. The geometric nonlinearities originate when the structural deformation is experiencing a noticeable strain to make the cable's stress sufficient to produce a state of equilibrium in deformed states. The efficiency of cable structures depends on prestressing to attain a desirable appearance and function with the required stability. The inserted prestressing effort offers advances in

structural inflexibility, the lessening of structural distortion, and the redistribution of internal stress, proffering a more cost-effective structure<sup>[1, 2]</sup>. As Kwan<sup>[3]</sup> stated, the behavior (initial stiffness) of cable nets depends on the prestressing rather than its axial stiffness. So, any improvement in finding new analysis techniques for such structures is demanded.

Various recent methods for analyzing cable structures have been thoroughly reviewed<sup>[3-10]</sup>. Most recent methods insist on algorithmic procedures, computer operation aspects, and programming, which contribute to their prorated complexity. In contrast, the vital attention in deriving the proposed technique in this paper is the lucidity of the essential characteristics of cable structures. Therefore, the essential emphases of this paper are: i) to propose a new method for analyzing simple and complex cable structures under static loadings; and ii) to compare and evaluate this approach with several highly nonlinear structural problems.

Various recent methods for analyzing cable structures have been reviewed, which recently exist thoroughly<sup>[3-10]</sup>, and are used for both the static and dynamic analysis of structural cables. The susceptibilities of these solution approaches are dissimilar from each other. Most of them are very complex and require sufficient experience to use. In this section, four of these popular approaches are described briefly.

\* Corresponding author  
 E-mail address: [najmadeen\\_saeed@uor.edu.krd](mailto:najmadeen_saeed@uor.edu.krd) (Instructor).  
 Peer-reviewed under the responsibility of the University of Garmian.



## P. 3. Nonlinear Prestress of Space Cable Net Structures


<https://doi.org/10.23918/eajse.v10i1p3>

<p>Eurasian J. Sci. Eng., 2024, 10(1), 23-34  <a href="https://doi.org/10.23918/eajse.v10i1p3">https://doi.org/10.23918/eajse.v10i1p3</a></p>		<p>Published by Tishk International University          Available at: <a href="https://eajse.tiu.edu.iq/submit/">https://eajse.tiu.edu.iq/submit/</a></p>
RESEARCH ARTICLE		Open Access
<h3>Nonlinear Prestress of Space Cable Net Structures</h3>		
<p>Shna Jabar Abdulkarim<sup>1,2*</sup> , and Najmadeen Mohammed Saeed<sup>2,3</sup> </p>		
<p><sup>1</sup> Civil Engineering Department, Erbil Technical Engineering College, Erbil Polytechnic University, Erbil, Iraq.  <sup>2</sup> Civil Engineering Department, University of Raparin, Rania, Iraq.  <sup>3</sup> Civil Engineering Department, Faculty of Engineering, Tishk International University, Erbil, Iraq.</p>		
<p><b>Article History</b>  <i>Received: 25.11.2022</i>  <i>Revised: 22.12.2022</i>  <i>Accepted: 18.02.2024</i>  <i>Published: 28.03.2024</i>  <i>Communicated by: Asst. Prof. Dr. Abubakar M. Ashir</i>  <i>*Email address: <a href="mailto:shna.jabar@suor.edu.krd">shna.jabar@suor.edu.krd</a></i>  <i>*Corresponding Author</i></p>	<p><b>Abstract:</b>          Cable-net structures are used for many structural purposes, such as stadiums, roofs, bridges... etc. They are lightweight structures that can be used in unique construction at an effective cost. Geometrical nonlinearity governs the performance of cable net systems. This particular system can equilibrate applied loads by undergoing significant deformations with small strains. Therefore, the cable-net structures require to attain a suitable degree of prestressing to prevent cables from slacking and to obtain specific geometry and function. The effective numerical approach is applied for computing the desired level of prestress for a three-dimensional cable-net model and a conical cable-net model. The targeted prestress is achieved considering the nonlinear behavior of cables. The nonlinear member variation is introduced as a second-order function of displaced joints. Then used in determining the desired prestress. Two numerical examples are conducted using the present technique and the nonlinear analysis of SAP2000. Both of the analysis outcomes for the models showed a very well agreement with reaching the target. However, using the Euclidean norm index with a value of 0.0809 in the first example confirmed that the current technique is more approachable to the desired prestress. In addition, when the value of actuation is pre-determined and used in computing the degree of prestress, both the present approach and SAP2000 software work equivalently, as seemed in the second example, which showed 0.04% of the maximum difference in the prestress computation.</p>	<p>          Copyright: © 2023 by the author. Licensee Tishk International University, Erbil, Iraq. This article is an open access article distributed under the terms and conditions of the Creative Commons Attribution-NonCommercial 2.0 Generic License (CC BY-NC 2.0) <a href="https://creativecommons.org/licenses/by-nc/2.0/">https://creativecommons.org/licenses/by-nc/2.0/</a></p>
<p><b>Keywords:</b> Cable-net; Prestress; Geometric Nonlinearity; Self-Equilibrate; Force Method.</p>		
<p><b>1. Introduction</b></p>		
<p>Cable-net structures are tensile structures whose stability is dependent on the axial tensile force alone. The majority of cable-net structures are kinematically indeterminates; therefore, they rely on their geometrical flexibility follow-on their self-equilibrated state [1]. Prestressing is essential in cable-net systems to attain the looked-for shape, stiffness, and stability [2]. Moreover, the level of prestressing has a direct influence on indicating the load tolerance capability, expenses, and shape deformation [3]. The cable-net form is generally determined via its nodal positions, and it has highly flexible geometry. Thus, taking into account the geometric nonlinearity during the prestressing is crucial [4-7].</p>		
<p>Many research publications have been conducted to find out the optimal degree of prestressing for various tensile structures. Pellegrino [8] developed an approach based on the linear force method, assuming small deformation, to find out the prestressed mechanism and the loading conditions that have an effect on causing cable looseness. Kwan and Pellegrino [9] used the least squares analysis technique to calculate the state of prestress in particular and optimal situations with preselected actuators equal to the number of self-stress states. However, You [10] prestressed cable structure by altering the member length of the cables, and similarly controlled the nodal positions by charging the</p>		

## P. 4. Statical Nonlinear Analysis of Spherical Assemblies Utilizing Pade Approximation

<https://doi.org/10.23918/eajse.v10i1p9>



Eurasian J. Sci. Eng., 2024, 10(1), 103-112  
<https://doi.org/10.23918/eajse.v10i1p9>



Published by Tishk International University  
 Available at: <https://eajse.tiu.edu.iq/submit/>

RESEARCH ARTICLE
Open Access

### Statical Nonlinear Analysis of Spherical Assemblies Utilizing Pade Approximation


Shna Jabar Abdulkarim<sup>1,2\*</sup> , and Najmadeen Mohammed Saeed<sup>2,3</sup> 

<sup>1</sup>Civil Engineering Department, Erbil Technical Engineering College, Erbil Polytechnic University, Erbil, Iraq.  
<sup>2</sup>Civil Engineering Department, University of Raparin, Rania, Iraq.  
<sup>3</sup>Civil Engineering Department, Faculty of Engineering, Tishk International University, Erbil, Iraq.

**Abstract:**  
 A new numerical technique for computing the displacement and internal force is presented and applied to the double-layer spherical model. This numerical approach takes into consideration the geometrical nonlinear response of the pin-jointed rigid systems. The presented method performs a practical way of employing the large deformation within the elastic limit for analyzing space structures. In the proposed technique the nonlinear geometrical response of the assembly is modeled and analyzed as a system of algebraic nonlinear equations. The Pade approximation method is conducted in the derivation to give a high rate of convergent ratio in solving the nonlinear equations. The result is validated using the nonlinear finite element software SAP2000 and the linear force method. The discrepancies between the proposed technique and SAP2000 analysis results for external nodal displacement difference and internal element force difference are computed and compared with the linear technique outcomes. The Euclidean norm index is also used to test the precision of calculated nonlinear nodal displacements. The findings showed more closeness to nonlinear SAP2000 results than the linear method.

**Keywords:** Geometric Nonlinearity; Nonlinear Analysis; Statical Analysis; Spherical; Force Method.

**Article History**  
 Received: 04.12.2022  
 Revised: 12.01.2023  
 Accepted: 18.02.2024  
 Published: 03.04.2024  
 Communicated by: Asst. Prof. Dr. Abubakar M. Ashir  
 \*Email address: [shna.jabar@uor.edu.iq](mailto:shna.jabar@uor.edu.iq)  
 \*Corresponding Author



Copyright: © 2023 by the author. Licensee Tishk International University, Erbil, Iraq. This article is an open access article distributed under the terms and conditions of the Creative Commons Attribution-NonCommercial 2.0 Generic License (CC BY-NC 2.0) <https://creativecommons.org/licenses/by-nc/2.0/>

#### 1. Introduction

Spheres are always considered unique and elegant geometry for structures [1, 2]. Architects and engineers have built a variety of spherical forms all over the world. Many spherical buildings can be seen as landmarks, such as Al Wasl Plaza in Dubai in UAE as shown in Figure 1 [3]. Due to the geometrical characteristics of spheres, they are used to afford a wide span as a lightweight structure with economical choice. When they are affected by specific external loads, they face notable deformation [4, 5]. Therefore, they require a very precise computation during the analysis and design process considering their geometrical nonlinear behavior [6].

Many nonlinear analysis techniques have been established for analyzing the nonlinear static and dynamic responses of structures. In the early stages when researchers considered the geometric nonlinearity behavior, they applied techniques of incremental stiffness, Newton Raphson, and iteration procedure [7]. The dynamic relaxation method is one of the popular methods conducted in dealing with geometrically nonlinear static analysis at a steady state [8-13]. Improving the tangent stiffness matrix in the finite element method is another way for performing nonlinear analysis with geometrical consideration [14-17]. Minimum potential energy is an additional different method depending on minimizing the total potential energy of the entire set to provide the equilibrium state [18-21]. The further analysis technique is the nonlinear force method (NFM). In this approach, the three basic



## APPENDIX

## MATLAB Codes for computing prestressing, analysis, and preservation

## A: MATLAB Code for Numerical Prestressing of Illustrative Example in 3.2.5 by fsolve

```

function F=TripleLink(X)    % TripleLink: name of saved m. file

%Copy and paste the below calling function to Command Windows.
%clc; clear all;[result, fval]=fsolve(@TripleLink,
[zeros(1,5)]);result'

%coor: matrix for the coordinates of the members of triple link
structure

coor=[    0      800    0  1  1  1      ; %Node no.1
        0      300    0  0  0  1      ; %Node no.2
       -400     0    0  1  1  1      ; %Node no.3
        400     0    0  1  1  1      ]; %Node no.4

%conn: connectivity matrix between coors to create the cables

conn=[1 2 0 %Cable no. i
      2 3 0 %Cable no. ii
      2 4 0]; %Cable no. iii

%EA: Define the axial stiffness of the cables

EA=10000*ones(1,3);

% nD: no. of degree of freedom
% nB & nJ to calculate number of cables and joints automatically

[nD a]=size(find(coor(:,4:6)==0));
[nB a]=size(conn);
[nJ a]=size(coor);

% data structure for coor
dx=zeros(1,nJ);
dy=zeros(1,nJ);
dz=zeros(1,nJ);
t=zeros(1,nB);
%Need to copy data from X into the non-zero dx's, dy's & dz's, and t's

dx(2)=X(1);
dy(2)=X(2);

t=X(3:5);

act=[ -1    %ei
      0     %eii
      0]; %eiii

```

## APPENDIX

```

% to create nB compatibility & flexibility equations.

F=zeros(1,(nD+nB));
for i=1:nB,
    j1=conn(i,1); j2=conn(i,2);
    x21=(coor(j2,1)-coor(j1,1));
    y21=(coor(j2,2)-coor(j1,2));
    z21=(coor(j2,3)-coor(j1,3));
    L=sqrt(x21^2+y21^2+z21^2);

% Combined compatibility and flexibility equations (to solve in one
step)

F(i)= (4*L*x21*(dx(j2)-dx(j1))+4*L*y21*(dy(j2)-dy(j1))+...
    4*L*z21*(dz(j2)-dz(j1))-2*L*((dx(j2)-dx(j1))^2)-...
    2*L*((dy(j2)-dy(j1))^2)-2*L*((dz(j2)-
    dz(j1))^2))/(4*(L^2)-(2*x21*(dx(j2)-dx(j1)))-...
    (2*y21*(dy(j2)-dy(j1))-(2*z21*(dz(j2)-dz(j1)))+...
    ((dx(j2)-dx(j1))^2)+((dy(j2)-dy(j1))^2)+...
    ((dz(j2)-dz(j1))^2)))+t(i)*L/EA(i)+act(i);

if t(i)<0; t(i)=0; end % to indicate the slackened cables
end

% nD equilibrium equations; it will generate 3*nJ equations

G=zeros(1,(3*nJ));

for i=1:nB,

    j1=conn(i,1);
    j2=conn(i,2);
    x21=(coor(j2,1)-coor(j1,1));
    y21=(coor(j2,2)-coor(j1,2));
    z21=(coor(j2,3)-coor(j1,3));

    L=sqrt(x21^2+y21^2+z21^2);

    dx21=(dx(j2)-dx(j1));
    dy21=(dy(j2)-dy(j1));
    dz21=(dz(j2)-dz(j1));

    COSALPHA=((4*x21*L^2)-(4*dx21*L^2)-(2*(x21^2)*dx21)-(2*x21*y21*dy21)-
    (2*x21*z21*dz21))/...

    ((4*L^3)-(6*L*x21*dx21)-(6*L*y21*dy21)-(6*L*z21*dz21));

    COSBETA=((4*y21*L^2)-(4*dy21*L^2)-(2*(y21^2)*dy21)-(2*y21*x21*dx21)-
    (2*y21*z21*dz21))/...

    ((4*L^3)-(6*L*x21*dx21)-(6*L*y21*dy21)-(6*L*z21*dz21));

    COSGAMA=((4*z21*L^2)-(4*dz21*L^2)-(2*(z21^2)*dz21)-(2*z21*x21*dx21)-
    (2*z21*y21*dy21))/...

    ((4*L^3)-(6*L*x21*dx21)-(6*L*y21*dy21)-(6*L*z21*dz21));

```

## APPENDIX

---

```
if coor(j1,4)==0,
    G(3*(j1-1)+1)=G(3*(j1-1)+1) - t(i)*COSALPHA;
end;

if coor(j1,5)==0,
    G(3*(j1-1)+2)=G(3*(j1-1)+2) - t(i)*COSBETA;
end;

if coor(j1,6)==0,
    G(3*(j1-1)+3)=G(3*(j1-1)+3) - t(i)*COSGAMA;
end;

if coor(j2,4)==0,
    G(3*(j2-1)+1)=G(3*(j2-1)+1) + t(i)*COSALPHA;
end;

if coor(j2,5)==0,
    G(3*(j2-1)+2)=G(3*(j2-1)+2) + t(i)*COSBETA;
end;

if coor(j2,6)==0,
    G(3*(j2-1)+3)=G(3*(j2-1)+3) + t(i)*COSGAMA;
end;

end;

for i=1:nJ,
    G(3*(i-1)+1)=G(3*(i-1)+1);
    G(3*(i-1)+2)=G(3*(i-1)+2);
    G(3*(i-1)+3)=G(3*(i-1)+3);
end;

% now put the nonzero G in F
B=coor(:,4:6)'; F(nB+1:nB+nD)=G(find(B==0));
```

## B: MATLAB Code for Numerical Analysis by fsolve

```

function F=AnalysisSpaceCableNet(X)
% 1st Run ; 2nd copy and paste the next written line into (Command
Windows)to call the fsolve function
%clc; clear all;[result, fval]=fsolve(@AnalysisSpaceCableNet,
[zeros(1,139)]);result(76:139)';clc;d=result(:, [1:75])',t=result(:, [76
:139])'

% coor: deformed nodal coordinates of the model(coor after prestress)

coor=[920      920      400      1      1      1      ; %Node no.1
      460      920      200      1      1      1      ; %Node no.2
      692.29   692.29   251.50   0      0      0      ; %Node no.3
      920      460      200      1      1      1      ; %Node no.4
      0        920      0        1      1      1      ; %Node no.5
      229.17   692.06   91.66    0      0      0      ; %Node no.6
      462.34   462.34   139.73   0      0      0      ; %Node no.7
      692.06   229.17   91.66    0      0      0      ; %Node no.8
      920      0        0        1      1      1      ; %Node no.9
      -460     920     -200     1      1      1      ; %Node no.10
      -230.35  692.05  -88.97   0      0      0      ; %Node no.11
      -1.11    461.49  -2.18    0      0      0      ; %Node no.12
      231.34   231.33   42.71    0      0      0      ; %Node no.13
      461.51   -1.12   -2.19    0      0      0      ; %Node no.14
      692.06  -230.36  -88.97   0      0      0      ; %Node no.15
      920     -460     -200     1      1      1      ; %Node no.16
      -920     920     -400     1      1      1      ; %Node no.17
      -691.97  691.97  -262.10  0      0      0      ; %Node no.18
      -461.62  461.62  -134.09  0      0      0      ; %Node no.19
      -230.31  230.31  -41.95   0      0      0      ; %Node no.20
      0.01     0.00     2.88    0      0      0      ; %Node no.21
      230.32  -230.31  -41.95   0      0      0      ; %Node no.22
      461.63  -461.63  -134.08  0      0      0      ; %Node no.23
      691.97  -691.97  -262.10  0      0      0      ; %Node no.24
      920     -920     -400     1      1      1      ; %Node no.25
      -920     460     -200     1      1      1      ; %Node no.26
      -692.05  230.36  -88.96   0      0      0      ; %Node no.27
      -461.51   1.12   -2.16    0      0      0      ; %Node no.28
      -231.32  -231.31  42.74    0      0      0      ; %Node no.29
      1.12    -461.50  -2.16    0      0      0      ; %Node no.30
      230.36  -692.05  -88.95   0      0      0      ; %Node no.31
      460     -920     -200     1      1      1      ; %Node no.32
      -920     0        0        1      1      1      ; %Node no.33
      -692.07  -229.17   91.67    0      0      0      ; %Node no.34
      -462.33  -462.33  139.73   0      0      0      ; %Node no.35
      -229.17  -692.06   91.66    0      0      0      ; %Node no.36
      0        -920     0        1      1      1      ; %Node no.37
      -920     -460     200     1      1      1      ; %Node no.38
      -692.28  -692.28  251.49   0      0      0      ; %Node no.39
      -460     -920     200     1      1      1      ; %Node no.40
      -920     -920     400     1      1      1      ]; %Node no.41

% conn: (connectivity matrix)connection between the nodal coordinates
of the model
% conn(i,3) the present prestress of the members

conn=[1 3 255.58 ; % Cable No. 1
      2 3 89.07 ; % Cable No. 2
      3 4 89.07 ; % Cable No. 3

```

## APPENDIX

2	6	122.99	;	%	Cable No.	4
3	7	243.64	;	%	Cable No.	5
4	8	122.96	;	%	Cable No.	6
5	6	39.50	;	%	Cable No.	7
6	7	37.57	;	%	Cable No.	8
7	8	37.57	;	%	Cable No.	9
8	9	39.49	;	%	Cable No.	10
5	11	85.39	;	%	Cable No.	11
6	12	121.58	;	%	Cable No.	12
7	13	239.77	;	%	Cable No.	13
8	14	121.55	;	%	Cable No.	14
9	15	85.44	;	%	Cable No.	15
10	11	156.59	;	%	Cable No.	16
11	12	153.01	;	%	Cable No.	17
12	13	148.71	;	%	Cable No.	18
13	14	148.71	;	%	Cable No.	19
14	15	153.02	;	%	Cable No.	20
15	16	156.62	;	%	Cable No.	21
10	18	18.98	;	%	Cable No.	22
11	19	82.13	;	%	Cable No.	23
12	20	118.86	;	%	Cable No.	24
13	21	229.98	;	%	Cable No.	25
14	22	118.83	;	%	Cable No.	26
15	23	82.18	;	%	Cable No.	27
16	24	18.97	;	%	Cable No.	28
17	18	219.33	;	%	Cable No.	29
18	19	216.40	;	%	Cable No.	30
19	20	208.91	;	%	Cable No.	31
20	21	204.04	;	%	Cable No.	32
21	22	204.05	;	%	Cable No.	33
22	23	208.92	;	%	Cable No.	34
23	24	216.41	;	%	Cable No.	35
24	25	219.35	;	%	Cable No.	36
18	26	18.98	;	%	Cable No.	37
19	27	82.12	;	%	Cable No.	38
20	28	118.87	;	%	Cable No.	39
21	29	229.97	;	%	Cable No.	40
22	30	118.83	;	%	Cable No.	41
23	31	82.18	;	%	Cable No.	42
24	32	18.97	;	%	Cable No.	43
26	27	156.42	;	%	Cable No.	44
27	28	152.84	;	%	Cable No.	45
28	29	148.53	;	%	Cable No.	46
29	30	148.51	;	%	Cable No.	47
30	31	152.82	;	%	Cable No.	48
31	32	156.40	;	%	Cable No.	49
27	33	85.38	;	%	Cable No.	50
28	34	121.60	;	%	Cable No.	51
29	35	239.73	;	%	Cable No.	52
30	36	121.56	;	%	Cable No.	53
31	37	85.44	;	%	Cable No.	54
33	34	39.56	;	%	Cable No.	55
34	35	37.63	;	%	Cable No.	56
35	36	37.63	;	%	Cable No.	57
36	37	39.56	;	%	Cable No.	58
34	38	123.02	;	%	Cable No.	59
35	39	243.60	;	%	Cable No.	60
36	40	122.97	;	%	Cable No.	61
38	39	89.11	;	%	Cable No.	62
39	40	89.11	;	%	Cable No.	63
39	41	255.53	];	%	Cable No.	64

## APPENDIX

```
% EA: effective axial stiffness of the members

EA=[179811.80; 166387.23; 161749.38; 166282.76; 166352.14;
    169376.68; 165663.58; 162465.38; 158755.97; 167620.04;
    163100.19; 162686.60; 163226.46; 161577.91; 163100.19;
    164659.92; 162666.37; 161238.01; 161238.01; 163039.52;
    172087.92; 167726.70; 158715.67; 158702.74; 160458.22;
    161284.35; 160922.71; 164574.69; 170181.03; 166944.71;
    164188.74; 159837.54; 165548.59; 164950.26; 165445.81;
    172153.68; 162664.14; 160180.24; 160910.42; 160898.37;
    158340.67; 161296.53; 164189.00; 166169.93; 163790.97;
    159457.56; 159457.56; 160462.87; 165034.84; 163100.19;
    163434.22; 161987.60; 164188.74; 163100.19; 167620.04;
    159484.24; 162086.66; 166440.66; 171369.53; 166352.14;
    167045.60; 162125.97; 170043.99; 174389.10];

% Load Case 1 (vertical loading)

P=[ 0 0 0 ; % Node 1
    0 0 0 ; % Node 2
    0 0 0 ; % Node 3
    0 0 0 ; % Node 4
    0 0 0 ; % Node 5
    0 0 -20 ; % Node 6
    0 0 0 ; % Node 7
    0 0 -20 ; % Node 8
    0 0 0 ; % Node 9
    0 0 0 ; % Node 10
    0 0 -20 ; % Node 11
    0 0 -20 ; % Node 12
    0 0 -20 ; % Node 13
    0 0 -20 ; % Node 14
    0 0 -20 ; % Node 15
    0 0 0 ; % Node 16
    0 0 0 ; % Node 17
    0 0 -20 ; % Node 18
    0 0 -20 ; % Node 19
    0 0 -20 ; % Node 20
    0 0 -20 ; % Node 21
    0 0 -20 ; % Node 22
    0 0 -20 ; % Node 23
    0 0 -20 ; % Node 24
    0 0 0 ; % Node 25
    0 0 0 ; % Node 26
    0 0 -20 ; % Node 27
    0 0 -20 ; % Node 28
    0 0 -20 ; % Node 29
    0 0 -20 ; % Node 30
    0 0 -20 ; % Node 31
    0 0 0 ; % Node 32
    0 0 0 ; % Node 33
    0 0 -20 ; % Node 34
    0 0 0 ; % Node 35
    0 0 -20 ; % Node 36
    0 0 0 ; % Node 37
    0 0 0 ; % Node 38
    0 0 0 ; % Node 39
    0 0 0 ; % Node 40
    0 0 0 ]; % Node 41
```

## APPENDIX

```

% nD: no. of degree of freedom, nB & nJ To calculated automatically
number of members(bars) and number of joints

[nD a]=size(find(coor(:,4:6)==0));[nB a]=size(conn);[nJ a]=
size(coor);

% data structure for coor
dx=zeros(1,nJ);
dy=zeros(1,nJ);
dz=zeros(1,nJ);

%Need to copy data from X into the non-zero dx's, dy's & dz's

dx(3)=X(1);      dy(3)=X(2);      dz(3)=X(3);
dx(6)=X(4);      dy(6)=X(5);      dz(6)=X(6);
dx(7)=X(7);      dy(7)=X(8);      dz(7)=X(9);
dx(8)=X(10);     dy(8)=X(11);     dz(8)=X(12);
dx(11)=X(13);    dy(11)=X(14);    dz(11)=X(15);
dx(12)=X(16);    dy(12)=X(17);    dz(12)=X(18);
dx(13)=X(19);    dy(13)=X(20);    dz(13)=X(21);
dx(14)=X(22);    dy(14)=X(23);    dz(14)=X(24);
dx(15)=X(25);    dy(15)=X(26);    dz(15)=X(27);
dx(18)=X(28);    dy(18)=X(29);    dz(18)=X(30);
dx(19)=X(31);    dy(19)=X(32);    dz(19)=X(33);
dx(20)=X(34);    dy(20)=X(35);    dz(20)=X(36);
dx(21)=X(37);    dy(21)=X(38);    dz(21)=X(39);
dx(22)=X(40);    dy(22)=X(41);    dz(22)=X(42);
dx(23)=X(43);    dy(23)=X(44);    dz(23)=X(45);
dx(24)=X(46);    dy(24)=X(47);    dz(24)=X(48);
dx(27)=X(49);    dy(27)=X(50);    dz(27)=X(51);
dx(28)=X(52);    dy(28)=X(53);    dz(28)=X(54);
dx(29)=X(55);    dy(29)=X(56);    dz(29)=X(57);
dx(30)=X(58);    dy(30)=X(59);    dz(30)=X(60);
dx(31)=X(61);    dy(31)=X(62);    dz(31)=X(63);
dx(34)=X(64);    dy(34)=X(65);    dz(34)=X(66);
dx(35)=X(67);    dy(35)=X(68);    dz(35)=X(69);
dx(36)=X(70);    dy(36)=X(71);    dz(36)=X(72);
dx(39)=X(73);    dy(39)=X(74);    dz(39)=X(75);

t=X(76:139); %t: member's axial force

% nB compatibility & flexibility equations (matrix)

F=zeros(1,(nD+nB));

for i=1:nB
    j1=conn(i,1); j2=conn(i,2);
    x21=(coor(j2,1)-coor(j1,1));
    y21=(coor(j2,2)-coor(j1,2));
    z21=(coor(j2,3)-coor(j1,3));
    L=sqrt(x21^2+y21^2+z21^2);
    % Eq. 3.34
    F(i)=(4+(3/L^2)*((dx(j2)-dx(j1))^2)+(6/L^2)*(x21*(dx(j2)-dx(j1)))+...
        (3/L^2)*((dy(j2)-dy(j1))^2)+(6/L^2)*(y21*(dy(j2)-dy(j1)))+...
        (3/L^2)*((dz(j2)-dz(j1))^2)+(6/L^2)*(z21*(dz(j2)-dz(j1))))/...
        (4+(1/L^2)*((dx(j2)-dx(j1))^2)+(2/L^2)*(x21*(dx(j2)-dx(j1)))+...
        (1/L^2)*((dy(j2)-dy(j1))^2)+(2/L^2)*(y21*(dy(j2)-dy(j1)))+...
        (1/L^2)*((dz(j2)-dz(j1))^2)+(2/L^2)*(z21*(dz(j2)-dz(j1))))-
        t(i)/EA(i)-1;
end

```

## APPENDIX

```

% nD equilibrium equations; originally, buildup 3*nJ equations

G=zeros(1, (3*nJ));

for i=1:nB,
    j1=conn(i,1); j2=conn(i,2);
    x21=(coor(j2,1)-coor(j1,1));
    y21=(coor(j2,2)-coor(j1,2));
    z21=(coor(j2,3)-coor(j1,3));
    L=sqrt(x21^2+y21^2+z21^2);
    dx21=(dx(j2)-dx(j1));
    dy21=(dy(j2)-dy(j1));
    dz21=(dz(j2)-dz(j1));

    COSALPHA=((4*x21*L^2)+(4*dx21*L^2)+(2*(x21^2)*dx21)+(2*x21*y21*dy21)+(
    2*x21*z21*dz21))/...
        ((4*L^3)+(6*L*x21*dx21)+(6*L*y21*dy21)+(6*L*z21*dz21));

    COSBETA=((4*y21*L^2)+(4*dy21*L^2)+(2*(y21^2)*dy21)+(2*y21*x21*dx21)+(2
    *y21*z21*dz21))/...
        ((4*L^3)+(6*L*x21*dx21)+(6*L*y21*dy21)+(6*L*z21*dz21));

    COSGAMA=((4*z21*L^2)+(4*dz21*L^2)+(2*(z21^2)*dz21)+(2*z21*x21*dx21)+(2
    *z21*y21*dy21))/...
        ((4*L^3)+(6*L*x21*dx21)+(6*L*y21*dy21)+(6*L*z21*dz21));

    if coor(j1,4)==0,
        G(3*(j1-1)+1)=G(3*(j1-1)+1) - (t(i)+conn(i,3))*COSALPHA;
    end;

    if coor(j1,5)==0,
        G(3*(j1-1)+2)=G(3*(j1-1)+2) - (t(i)+conn(i,3))*COSBETA;
    end;

    if coor(j1,6)==0,
        G(3*(j1-1)+3)=G(3*(j1-1)+3) - (t(i)+conn(i,3))*COSGAMA;
    end;
    if coor(j2,4)==0,
        G(3*(j2-1)+1)=G(3*(j2-1)+1) + (t(i)+conn(i,3))*COSALPHA;
    end;
    if coor(j2,5)==0,
        G(3*(j2-1)+2)=G(3*(j2-1)+2) + (t(i)+conn(i,3))*COSBETA;
    end;
    if coor(j2,6)==0,
        G(3*(j2-1)+3)=G(3*(j2-1)+3) + (t(i)+conn(i,3))*COSGAMA;
    end;
end;

for i=1:nJ,
    G(3*(i-1)+1)=G(3*(i-1)+1) - P(i,1);
    G(3*(i-1)+2)=G(3*(i-1)+2) - P(i,2);
    G(3*(i-1)+3)=G(3*(i-1)+3) - P(i,3);
end;

% now put the nonzero G in F
B=coor(:,4:6)'; F(nB+1:nD+nB)=G(find(B==0));

```



## C: MATLAB Code for Numerical Displacement preservation by fsolve

```

function F=DisplacementPreservationSpaceCableNet(X)
% Run the calling function with the commands
%clc; clear all;[result,
fval]=fsolve(@DisplacementPreservationSpaceCableNet,
[zeros(1,139)]);result';clc;d=result(:,[1:75])',e0=result(:,[76:139])'

% coor: deformed nodal coordinates of the model(coor after prestress)

coor=[920      920      400      1      1      1      ; %Node no.1
      460      920      200      1      1      1      ; %Node no.2
      692.29   692.29   251.50   0      0      0      ; %Node no.3
      920      460      200      1      1      1      ; %Node no.4
      0        920      0        1      1      1      ; %Node no.5
      229.17   692.06   91.66    0      0      0      ; %Node no.6
      462.34   462.34   139.73   0      0      0      ; %Node no.7
      692.06   229.17   91.66    0      0      0      ; %Node no.8
      920      0        0        1      1      1      ; %Node no.9
      -460     920     -200     1      1      1      ; %Node no.10
      -230.35  692.05   -88.97   0      0      0      ; %Node no.11
      -1.11    461.49   -2.18    0      0      0      ; %Node no.12
      231.34   231.33   42.71    0      0      0      ; %Node no.13
      461.51   -1.12    -2.19    0      0      0      ; %Node no.14
      692.06   -230.36  -88.97   0      0      0      ; %Node no.15
      920      -460     -200     1      1      1      ; %Node no.16
      -920     920     -400     1      1      1      ; %Node no.17
      -691.97  691.97  -262.10   0      0      0      ; %Node no.18
      -461.62  461.62  -134.09   0      0      0      ; %Node no.19
      -230.31  230.31  -41.95    0      0      0      ; %Node no.20
      0.01     0.00     2.88     0      0      0      ; %Node no.21
      230.32  -230.31  -41.95    0      0      0      ; %Node no.22
      461.63  -461.63  -134.08   0      0      0      ; %Node no.23
      691.97  -691.97  -262.10   0      0      0      ; %Node no.24
      920      -920     -400     1      1      1      ; %Node no.25
      -920     460     -200     1      1      1      ; %Node no.26
      -692.05  230.36  -88.96    0      0      0      ; %Node no.27
      -461.51   1.12    -2.16    0      0      0      ; %Node no.28
      -231.32  -231.31  42.74     0      0      0      ; %Node no.29
      1.12    -461.50  -2.16    0      0      0      ; %Node no.30
      230.36  -692.05  -88.95    0      0      0      ; %Node no.31
      460      -920     -200     1      1      1      ; %Node no.32
      -920     0        0        1      1      1      ; %Node no.33
      -692.07  -229.17   91.67    0      0      0      ; %Node no.34
      -462.33  -462.33  139.73   0      0      0      ; %Node no.35
      -229.17  -692.06   91.66    0      0      0      ; %Node no.36
      0        -920     0        1      1      1      ; %Node no.37
      -920     -460     200     1      1      1      ; %Node no.38
      -692.28  -692.28  251.49   0      0      0      ; %Node no.39
      -460     -920     200     1      1      1      ; %Node no.40
      -920     -920     400     1      1      1      ]; %Node no.41

% conn: (connectivity matrix)connection between the nodal coordinates
of the model
conn=[1 3 0; % Cable No. 1
      2 3 0 ; % Cable No. 2
      3 4 0 ; % Cable No. 3
      2 6 0 ; % Cable No. 4
      3 7 0 ; % Cable No. 5

```

## APPENDIX

---

4	8	0	;	%	Cable No.	6
5	6	0	;	%	Cable No.	7
6	7	0	;	%	Cable No.	8
7	8	0	;	%	Cable No.	9
8	9	0	;	%	Cable No.	10
5	11	0	;	%	Cable No.	11
6	12	0	;	%	Cable No.	12
7	13	0	;	%	Cable No.	13
8	14	0	;	%	Cable No.	14
9	15	0	;	%	Cable No.	15
10	11	0	;	%	Cable No.	16
11	12	0	;	%	Cable No.	17
12	13	0	;	%	Cable No.	18
13	14	0	;	%	Cable No.	19
14	15	0	;	%	Cable No.	20
15	16	0	;	%	Cable No.	21
10	18	0	;	%	Cable No.	22
11	19	0	;	%	Cable No.	23
12	20	0	;	%	Cable No.	24
13	21	0	;	%	Cable No.	25
14	22	0	;	%	Cable No.	26
15	23	0	;	%	Cable No.	27
16	24	0	;	%	Cable No.	28
17	18	0	;	%	Cable No.	29
18	19	0	;	%	Cable No.	30
19	20	0	;	%	Cable No.	31
20	21	0	;	%	Cable No.	32
21	22	0	;	%	Cable No.	33
22	23	0	;	%	Cable No.	34
23	24	0	;	%	Cable No.	35
24	25	0	;	%	Cable No.	36
18	26	0	;	%	Cable No.	37
19	27	0	;	%	Cable No.	38
20	28	0	;	%	Cable No.	39
21	29	0	;	%	Cable No.	40
22	30	0	;	%	Cable No.	41
23	31	0	;	%	Cable No.	42
24	32	0	;	%	Cable No.	43
26	27	0	;	%	Cable No.	44
27	28	0	;	%	Cable No.	45
28	29	0	;	%	Cable No.	46
29	30	0	;	%	Cable No.	47
30	31	0	;	%	Cable No.	48
31	32	0	;	%	Cable No.	49
27	33	0	;	%	Cable No.	50
28	34	0	;	%	Cable No.	51
29	35	0	;	%	Cable No.	52
30	36	0	;	%	Cable No.	53
31	37	0	;	%	Cable No.	54
33	34	0	;	%	Cable No.	55
34	35	0	;	%	Cable No.	56
35	36	0	;	%	Cable No.	57
36	37	0	;	%	Cable No.	58
34	38	0	;	%	Cable No.	59
35	39	0	;	%	Cable No.	60
36	40	0	;	%	Cable No.	61
38	39	0	;	%	Cable No.	62
39	40	0	;	%	Cable No.	63
39	41	0]	;	%	Cable No.	64

## APPENDIX

```
% EA: effective axial stiffness of the members

EA=[179811.80; 166387.23; 161749.38; 166282.76; 166352.14;
    169376.68; 165663.58; 162465.38; 158755.97; 167620.04;
    163100.19; 162686.60; 163226.46; 161577.91; 163100.19;
    164659.92; 162666.37; 161238.01; 161238.01; 163039.52;
    172087.92; 167726.70; 158715.67; 158702.74; 160458.22;
    161284.35; 160922.71; 164574.69; 170181.03; 166944.71;
    164188.74; 159837.54; 165548.59; 164950.26; 165445.81;
    172153.68; 162664.14; 160180.24; 160910.42; 160898.37;
    158340.67; 161296.53; 164189.00; 166169.93; 163790.97;
    159457.56; 159457.56; 160462.87; 165034.84; 163100.19;
    163434.22; 161987.60; 164188.74; 163100.19; 167620.04;
    159484.24; 162086.66; 166440.66; 171369.53; 166352.14;
    167045.60; 162125.97; 170043.99; 174389.10];

% nD: no. of degree of freedom, nB & nJ To calculated automatically
number of members(bars) and number of joints

[nD a]=size(find(coor(:,4:6)==0));[nB a]=size(conn);[nJ a]=
size(coor);

% data structure for coor
dx=zeros(1,nJ);
dy=zeros(1,nJ);
dz=zeros(1,nJ);

%Need to copy data from X into the non-zero dx's, dy's & dz's

dx(3)=X(1);      dy(3)=X(2);      dz(3)=X(3);
dx(6)=X(4);      dy(6)=X(5);      dz(6)=X(6);
dx(7)=X(7);      dy(7)=X(8);      dz(7)=X(9);
dx(8)=X(10);     dy(8)=X(11);     dz(8)=X(12);
dx(11)=X(13);    dy(11)=X(14);    dz(11)=X(15);
dx(12)=X(16);    dy(12)=X(17);    dz(12)=X(18);
dx(13)=X(19);    dy(13)=X(20);    dz(13)=X(21);
dx(14)=X(22);    dy(14)=X(23);    dz(14)=X(24);
dx(15)=X(25);    dy(15)=X(26);    dz(15)=X(27);
dx(18)=X(28);    dy(18)=X(29);    dz(18)=X(30);
dx(19)=X(31);    dy(19)=X(32);    dz(19)=X(33);
dx(20)=X(34);    dy(20)=X(35);    dz(20)=X(36);
dx(21)=X(37);    dy(21)=X(38);    dz(21)=X(39);
dx(22)=X(40);    dy(22)=X(41);    dz(22)=X(42);
dx(23)=X(43);    dy(23)=X(44);    dz(23)=X(45);
dx(24)=X(46);    dy(24)=X(47);    dz(24)=X(48);
dx(27)=X(49);    dy(27)=X(50);    dz(27)=X(51);
dx(28)=X(52);    dy(28)=X(53);    dz(28)=X(54);
dx(29)=X(55);    dy(29)=X(56);    dz(29)=X(57);
dx(30)=X(58);    dy(30)=X(59);    dz(30)=X(60);
dx(31)=X(61);    dy(31)=X(62);    dz(31)=X(63);
dx(34)=X(64);    dy(34)=X(65);    dz(34)=X(66);
dx(35)=X(67);    dy(35)=X(68);    dz(35)=X(69);
dx(36)=X(70);    dy(36)=X(71);    dz(36)=X(72);
dx(39)=X(73);    dy(39)=X(74);    dz(39)=X(75);
e0=X(76:139);%e0:required member actuation for displacement preservation

e0(1:4)=0;e0(6)=0;e0(7)=0;
e0(10:22)=0;e0(24:26)=0;
e0(28:37)=0;e0(39:41)=0;
e0(43:55)=0;e0(58)=0;e0(59)=0;e0(61:64)=0;
```

```

% nB compatibility & flexibility equations (matrix)
F=zeros(1,(nD+nB));
for i=1:nB
    j1=conn(i,1); j2=conn(i,2);
    x21=(coor(j2,1)-coor(j1,1));
    y21=(coor(j2,2)-coor(j1,2));
    z21=(coor(j2,3)-coor(j1,3));
    L=sqrt(x21^2+y21^2+z21^2);

% Eq. 3.38
F(i)=(x21*(dx(j2)-dx(j1)))/L+...
      (y21*(dy(j2)-dy(j1)))/L+...
      (z21*(dz(j2)-dz(j1)))/L-...
      (((dx(j2)-dx(j1))^2)/(2*L)-...
       ((dy(j2)-dy(j1))^2)/(2*L)-...
       ((dz(j2)-dz(j1))^2)/(2*L)+...
       (((x21)^2)*((dx(j2)-dx(j1))^2))/(2*(L^3))+...
       (((y21)^2)*((dy(j2)-dy(j1))^2))/(2*(L^3))+...
       (((z21)^2)*((dz(j2)-dz(j1))^2))/(2*(L^3))+...
       (x21*(dx(j2)-dx(j1))*y21*(dy(j2)-dy(j1)))/(L^3)+...
       (x21*(dx(j2)-dx(j1))*z21*(dz(j2)-dz(j1)))/(L^3)+...
       (y21*(dy(j2)-dy(j1))*z21*(dz(j2)-dz(j1)))/(L^3)-e0(i);
end
% nD equilibrium equations; originally, buildup 3*nJ equations
G=zeros(1,(3*nJ));
for i=1:nB,
    j1=conn(i,1); j2=conn(i,2);
    x21=(coor(j2,1)-coor(j1,1)); y21=(coor(j2,2)-coor(j1,2));
    z21=(coor(j2,3)-coor(j1,3)); L=sqrt(x21^2+y21^2+z21^2);
    dx21=(dx(j2)-dx(j1)); dy21=(dy(j2)-dy(j1)); dz21=(dz(j2)-dz(j1));

COSALPHA=((x21-dx21)*L)/((L^2)-(x21*dx21)-(y21*dy21)-(z21*dz21));
COSBETA=((y21-dy21)*L)/((L^2)-(x21*dx21)-(y21*dy21)-(z21*dz21));
COSGAMA=((z21-dz21)*L)/((L^2)-(x21*dx21)-(y21*dy21)-(z21*dz21));

    if coor(j1,4)==0,
        G(3*(j1-1)+1)=G(3*(j1-1)+1) - t(i)* COSALPHA;
    end;
    if coor(j1,5)==0,
        G(3*(j1-1)+2)=G(3*(j1-1)+2) - t(i)* COSBETA;
    end;
    if coor(j1,6)==0,
        G(3*(j1-1)+3)=G(3*(j1-1)+3) - t(i)* COSGAMA;
    end;
    if coor(j2,4)==0,
        G(3*(j2-1)+1)=G(3*(j2-1)+1) + t(i)* COSALPHA;
    end;
    if coor(j2,5)==0,
        G(3*(j2-1)+2)=G(3*(j2-1)+2) + t(i)*COSBETA;
    end;
    if coor(j2,6)==0,
        G(3*(j2-1)+3)=G(3*(j2-1)+3) + t(i)*COSGAMA;
    end;
end;
for i=1:nJ,
    G(3*(i-1)+1)=G(3*(i-1)+1);
    G(3*(i-1)+2)=G(3*(i-1)+2);
    G(3*(i-1)+3)=G(3*(i-1)+3);
end; % now put the nonzero G in F
B=coor(:,4:6)'; F(nB+1:nB+nD)=G(find(B==0));

```

## D: MATLAB Code for Numerical Force preservation by fsolve

```

function F=ForcePreservationSpaceCableNet(X)
% Run in the Command Windows
%clc; clear all;[result, fval]=fsolve(@ForcePreservationSpaceCableNet,
[result, fval]=fsolve(@ForcePreservationSpaceCableNet,
[zeros(1,203)]);result';clc;d=result(:,[1:75])',t=result(:,[76:139])',
e0=result(:,[140:203])'

%coor: deformed nodal coordinates of the model after prestress and
loading

coor=[920      920      400      1      1      1      ; %Node no.1
      460      920      200      1      1      1      ; %Node no.2
      693.01    693.09    249.77    0      0      0      ; %Node no.3
      920      460      200      1      1      1      ; %Node no.4
      0        920      0        1      1      1      ; %Node no.5
      222.68    692.20    106.43    0      0      0      ; %Node no.6
      464.25    467.33    127.85    0      0      0      ; %Node no.7
      692.28    231.08    87.33     0      0      0      ; %Node no.8
      920      0        0        1      1      1      ; %Node no.9
      -460     920     -200     1      1      1      ; %Node no.10
      -233.10   692.46   -82.96    0      0      0      ; %Node no.11
      -4.63    461.81    5.19     0      0      0      ; %Node no.12
      232.04    234.23    39.07    0      0      0      ; %Node no.13
      461.46    1.23     -6.81    0      0      0      ; %Node no.14
      691.93   -226.64   -97.32    0      0      0      ; %Node no.15
      920     -460     -200     1      1      1      ; %Node no.16
      -920     920     -400     1      1      1      ; %Node no.17
      -691.27   691.36   -263.07    0      0      0      ; %Node no.18
      -459.62   459.60   -139.08    0      0      0      ; %Node no.19
      -228.09   227.75   -48.07    0      0      0      ; %Node no.20
      3.33     -0.40    2.54     0      0      0      ; %Node no.21
      233.23   -232.50   -35.42    0      0      0      ; %Node no.22
      465.45   -464.44   -123.65    0      0      0      ; %Node no.23
      692.49   -692.41   -261.15    0      0      0      ; %Node no.24
      920     -920     -400     1      1      1      ; %Node no.25
      -920     460     -200     1      1      1      ; %Node no.26
      -691.98   231.68   -86.10    0      0      0      ; %Node no.27
      -461.32    1.95    -0.56    0      0      0      ; %Node no.28
      -230.02  -229.23   45.70    0      0      0      ; %Node no.29
      0.13     -461.13   -3.48    0      0      0      ; %Node no.30
      229.04  -691.79   -91.62    0      0      0      ; %Node no.31
      460     -920     -200     1      1      1      ; %Node no.32
      -920      0        0        1      1      1      ; %Node no.33
      -691.93  -229.12    91.69    0      0      0      ; %Node no.34
      -460.99  -460.47   143.10    0      0      0      ; %Node no.35
      -231.21  -692.06    87.11    0      0      0      ; %Node no.36
      0        -920      0        1      1      1      ; %Node no.37
      -920     -460     200     1      1      1      ; %Node no.38
      -691.37  -691.30   253.24    0      0      0      ; %Node no.39
      -460     -920     200     1      1      1      ; %Node no.40
      -920     -920     400     1      1      1      ]; %Node no.41

% conn: (connectivity matrix)connection between the nodal coordinates
of the model
conn=[1 3 0; % Cable No. 1
      2 3 0 ; % Cable No. 2
      3 4 0 ; % Cable No. 3
      2 6 0 ; % Cable No. 4
      3 7 0 ; % Cable No. 5

```

## APPENDIX

---

4	8	0	;	% Cable No.	6
5	6	0	;	% Cable No.	7
6	7	0	;	% Cable No.	8
7	8	0	;	% Cable No.	9
8	9	0	;	% Cable No.	10
5	11	0	;	% Cable No.	11
6	12	0	;	% Cable No.	12
7	13	0	;	% Cable No.	13
8	14	0	;	% Cable No.	14
9	15	0	;	% Cable No.	15
10	11	0	;	% Cable No.	16
11	12	0	;	% Cable No.	17
12	13	0	;	% Cable No.	18
13	14	0	;	% Cable No.	19
14	15	0	;	% Cable No.	20
15	16	0	;	% Cable No.	21
10	18	0	;	% Cable No.	22
11	19	0	;	% Cable No.	23
12	20	0	;	% Cable No.	24
13	21	0	;	% Cable No.	25
14	22	0	;	% Cable No.	26
15	23	0	;	% Cable No.	27
16	24	0	;	% Cable No.	28
17	18	0	;	% Cable No.	29
18	19	0	;	% Cable No.	30
19	20	0	;	% Cable No.	31
20	21	0	;	% Cable No.	32
21	22	0	;	% Cable No.	33
22	23	0	;	% Cable No.	34
23	24	0	;	% Cable No.	35
24	25	0	;	% Cable No.	36
18	26	0	;	% Cable No.	37
19	27	0	;	% Cable No.	38
20	28	0	;	% Cable No.	39
21	29	0	;	% Cable No.	40
22	30	0	;	% Cable No.	41
23	31	0	;	% Cable No.	42
24	32	0	;	% Cable No.	43
26	27	0	;	% Cable No.	44
27	28	0	;	% Cable No.	45
28	29	0	;	% Cable No.	46
29	30	0	;	% Cable No.	47
30	31	0	;	% Cable No.	48
31	32	0	;	% Cable No.	49
27	33	0	;	% Cable No.	50
28	34	0	;	% Cable No.	51
29	35	0	;	% Cable No.	52
30	36	0	;	% Cable No.	53
31	37	0	;	% Cable No.	54
33	34	0	;	% Cable No.	55
34	35	0	;	% Cable No.	56
35	36	0	;	% Cable No.	57
36	37	0	;	% Cable No.	58
34	38	0	;	% Cable No.	59
35	39	0	;	% Cable No.	60
36	40	0	;	% Cable No.	61
38	39	0	;	% Cable No.	62
39	40	0	;	% Cable No.	63
39	41	0]	;	% Cable No.	64

## APPENDIX

```
% nD: no. of degree of freedom, nB & nJ To calculated automatically
number of members(bars) and number of joints

[nD a]=size(find(coor(:,4:6)==0));[nB a]=size(conn);[nJ a]=
size(coor);

% data structure for coor

dx=zeros(1,nJ);
dy=zeros(1,nJ);
dz=zeros(1,nJ);

%Need to copy data from X into the non-zero dx's, dy's & dz's

dx(3)=X(1);      dy(3)=X(2);      dz(3)=X(3);
dx(6)=X(4);      dy(6)=X(5);      dz(6)=X(6);
dx(7)=X(7);      dy(7)=X(8);      dz(7)=X(9);
dx(8)=X(10);     dy(8)=X(11);     dz(8)=X(12);
dx(11)=X(13);    dy(11)=X(14);    dz(11)=X(15);
dx(12)=X(16);    dy(12)=X(17);    dz(12)=X(18);
dx(13)=X(19);    dy(13)=X(20);    dz(13)=X(21);
dx(14)=X(22);    dy(14)=X(23);    dz(14)=X(24);
dx(15)=X(25);    dy(15)=X(26);    dz(15)=X(27);
dx(18)=X(28);    dy(18)=X(29);    dz(18)=X(30);
dx(19)=X(31);    dy(19)=X(32);    dz(19)=X(33);
dx(20)=X(34);    dy(20)=X(35);    dz(20)=X(36);
dx(21)=X(37);    dy(21)=X(38);    dz(21)=X(39);
dx(22)=X(40);    dy(22)=X(41);    dz(22)=X(42);
dx(23)=X(43);    dy(23)=X(44);    dz(23)=X(45);
dx(24)=X(46);    dy(24)=X(47);    dz(24)=X(48);
dx(27)=X(49);    dy(27)=X(50);    dz(27)=X(51);
dx(28)=X(52);    dy(28)=X(53);    dz(28)=X(54);
dx(29)=X(55);    dy(29)=X(56);    dz(29)=X(57);
dx(30)=X(58);    dy(30)=X(59);    dz(30)=X(60);
dx(31)=X(61);    dy(31)=X(62);    dz(31)=X(63);
dx(34)=X(64);    dy(34)=X(65);    dz(34)=X(66);
dx(35)=X(67);    dy(35)=X(68);    dz(35)=X(69);
dx(36)=X(70);    dy(36)=X(71);    dz(36)=X(72);
dx(39)=X(73);    dy(39)=X(74);    dz(39)=X(75);

t=X(76:139);

t(2)=54 ;
t(7)=19 ;
t(8)=18 ;
t(27)=33 ;
t(28)=53 ;

e0(1:64)=X(140:203);

e0(1:64)=0;
e0(2)=X(141);
e0(3)=X(142);
e0(7)=X(146) ;
e0(8)=X(147);
e0(27)=X(166) ;
e0(28)=X(167);
e0(36)=X(175) ;
e0(43)=X(182);
```

## APPENDIX

```

% nB compatibility & flexibility equations (matrix)
F=zeros(1, (nD+nB));
for i=1:nB
    j1=conn(i,1); j2=conn(i,2);
    x21=(coor(j2,1)-coor(j1,1));
    y21=(coor(j2,2)-coor(j1,2));
    z21=(coor(j2,3)-coor(j1,3));
    L=sqrt(x21^2+y21^2+z21^2);

F(i)= (x21*(dx(j2)-dx(j1)))/L+...
      (y21*(dy(j2)-dy(j1)))/L+...
      (z21*(dz(j2)-dz(j1)))/L-...
      (((dx(j2)-dx(j1))^2)/(2*L)-...
      ((dy(j2)-dy(j1))^2)/(2*L)-...
      ((dz(j2)-dz(j1))^2)/(2*L)+...
      (((x21)^2)*((dx(j2)-dx(j1))^2)/(2*(L^3))+...
      (((y21)^2)*((dy(j2)-dy(j1))^2)/(2*(L^3))+...
      (((z21)^2)*((dz(j2)-dz(j1))^2)/(2*(L^3))+...
      (x21*(dx(j2)-dx(j1))*y21*(dy(j2)-dy(j1)))/(L^3)+...
      (x21*(dx(j2)-dx(j1))*z21*(dz(j2)-dz(j1)))/(L^3)+...
      (y21*(dy(j2)-dy(j1))*z21*(dz(j2)-dz(j1)))/(L^3) +t(i)*L/EA(i)+e0(i);

    end
% nD equilibrium equations; originally, buildup 3*nJ equations
G=zeros(1, (3*nJ));
for i=1:nB,
    j1=conn(i,1); j2=conn(i,2);
    x21=(coor(j2,1)-coor(j1,1)); y21=(coor(j2,2)-coor(j1,2));
    z21=(coor(j2,3)-coor(j1,3)); L=sqrt(x21^2+y21^2+z21^2);
    dx21=(dx(j2)-dx(j1)); dy21=(dy(j2)-dy(j1)); dz21=(dz(j2)-dz(j1));

COSALPHA=((x21-dx21)*L)/((L^2)-(x21*dx21)-(y21*dy21)-(z21*dz21));
COSBETA=((y21-dy21)*L)/((L^2)-(x21*dx21)-(y21*dy21)-(z21*dz21));
COSGAMA=((z21-dz21)*L)/((L^2)-(x21*dx21)-(y21*dy21)-(z21*dz21));

    if coor(j1,4)==0,
        G(3*(j1-1)+1)=G(3*(j1-1)+1) - t(i)* COSALPHA;
    end;
    if coor(j1,5)==0,
        G(3*(j1-1)+2)=G(3*(j1-1)+2) - t(i)* COSBETA;
    end;
    if coor(j1,6)==0,
        G(3*(j1-1)+3)=G(3*(j1-1)+3) - t(i)* COSGAMA;
    end;
    if coor(j2,4)==0,
        G(3*(j2-1)+1)=G(3*(j2-1)+1) + t(i)* COSALPHA;
    end;
    if coor(j2,5)==0,
        G(3*(j2-1)+2)=G(3*(j2-1)+2) + t(i)*COSBETA;
    end;
    if coor(j2,6)==0,
        G(3*(j2-1)+3)=G(3*(j2-1)+3) + t(i)*COSGAMA;
    end;
end;
for i=1:nJ,
    G(3*(i-1)+1)=G(3*(i-1)+1);
    G(3*(i-1)+2)=G(3*(i-1)+2);
    G(3*(i-1)+3)=G(3*(i-1)+3);
end; % now put the nonzero G in F
B=coor(:,4:6)'; F(nB+1:nB+nD)=G(find(B==0));

```



گۆراوه ديارى كراوه كان. كاريگه رى پرۆسه ي پاراستن په يوه سته به دانانى كاريپكه ر(ئه كچوئته ر)، شيكاري هه ستيا رى ئه ندامى، و هه لېژاردنى گونجاوى ئامانجه كانى بى كاريپكه ردىن.

چه سپاندى ئه م ته كنيكانه بريتى بوو له توپژينه وهى كه يسى ژماره يى و تاقىكه ردىنه وهى ئه زموونى له سه ر مۆديلى تۆرى كيپلى بۆشايى پارابۆلۆيدى هايپه ربۆليك كه 64 ئه ندام و 41 جومگه ي تىدا بوو. ئه نجامه كان ريككه وتنيكى به هيژيان نيشان دا، له گه ل زۆرترين و كه مترين ريژه ي ناته بايى به ريژه ي 7% و 0%، له نيوان پيوانه ي تيۆرى و تاقىگه ييه كاندا. ئه م تيزه چوارچيوه يه كى نويبووه وه ده خاته روو كه به شيوه يه كى به رچاو وردى، كارايى و كونترولكه ردى كاردانه وهى پيشبينيكا راي پيكه اته يى به رز ده كاته وه، پيشكه وتنيكى به رچاو له بوارى پيكه اته بۆشاييه په يوه سته كراوه كانى پينه كاندا به رده ست ده خات.

## پوخته

لەم تیزەدا، سێ تەکنیکی ناھێلی پەرەیان پێدراوە کە ئەوانیش تەکنیکەکانی فشاری پێشوخەخت و شیکردنەووە پاراستنە لەسەر بنەمای رێبازی ھیز بە ڕەچاوکردنی ناھێلییە ئەندازەییەکان لە پیکھاتە بۆشاییە پەيوەستکراوەکانی پین. ئەم تەکنیکانە چوارچۆیەکی گشتگیر بۆ ئەنجامدانی وردی فشاری پێشوخەختە و شیکردنەووە و پاراستنی کۆبوووەوی بۆشایی دابین دەکەن، کە لە رێگەی لیکۆلینەووی چری ژمارەیی و تاقیکارییەو پشتراستکراونەتەووە.

توێژینەووەکە رێبازە ناھێلکارییەکان بەشیووی راستەوخۆ دەناسینیت، بەتایبەتی بۆ فشاری پێشوخەختە پاراستن، کە زال دەبن بەسەر سنوورەکانی شیوازە دووبارەبوووەکان و نزیکبوونەووە ھێلییەکان. ھاوکێشە ناھێلییە دارپێژراوەکان، کە وەک کارکردیک بۆ جیگۆرکی جومگەکان دەربدراون، وە بەشیوویەکی کارا بە بەکارھێنانی ئیفسۆلفی ماتلاب شیتەل کراون، ئەمەش وادەکات کە بەکارھێنانی بەھیزی بۆ ھەردوو سیستمی فەزایی سادە و ئالۆز نیشان بدات. تەکنیکە پێشنیار کراوەکە فشاری پێشوخەختە ئاستی پێش فشاری خوازاو بە ھەژمارکردنیک ورد بۆ گۆرانکارییە ناھێلییەکانی ئەندامەکانی ھەژمار دەکات، رێگری دەکات لە شلبوونەووی کێیلەکان، و پاراستنی ریکخستن ھاوتا لەگەڵ شیتەلکەرەکانی نەرمەکالا لە ژێر بارودۆخی کارپیکردنی پێشوخەختە دیاری دەکات.

شیوازی شیکاری پەرەپێدراو کارا و وردە، توانای ھەژمارکردنی فشارەکانی ناوہووی ئەندامەکان و ھیزەکانی تەوہرەیی ھەبە بۆ ھەردوو ئەندامی رەق و نەرم، لە ھەمان کاتدا ناھێلکارییە ئەندازەییەکان لە ژێر بارودۆخی بارە جیاوازیەکاندا لەخۆدەگریت. بە ھەمان شیوہ، تەکنیکەکانی پاراستن بەشیوویەکی متمانەپیکراو ئەندازە تیکچوووەکان، جیگۆرکی گریکان و ھیزە ناوخواييەکان دەگەرینیتەووە، لەگەڵ کۆنترۆلی ئامانجدار بۆ



زانكۆی پۆلیتیه كنیکی هه ولیر  
ERBIL POLYTECHNIC UNIVERSITY

## فشاری پیش وه ختی ناهیلی و پاراستنی ئەندازهیی پیکهاته بۆشاییه کان

تیزه که

پیشکەشی ئەنجومه نی کۆلیژی ته کنیکی ئەندازیاری هه ولیر کراوه له زانکۆی  
پۆلیتیه کنیکی هه ولیر وه کو به شیک له پیداو یستیه کانی به دهست هیئانی پلهی  
دکتۆرای فه لسه فه له ئەندازیاری بیناکاری

له لایه ن

شنه جبار عبدالکریم

به کالۆریۆس له ئەندازیاری بیناکاری – زانکۆی سلیمانی – ۲۰۰۷  
ماسته ر له ئەندازیاری بیناکاری – زانکۆی زانستی مالیزیا – ۲۰۱۴

به سه ره پهرشتی

پ. ی. د. نجم الدین محمد سعید

هه ولیر - کوردستان

تشرینی یه که م ۲۰۲۴